

**A Study of Flavocytochrome b_2
and Flavocytochrome c_3**

Ruth Moysey



**Thesis presented for the degree of
Doctor of Philosophy
The University Of Edinburgh
January 2001**



The work presented in this thesis is the original work of the author, except where specific reference is made to other sources. It has not been submitted in part, or in whole, for any other degree. Some of the results have already been published.

“The most exciting phrase to hear in science, the one that heralds new discoveries, is not ‘Eureka!’ but ‘That’s funny...’ “

(Isaac Asimov)

Acknowledgements

I would like to thank my supervisors Steve Chapman and Graeme Reid for their help and support throughout my PhD and the Chapman/Reid group for making my stay in Edinburgh an enjoyable one. In particular I am grateful to Caroline Miles for the preparation of the mutant enzymes, Chris Mowat for the crystallography and to Kate and Mary for their contribution to work on fcc.

Abstract

Flavocytochrome b_2 from *Saccharomyces cerevisiae* is a tetramer of identical subunits each with M_r 57,500. The enzyme catalyses the oxidation of L-lactate to pyruvate and transfers electrons to cytochrome c . Each subunit consists of two distinct domains: an N-terminal cytochrome domain and a C-terminal flavin domain. The flavin domain (FDH) has been expressed independently of the cytochrome domain and retains its ability to function as an L-lactate dehydrogenase. However in the absence of the haem domain electron transfer to cytochrome c is extremely slow. Site directed mutagenesis has been used to create a recognition site for cytochrome c on the surface of the flavin domain. Complementary charges were introduced by the mutations K201E, K324A and F325E and a loop section replaced with a 5-glycine linker (FDH_{5GLY}). However binding studies were inconclusive as to whether any significant complex formation between FDH_{5GLY} and cytochrome c actually occurred.

In order to engineer an enzyme selective for glycolate over L-lactate two mutants have been constructed. FDH_{L230W} incorporates the single amino acid change of Leu230 to tryptophan. The triple mutant (FDH_{TRIP}) combines the mutation L230W, with T197A and A283T. FDH_{TRIP} was found to preferentially bind glycolate over lactate with K_m values of 16 mM and 26 mM respectively. In addition FDH_{L230W} and FDH_{TRIP} were tested for their ability to function as oxidases. However no significant increase in oxidase activity compared to wild-type was observed.

Flavocytochrome c_3 is a fumarate reductase expressed by the marine bacterium *Shewanella frigidimarina* during anaerobic growth in the presence of fumarate. This soluble periplasmic enzyme is composed of three domains; a flavin domain containing non-covalently bound FAD, a cytochrome domain and a clamp domain. The active site is located in the

flavin domain at the interface with the clamp domain. The enzyme catalyses the reduction of fumarate to succinate with a k_{cat} of $509 \pm 15 \text{ s}^{-1}$ and K_m of $25 \pm 2 \mu\text{M}$ at pH 7.2, 25°C. Reduction of fumarate requires hydride transfer from the FAD and protonation by an active site acid. Residues implicated in catalysis have been studied using site directed mutagenesis. Substitution of Arg402 by alanine leads to complete loss of activity whereas neither of the two active site histidines (His504 and His365) is essential for catalysis. The H365A:H504A double mutant enzyme was found to have a k_{cat} of $0.84 \pm 0.05 \text{ s}^{-1}$ at pH 7.2. Substitution of Arg402 by lysine, histidine or tyrosine led to a fall in k_{cat} to 0.55 s^{-1} , 0.091 s^{-1} and 0.05 s^{-1} respectively. Substrate specificity and inhibition studies have been carried out to probe the active site structure. Fcc₃ was unable to catalyse the reduction of alternative enoates to fumarate. However, oxaloacetate, methylsuccinate and 3-nitropropionate were found to be inhibitors of succinate oxidation with K_i values of $5.3 \mu\text{M}$, 1.7 mM , and 0.5 mM respectively.

Contents

Declaration	ii
Acknowledgements	iv
Abstract	v
Index	vii

Part 1 Flavocytochrome b_2

Chapter 1 Introduction to Flavocytochrome b_2

1.1 The Family of α -hydroxy acid dehydrogenases/oxidases	1
1.2 Flavin mononucleotide	2
1.3 Haem	3
1.4 Flavocytochrome b_2	4
1.4.1 Electron Transfer	6
1.4.2 The Flavin Domain	7
1.4.3 Substrate Binding	7
1.4.4 Substrate Specificity	8
1.4.4.1 Redesign of the Active Site	9
1.4.5 The Hydride Transfer Mechanism	11
1.5 Glycolate Oxidase	12
1.6 L-lactate Monooxygenase	16
1.7 Re-oxidation of FMN by Molecular Oxygen	17
1.8 Project Aims	18

Chapter 2 Materials and Methods

2.1 Buffers	20
2.2 Growth Media	23
2.3 Molecular Biology	23

2.4	Hybrid PCR	27
2.5	Protein Isolation and Purification	32
2.6	Purity Determination	34
2.7	Kinetic Analysis	36
2.8	Oxidase Activity	37
2.9	Redox Potentiometry	38
2.10	Microcalorimetry	39

Chapter 3 The Flavin Domain of Flavocytochrome b_2

3.1	Substrate Specificity	40
3.1.1	Steady-State Kinetics	40
3.1.2	Pre-Steady-State Kinetic Analysis	43
3.2	Potentiometry	44
3.3	Oxidase Activity	46
3.3.1	Steady-State Analysis	46
3.3.2	Pre-Steady-State Oxidation with O_2	47
3.4	Recognition for Cytochrome c	48
3.4.1	Replacement of the Loop	52
3.4.2	Steady-State Analysis	53
3.4.3	Ionic Strength Plots	54
3.4.4	Microcalorimetry and Molecular Recognition	56
3.4.4.1	Differential Scanning Calorimetry	56
3.4.4.2	Isothermal Calorimetric Titrations	58
3.5	Discussion	59
	References	63

Part 2 Flavocytochrome c_3

Chapter 4 Introduction to Flavocytochrome c_3

4.0 Introduction	68
4.1 Comparison of Fumarate Reductases	69
4.1.1 Global Structure	70
4.1.2 The Flavoprotein Subunit	74
4.1.2.1 Mechanism	76
4.1.2.2 Proton Delivery	79
4.1.3 The Clamp Domain	81
4.1.4 The Haem Domain	82
4.1.5 The Membrane Anchor Subunit	84
4.1.6 Electron Donors	86
4.2 Project Aims	87

Chapter 5 Materials and Methods

5.1 Media and Solutions	88
5.2 Protein Preparation	90
5.3 Purity Determination	92
5.4 Kinetic Analysis	95
5.5 Solvent Isotope Studies	97

Chapter 6 Structure and Function of Flavocytochrome c_3

6.1 Probing the Active Site Structure	98
6.1.1 Substrate Specificity	100
6.1.2 Inhibition Studies	103
6.2 The Active Site Catalyst	109
6.2.1 The Roles of the Active Site Histidines	109
6.2.2 H365A:H504A- fcc_3	112

6.2.2.1	The Effect of H365A:H504A on k_{cat} and K_m	112
6.2.2.2	The pH Dependence of H365A:H504A- fcc_3	114
6.2.3	Substitution of the Active-Site Acid	115
6.2.4	The Crystal Structure of R402A	118
6.2.5	R402K- fcc_3	119
6.2.5.1	The Crystal Structure of R402K	121
6.2.6	R402H- fcc_3	122
6.2.7	R402Y- fcc_3	123
6.2.7.1	Comparison of the pH Profiles of R402K- fcc_3 , R402H- fcc_3 and R402Y- fcc_3	124
6.3	Solvent Isotope Effect	125
6.3.1	Introduction	125
6.3.2	Solvent Isotope Studies on wild-type	127
6.3.3	Solvent Isotope Studies on R402K- fcc_3 and R402H- fcc_3	128
6.4	Conclusions and Future Work	131
References		133

Appendix

7.1	Abbreviations	138
7.2	Derivation of Michaelis-Menten Equation	139
7.1.1	Competitive inhibition	142
7.3	Debye-Hückel Theory	143
7.4	pH profile equation	144
7.5	Solvent Isotope effect	145
7.6	Conferences and Courses Attended	149
7.7	Publications	149

Figures

1.1	Different modes of FMN re-oxidation in the family of α -hydroxy acid dehydrogenases/oxidases.	1
-----	--	---

1.2	The different oxidation states of FMN	3
1.3	The structure of protohaem IX (haem <i>b</i>), haem <i>a</i> and haem <i>c</i> .	4
1.4	Conversion of L-lactate to pyruvate.	4
1.5	A single subunit of flavocytochrome <i>b</i> ₂ .	5
1.6	The catalytic cycle of flavocytochrome <i>b</i> ₂ .	6
1.7	The flavin domain	7
1.8	The structure of flavocytochrome <i>b</i> ₂ active site.	8
1.9	Comparison of residues at the equivalent position 230 and corresponding substrates.	9
1.10	The active site of flavocytochrome <i>b</i> ₂ highlighting residues which have been studied with regard to substrate specificity.	10
1.11	The hydride transfer mechanism.	12
1.12	Conversion of glycolate to glyoxylate.	12
1.13	Glycolate oxidase	13
1.14	Comparison of the active site structure of glycolate oxidase with flavocytochrome <i>b</i> ₂ .	13
1.15	Location of a water molecule close to the FMN in glycolate oxidase which is absent in the active site of flavocytochrome <i>b</i> ₂ .	15
1.16	Comparison of active site residues in glycolate oxidase and flavocytochrome <i>b</i> ₂ .	16
1.17	Re-oxidation of the Flavin by molecular oxygen	18
2.1	Replacement of DNA sequence encoding for the loop with sequence encoding for 5 glycine residues.	27
2.2	Generation of the double stranded DNA fragment encoding for the flavin domain between the loop and H ₃ end.	29
2.3	Generation of the double stranded DNA fragment encoding for the flavin domain between the loop and R ₁ end.	30
2.4	Formation of the double stranded DNA fragment encoding for the flavin domain with the loop replaced by 5 glycine residues.	31
2.5	Ligation of double stranded PCR product into the expression vector pJF118.	32
2.6	Spectrum of purified flavin domain.	34

3.1	Examples of steady-state traces obtained for the reduction of $[\text{Fe}(\text{CN})_6]^{3-}$	40
3.2	Michaelis-Menten plot for FDH_{wt} with glycolate as substrate.	41
3.3	Semi-log plot comparing K_m values for L-lactate and glycolate for glycolate oxidase, FDH_{wt} , $\text{FDH}_{\text{L230W}}$ and FDH_{TRIP} .	42
3.4	Comparison of enzyme efficiency of glycolate oxidase, FDH_{wt} , $\text{FDH}_{\text{L230W}}$ and FDH_{TRIP} with L-lactate and glycolate.	43
3.5	Pre-steady-state analysis for the reduction of FDH_{WT} by L-lactate.	43
3.6	Redox titration spectra of FDH_{TRIP} .	44
3.7	Plot of percentage oxidised FMN at 454 nm against the measured reduction potential.	45
3.8	The coupled assay system used to monitor oxidase activity of $\text{FDH}_{\text{L230W}}$	46
3.9	Example trace of steady-state oxidase activity of $\text{FDH}_{\text{L320W}}$ with L-lactate.	46
3.10	Comparison of pre-steady-state oxidase activity for FDH_{WT} and $\text{FDH}_{\text{L230W}}$.	48
3.11	Charged residues surrounding the haem of cytochrome <i>c</i> .	49
3.12	Location of residues mutated in an attempt to engineer a binding site for cytochrome <i>c</i> .	50
3.13	The closest approach of cytochrome <i>c</i> (haem) to FDH_{WT} (FMN) allowed by the modelled loop.	51
3.14	The closest approach of cytochrome <i>c</i> (haem) to FDH_{5GLY} (FMN) in which the loop has been replaced by a 5 glycine linker.	52
3.15	Confirmation of FDH_{5GLY} by western Blott and mass spectrometry.	52
3.16	Michaelis-Menten plot for FDH_{5GLY} under saturating lactate conditions using cytochrome <i>c</i> as electron acceptor.	53
3.17	Ionic strength data for FDH_{WT} and FDH_{5GLY}	55
3.18	Differential scanning calorimetry trace of cytochrome <i>c</i> , FDH_{WT} and a 1:1 mixture	57
3.19	Differential scanning calorimetry trace of cytochrome <i>c</i> , FDH_{5GLY} and a 1:1 mixture	58
3.20	Isothermal titration calorimetry of cytochrome <i>c</i> into FDH_{5GLY}	59

3.21	Electron density of the FAD in D-amino acid oxidase showing the presence of a diatomic species proposed to be peroxide.	61
4.1	Reduction of fumarate to succinate	68
4.2	The crystal structure of flavocytochrome c_3	71
4.3	Structural comparison of the fumarate reductases from <i>W. succinogenes</i> , <i>E. coli</i> and <i>Shewanella</i> .	73
4.4	An octahedrally coordinated sodium ion is found buried in the flavin domain close to the active site.	74
4.5	Conservation of active site residues in fumarate reductases and succinate dehydrogenases.	75
4.6	The active site of flavocytochrome c_3	77
4.7	Schematic representation of the mechanism	78
4.8	The proton pathway	79
4.9	Comparison of the active site structures of the fumarate reductases from <i>E. coli</i> , <i>W. succinogenes</i> and <i>Shewanella</i> .	80
4.10	Movement of the clamp domain in flavocytochrome c_3 from <i>S. putrefaciens</i> .	81
4.11	Comparison of the clamp domain positions of L-aspartate oxidase and flavocytochrome c_3 .	82
4.12	The arrangement of c -type haems and FAD which together form a 40 Å 'molecular wire'.	83
4.13	NMR structure of cytochrome c_3	84
4.14	Redox cofactors found in the membrane bound fumarate reductases from <i>E. coli</i> and <i>W. succinogenes</i> .	85
4.15	Quinone structures	86
5.1	SDS gel showing purity of samples at each subsequent purification step.	94
5.2	UV/vis spectrum of purified flavocytochrome c_3	94
6.1	The active site cavity of flavocytochrome c_3	98
6.2	The active site of flavocytochrome c_3 highlighting the hydrogen bonding network.	100
6.3	Key components of the substrate required for catalysis.	101
6.4	Structures of potential substrates.	101

6.5	Traces obtained for succinate oxidation in the absence and in the presence of an inhibitor.	103
6.6	Inhibitors and potential inhibitors	104
6.7	Inhibition curve of succinate oxidation by oxaloacetate	105
6.8	Michaelis plots of succinate oxidation at different inhibitor concentrations.	106
6.9	Reciprical plot confirming competitive inhibition.	107
6.10	Substitution of histidine with alanine.	110
6.11	The active site of H365A in comparison to wild-type.	111
6.12	The proton transfer pathway of H365A in comparison to wild-type.	111
6.13	Michaelis plot of H365A:H504A- <i>fcc</i> ₃ with fumarate at pH 7.2.	113
6.14	A comparison of the pH profile of wild-type <i>fcc</i> ₃ with H365A:H504A- <i>fcc</i> ₃ .	115
6.15	Structures of amino acid residues substituted for Arg402.	117
6.16	The pK _a values of the protonatable side-chain of Arg, Lys, His and Tyr.	119
6.17	A comparison of the active site of R402A with wild-type.	120
6.18	Michaelis plot of fumarate reduction by R402K at pH7.2	121
6.19	Overlay of the active site structure of wild-type and <i>fcc</i> ₃ -R402K.	122
6.20	Comparison of the proton transfer pathway in <i>fcc</i> ₃ -R402K and wild-type.	123
6.21	Comparison of pH profiles of R402H, R402K and R402Y.	125
6.22	Free energy diagram for enzyme catalyses reactions.	126
6.23	Equation for the solvent isotope effect.	126
6.24	Solvent isotope effect observed for wild-type at pH 7.2.	127
6.25	Solvent isotope effect observed for wild-type at pH 9.5.	128
6.26	Solvent isotope effect observed for R402K at pH 7.2.	129
6.27	Solvent isotope effect observed for R402H at pH 7.2.	129
6.28	The proton transfer pathway.	130

Chapter 1

Introduction to Flavocytochrome b_2

1.0 Introduction to Flavocytochrome b_2

1.1 The Family of α -hydroxy acid dehydrogenases/oxidases

L-lactate dehydrogenase is a member of the family of FMN dependent α -hydroxy acid dehydrogenases/oxidases that include glycolate oxidases (Lindqvist 1989, lactate monooxygenase (Hayaishi *et al.*, 1957, Lockridge *et al.*, 1972), long-chain hydroxyacid oxidase (Belmouden *et al.*, 1993) and mandelate dehydrogenase (Fewson *et al.*, 1988). The ultimate oxidant depends on the particular enzyme. Molecular oxygen is the electron acceptor for the oxidases, whereas the flavocytochromes b_2 (lactate and mandelate dehydrogenases) utilise an intramolecular haem. The membrane associated bacterial mandelate dehydrogenases transfer an electron from the reduced FMN to a component of the electron transport chain located in the membrane (Mitra *et al.*, 1993).

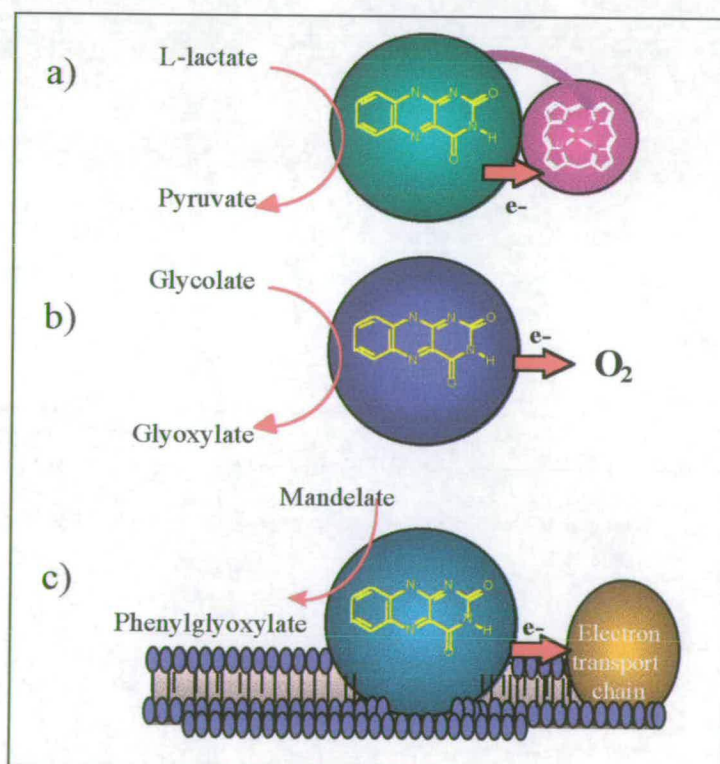


Figure 1.1 Different modes of FMN re-oxidation. a) via an intramolecular haem (flavocytochrome b_2), b) by molecular oxygen in oxidases (GOX) and c) to a component of the electron transport chain (bacterial mandelate dehydrogenase).

Although the method of FMN re-oxidation is different there is significant sequence similarity within this family of enzymes (Lê *et al.*, 1991). Lactate dehydrogenase from *S. cerevisiae* shall be referred to as flavocytochrome b_2 ($fc b_2$).

	GOX (Spinach)	HaOX (rat)	LMO (<i>M. smegmatis</i>)	MDH (<i>P. putida</i>)
Fcb_2 Flavin domain (<i>S. cerevisiae</i>)	37%	37%	28%	29%

Table 1.1 Sequence identity between the flavin domain of $fc b_2$ and glycolate oxidase (GOX), long-chain hydroxyacid oxidase (HaOX), L-lactate monooxygenase and mandelate dehydrogenase (MDH).

1.2 Flavin mononucleotide

Flavins undergo two electron oxidation/reduction reactions, but are distinctive in having a stable one-electron species, a semiquinone free radical. The ability of the flavin to form the semiquinone enables it to mediate electron transfer between organic substrate (two-electron donor/acceptor) and a one-electron donor/acceptor such as haem. The three stable forms of the flavin, (oxidised, semiquinone and reduced) differ sequentially by single electrons in their oxidation states (Figure 1.2). The oxidised form of the flavin is bright yellow due to strong absorbance in the 350-450 nm region of the spectrum. The functional part of the flavin, the isoalloxazine ring, is attached to a ribitol group of which the 5' carbon is attached to phosphate. Flavin adenine dinucleotide (FAD) is an adenylated derivative of FMN which undergoes virtually identical electron transfer reactions. The ribose side-chain is used to anchor the molecule to the protein. The free energy change (ΔG) of an oxidation-reduction reaction under a particular set of conditions is related to the reduction potentials of the redox pairs under the same conditions by the equation $\Delta G = -nF\Delta E$.

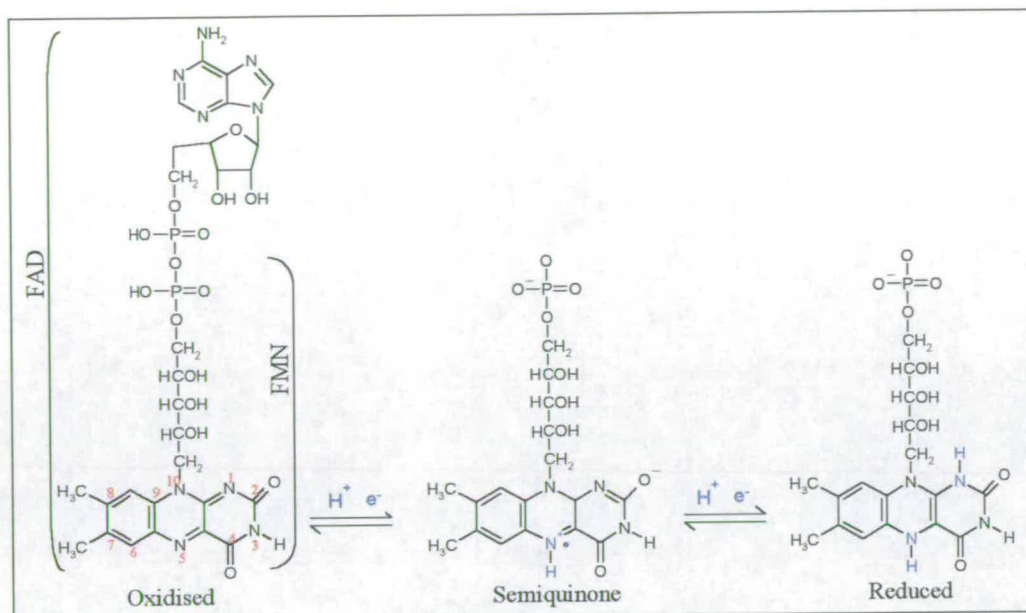


Figure 1.2 Different oxidation states of the FMN (oxidised, semiquinone and reduced)

1.3 Haem

Cytochromes are iron containing electron transfer proteins. The characteristic strong colours of cytochromes are produced by the haem prosthetic group. There are three main classes of cytochromes distinguished by differences in their light-absorption spectra and designated *a*, *b* and *c* (Figure 1.3). The prosthetic groups of cytochromes have four five-membered, nitrogen-containing rings in a cyclic structure called a porphyrin. The four nitrogens are co-ordinated with a central Fe ion that can be either Fe²⁺ or Fe³⁺. Iron protoporphyrin IX is found in *b*-type cytochromes and is non-covalently bound. Two histidine residues provide the fifth and sixth ligands to the Fe ion. Haem *c* is bound covalently through thioether bonds to two cysteine residues of the protein, e.g. cytochrome *c*. Haem *a*, found in *a*-type cytochromes such as cytochrome *aa*₃, a component of the cytochrome oxidase system, has a long isoprenoid tail attached to one of the five-membered rings. Haem containing proteins can mediate single electron transfers or they can couple electron transfer to carrying out enzymatic reactions. The driving force for carrying out redox reactions will depend on the potential of the haem. This is modulated by the structure and environment of the haem in the protein.

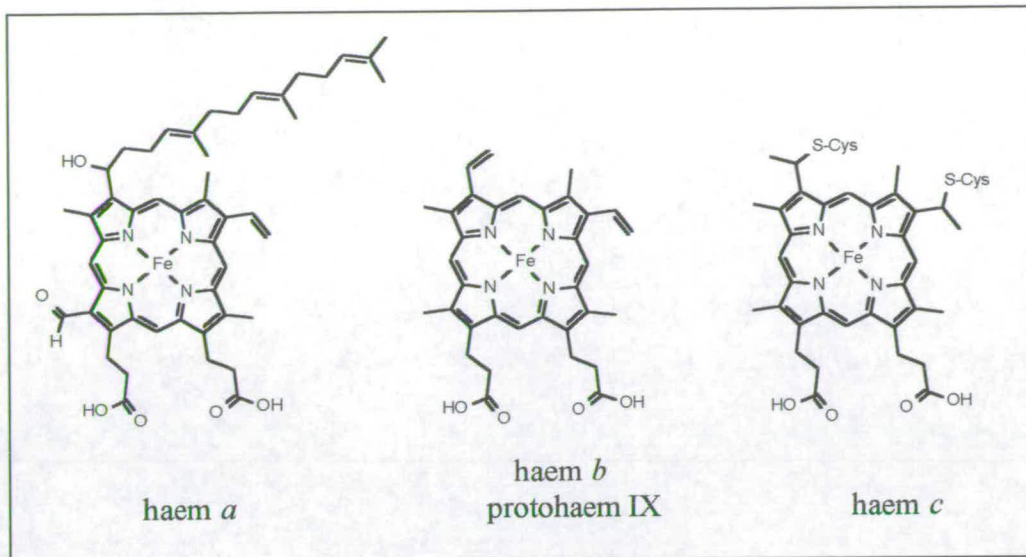


Figure 1.3 The structure of protohaem IX (haem *b*), haem *a* and haem *c*.

1.4 Flavocytochrome b_2

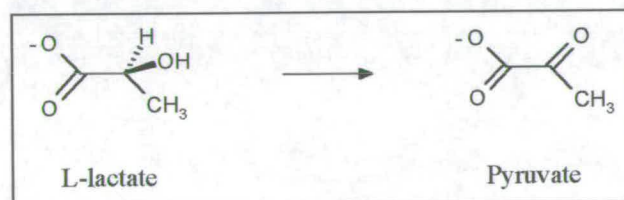


Figure 1.4 Flavocytochrome b_2 catalyses the reaction of L-lactate to pyruvate

Flavocytochrome b_2 from *Saccharomyces cerevisiae* (Jacq and Lederer 1974) catalyses the oxidation of L-lactate to pyruvate (Figure 1.4) with subsequent transfer of electrons to cytochrome *c* (Appelby and Morton 1954) in the mitochondrial intermembrane space (Daum *et al.*, 1982). It forms part of a secondary electron transport chain with cytochrome *c* terminating in cytochrome *c* oxidase that ensures growth on lactate, even if the rest of the mitochondrial electron transport chain is blocked. The enzyme is a homotetramer (4×58 kDa); each subunit is composed of two distinct domains, one of which contains FMN, the other a haem. The crystal structure of flavocytochrome b_2 has been solved to 2.4 Å resolution (Xia and Mathews 1990). The asymmetric unit contains two distinguishable subunits. In one, substrate is absent from the active site and the cytochrome domain is resolved (Figure

1.5). In the other, where pyruvate is bound at the active site no electron density is observed for the cytochrome domain, suggesting that it is positionally disordered. The closest distance between the haem and the FMN is 9.6 Å.

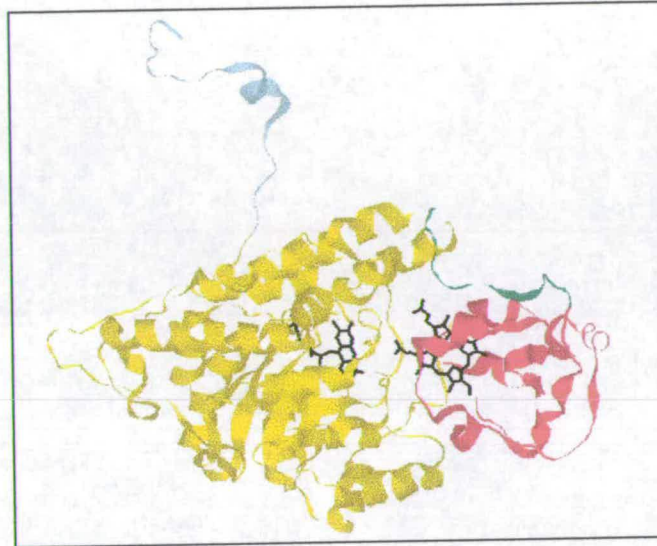


Figure 1.5 Subunit of flavocytochrome b_2 . The flavin domain (yellow) is linked via the hinge (green) to the haem domain (red). The c-terminal tail (blue) forms a number of contacts with the other three subunits in the tetramer. Redox cofactors are shown in black.

The active site is located in the flavin domain where dehydrogenation takes place. Electrons then pass one at a time to the haem and onto cytochrome c . The cytochrome domain and flavin binding domain are in close contact and are joined by a short hinge. The hinge has little influence on the lactate dehydrogenase activity of the enzyme but is important in orientating the two domains for efficient electron transfer (White *et al.*, 1993, Sharp *et al.*, 1994, Bell *et al.*, 1997). The interaction with cytochrome c has been studied and a number of models have been proposed (Tegoni *et al.*, 1993, Short *et al.*, 1997). The model proposed by Short *et al.* (1998) in which one cytochrome c molecule interacts with a single fc_b_2 subunit seems the most likely. The location of the binding site in this model enables the b_2 -haem and c -haem to be as close together as possible. Complementary electrostatic interactions between the two surfaces initially orientate the two proteins prior to electron transfer. Kinetic studies support the idea of one main docking site (Daff *et al.*, 1996a and 1996b).

1.4.1 Electron transfer

The route of electron transfer in $fc b_2$, L-lactate \rightarrow FMN \rightarrow b_2 -haem \rightarrow cytochrome c , has been the subject of much research (Capeillère-Blandin *et al.*, 1975, Chapman *et al.*, 1991, Lederer 1991). The catalytic cycle under saturating concentrations of L-lactate and cytochrome c is represented in Figure 1.6 (Daff *et al.*, 1996a). Following substrate binding FMN is reduced and L-lactate is oxidised to pyruvate (step 1). The rate constant for the reduction of FMN by L-lactate has been determined by stopped-flow kinetics to be $604 \pm 60 \text{ s}^{-1}$ (Miles *et al.*, 1992). Interdomain electron transfer then occurs from fully reduced FMN to b_2 -haem, generating reduced haem and FMN semiquinone (step 2). This has been estimated to occur at $\sim 1500 \text{ s}^{-1}$ (Chapman *et al.*, 1994). Electrons are then transferred from b_2 -haem to cytochrome c (step 3 and step 5). The rate of cytochrome c reduction has been shown to be in excess of 1000 s^{-1} (Daff *et al.*, 1996b). The rate limiting step (step 4) involves interdomain electron transfer between flavin semiquinone and haem at a rate of 120 s^{-1} . The rate constant for this step has been shown to correlate with the driving force (ΔG) (Tegoni *et al.*, 1998) and is therefore under thermodynamic control.

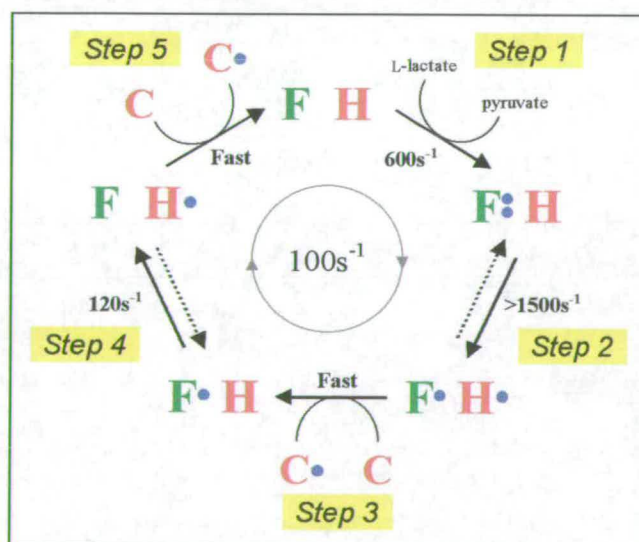


Figure 1.6 Model proposed to explain the electron transfer events which make up the catalytic cycle of flavocytochrome b_2 in saturating amount of L-lactate and cytochrome c . F = FMN, H = b_2 haem, C = cytochrome c and • = electron

1.4.2 The Flavin Domain

The flavin domain (FDH) has been expressed independently of the haem domain and retains its ability to function as an L-lactate dehydrogenase with the artificial electron acceptor ferricyanide but has only residual activity with cytochrome c (Balme *et al.*, 1995). Steady-state activity with cytochrome c as electron acceptor has fallen from $207 \pm 10 \text{ s}^{-1}$ in $fc b_2$ to $0.22 \pm 0.05 \text{ s}^{-1}$ in FDH. However with ferricyanide rates for $fc b_2$ and FDH are $400 \pm 10 \text{ s}^{-1}$ and $273 \pm 6 \text{ s}^{-1}$ respectively. Until now the crystal structure of the flavin domain from intact $fc b_2$ has been used as a realistic representation of the isolated flavin domain. The recent determination of the flavin domain structure to 2.4 \AA resolution (Figure 1.7) (Mathews, personal communication) now allows direct comparison between it and the intact enzyme.

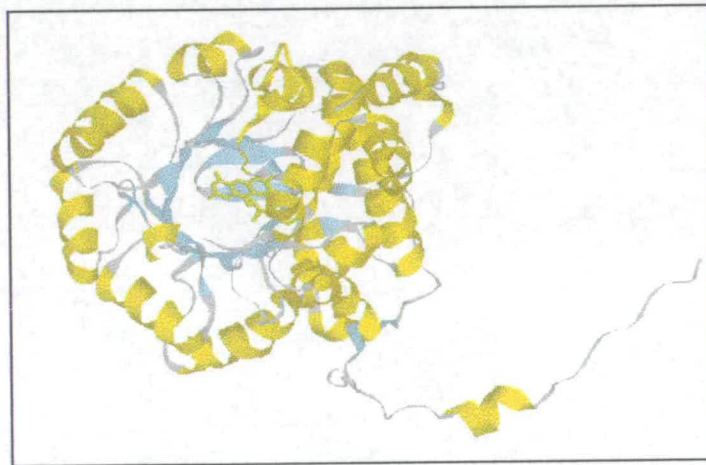


Figure 1.7 The flavin domain showing the $\alpha_8\beta_8$ barrel structure with α helices in yellow and β sheets in blue. FMN is located near the center of the barrel..

1.4.3 Substrate Binding

The crystal structure of $fc b_2$ shows pyruvate bound in the active site of one subunit (Xia *et al.*, 1990) (Figure 1.8). The active site residues of $fc b_2$ have been studied in detail using site-directed mutagenesis (Chapman *et al.*, 1991, Lederer *et al.*, 1991). The carboxyl group forms an electrostatic interaction with the positively charged

Arg376 and hydrogen bonds from one of the two carboxyl groups to Tyr143. Tyr143 is believed to be important in controlling the orientation of the substrate and is essential for intra-molecular electron transfer (Miles *et al.*, 1992). The keto oxygen of pyruvate interacts with His373, the active site base (Gaume *et al.*, 1995). Mutation of His373 causes a 10^5 -fold loss in activity. Tyr254 is involved in transition state stabilisation (Reid *et al.*, 1988, Gondry *et al.*, 1995) and not as previously reported in Michaelis complex formation. These conserved residues occupy identical positions in the FDH structure (Figure 1.8 inset)

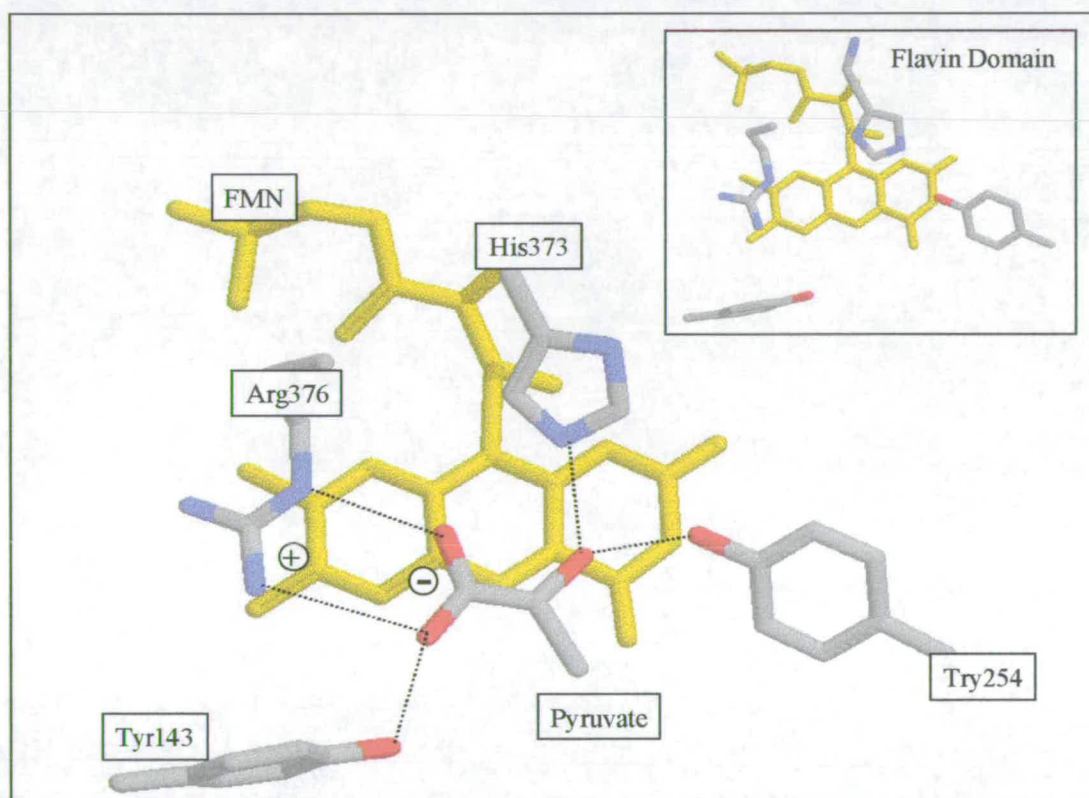


Figure 1.8 The structure of flavocytochrome b_2 active site. Residues important for catalysis are shown. Pyruvate the product of the reaction is bound at the active site. Inset :Active site of the isolated flavin domain.

1.4.4 Substrate Specificity

Sequence comparisons show that in enzymes that have L-lactate as a primary substrate (*S. cerevisiae* L-ldh, *H. anomala* L-ldh, and L-lactate monooxygenase from

M. smegmatis; Guiard *et al.*, 1995, Black *et al.*, 1989 and Giegel *et al.*, 1990 respectively) the equivalent of Leu230 is conserved, whereas in spinach glycolate oxidase the position of Leu230 is occupied by a larger tryptophan residue (Volkita *et al.* 1998). In L-mandelate dehydrogenase from *P. putida* Leu230 is replaced by a smaller glycine residue (Tsou *et al.*, 1990). The size of this residue is therefore seen to correspond inversely to the size of the substrate side chain (Figure 1.9).




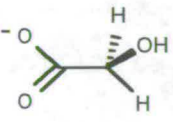
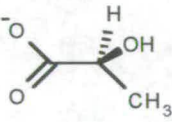
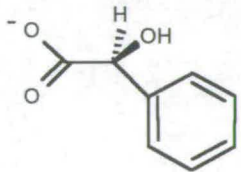
GOX (Spinach)	L-LDH ($fc b_2$) (<i>S. cerevisiae</i>)	L-MDH (<i>P. putida</i>)
		
Tryptophan	Leucine	Glycine
		
Glycolate	L-Lactate	L-Mandelate

Figure 1.9 Comparison of residues at the equivalent position 230 and corresponding substrates.

1.4.4.1 Redesign of the Active Site

The substrate specificity of $fc b_2$ has been investigated previously by Daff *et al.* (1994a), Sinclair *et al.*, (1998). In an attempt to modify the substrate specificity in favour of larger substrates, three mutant enzymes: A198G, L230W and the double mutant A198G/L230A were studied (Figure 1.10). The A198G mutation was found to weaken substrate binding but the substrate specificity was largely unaffected. So, although Ala198 influences catalysis it is not responsible for the selection of L-lactate,

over other substrates. The result of the L230A mutation is to produce an enzyme that is selective for long-chain 2-hydroxy acids. This mutation resulted in an 80-fold swing in selectivity from L-lactate to 2-hydroxyoctanoate. The double mutant A198G/L230A resulted in poor substrate binding properties and activity levels similar to those seen for L230A. The role of Ile326 has also been investigated (Daff PhD thesis 1996). The crystal structure shows this residue to be slightly further away from the substrate than Ala198 or Leu230. However the side chain of Ile326 appears to be in contact with the side chain of Leu230. The mutation I326A removes significant bulk from the active site and this enzyme was shown to create a 160-fold swing in substrate specificity towards 2-hydroxy octanoate.

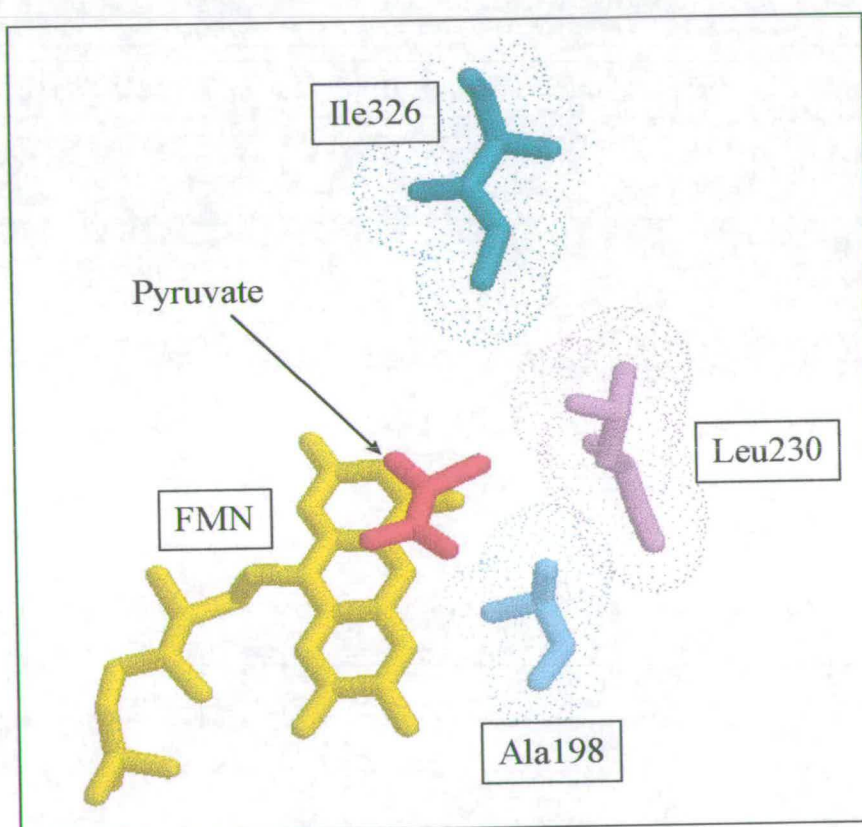


Figure 1.10 The active site of flavocytochrome b_2 highlighting residues which have been studied with regard to substrate specificity. Leu230 is important in selecting for L-lactate. Mutation of Ala198 was found to weaken the substrate binding. Ile326 though farther away from the substrate contacts the side chain of Leu230.

1.4.5 The hydride transfer mechanism

The mechanism of dehydrogenation has in the past been the subject of some controversy (Chapman *et al.*, 1991, Lederer 1991). Questions have revolved around the issue of where the electron pair resides when the substrate α -carbon hydrogen bond is broken. It has been deduced from recent mechanistic studies with D-amino acid oxidase (Mattevi *et al.*, 1996, Harris, unpublished results) that a direct hydride transfer mechanism operates in this enzyme. The implications for the mechanistically related α -hydroxy acids is that they also proceed by hydride transfer (Figure 1.11). The alternative carbanion mechanism (Walsh *et al.*, 1971) involving abstraction of a proton from the α -carbon is based largely on earlier experimental evidence from D-amino acid oxidase.

The hydride transfer mechanism involves removal of the hydroxyl proton from the substrate by an active site base with concomitant loss of a hydride ion from the substrate to FMN. Evidence from D-amino acid oxidase is consistent with a transition state in which rupture of the two substrate bonds to hydrogen is concerted (Mattevi *et al.*, 1999). A highly conserved histidine residue in *fc_{b2}*, His373 acts as a base for the reaction. Mutation of His373 to glutamate decreases the rate of lactate oxidation by at least 10^5 , consistent with a role for this residue as an active site base. The activity reported for H373Q (Miles *et al.*, 1992) is consistent with the Gln codon being misinterpreted for wild-type during DNA translation. The homologous histidine in MDH is His274 and in GOX His254. The importance of the conserved histidine in catalysis has been confirmed by the results of mutagenesis studies on lactate monooxygenase from *S. smegmatis*, *fc_{b2}* and L-MDH. A charged lysine residue (Lys349) is thought to stabilise the charge on the N1-C2=O locus in the reduced flavin by electrostatic interactions. The fact that a K349R mutant exhibits no dehydrogenase activity supports this proposal (Reid *et al.*, 1988). An equivalent lysine residue is conserved within this family of enzymes.

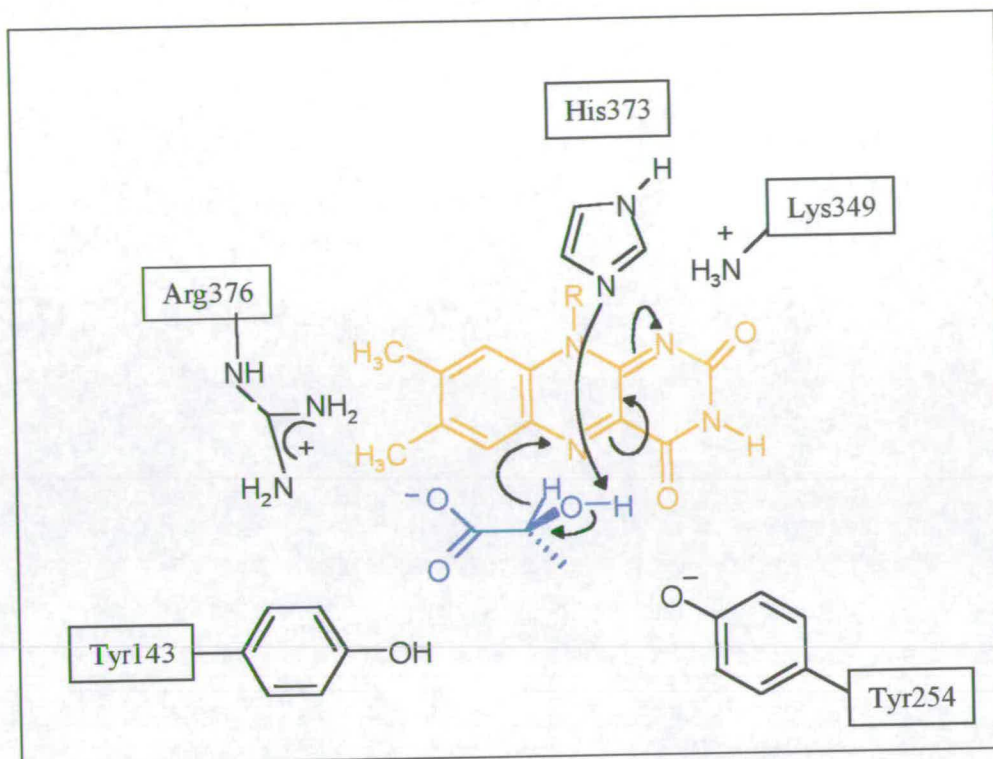


Figure 1.11 Mechanism of dehydrogenation proceeds via direct hydride transfer from substrate to N(5)

1.5 Glycolate Oxidase

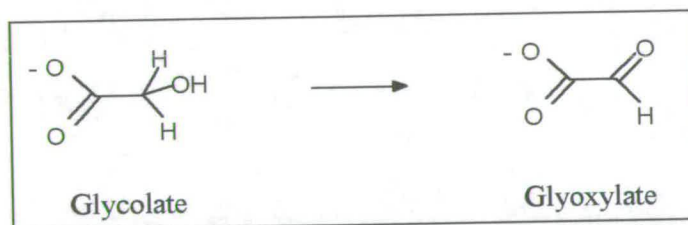


Figure 1.12 Glycolate oxidase catalyses the reaction of glycolate to glyoxylate.

In green plants, glycolate oxidase (GOX) is one of the key enzymes in photorespiration where it oxidises glycolate to glyoxylate (Figure 1.12). Glycolate oxidase from spinach has a subunit of 40,000 M_r and is 37 % identical in amino acid sequence to the flavin domain of fb_2 (Guiard 1985, Lederer *et al.*, 1985, Volokita *et al.*, 1987) The crystal structure of GOX is available at 2.0 Å resolution (Lindqvist *et al.*, 1991). GOX like FDH forms the common $\alpha_8\beta_8$ barrel structure (Scrutton 1994) (Figure 1.13).

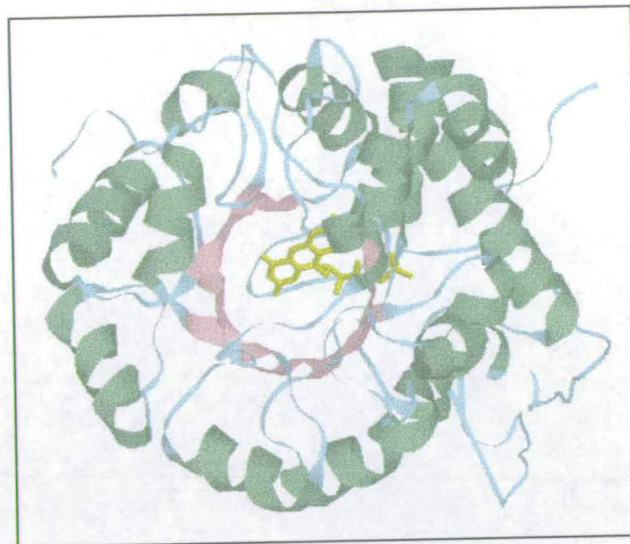


Figure 1.13 Glycolate oxidase showing the $\alpha_8\beta_8$ barrel structure with α helices in green and β sheet in pink. FMN (yellow) is bound at the centre of the barrel.

When the structures of FDH and GOX are superimposed the 3 dimensional structures are largely identical. Conservation of the equivalent active site residues, Arg257, Tyr24, Tyr129 and His254 (GOX numbering) indicates that glycolate would be bound in a similar manner to that observed for pyruvate in fc_b_2 (Figure 1.14).

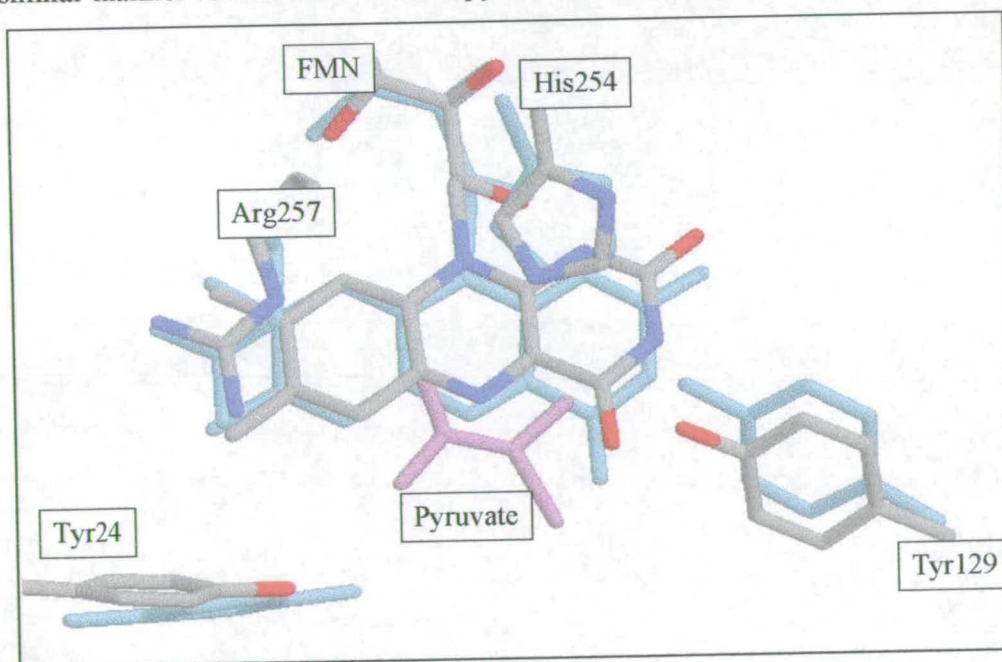


Figure 1.14 The active site structure of glycolate oxidase (atom coloured, GOX numbering) compared to flavocytochrome b_2 (blue). The structure of fc_b_2 contains the product of the reaction, pyruvate (pink). It is predicted that glycolate would bind in a similar manner in glycolate oxidase.

Although $fc b_2$ /FDH and GOX have a high degree of structural similarity there are some differences. In GOX a loop region of 29 residues between strand 4 and helix 4 of the barrel covers the active site cleft where the substrate is bound. In $fc b_2$ and FDH the loop region of 24 residues is disordered in the crystal structure. In $fc b_2$ it is predicted that the loop is pushed to one side by the presence of the haem domain. This might constitute the basis of their different re-oxidation modes. The mechanism for the first half reaction, substrate oxidation/FMN reduction is conserved. The difference in reactivity of the flavins to oxidants could be derived from the accessibility of the active site. Both the main chain and side chain conformation of Thr78/197 differ in the two structures. Thr197 lies in close proximity to the isoalloxazine ring which differs in position between the two enzymes. In $fc b_2$ /FDH a hydrogen bond forms between N5 of FMN and the main-chain amide of Ala198. In glycolate oxidase where the ring system is tilted away from Thr197 a pocket with a water molecule is found near the *re*-face of the FMN ring (Figure 1.15). This pocket is believed to be important for oxidase activity either as a binding site for dioxygen or to accommodate the O4 oxygen of FMN (Walsh *et al.*, 1980). Structures of glycolate oxidase, with inhibitors at the active site show the FMN in the same orientation as in $fc b_2$ (Stenberg *et al.*, 1997). This implies some degree of mobility of the FMN in glycolate oxidase whereas the isoalloxazine ring of $fc b_2$ has the same orientation irrespective of whether pyruvate is bound which indicates a less mobile FMN molecule. FMN mobility in the oxidase may be important in enabling the formation of the C4- α hydroperoxide which imposes bending on the otherwise planar isoalloxazine system.

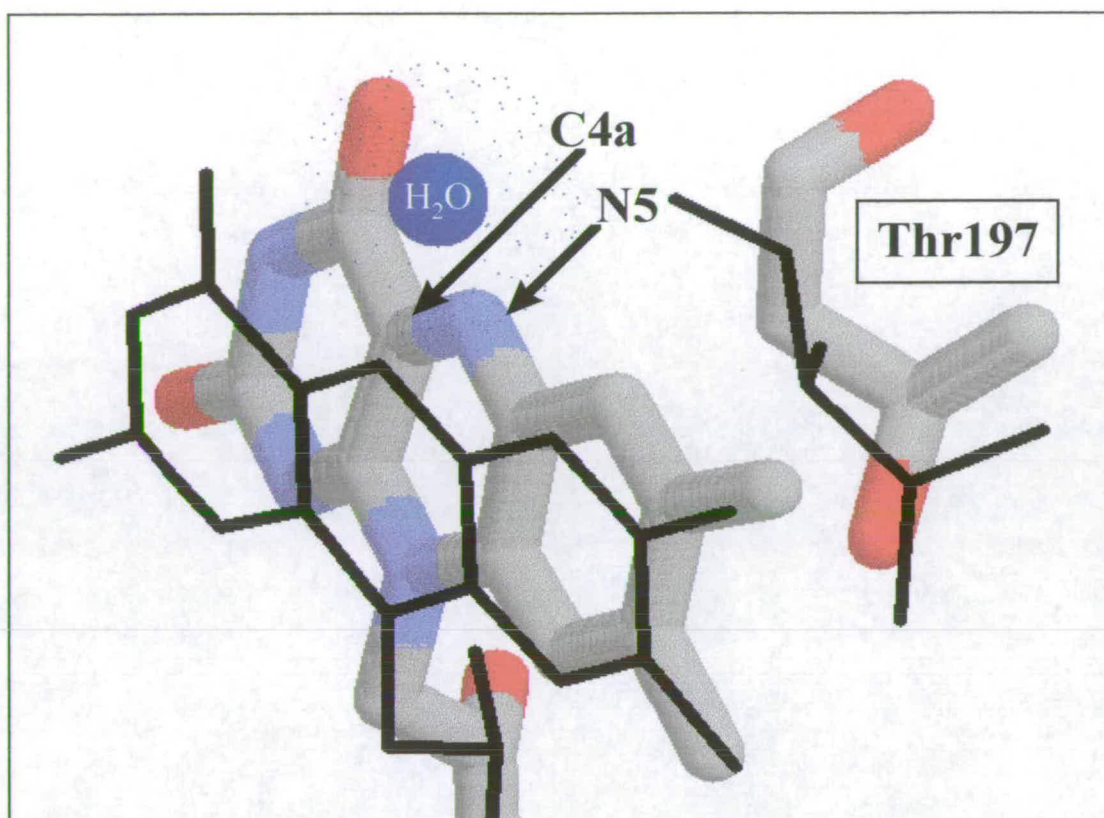


Figure 1.15 Thr197 may govern the mobility of the FMN enabling a water molecule (blue) to fit into a pocket on the re-side of the FMN in glycolate oxidase (black) but not in flavocytochrome b_2 (coloured).

In glycolate oxidase the active-site base (His254) forms hydrogen bonds to Asp157 and the adjacent residue Thr158. In $fc b_2$, the equivalent residues are Asp282 and Ala283 of which only the former can form a hydrogen bond with His373 (Figure 1.16). Sequence alignments show that a threonine is conserved at this position in glycolate oxidase and all other family members which react with molecular oxygen (Lederer *et al.*, 1991). It has therefore been suggested that the interaction of Thr158 in GOX with His254 might play a role in governing oxidase activity. Ala283 is close to the active site so could also effect the substrate specificity of the enzyme. The role of Leu230 in controlling substrate specificity has already been discussed.

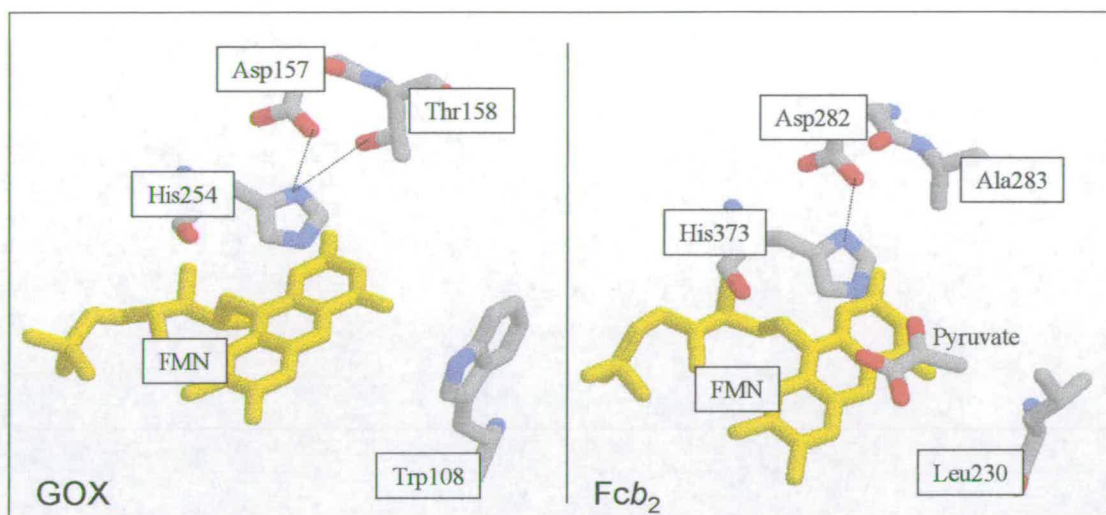


Figure 1.16 Comparison of the active sites of GOX and $fc b_2$. In GOX Thr158 and Asp157 each form hydrogen bonds to His254, the active site base. In $fc b_2$ Ala283 is unable to form a hydrogen bond to His373. Leu230 and the equivalent residue, Trp108, control substrate specificity.

1.6 L-lactate monooxygenase

L-lactate monooxygenase (LMO) from *M. smegmatis* is a member of the L- α -hydroxy acid oxidases. It catalyses the oxidation of L-lactate to pyruvate (Hayaishu *et al.*, 1957, Lockridge *et al.*, 1972, Ghisla and Massey 1991). LMO is unique within this family in that dissociation of the initial oxidation product pyruvate occurs much more slowly than the reaction of the reduced enzyme-pyruvate complex with oxygen. The resultant H_2O_2 decarboxylates pyruvate within the active site to the final products, acetate, CO_2 and water. The crystal structure is not available but there is close sequence similarity to $fc b_2$. For each of the residues implicated in binding and catalysis there is an identical residue in the amino acid sequence of LMO (Giegel *et al.*, 1990, Maeda-Yorita *et al.*, 1995, Sanders *et al.*, 1999, Müh *et al.*, 1994a and 1994b) The mutation G99A in the vicinity of the flavin resulted in a dramatic change in the oxygen reactivity of the enzyme (Sun *et al.*, 1996). The G99A enzyme is reduced by L-lactate at a similar rate to that of wild-type enzyme but produces

pyruvate instead of the decarboxylation products. This enzyme reacts with O_2 at a rate ~ 100 -fold slower than wild-type. Due to the very low oxygen reactivity of the reduced enzyme, G99A catalyses the oxidation of L-lactate to pyruvate and H_2O_2 instead of acetate, CO_2 and H_2O , the normal decarboxylation products. It is suggested that the small steric change close to the N(5) of the flavin causes a profound change in the electrostatic distribution of the isoalloxazine ring. This implies that electrostatic interactions provide an important factor for control of O_2 reactivity.

1.7 Flavin Reoxidation by molecular oxygen

A detailed comparison of the active site structure of GOX and $fc b_2$ has suggested the origin of their different re-oxidation modes lies in the existence of a putative oxygen binding pocket on the re-side of the cofactor in GOX (Figure 1.17). The *si*-side of the flavin being crowded by catalytic residues. The amino acid sequence for long chain α -hydroxy acid oxidase is also available but alignment with GOX does not shed any light on what might control oxidase activity. The first step in re-oxidation of the reduced flavin is the transfer of an electron from the flavin to molecular oxygen. Spin inversion then occurs and a covalent flavin 4a-hydroperoxide forms. This will occur if the distance and orientation of the flavin and superoxide is such to enable a thermodynamically stable bond to form. Hydroperoxide then dissociates heterolytically to yield oxidised flavin and hydrogen peroxide.

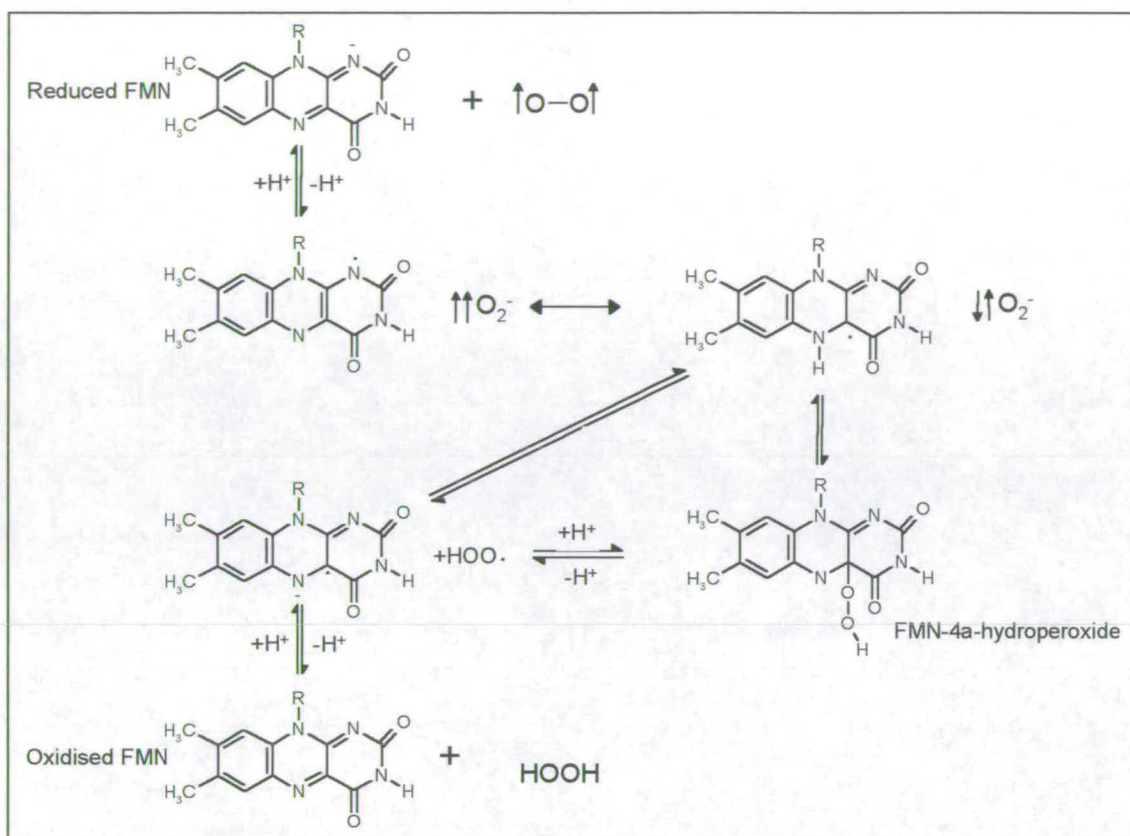


Figure 1.17 Mechanism of re-oxidation of the flavin by molecular oxygen.

1.8 Project Aims

The flavin domain (FDH) expressed independently of the haem domain retains its ability to act as a lactate dehydrogenase and this project focuses on three areas that affect how FDH functions:-

- i) Substrate specificity and ii) reactivity towards molecular oxygen.

Two mutant enzymes were constructed, the first involved a single amino acid change of Leu230 to tryptophan - $\text{FDH}_{\text{L230W}}$. The second mutant was designed to encompass the major structural differences seen at the active sites to see if their collective effect yielded improved oxidase activity or glycolate selectivity. In addition to the mutation L230W, residue Thr197 was mutated to alanine in an attempt to create a pocket on

the *re*-side of the FMN and Ala283 was mutated to threonine. This triple mutant enzyme is referred to as FDH_{TRIP}.

iii) recognition for cytochrome *c*.

In the absence of the haem domain direct electron transfer from flavin to cytochrome *c* is extremely slow. This is thought to be due to poor recognition between the two protein surfaces. The effect of creating a recognition site for cytochrome *c* on the surface of the flavin domain to increase the efficiency of electron transfer is investigated.

Chapter 2
Materials and Methods

2.0 Materials and Methods

2.1 Buffers

0.5 M Phosphate pH 7.0

305 mM Na₂HPO₄ solution, dibasic potassium salt

195 mM NaH₂PO₄ solution, monobasic potassium salt

0.1 M Tris.HCl pH 7.5, I=0.1M (Tris[hydroxymethyl]aminomethane)

dH₂O 500 ml

Trizma base 12.1 g

NaCl 5.265 g

Adjusted to pH 7.5 using 1M HCl and made up to 1 l with dH₂O

0.1 M MOPS pH 7.5 (3-[N-Morpholino]propanesulfonic acid)

dH₂O 500 ml

MOPS 20.93 g

Adjusted to pH 7.5 using 1M HCl and made up to 1 l with dH₂O

Lysis Buffer

Phosphate buffer pH 7.0 100 mM

Lactate 10 mM

EDTA 10 mM

PMSF 1 mM

egg white lysozyme 0.2 mg/ml

L-lactate/ferricyanide activity assay

Tris.HCl pH 7.5, I= 0.1 M.

L-lactate lithium salt 10 mM

Potassium ferricyanide. 2 mM

3 × SDS gel-loading buffer

Tris.HCl pH 6.8	50 mM
Dithiothreitol	100 mM
SDS (electrophoresis grade)	2 %
Bromophenol blue	0.1 %
glycerol	10 %

SDS resolving Buffer (1.5 M Tris.HCl pH 8.8)

Trizma base	181.6 g
SDS	4.0 g
dH ₂ O	600 ml

Adjusted to pH 8.8 with HCl and made up to 1 l with dH₂O

Stacking Buffer (0.5 M Tris.HCl pH 6.8)

Trizma base	30.28 g
SDS	2.0 g
dH ₂ O	450 ml

Adjusted to pH 6.8 with HCl and made up to 0.5 l with dH₂O

5×tris-glycine running buffer

Trizma base	15.1 g
glycine	94 g
10 % SDS	50 ml

Tris-Acetate (TAE)

Trizma base	242 g
Glacial acetic acid	57.1 ml
0.5 M EDTA (pH 8.0)	100 ml

Tris-buffered saline (TBS)

1 M Tris.HCl pH 7.5	10 ml
4M NaCl	37.5 ml
dH ₂ O to 1 l	

Transfer Buffer (10×)

1 M Tris.HCl pH 8.3	250 ml
Glycine	112.6g
dH ₂ O to 1 l	

Developing solution

<i>o</i> -dianisidine 5 mg/ml	500 µl
Imidazole	1 ml
Hydrogen peroxide (30 %)	0.1 ml
H ₂ O	8.4 ml

TEG/Lysozyme

Tris.HCl pH 8.0	25 mM
EDTA	10 mM
Glucose	50 mM

Solution B

Tris.HCl pH 8.0	40 mM
EDTA	1 mM
Na Acetate	0.1 M
SDS	0.1 %

2.2 Growth Media

Luria Broth

Bacto Tryptone	10 g/l
Bacto Yeast Extract	5 g/l
NaCl	5 g/l

Terrific Broth

Bacto Tryptone	12 g/l
Bacto Yeast Extract	24 g/l
glycerol	4 ml/l
K ₂ HPO ₄	12.54 g/l
KH ₂ PO ₄	2.31 g/l

SOC Medium

Bacto Tryptone	20 g/l
Bacto Yeast Extract	50 g/l
NaCl	10 mM
KCl	2.5 mM
MgSO ₄	10 mM
Glucose	20 mM

All media was sterilised prior to use at 121 °C for twenty minutes in a Kestral autoclave.

2.3 Molecular Biology

2.3.1 DNA Digest

Plasmid DNA	1-2 µl (~5-10 µg)
Multicore Buffer (Promega)	1.5 µl
<i>Eco</i> R1	1 µl
<i>Hind</i> III	1 µl
dH ₂ O	10 µl

Reactants were mixed under standard sterile conditions in an Eppendorf and incubated at 37 °C for at least 1 hr.

2.3.2 DNA Ligation

Vector DNA	0.5 μ l (~5 μ g)
Insert DNA	1 μ l (~5-10 μ g)
5 \times Ligase buffer (NEB 2)	2 μ l
Bovine serum albumin	100 μ g/ μ l
DNA Ligase (NEB)	1 μ l
dH ₂ O	6.5 μ l

Reactants were mixed under standard sterile conditions in an Eppendorf and incubated for 1-4 hours at room temperature.

2.3.1 Agarose Gel Electrophoresis

Agarose, high purity	0.17 g
1 \times TAE buffer	25 ml
Ethidium Bromide (10 mg/ml)	2 μ l

Agarose gels (0.7 %) were used to determine purity and quantity of DNA and to separate digested DNA fragments. Agarose was dissolved in TAE buffer by heating then allowed to cool until room temperature before addition of ethidium bromide to a concentration of 0.5 μ g/ml as DNA marker and poured into a the mould and comb inserted. Once the gel was set the comb was removed and electrophoresis buffer added until the gel was covered. Samples of DNA were mixed with gel loading buffer and loaded into the slots of the submerged gel along with 1 kb marker ladder (Gibco BRL). The gel was run for 30-60 minutes at 38 mA or until the dye front had migrated the appropriate distance. The gel was visualised under ultraviolet illumination and the required band cut out using a scalpel. The piece of DNA was then purified using the QIAEX II agarose gel extraction kit. This uses a silica matrix EZ-GLASSMILKTM to bind DNA, which was then eluted.

2.3.4 DNA Isolation

2.3.4.1 Plasmid DNA Preparation (large scale)

A single colony was used to inoculate 50 ml Luria Broth containing 50 mg/ml ampicillin which was grown overnight at 37 °C. Cells were pelleted by centrifugation at 4000 rpm (SLA1500 rotor, Sorval RC-5B centrifuge) for 10 minutes in silinated corex tubes. Cell pellets were resuspended in 2 ml TEG/lysozyme mixed by inversion and left on ice for 20 minutes. To this solution 4 ml 0.2 M NaOH/1% SDS was added, mixed by inversion and left on ice for 5 mins. 3 ml of 3 M Na Acetate pH 5.2 was added and again the solution was mixed by inversion. The solution was spun at 10,000 rpm for 10 minutes to remove chromosomal DNA. The supernatant was precipitated by adding 16 ml of EtOH and incubating on ice for 15 minutes followed by centrifuging at 10,000 rpm (Biofuge, pico, Heraeus) for 10 mins to pellet plasmid DNA. The plasmid DNA was resuspended in 4 ml solution B and then extracted with 4 ml of phenol/chloroform 1:1. Removing the aqueous phase to a clean test-tube, the organic phases were combined, mixed with 8 ml ethanol, incubated on ice for 15 minutes and centrifuged at 10,000 rpm (Heraeus, Biofuge, pico) for 10 minutes. The pellet was resuspended in 400 µl TE buffer transferred to an Eppendorf and incubated with 20 µl boiled RNase (10 mg/ml) at 37 °C for 1 hour. To the aqueous phase 20 µl of 4 M NaCl was added and the solution extracted with 3 × 500 µl phenol/chloroform, followed by one extraction with 500 µl chloroform. The aqueous phase was incubated on ice for 10 minutes with 800 µl EtOH to produce a white precipitate. The plasmid DNA pellet was spun in a microcentrifuge at 13,000 rpm (Heraeus, Biofuge, pico) for 5 minutes, excess solution removed and the pellet washed with 300 µl EtOH (70 %) before drying. Plasmid DNA was resuspended in 200 µl dH₂O and stored at -20 °C.

2.3.4.2 Plasmid DNA Preparation (small scale)

Plasmids were purified from 2-3 ml overnight culture using GFX micro plasmid prep kit. A single colony was used to inoculate 5 ml LB, 50 µg/µl ampicillin which was

incubated at 37 °C overnight. A 1-1.5 ml culture was centrifuged for 1 minute (Heraeus, Biofuge, pico) 13,000 rpm, supernatant removed, additional aliquots of culture added centrifuged and supernatant removed. The cell pellet was resuspended in 300 µl solution 1. Cells were then lysed by alkali treatment and chromosomal DNA and proteins denatured. The solution was then neutralised with an acetate solution and transferred onto a GFX column which binds DNA, washed and then eluted from glass fibre matrix into low ionic strength buffer (20 µl).

2.3.5 Transformation

Plasmid solution (5 µl, from miniprep) was added to 200 µl competent cells (*E.coli* TG1) kept on ice for 30 minutes. Cells were then subjected to heat shock at 42 °C for 45 seconds followed by immediate immersion in ice for 2 minutes. 800 µl SOC medium was added and the solution incubated at 37 °C for 1 hour with shaking. Cells were pelleted, resuspended in 100 µl H₂O and spread on agar/ampicillin plates which were then incubated at 37 °C overnight. Plates spread with vector or insert were used as controls.

2.3.6 Growth and Maintenance of Cell Stocks

Standard sterile techniques were employed. Media and equipment were sterilised at 121 °C for twenty minutes in a Kestral autoclave to avoid contamination.

Agar plates.

Single colonies from transformations were streaked on agar/ampicillin plates and stored at 4 °C for up to 3 weeks.

-80°C freezer stocks.

Single colonies were used to inoculate 5 ml starter cultures. These were incubated at 37 °C until mid-log phase then stored with glycerol at a concentration of 50 % v/v at -80 °C. Cell stocks were used to re-streak agar plates or used directly to inoculate 5 ml starter cultures.

2.4 Hybrid PCR

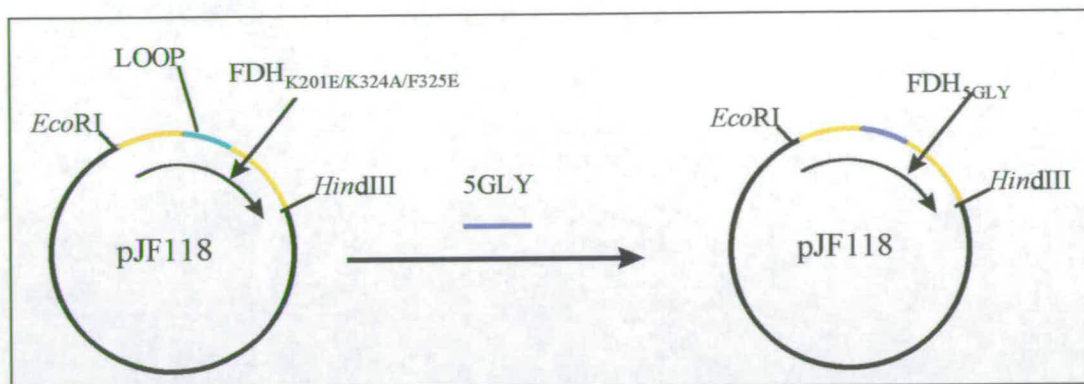


Figure 2.1 Replacement of DNA encoding for the loop section with that encoding for 5 glycine residues.

PCR was used to replace a section of the loop region, residues 298-320 inclusive, with either 5 glycine or 7 glycine residue linker (Figure 2.1). Primer sequences used are shown in Table 2.1. Template DNA for the flavin domain contained the mutations K201E, K324A, F325E.

2.4.1 Primers

Primer	DNA base sequence
5 GLYB2LOOP	GGT GGT GGT GGT GGT CAA GGT GCT TCG AGA GCG
H3B2LOOP	CTC CGG AAG CTT CAG AAA GTA GCC TTA AAG C
5GLYB2REVCOM	ACC ACC ACC ACC ACC TTT CAG CTT CAT ATC
B-2074A-98	CTC CTG GTT GAA TTC ATG GAA ACT AAG G
7GLYB2LOOP	GGT GGT GGT GGT GGT GGT GGT GCG TTA TCA GCG GAA ATT GAC CC
B2CTERMVECT	GCC TAG CTT TAA GGC TAC TTT CTG
VECTB2CTERM	CAG AAA GTA GCC TTA AAG CTA GGC

Table 2.1 DNA base sequences of primers used in PCR reactions

2.4.2 PCR Conditions

PCR conditions are described in Table 2.2. The sample was overlaid with 50 μ l mineral oil to prevent evaporation of the sample during repeated heating and cooling cycles. The process was carried out for 20 cycles. PCR products were visualised by and purified from agarose gel electrophoresis before subsequent steps.

Cycle	Denaturation		Annealing		Polymerisation	
	First cycle	5 mins	95 °C	2 mins	41 °C	3 mins
Subsequent cycle	1 min	95 °C	2 mins	41 °C	3 mins	72 °C

Table 2.2 PCR conditions

PCR was used to amplify the sequence of the flavin between the loop and H3 end introducing a region encoding for 5 glycine residues (Figure 2.2, step 1) and between the loop and R1 end introducing complementary sequence to the 5 glycine residues (Figure 2.3, step 2) (Table 2.3). Reactants were mixed under sterile conditions in a 0.5 ml microfuge tube in the following order and overlaid with 100 μ l mineral oil to prevent evaporation.

	Step 1	Step 2
Template DNA	1-2 μ g	1-2 μ g
Primer	5GLYB2LOOP (10 pmol)	5GLYB2REVCOM 10 pmol
Primer	H3B2LOOP (10 pmol)	B2074A-98 (10 pmol)
Mix. of four dNTPs, each at concentration of 10 mM	2 μ l	2 μ l
Buffer (Promega, 10 \times conc.)	5 μ l	5 μ l
MgCl ₂ (25 mM)	3 μ l	3 μ l
H ₂ O	To 50 μ l	To 50 μ l
Taq DNA polymerase (5 units/ μ l)	0.5 μ l	0.5 μ l

Table 2.3 Components of step 1 and step 2 PCR

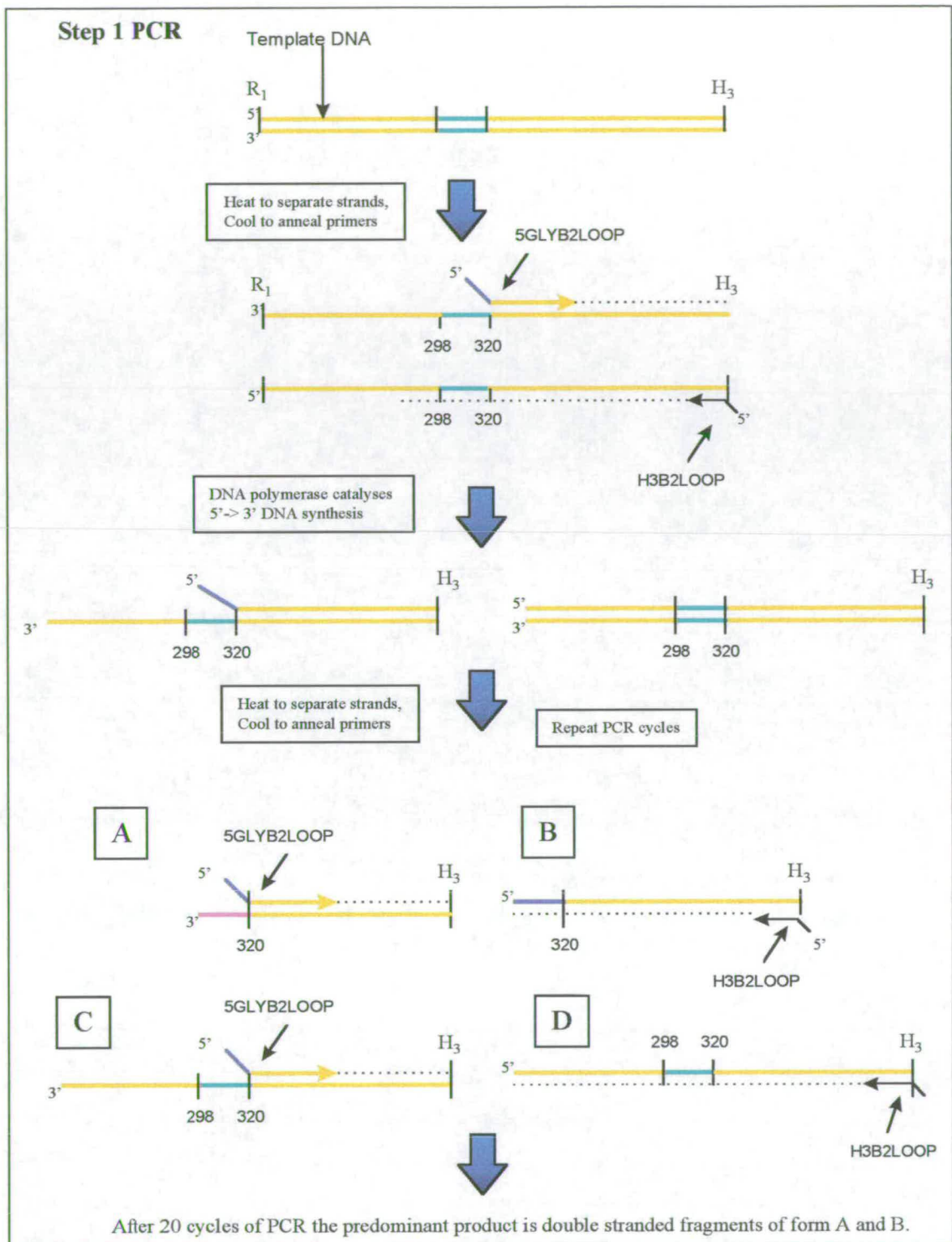


Figure 2.2 Step 1 PCR. Generation of the double stranded DNA fragment encoding for the flavin domain (yellow) between the loop and H3 end. Sequence encoding for (blue) and complementary (pink) to 5 glycine residues. Original loop section (green).

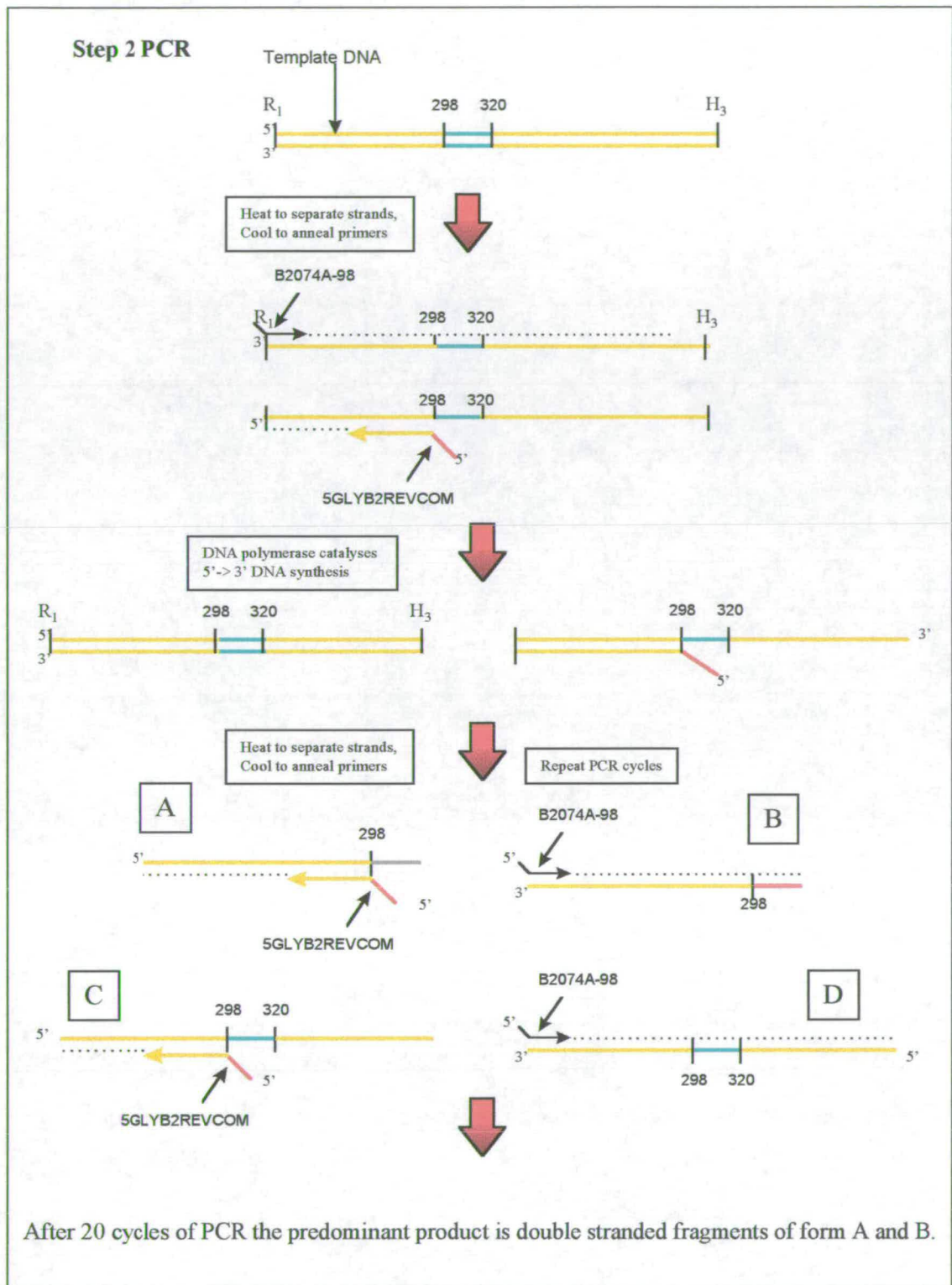


Figure 2.3 Step 2 PCR. Generation of the double stranded DNA fragment encoding for the flavin domain (yellow) between the loop and R_1 end. Sequence encoding for (grey) and complementary (red) to 5 glycine residues. Original loop section (green).

DNA fragments from PCRs step 1 and 2 were purified from agarose gel before PCR to create the gene for the flavin domain with the 5 glycine replacement (Figure 2.4) (Table 2.4). Reactants were mixed in the following order under sterile conditions to a 0.5 ml microfuge tube and overlaid with 100 μ l mineral oil to prevent evaporation.

	Step 3
PCR product Step 1	1 μ l (100 pmol)
PCR product Step 2	1 μ l (100 pmol)
dNTPs (5 mM)	2 μ l
Buffer (Promega 10 \times conc.)	5 μ l
MgCl ₂ 25 mM	3 μ l
Primer H3B2LOOP	2.5 μ l
Primer B2074A-98	2.5 μ l
dH ₂ O (to final vol. of 50 μ l)	32.5 μ l
Taq DNA polymerase 5units/ μ l	0.5 μ l

Table 2.4 Components of PCR Step3

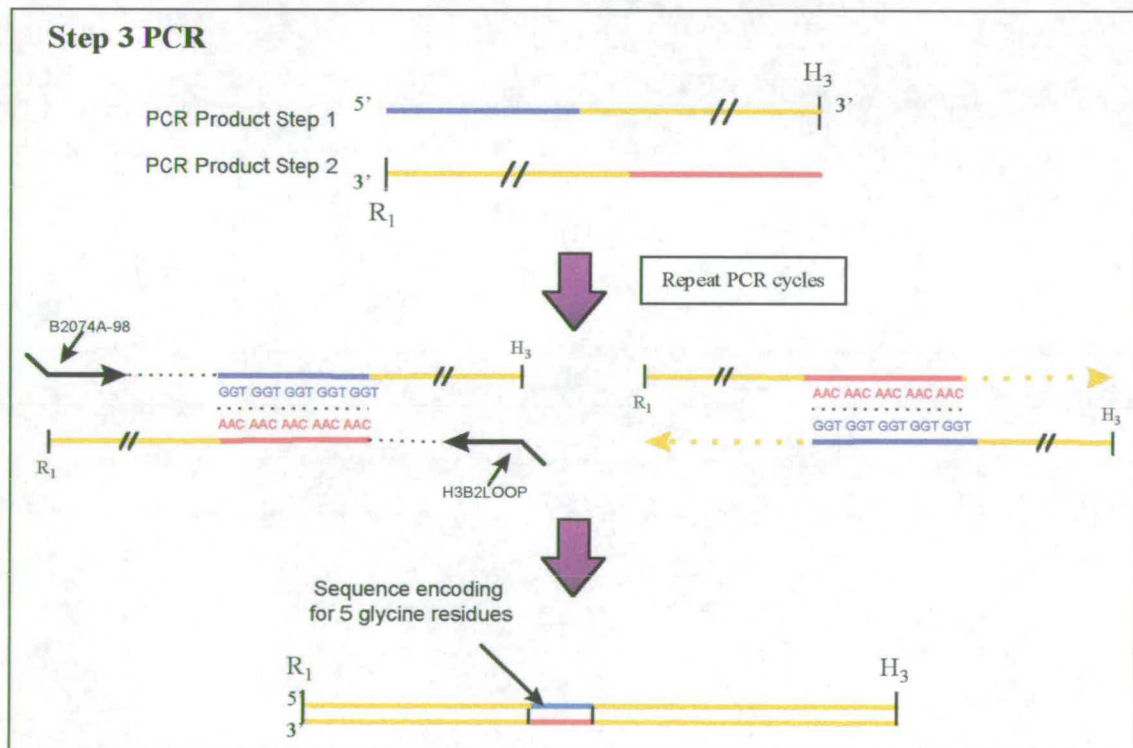


Figure 2.4 Step 3 PCR Formation of the double stranded DNA fragment encoding for the flavin domain with the loop replaced by a 5 glycine linker.

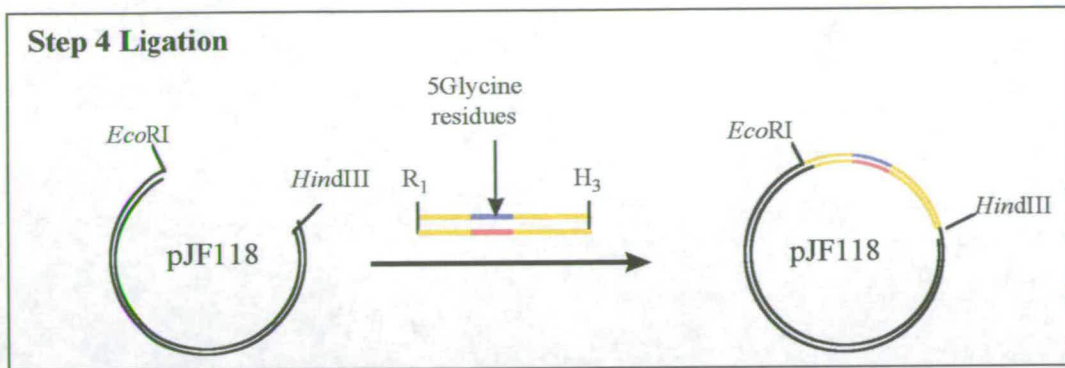


Figure 2.5 Ligation of double stranded PCR product into the expression vector pJF118EH (Fürste *et al.*, 1986).

2.5 Protein Isolation and Purification

2.5.1 Cell Growth

2.5.1.1 pop2136 (pRC23)

Starter cultures (5 ml) were grown overnight and were used to inoculate 1 l flasks containing 500 ml Luria broth, 100 $\mu\text{g/ml}$ carbenicillin. Cultures were incubated at 30°C shaking at 200 rpm until mid-log phase (approx. 5-6 hours). Protein over-expression was induced by increasing the growth temperature to 42 °C for 10 hours. A typical growth yielded approximately 4 g l^{-1} wet cell mass.

2.5.1.2 TG1 (pJF118)

Starter cultures (5 ml) were grown overnight and were used to inoculate 2 l flasks containing 500 ml of Terrific broth, 50 $\mu\text{g/ml}$ of ampicillin. Flasks were incubated at 37 °C and 200 rpm until mid log phase (O.D.=0.6 at 600nm). Cultures were induced with 0.5 mM IPTG (isopropyl- β -D-1thiogalactopyranoside) for 10-12 hours. A typical growth yielded approximately 8-10 g/l wet cell mass.

2.5.2 Cell Lysis

A typical preparation used 20-30 g of wet cell mass. The cells were snap frozen in liquid nitrogen, resuspended and stirred in 100 ml lysis buffer for 2 hrs at 4 °C

followed by sonication to ensure maximum release of protein. Sonication was carried out at intensity 8 for 3-4 minutes (20 sec bursts) using an MSE Soniprep150 while the cells were kept on ice. Cell debris was removed by centrifugation at 15000 rpm using a ss34 rotor and Sorval RC-5B centrifuge. The cell lysis solution was diluted approximately 4-fold in dH₂O/10 % glycerol to provide the correct ionic strength for column chromatography. The addition of glycerol has been shown to help prevent flavin loss but it is not known why.

2.5.3 Anion Exchange Chromatography

Diethylaminoethyl, DE52 column material (Whatman) was prepared by re-suspending in 100 mM phosphate buffer pH 7.0 before equilibrating in 10 mM phosphate buffer pH 7.0. A column approximately 10 cm long and 2 cm in diameter was poured and washed with two column volumes of 10 mM phosphate buffer. The diluted supernatant was loaded directly onto the DE52. FDH binds to the column, remaining protein is washed through. Eluate was tested for L-lactate/ferricyanide oxidoreductase activity to ensure FDH was binding to the column material. The column was washed with 10 mM phosphate pH 7.0 until the UV absorbance at 270 nm was minimal. FDH was eluted with ≥ 60 mM phosphate buffer in a tight band.

2.5.4 Ammonium Sulphate Precipitation

FDH in the eluent was precipitated with 80 % ammonium sulphate. The 80 % solution was stirred at 4 °C for 2 hours then centrifuged at 15000 g for 15-20 minutes to give a pellet containing FDH. The pellet was dissolved in the minimum of 0.1 M Tris.HCl pH 7.5 buffer (2-3 ml) and desalted by gel filtration chromatography. The protein solution was collected in fractions and its purity determined. Protein was stored at -80 °C

2.5.5 Gel Filtration Chromatography

Sephadex G25 was equilibrated in Tris.HCl pH 7.5 I=0.1M. A column approximately 25 cm long, diameter 1-2 cm was poured. A 2-3 ml aliquot of concentrated protein solution were then passed through the column.

2.6 Purity Determination

The purity of the protein was assessed by UV/vis spectrophotometry. A ratio of A_{270}/A_{454} of 8 was considered pure (Figure 2.6).

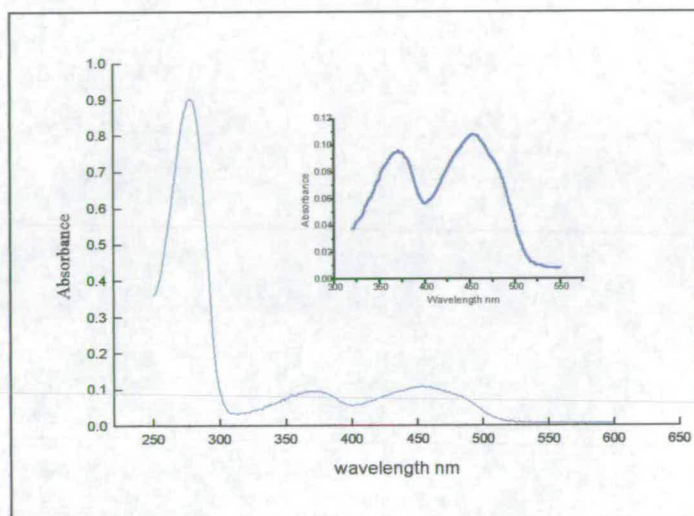


Figure 2.6 Spectrum of purified flavin domain.

2.6.1 SDS Page Gel Electrophoresis

	4 % Stacking Gel	12 % Separation Gel
dH ₂ O	3.05 μ l	3.5 ml
0.5 M Tris.HCl, pH 6.8	1.25 ml	-
1.5 M Tris.HCl, pH 8.8	-	2.5 ml
10% (w/v)SDS	50 μ l	100 μ l
Acrylamide (30% stock)	0.65 ml	4 ml
Ammonium persulfate (10%)	25 μ l	50 μ l
TEMED	8 μ l	5 μ l

Table 2.5 Components of SDS gel

The polyacrylamide gel was prepared in two phases, a resolving gel for the separation of the protein samples and a stacking gel for the concentration of protein samples

before separation (Table 2.5). Gels were prepared by combining all solutions except TEMED. Polymerisation was initiated by addition of TEMED and ammonium persulfate. The resolving gel was poured between two glass plates and overlaid with water saturated butanol. Once polymerised (30 minutes) the water saturated butanol was rinsed off with distilled water and the stacking gel was prepared. The stacking gel was mixed and then poured in top of the resolving gel. A comb was then inserted into the top of the stacking gel and the gel was allowed to polymerise for 30 minutes. Once polymerised the gel was clamped into a vertical electrophoresis tank with $1 \times$ running buffer. The comb was then carefully removed and the protein samples were loaded into the wells with one lane of prestained protein markers (BioLabs, broadrange). Gels were run at 200 volts for 45 minutes. The gels were stained with 1 % Coomassie blue in 40 % MeOH/10 % HOAc for 30 minutes followed by destaining in 40 % MeOH/10 % HOAc until bands became visible (usually 1-3 hours).

2.6.2 Western Blotting

An SDS-PAGE gel was run and then soaked in $1 \times$ transfer buffer for two minutes. It was then assembled into a sandwich with the gel adjacent to a piece of nylon membrane (Hybond-N) placed between 2×2 layers of 3 mm filter paper and foam sponge, (all pre-soaked in $1 \times$ transfer buffer). The proteins were then transferred onto the membrane by immersing the sandwich in a tank containing $1 \times$ transfer buffer and passing a current of 1 Amp through it for 2 hours. The membrane was on the positive electrode side, since proteins migrate towards the electrode. The membrane was then used for immunodetection.

The membrane filters were blocked by agitating in 20 % milk protein solution in TBS overnight. Milk solution was removed and 30 μ l rabbit antiserum B2-3 in 40 ml 5 % milk protein added and the solution agitated gently for 3 hrs before washing thoroughly in TBS for 30 minutes, changing TBS frequently. TBS buffer was then removed and 10 μ l goat (antirabbit) antibody in 40 ml 5 % milkprotein added and

again the solution was agitated gently for 2 hrs followed by copious washing as before. Membranes were developed by shaking the membrane in 10 ml of developing solution until an orange band appeared. The reaction was stopped by rinsing the membrane in distilled water.

2.7 Kinetic Analysis

2.7.1 Steady-State

Steady-state experiments were performed on a Shimadzu 2101 UV/vis spectrophotometer at 25 °C. Assays were carried out in Tris.HCl pH 7.5, I = 0.1M, except were the ionic strength of the solution needed to be varied. Protein solution was kept on ice during the experiment until required and remained fully active for up to 2 hours. Assay solutions were made up in spectrophotometric cuvettes without protein and incubated in a water bath at 25 °C for 5-10 minutes prior to measurement. Reactions were initiated by addition of protein. The rate of change of absorbance of the acceptor ($\Delta A/\Delta T$) was followed over 2 minutes at the relevant wavelength. Using the value of $\Delta A/\Delta T$, k_{obs} was calculated from the equation shown below. Values were plotted against the concentrations of the substrate to generate a Michaelis-Menten curve, allowing calculation of the kinetic parameters k_{cat} and K_m .

$$k_{\text{obs}} (\text{s}^{-1}) = \frac{\Delta A/\Delta T (\text{min}^{-1}) \times \text{assay vol (l)} / \epsilon \times 60 (\text{s}) \times \text{p.l. (cm)} \times \text{protein vol (l)}}{[\text{protein}] (\text{M})}$$

where k_{obs} = The observed reaction rate.

ϵ = The extinction coefficient of cytochrome *c* or $[\text{Fe}(\text{CN})_6]^{3-}$.

p.l. = The pathlength of the cuvette.

2.7.2 Electron Acceptor Dependence

The concentration of ferricyanide or cytochrome *c* was varied while the concentration of L-lactate was kept constant and saturating.

2.7.3 Pre-steady-state Kinetics

All experiments were performed on an Applied Photophysics SF.17 Micro volume stopped-flow spectrophotometer at 25 °C, in Tris.HCl pH 7.5, I=0.1M buffer. The reaction was initiated by the rapid mixing of protein (typically ~ 6 μ M) and substrate (saturating concentrations). The reaction was monitored at 454 nm. At least 3 consistent traces were obtained before averaging and fitting to a single exponential.

2.8 Oxidase Activity

2.8.1 Steady-State

Reactions were carried out in a 1 ml glass cuvet with a 1 cm light path.

Oxidase activity under steady-state conditions can be obtained by using a coupled assay system.

Stock Solutions	8 mM <i>o</i> -dianisidine
	0.0025 g in 1 ml buffer/ 80 % triton x100
	Horse Radish Peroxidase 1 mg/ml
	0.1 M MOPS pH 7.5

To a solution containing 0.04 mM *o*-dianisidine, 2 μ l HRP (1 mg/ml), 0.5 mM L-lactate, buffer was added to give a final volume of 1 ml. The reaction was initiated by addition of 10 μ l FDH (100 μ M). Oxidase activity was measured as an increase in absorbance at 440 nm corresponding to that of reduced *o*-dianisidine.

2.8.2 Pre-Steady-State Analysis

The procedure was carried out as in section 2.7.3. The concentration of protein samples and substrate samples were 40 μ M and 60 μ M respectively, which on mixing were lowered to half these concentrations. The rate of re-oxidation of the FMN by oxygen saturated buffers was monitored at 454 nm over 100 ms. At least three consistent traces were obtained before averaging and fitting to a single exponential.

2.9 Redox Potentiometry

2.9.1 Redox Solutions and Mediators

Ferricyanide 30 mg in 5 ml 100 mM phosphate buffer pH 7.0

L-lactate 0.01g in 5 ml 100 mM phosphate buffer pH 7.0

HNQ (2-hydroxy-1-4-napthaquinone sulphite) $E_m = -140$ mV

MV (Methyl Viologen) $E_m = -430$ mV

ANQ (Anthraquinone) $E_m = -220$ mV

2.9.2 Procedure

Redox titrations were carried out under anaerobic conditions using a calomel electrode. Mediator solutions were made up to concentrations of 10 mM with degassed buffer. Protein was fully degassed by passing through a 10×2 cm gel filtration column (sephadex G25). Protein solution was then diluted with degassed buffer until an absorption of 0.7 at 452 nm ($\sim 60 \mu\text{M}$) was obtained in a volume of 10 ml. 10 μl of each mediator were added. The protein solution was fully re-oxidised by addition of ferricyanide, then reduced in step wise increments of ~ 5 mV by the addition of L-lactate and allowed to reach equilibration before recording the spectrum (700-250 nm). Once the protein had been fully reduced re-oxidation was carried out by addition of ferricyanide and the spectrum recorded at each new potential until full oxidation had been achieved. To analyse the data, the percentage oxidised protein was plotted against its corresponding potential, corrected relative to the standard hydrogen electrode (SHE) by $E_h = E + 244$ mV. This gave a sigmoidal curve which was fitted to a single electron Nernst equation and the midpoint calculated. The slope, if the system was in equilibrium is 29.5 ± 5 indicating a two electron transfer process.

The Nernst Equation is given by: $E = E_h + RT / nF \ln[\text{ox}]/[\text{red}]$

E = measured potential (mV)

E_h = mid-point potential (mV)

T = temperature (K)

R = molar gas constant ($\text{J mol}^{-1} \text{K}^{-1}$)

$[\text{red}]$ = concentration of reduced species

F = Faraday constant (C mol^{-1})

$[\text{ox}]$ = concentration of oxidised species

n = number of electrons

2.10 Microcalorimetry

2.10.1 Differential Scanning Calorimetry

Samples for calorimetry were dialysed extensively against the required buffer at 4 °C. Aliquots of the final dialysis buffer were used for the DSC reference and base line corrections. DSC was performed using a Microcal MC-2D instrument at a scan rate of 60 °C h⁻¹. Samples and reference samples were degassed under vacuum with gentle stirring before being loaded, and were held under 2-3 atm N₂ pressure during DSC to inhibit degassing and bubble formation at higher temperatures.

2.10.2 Isothermal Titration Calorimetry

Protein-protein titration isotherms were measured at 25 °C using microcal Omega titration microcalorimeter. A typical titration sequence involved 20 injections at 3 minute intervals of 5 µl aliquots of cytochrome *c* (~ 300 µM) solution into the stirred calorimeter cell (total volume 1.4 ml) containing FDH solution (~15 µM) so that each titration was completed in approximately 1 hour. Control experiments for heats of dilution of cytochrome *c* and FDH were performed under identical conditions and used for data correction in subsequent analysis. FDH was fully reduced with sodium dithionite then passed down a gel filtration column to remove excess. Protein samples for microcalorimetry were dialysed extensively against the appropriate buffer and briefly degassed prior to loading in the calorimeter cell. Cytochrome *c* was dissolved in the same dialysis buffer to minimise dilution artefacts and loaded in the injection syringe at typically 10 to 20 × concentration of FDH.

Chapter 3

The Flavin Domain of Flavocytochrome *b*₂

3.0 The Flavin Domain of Flavocytochrome b_2

3.1 Substrate Specificity

3.1.1 Steady-State Kinetics

Steady-state experiments were carried out on FDH as described Section 2.7.1. The enzyme exhibits saturation kinetics with a K_m for ferricyanide of 0.26 mM (Miles *et al.*, 1992). Hence concentrations of 3 mM ferricyanide were used for the determination of all steady-state parameters. Assays were carried out over a range of glycolate or L-lactate concentrations (Figure 3.1). Data were then fitted to the Michaelis-Menten equation and k_{cat} and K_m values were calculated for each of the mutant enzymes (Figure 3.2). The values obtained are compared to those of FDH_{WT} and glycolate oxidase in Table 3.1.

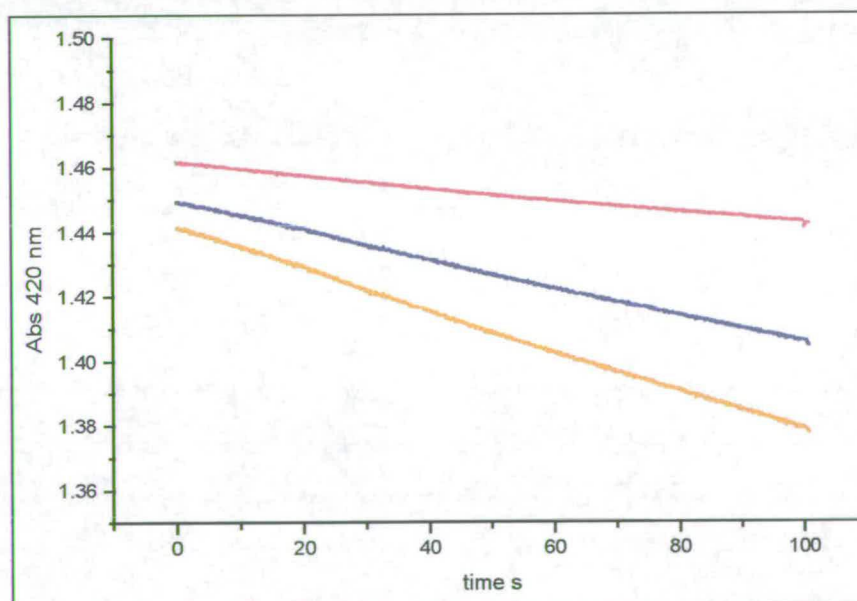


Figure 3.1 Examples of steady-state traces obtained for the reduction of $[\text{Fe}(\text{CN})_6]^{3-}$ by FDH_{WT}. The reaction was initiated by the addition of enzyme to the assay containing glycolate at concentrations of 3 mM (red), 6 mM (blue) and 15 mM (orange).

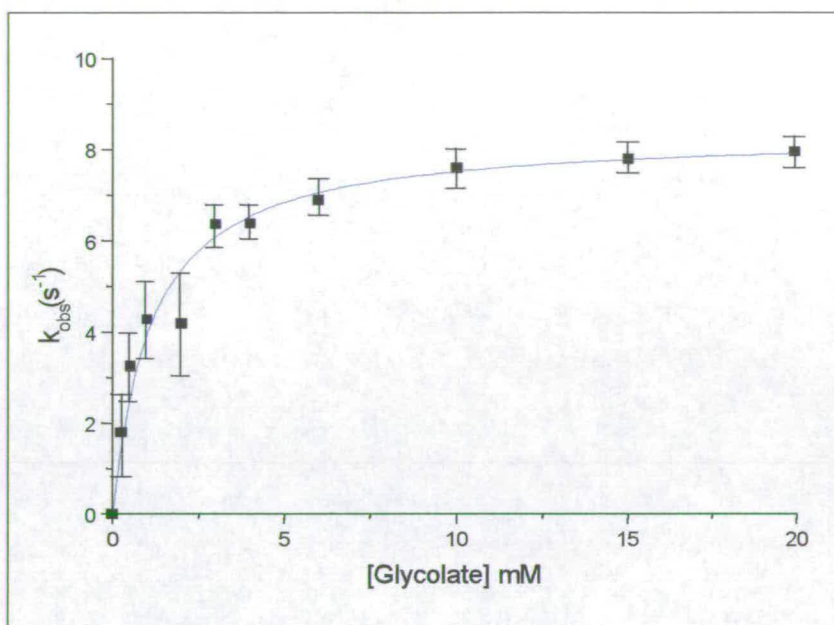


Figure 3.2 A Michaelis-Menten plot for FDH_{WT} with glycolate. Individual points were calculated from steady-state assays. The data was fitted by least squares regression analysis to the Michaelis-Menten equation using the program Microcal Origin.

Enzyme	Substrate : L-lactate			Substrate : Glycolate		
	k_{cat} s^{-1}	K_m (mM)	k_{cat}/K_m $M^{-1} s^{-1}$	k_{cat} s^{-1}	K_m (mM)	k_{cat}/K_m $M^{-1} s^{-1}$
GOX	17.5 ± 0.4	1.9 ± 0.2	9.21×10^3	20.0 ± 0.2	1.0 ± 0.1	20×10^3
FDH_{WT}	273 ± 2	0.20 ± 0.05	1.36×10^6	8.4 ± 0.6	1.1 ± 0.1	7.64×10^3
FDH_{L230W}	75.2 ± 3	3.9 ± 0.5	19.2×10^3	7.6 ± 0.6	7.3 ± 0.8	1.04×10^3
FDH_{TRIP}	9.5 ± 0.4	26 ± 3	3.7×10^2	3.7 ± 0.4	16.3 ± 1.5	0.23×10^3

Table 3.1 Comparison of steady-state kinetic parameters for L-lactate and glycolate dehydrogenation. Data for GOX taken from Macheroux et al (1991).

FDH_{WT} has a k_{cat} value with L-lactate of $273 s^{-1}$. Compared to this FDH_{L230W} shows a 4-fold decrease in k_{cat} to $75 s^{-1}$ and FDH_{TRIP} a 30-fold fall to $9.5 s^{-1}$. With glycolate as substrate the k_{cat} values for FDH_{WT} and FDH_{L230W} are similar (7.6 and $8.4 s^{-1}$ respectively), a two-fold lowering in comparison with glycolate oxidase. Rates for FDH_{TRIP} decrease further to $3.7 s^{-1}$, a fifth of that seen in glycolate oxidase.

The value of K_m , represents a measure of the affinity of the enzyme for the substrate. Low values indicate tight binding and high values weak binding. The K_m values for L-lactate increased from 0.2 mM for FDH_{WT} to 3.9 mM for FDH_{L230W} and 26 mM for FDH_{TRIP} . The K_m values for glycolate follow a similar pattern to that seen for lactate. K_m for glycolate has increased from 1.1 mM for FDH_{WT} to 7.3 mM for FDH_{L230W} and 16.3 mM for FDH_{TRIP} . Comparing values of K_m for lactate and glycolate, FDH_{WT} and FDH_{L230W} both bind lactate more tightly than glycolate but this preference is reversed for the mutant FDH_{TRIP} which binds glycolate more tightly than lactate. K_m values for glycolate and L-lactate are 16.3 mM and 26 mM, respectively

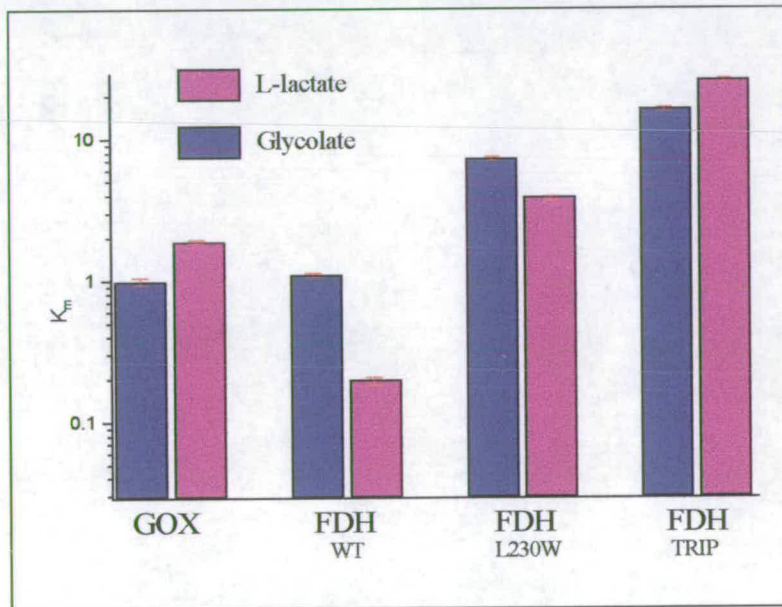


Figure 3.3 Semi-log plot comparing K_m values for L-lactate and glycolate for GOX, FDH_{WT} , FDH_{L230W} , FDH_{TRIP} . The K_m values were calculated from individual Michaelis plots.

The enzyme efficiency, k_{cat}/K_m with L-lactate has fallen from $10^6 M^{-1}s^{-1}$ for FDH_{WT} to $10^3 M^{-1}s^{-1}$ for FDH_{L230W} and $10^2 M^{-1}s^{-1}$ for FDH_{TRIP} . Comparing values of k_{cat}/K_m (Figure 3.4) for L-lactate and glycolate, FDH_{WT} is 10^3 -fold more efficient with L-lactate than with glycolate. FDH_{L230W} is still considerably better at oxidising L-lactate as a substrate but the difference has dropped to 30 times. In the triple mutant enzyme efficiency is only two-fold greater for lactate than glycolate although this has been accompanied by a general decrease in activity of the enzyme.

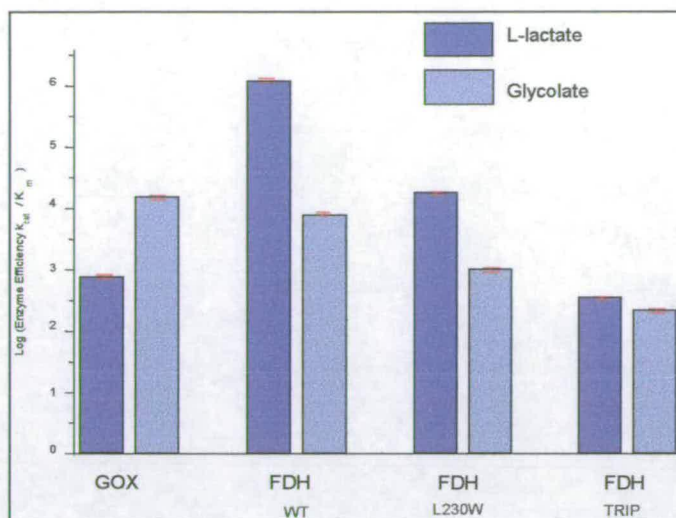


Figure 3.4 Comparison of enzyme efficiency of each for the enzymes with lactate and glycolate.

3.1.2 Pre-steady-state Kinetic Analysis

The pre-steady-state rates of flavin reduction by L-lactate and glycolate for each of the FDH mutants and FDH_{WT} were measured by stopped flow spectrophotometry at 454 nm (section 2.7.3). Experiments were carried out with saturating concentrations of either L-lactate or glycolate. Three consistent traces were obtained before averaging and fitting to a single exponential (Figure 3.5).

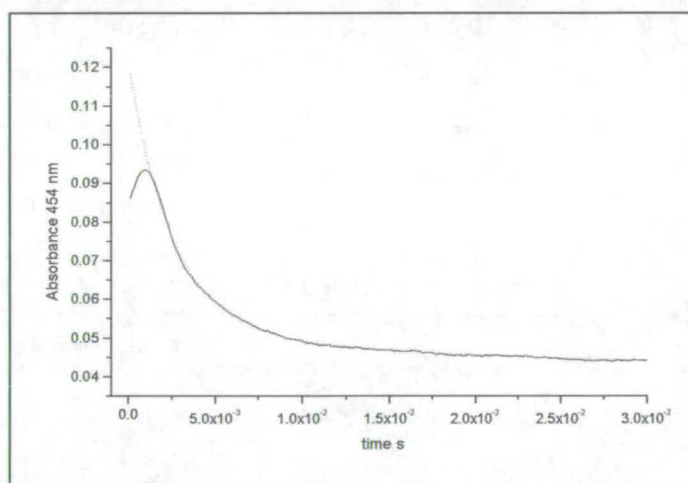


Figure 3.5 Pre-steady-state analysis for the reduction of FDH_{WT} by L-lactate was carried out by monitoring the rate of flavin reduction at 454 nm. The initial rise is due to the dead time of the instrument. This region of data was excluded from the fit. Trial fits using a range of equations were carried out but data was found to fit best to a single exponential.

Pre-steady-state k_{lim} values for mutants and FDH_{WT} are shown in Table 3.2.

Enzyme	L-lactate k_{lim} (s^{-1})	Glycolate k_{lim} (s^{-1})
FDH_{WT}	258 ± 25	6 ± 0.6
FDH_{L230W}	117 ± 15	5 ± 0.5
FDH_{TRIP}	2.9 ± 0.5	3.1 ± 0.5

Table 3.2 Pre-steady-state data for L-lactate and glycolate reduction by FDH_{WT} , FDH_{L230W} and FDH_{TRIP} .

3.2 Potentiometry

The introduction of different residues close to the FMN might affect the reduction potential of the flavin and therefore the driving force for the reaction (Pace *et al.*, 1986). It was assumed that should the triple mutant exhibit a reduction potential similar to wild type then the single mutant would not have a more significant effect. However, compensation effects in the triple mutant could mean that a single site mutation has a more significant effect than the triple mutation. The UV/vis spectra obtained for reductive and oxidative titrations for FDH_{TRIP} are shown in Figure 3.6.

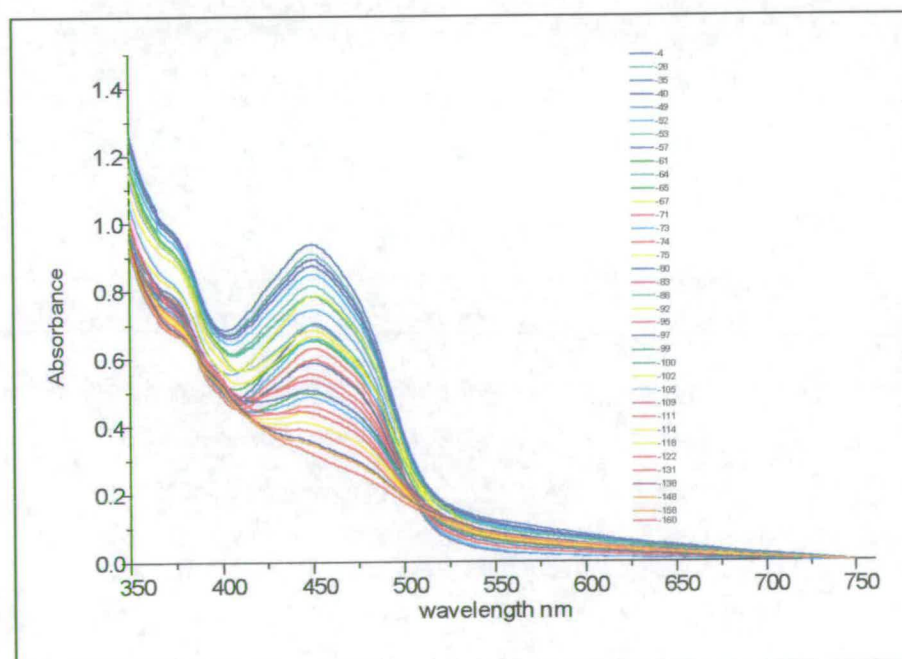


Figure 3.6 Redox titration spectra of FDH_{TRIP} . The enzyme was reduced by the addition of L-lactate and re-oxidised by $Fe(CN)_6^{3-}$. Spectra were monitored at each potential.

Due to the length of time required at 25°C protein precipitation and evaporation of the solution occurred over the course of the experiment. To correct for this, spectra were normalised to zero absorbance at 750 nm, where no absorbance would be expected, and corrected by multiplying by $(1-(1/\lambda))$. It was necessary to repeat the experiment twice; once to obtain the reductive curve and once for the oxidative curve using fresh protein stock each time to limit the amount of turbidity and protein precipitation. These data were combined and show that the reduction and oxidation of the enzyme is fully reversible under these conditions. The absorbances at 454 nm as a percentage of total FMN absorbance were then plotted against the measured reduction potential for each spectrum, corrected to the standard hydrogen electrode. The data were fitted to a single two electron Nernst equation. The redox potential of -100 ± 10 mV (Figure 3.7) compares favourably to that of FDH_{WT} and mandelate dehydrogenase, (-110 mV and -119 mV respectively). So the three mutations at the active site have not had a significant effect on the reduction potential of the FMN.

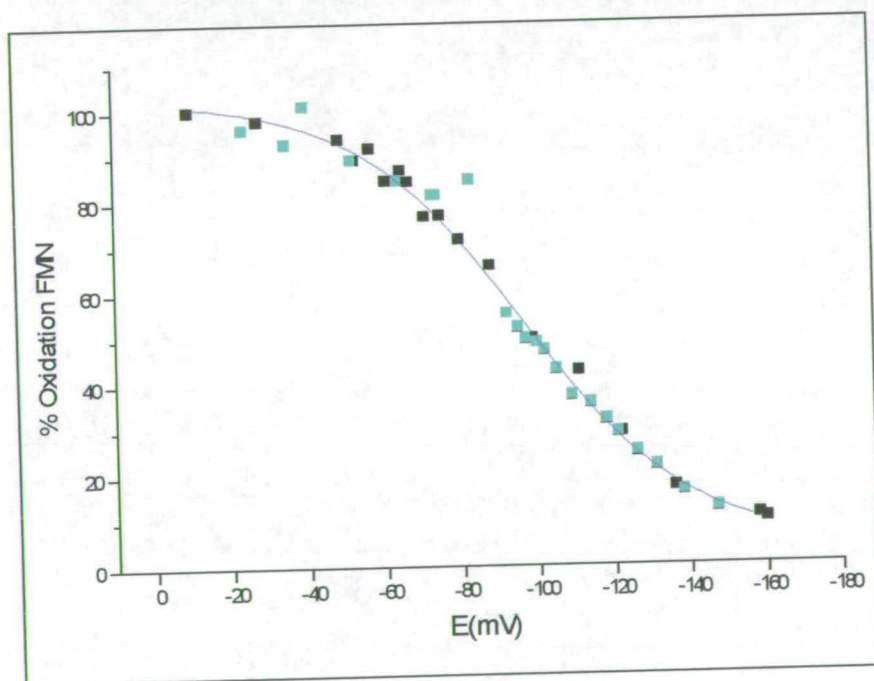


Figure 3.7 Plot of percentage oxidised FMN at 454 nm against measured potential (Vs SHE) Reduction data are shown in black, re-oxidation data in green. Data were fitted to a single two electron Nernst equation.

3.3 Oxidase Activity

3.3.1 Steady-State

Steady-state oxidase activity was measured using a coupled assay system (Figure 3.8). During lactate turnover hydrogen peroxide is produced as a result of FMN re-oxidation by molecular oxygen. The reduction of hydrogen peroxide by horseradish peroxidase (HRP) present in the assay is coupled to the oxidation of *o*-dianisidine which can be monitored at 440 nm. An example trace is shown in Figure 3.12.

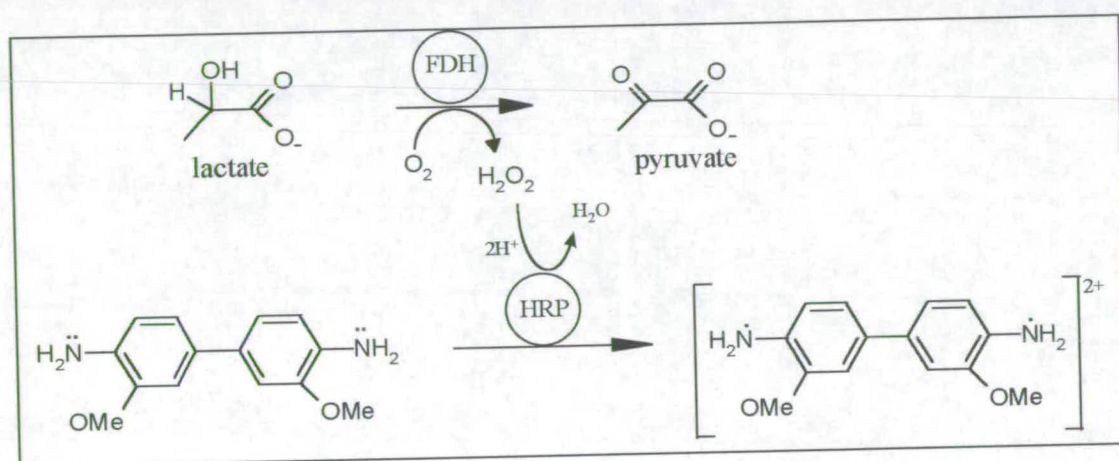


Figure 3.8 Coupled assay system used to monitor oxidase activity of FDH_{L230W}

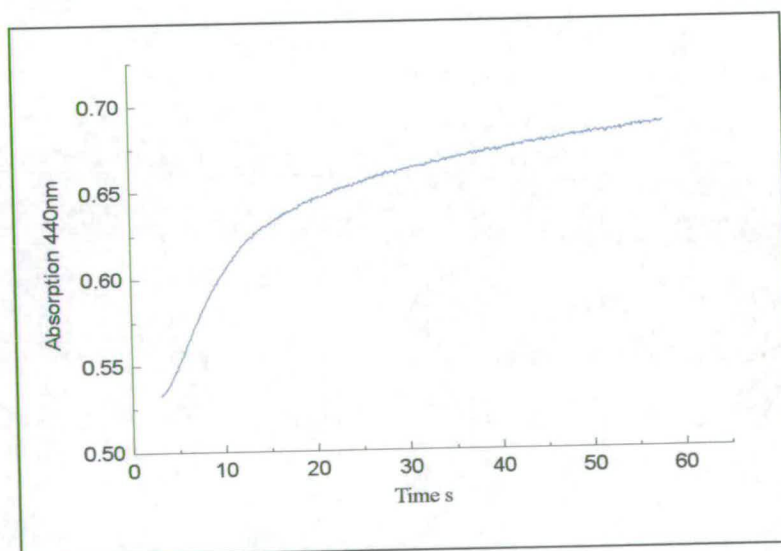


Figure 3.9 Example trace of steady-state oxidase activity of FDH_{L230W} with L-lactate.

The rate of oxidase activity is much greater at the beginning of the reaction and slows as the reaction proceeds. It is likely that oxide and superoxide radicals produced during catalysis are damaging to the enzyme. As the reaction proceeds an increasing proportion of the enzyme becomes damaged and is unable to catalyse the reaction leading to lowered rates. Due to the low amounts of enzyme used in the steady-state assays it was not possible to test this hypothesis by analysing reaction samples by mass spectrometry or SDS-PAGE. Initial rates of oxidase activity were measured over the first 10 seconds of the reaction at saturating lactate concentrations (Table 3.3).

	$k_{lim} (s^{-1})$
FDH _{WT}	0.045
FDH _{L230W}	0.034
FDH _{TRIP}	0.034

Table 3.3 Steady-state data of oxidase activity of FDH_{WT} and mutants.

3.3.2 Pre-steady-State Oxidation with O₂

The pre-steady-state measurement allows the determination of oxidase activity with the enzyme undergoing a single reduction oxidation step. This eliminates the problem of the enzyme becoming damaged in subsequent turnover steps. The enzyme was first reduced with glycolate then flavin re-oxidation by oxygen present in the buffers was monitored at 454 nm. At least 3 traces were obtained before averaging and fitting to a single exponential. The fitting range was set to allow for a time delay of 10-20 seconds to ensure that full reduction of FMN had been achieved (Figure 3.10).

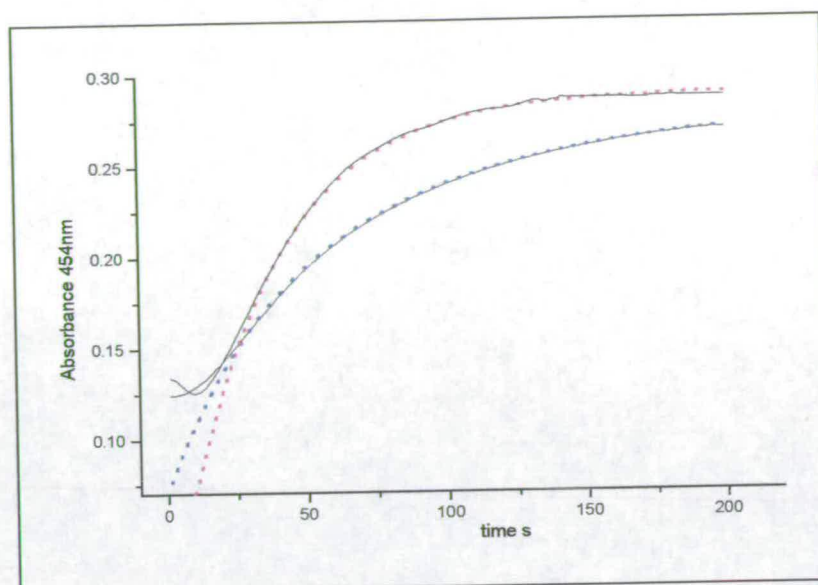


Figure 3.10 Comparison of pre-steady-state oxidase activity for FDH_{WT} and $\text{FDH}_{\text{L230W}}$. Data are shown in black. Fits to single exponentials are shown as dotted lines, blue - FDH_{WT} and magenta - $\text{FDH}_{\text{L230W}}$. Initial downward curve of the trace for L230W is due to the slower rate of reduction after initial mixing of this enzyme with lactate.

Enzyme	$k_{\text{lim}} (\text{s}^{-1})$
FDH_{WT}	0.015 ± 0.001
$\text{FDH}_{\text{L230W}}$	0.017 ± 0.002
FDH_{TRIP}	0.015 ± 0.002

Table 3.4 Pre-steady-state data for the re-oxidation of FDH and mutants by molecular oxygen.

3.4 Recognition for Cytochrome c

The nature of the interaction between fcb_2 and cytochrome c has been previously studied (Daff *et al.*, 1996). The surface of cytochrome c surrounding the haem consists of several positive charges arising from the side chains of Arg13, Lys72, Lys79 and Lys27 (Koppenol *et al.*, 1982) (Figure 3.11). These are thought to form electrostatic interactions with complementary charges on the haem domain of fcb_2 . Results are compatible with a model of one cytochrome c per haem domain and one main catalytically active binding site. Kinetic studies suggest a mechanism whereby

cytochrome c binding is slow and electron transfer rapid. The alternative mechanism in which complex formation is rapid and reversible but electron transfer within the complex is slow was found to be less likely. However cytochrome c reduction was still able to occur when ferrocytochrome was used as an inhibitor. This suggests that electron transfer occurs at more than one site and that intra-molecular transfer depends predominantly on the relative orientation and position of the two proteins.

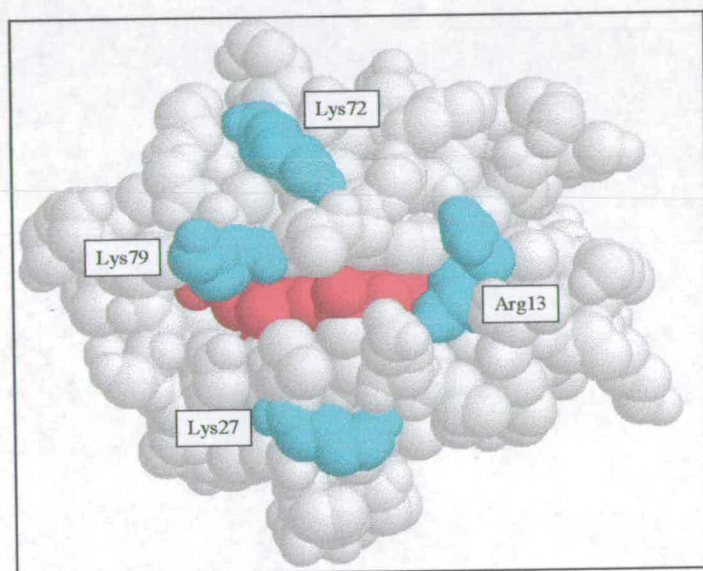


Figure 3.11 Charged residues surrounding the haem of cytochrome c

The isolated flavin domain of fc_b_2 shows very little activity with the physiological electron acceptor of fc_b_2 , cytochrome c (Balme *et al.*, 1995). This is surprising considering the large driving force for electron transfer between the two redox centres is approximately $1/3$ of a volt. Examination of the surface of the flavin domain around the solvent exposed C4a, N5 and C5a edge of the flavin show that residues are primarily positively charged or hydrophobic. Previous work attempted to create a docking site for cytochrome c on the surface of FDH. Three prominently positioned residues close to the flavin were engineered to complement the charges on cytochrome c (F. Welsh PhD thesis 1998). Two negatively charged residues were introduced by the mutations K201E and F325E while simultaneously removing a

positively charged lysine residue and a hydrophobic phenylalanine. The third mutation K324A also neutralised an exposed lysine (Figure 3.12). However, no increase in reactivity towards cytochrome c was observed.

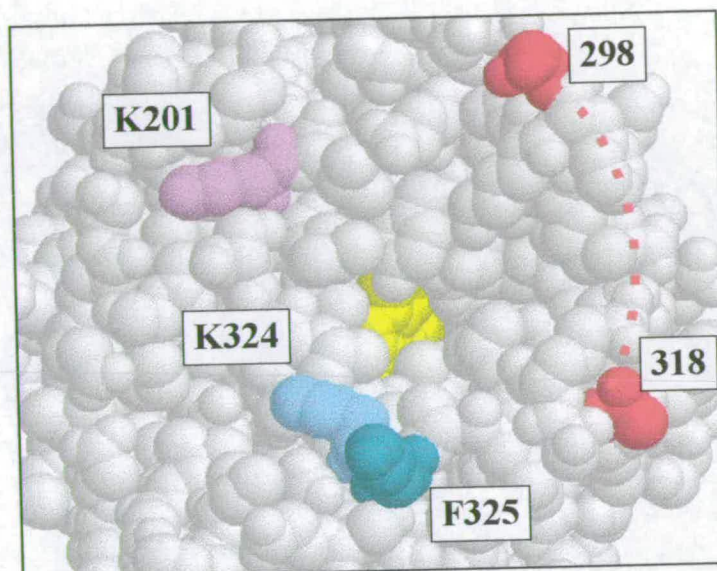


Figure 3.12 Prominent residues around the flavin which have been mutated are coloured. The loop shown as a dashed line connects residues 298 and 318.

In the crystal structures of FDH and intact $fc b_2$ the electron density for a large disordered loop of 20 amino acids is not visible. This flexible loop is situated on the surface of the flavin domain close to the FMN and would normally be pushed to one side by the haem domain. However in the absence of the haem domain it could adopt a conformation that sterically blocks cytochrome c from approaching close enough for efficient electron transfer. Molecular modelling experiments have demonstrated that this is likely to occur (Figure 3.13, R. Macfie, 1998). The model predicts the closest edge-to-edge distances between the two redox centres would be no less than 20 Å. For efficient electron transfer between redox centres distances of less than 14 Å are usually required (C. Moser *et al.*, 1992).

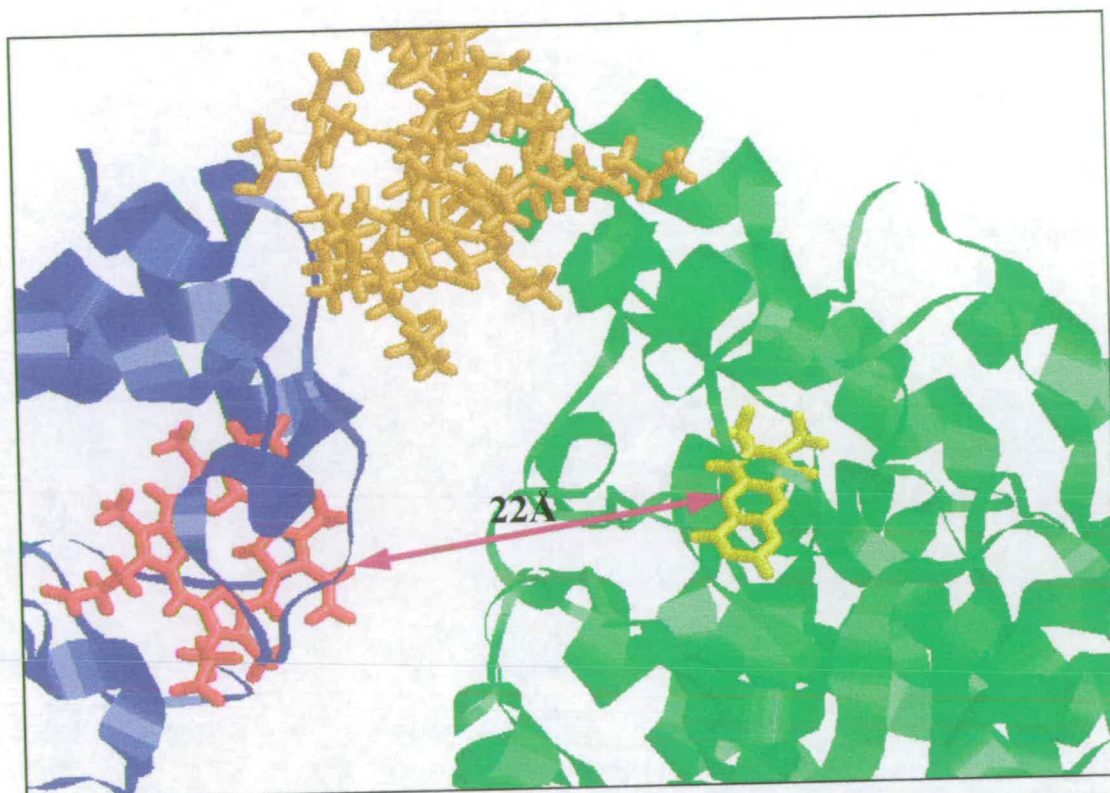


Figure 3.13 The closest approach of cytochrome *c* (blue) to FDH_{WT} (green) allowed by the modelled loop (orange).

Molecular modelling was used to re-design the loop so as to minimise its bulk but allow correct folding of the protein. A short amino-acid sequence of 5 or 7 glycine residues was found to be the most energetically favourable. Glycine residues were chosen to reduce attraction between the linker and the negatively charged residues introduced onto the surface. The minimum distance between the two redox centres was predicted by modelling to be approximately 13 Å (Figure 3.14).

In order to test these predictions two mutants were constructed. In combination with the three mutations K201E, K324A, F325E close to the flavin, the loop region was replaced with a short linker of 5 or 7 glycine residues. These mutants are referred to as FDH_{5GLY} and FDH_{7GLY}.

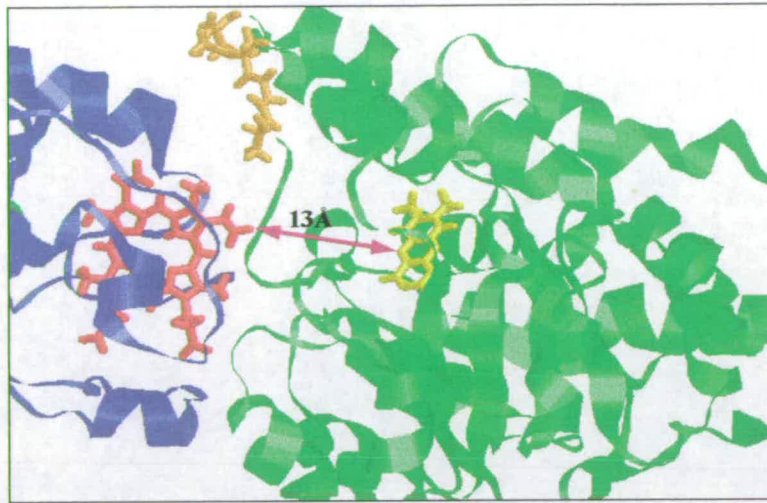


Figure 3.14 The closest approach of cytochrome c to $\text{FDH}_{5\text{GLY}}$, modelled 5 glycine linker in orange.

3.4.1 Replacement of the loop

Expression of $\text{FDH}_{5\text{GLY}}$ and $\text{FDH}_{7\text{GLY}}$ was confirmed by western blot. Purification of $\text{FDH}_{7\text{GLY}}$ proved problematic with loss of FMN and due to time constraints this mutant was not studied further. $\text{FDH}_{5\text{GLY}}$ was purified and confirmed to have a mass of 44014.6 (calculated 44013) by mass spectrometry (Figure 3.15).

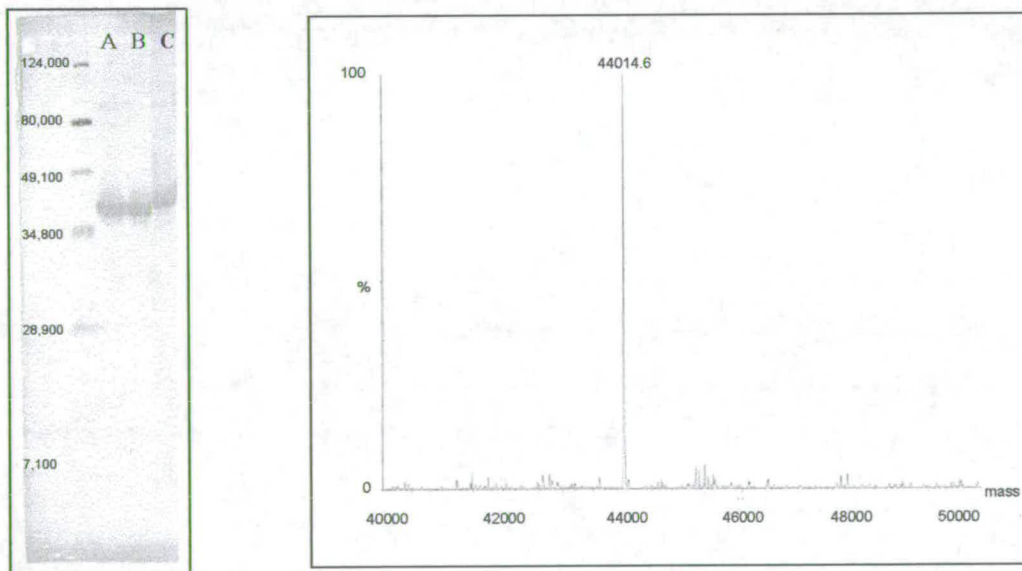


Figure 3.15 Western Blott of $\text{FDH}_{5\text{GLY}}$ (A), $\text{FDH}_{7\text{GLY}}$ (B), $\text{FDH}_{\text{K201E,K324A,F325E}}$ (C) and Confirmation of $\text{FDH}_{5\text{GLY}}$ by Mass spectrometry.

3.4.2 Steady-State Analysis

Steady-state analysis was carried out using ferricyanide and cytochrome c as electron acceptors (section 2.7.1) (Figure 3.16 and Table 3.5).

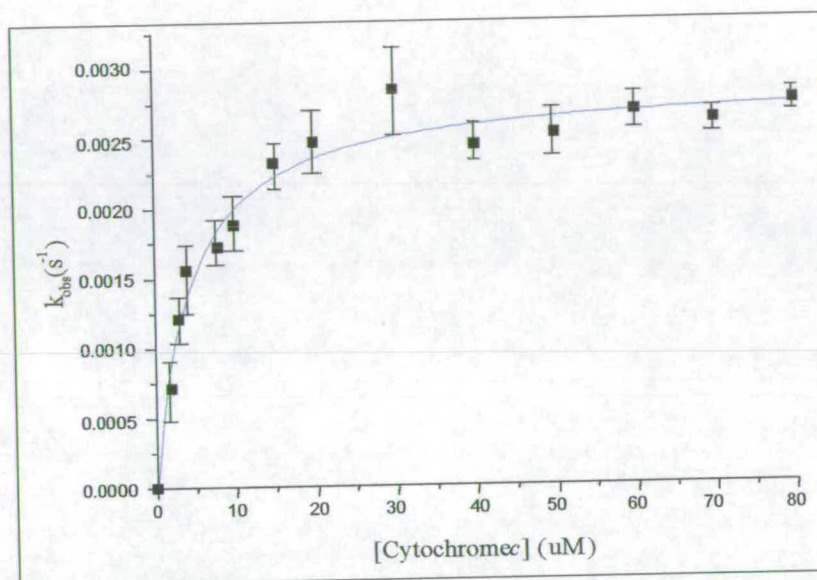


Figure 3.16 A Michaelis-Menten plot for $\text{FDH}_{5\text{GLY}}$ under saturating lactate conditions using cytochrome c as electron acceptor. Individual points were calculated from steady-state assays. The data was fitted by least squares regression analysis to the Michaelis-Menten equation using the program Microcal Origin.

	$\text{Fe}(\text{CN})_6^{3-}$		Cytochrome c	
	k_{cat} (s^{-1})	K_{m} (mM)	k_{cat} (s^{-1})	K_{m} (μM)
FDH_{WT}	273 ± 10	0.22 ± 0.02	0.02 ± 0.01	6.3 ± 0.2
$\text{FDH}_{\text{K201E,K324A,F325E}}$	14.6 ± 2	-	0.006 ± 0.001	15 ± 1.0
$\text{FDH}_{5\text{GLY}}$	16.8 ± 2	0.7 ± 0.1	0.004 ± 0.001	7.3 ± 0.5

Table 3.5 Parameters for FDH_{WT} and mutants with $[\text{Fe}(\text{CN})_6]^{3-}$ as electron acceptor and cytochrome c . Data for $\text{FDH}_{\text{K201E,K324A,F325E}}$ was taken from F. Welsh PhD thesis 1998.

The values of k_{cat} , at saturating L-lactate concentrations, for the reduction of $[\text{Fe}(\text{CN})_6]^{3-}$ by $\text{FDH}_{\text{K201E,K324A,F325E}}$ and $\text{FDH}_{5\text{GLY}}$ is considerably less than for FDH_{WT} . This is probably due to the electrostatic repulsion of $[\text{Fe}(\text{CN})_6]^{3-}$ and the negatively

charged glutamate residues. Molecular modelling studies have shown that $[\text{Fe}(\text{CN})_6]^{3-}$ is not hindered by the bulk of the loop and so rates of electron transfer are approximately the same for $\text{FDH}_{\text{K201E,K324A,F325E}}$ and $\text{FDH}_{5\text{GLY}}$. In contrast the interaction and electron transfer between $\text{FDH}_{\text{K201E,K324A,F325E}}$ and the much larger cytochrome c is adversely effected by the steric bulk of the loop. Yet removing the bulk of the loop did not improve the rate of electron transfer. K_m for cytochrome c remains approximately the same for FDH_{WT} , $\text{FDH}_{\text{K201E,K324A,F325E}}$ and $\text{FDH}_{5\text{GLY}}$.

3.4.3 Ionic Strength Plots

To investigate the nature of the interaction between cytochrome c and each of the enzymes FDH_{WT} and $\text{FDH}_{5\text{GLY}}$ Michaelis plots over a range of ionic strengths from $I=0.01\text{ M}$ to $I=0.40\text{ M}$ were obtained (Table 3.7 and 3.8). Values of $\log(k_{\text{cat}}/K_m)$ were plotted against $I^{1/2}$, to produce the ionic strength plots shown in Figure 3.17.

FDH _{5GLY}					
Ionic Strength (M)	k_{cat} (s ⁻¹)	K_m (μM)	k_{cat}/K_m	$I^{1/2}$	$\log k_{\text{cat}}/K_m$
0.01	0.0069	10.8	639	0.10	2.80
0.04	0.0041	4.1	993	0.20	3.00
0.05	0.0035	3.9	898	0.22	2.95
0.10	0.0036	7.3	494	0.32	2.69
0.12	0.0028	4.4	658	0.35	2.82
0.17	0.0030	8.4	177	0.41	2.25
0.20	0.0037	31.5	119	0.45	2.08
0.30	0.0030	43.6	69	0.55	1.84
0.40	0.0036	31.6	115	0.63	2.06

Table 3.7 Data for L-lactate dehydrogenation by $\text{FDH}_{5\text{GLY}}$. The kinetic parameters, k_{cat} and K_m , were calculated from Michaelis-Menten plots carried out at a range of ionic strengths.

FDH _{WT}					
Ionic Strength (M)	k_{cat} (s ⁻¹)	K_m (μM)	k_{cat}/K_m	$I^{1/2}$	$\log k_{cat}/K_m$
0.01	0.099	5.2	18929	0.10	4.30
0.04	0.065	10.7	6072	0.20	3.80
0.1	0.025	20.0	1250	0.32	3.10
0.2	0.004	69.1	58	0.45	1.76
0.3	0.002	28.1	71	0.55	1.85
0.4	0.002	54.6	36	0.63	1.56

Table 3.8 Data for L-lactate dehydrogenation by FDH_{WT}. The kinetic parameters, k_{cat} and K_m , were calculated from Michaelis-Menten plots carried out at a range of ionic strengths.

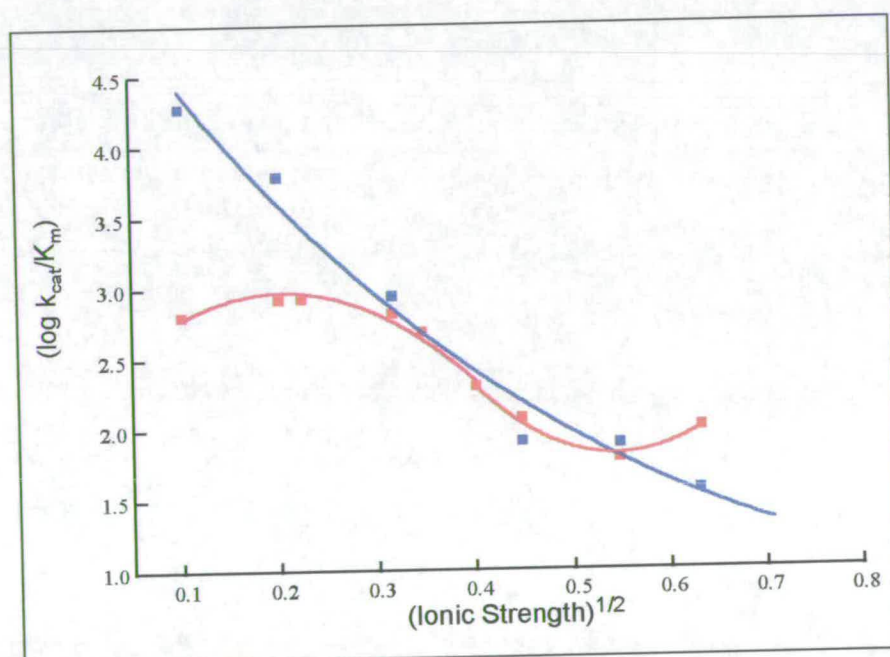


Figure 3.17 Ionic strength data for FDH_{WT} (blue) and FDH_{5GLY} (red). The data for FDH_{WT} have been fitted to the extended Debye-Hückel equation.

Values of K_m and k_{cat} were influenced by the ionic strength of the solution indicative of an interaction between oppositely charged surfaces. Data for FDH_{WT} were fitted to the extended Debye-Hückel equation (Appendix 7.3) and show an increase in rates of electron transfer at low ionic strength when the interaction of two charge surfaces is favoured. The shape of the ionic strength plot for FDH_{5GLY} is markedly different. As

ionic strength is lowered rates increase until $I=0.04$ M, then decrease to $I=0.01$ M. There are two possible scenarios which lead up to electron transfer. Either initial interaction of cytochrome c is followed by translational movement to an orientation favourable for electron transfer or a simple Ping-Pong mechanism operates. In both cases too strong an interaction would slow the exchange and release process down. At high ionic strengths an increase in rate is observed which is thought to be due to the non-ideal behaviour of protein-protein interactions in this region.

3.4.4 Microcalorimetry and Molecular Recognition

Microcalorimetry was used to investigate the strength of the electrostatic interaction. Isothermal titration (ITC) and differential scanning (DSC) calorimetry techniques can be used to study non covalent interactions involved in biomolecular recognition (Cooper *et al.*, 1993, Johnson *et al.*, 1992). Biomolecular recognition processes rely on a subtle balance of non covalent forces to control and mediate binding. Interactions involved include hydrogen bonding, hydrophobic and electrostatic forces. The free energy changes associated with non-covalent interactions involve a balance between enthalpic and entropic contributions.

3.4.4.1 Differential Scanning Calorimetry

Differential scanning calorimetry (DSC) involves the measurement of the differential heat energy uptake in a sample during a change in temperature. This experiment looks at the unfolding of proteins and the distinctive increase in excess heat capacity of the unfolded chain with respect to the folded protein. Experiments were carried out using a Microcal MC-2D instrument at a scan rate of 60 °C h^{-1} . Dilute protein solutions (less than 1 mg/ml) were used to limit protein-protein interactions. Protein solutions were exhaustively dialysed in 10 mM Hepes ($I=0.01$ M) and concentrations determined accurately before being degassed. DSC scans were normalised by

subtraction of control buffer data. DSC traces showing endothermic unfolding transitions of cytochrome c and FDH_{WT} individually and in a 1:1 ratio are shown in Figure 3.18 (Data Table 3.9).

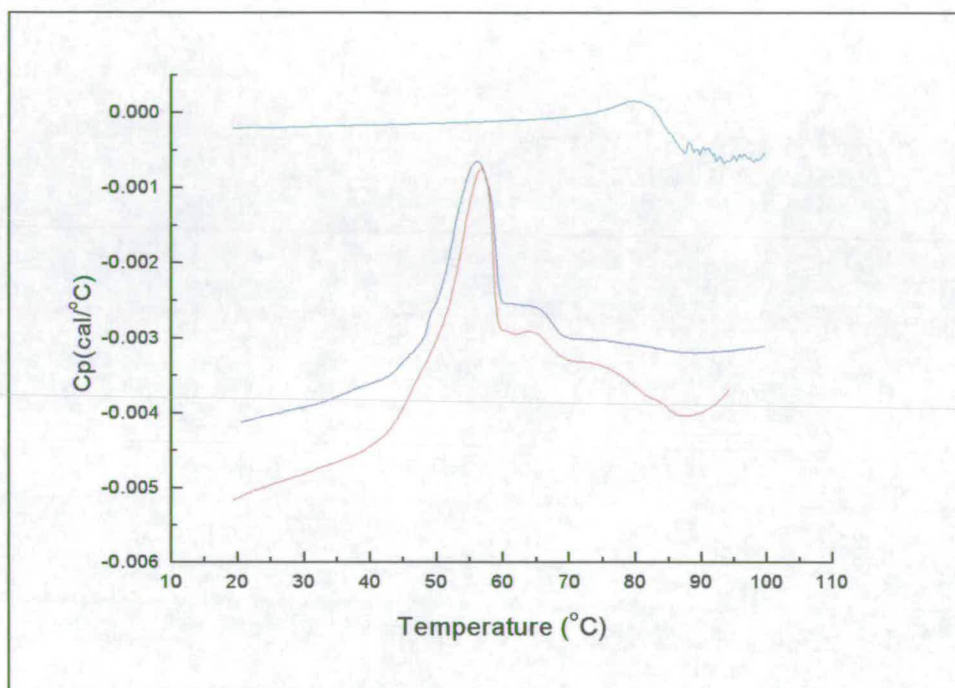


Figure 3.18 Differential scanning calorimetry trace of cytochrome c (green), FDH_{WT} (blue) and a 1:1 mixture (red). DSC scans were carried out in one direction only and were not reversible due to aggregation of the enzyme at high temperature.

The melting point of cytochrome c was determined to be 79.5 °C, much greater than FDH_{WT}, 56.0 °C. A 1:1 mixture of FDH_{WT} and cytochrome c gave a melting point of 60.0 °C, a 4 °C increase from that observed for FDH_{WT} alone. DSC scans for FDH_{5GLY}, cytochrome c and a 1:1 mixture are shown in Figure 3.19. The melting point of FDH_{5GLY} was determined to be 51.6 °C so thermal stability has decreased on replacing the loop section with a 5GLY linker. A 1:1 solution of cytochrome c and FDH_{5GLY} exhibits a melting point of 53.2 °C an increase of 1.6 °C. However the latter peak was not fully defined before exothermic aggregation of the protein took place.

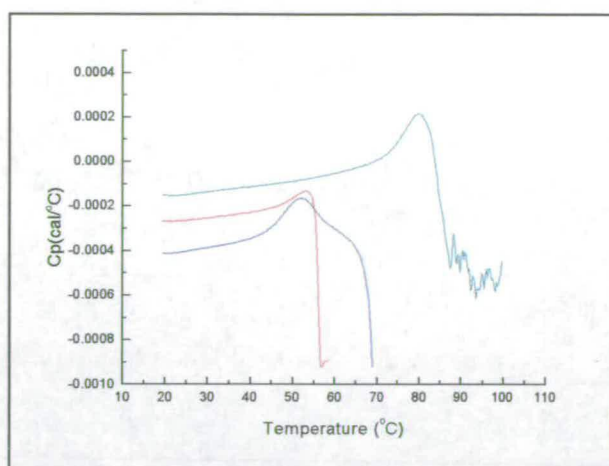


Figure 3.19 Differential scanning calorimetry trace of cytochrome c (green), $\text{FDH}_{5\text{GLY}}$ (blue) and a 1:1 mixture (red)

	Melting point
cytochrome c	79.5 °C
FDH_{WT}	56.0 °C
$\text{FDH}_{\text{WT}} / \text{cytochrome } c$	60.0 °C
$\text{FDH}_{5\text{GLY}}$	51.6 °C
$\text{FDH}_{5\text{GLY}} / \text{cytochrome } c$	~53.2 °C

Table 3.9 Melting point temperatures of FDH_{WT} and FDH mutants individually and in 1:1 ratio with cytochrome c .

3.4.4.2 Isothermal Calorimetric Titrations

Isothermal calorimetry can be used to study the thermodynamics of binding initiated on mixing a solution of the chosen biomolecules. Aliquots of cytochrome c were injected into a cell (typically 20 or more injections) containing $\text{FDH}_{5\text{GLY}}$ until the final molar ratio of $\text{FDH}_{5\text{GLY}}$ to cytochrome c was 1:2. Experiments were carried out as described in Section 2.10. No binding between $\text{FDH}_{5\text{GLY}}$ and cytochrome c was observed. Exothermic enthalpy changes seen were due to the dilution of cytochrome c as it was titrated into the FDH solution. The example shown has been corrected for

baseline drift (Figure 3.20). If binding were to occur in a 1:1 ratio enthalpy changes would be expected to be seen within the first 10 aliquot additions. The experiment was repeated with $fc b_2$, FDH_{WT} and $FDH_{K201E,K324A,F325E}$ but no binding of cytochrome c was detected for any of these proteins.

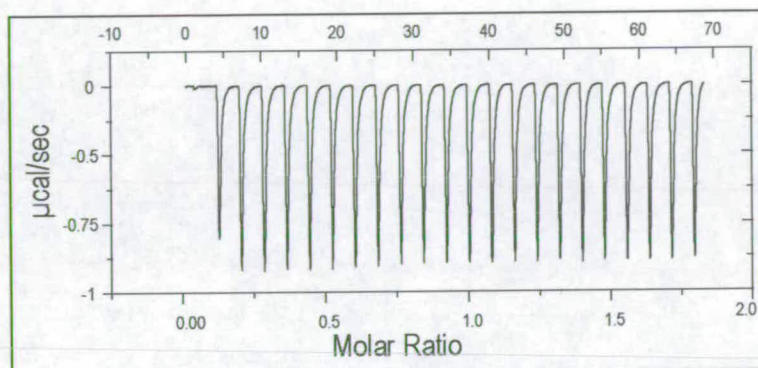


Figure 3.20 Isothermal titration calorimetry of cytochrome c into FDH_{5GLY} .

3.5 Discussion

The isolated flavin domain has been studied with regard to recognition for substrates and electron acceptors. The active site of FDH has been successfully redesigned by creating the mutations L230W, T197A, A283T to bind glycolate preferentially over L-lactate (K_m for lactate 26 mM, K_m for glycolate 16 mM). However this has been accompanied by a general decrease in enzyme efficiency as measured by k_{cat}/K_m and the enzyme is still more efficient at utilising lactate as a substrate than glycolate. As the K_m values for GOX and FDH_{TRIP} with glycolate are 1 mM and 26 mM respectively there remains some clear structural differences at the active site. It is likely that residues directly behind those that form the active site cavity influence the orientation of residues and their side chains which interact with the substrate. In particular the large planar ring of the tryptophan may lie in a different orientation in FDH to that seen in GOX. It has proved much more difficult to re-design FDH to be selective for smaller substrates than larger ones. Whereas larger substrates can be accommodated

by simply removing bulk from the active site the opposite does not hold true when engineering selectivity for smaller substrates.

None of the mutants studies showed any significantly improved ability to use molecular oxygen as an electron acceptor. All FDH enzymes were apparently sensitive to attack by hydrogen peroxide and superoxide radicals and their ability to act as an oxidase deteriorated rapidly with each subsequent turnover. What factors confer this protection on GOX and other oxidases has not been determined. The recently determined high resolution structures of D-amino acid oxidase complexed with D-alanine, D-trifluoroalanine and L-lactate (1.2 Å, 1.47 Å and 1.72 Å resolution respectively) has cast light on factors that confer oxidase activity (Umhau *et al.*, 2000). This enzyme, a member of the flavoprotein oxidase family catalyses the oxidation of D-amino acids. The hydride transfer mechanism of dehydrogenation is conserved but in the case of D-amino acid oxidase FAD is re-oxidised by molecular oxygen to yield FAD_{OX} and H_2O_2 . The high resolution electron density of the complex with D-alanine enables a diatomic species proposed to be peroxide to be resolved at the active site on the *re*-side of the flavin (Figure 3.21). One atom of the species is placed on the flavin plane between N(5) and C(4a). The second atom lies above and between C5a and C9a. With flavin monooxygenases, dioxygen activation has been shown to proceed via C(4a) covalent hydroperoxides which supports a link to C(4a) in preference to N5a. The peroxide species lies on the same side of the FMN as the water molecule found in GOX. This lends support to the idea that space occupied by the water molecule in GOX is important for oxidase activity. It is therefore not surprising that the single mutant $\text{FDH}_{\text{L230W}}$ did not show any improvement in oxidase activity. This tryptophan residue has been shown to influence substrate specificity but it is not important for oxidase activity. FDH_{TRIP} also showed no increase in oxidase activity. Although the mutation T197A was created on the *re*-side of the flavin this residue may be too far from the proposed peroxide binding site of C(4a) seen in D-amino acid oxidase.

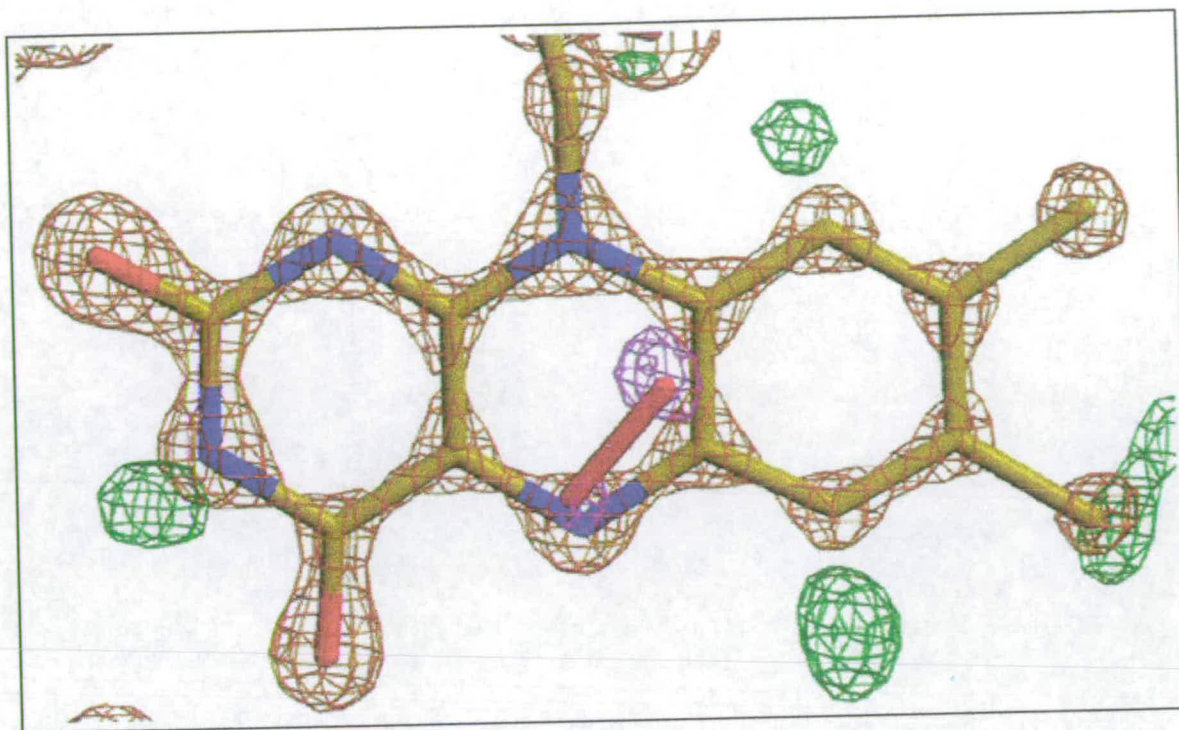


Figure 3.21 Electron density of the FAD in D-amino acid oxidase. The high resolution electron density enables a diatomic species proposed to be peroxide (red) to be resolved at the active site.

In the absence of the haem domain electron transfer direct from flavin to cytochrome c is extremely slow. A docking site for cytochrome c has been engineered on the surface of FDH however this has not led to improved electron transfer rates. Ionic strength studies indicate that there is an electrostatic interaction between FDH_{WT} and cytochrome c . The mutant $\text{FDH}_{5\text{GLY}}$ displays different characteristics to FDH_{WT} . At ionic strengths of less than 20 mM rate constants decrease in contrast to FDH_{WT} where rate constants continue to increase.

DSC and ITC were used to investigate the strength of this interaction. ITC detected no binding between the following; FDH_{WT} : cytochrome c , $\text{FDH}_{\text{K201E,K324A,F325E}}$: cytochrome c and $\text{FDH}_{5\text{GLY}}$:cytochrome c . DSC showed cytochrome c to increase the thermal stability of FDH_{WT} and to a lesser extent that of $\text{FDH}_{5\text{GLY}}$. As the melting point temperature increases in the presence of cytochrome c it would suggest that weak non-covalent interactions form between cytochrome c and the native conformation of FDH. However this is not proof of FDH/cytochrome c complex formation at the engineered binding site. The values obtained could be equally

accounted for by non-specific protein protein interactions. These results are inconclusive as to whether there is any significant complex formation between either FDH_{5GLY} or FDH_{WT} and cytochrome c . Another technique which could be employed to analyse protein-protein interactions but which was not available is ultra centrifugation. If there is more than one cytochrome c binding site on the haem domain of fc_b_2 as shown by Daff *et al.*, (1996a), then this suggests that the orientation and position of the two redox cofactors relative to each other may be more important for efficient electron transfer than actual binding.

Part 1
References

- Appelby, C. A., and Morten, R. K. (1954) *Nature* **173**, 749-752.
- Balme, A., Brunt, C. E., Pallister, R. L., Chapman, S. K., and Reid, G. A., (1995), *Biochem. J.*, **309**, 601-605.
- Bell, C., Uhrinova, S., Barlow, P. N., Chapman, S. K., and Reid, G. A., (1997). *Flavins and Flavoproteins 1996*, University of Calgary Press, Calgary, Alberta, 555-558.
- Belmouden, A., Le, K. H. D., Lederer, F. and Garchon, H. J. (1993) *Eur. J. Biochem.* **214**, 17-25.
- Black, M. T., White, S. A., Reid, G. A., and Chapman, S. K., (1989) *Biochem. J.*, **258**, 255-259.
- Brunt, C. E., Miles, C. S., Pallister, R. L., Reid, G. A., and Chapman, S. K., (1990) *Flavins and Flavoproteins*. 10th Int. Symposium, 787-790.
- Capeillère-Blandin, C., (1975), *Eur. J. Biochem.*, **56**, 91-101.
- Chapman, S. K., Reid, G. A., Bell, C., Daff, S., Sharp, R. E., White, P., Manson, F.D.C., and Lederer, F., (1994), *Biochem. Soc. Trans.*, **22**, 713-718.
- Chapman, S. K., White, S. A. and Reid, G. A., (1991), *Adv. Inorg. Chem.*, **36**, 257-301.
- Cooper, A. and McAuleyhecht K. E., (1993), *Philos. Trans. R. Soc. Lond. Ser. A-Math. Phys. Eng. Sci.*, **345**, 23-35.
- Daff, S., Manson, F. D. C., Reid, G. A., and Chapman, S. K. (1994a) *Biochem. J.*, **301**, 829-834
- Daff, S., Manson, F. D. C., Reid, G. A., and Chapman, S. K. (1994b) *Biochem. Soc. Trans.*, **22**, 282
- Daff, S., Ingledew, W. J., Reid, G. A., and Chapman, S. K., (1996a), *Biochemistry*, **35**, 6345-6350.

- Daff, S., Sharp, R. E., Short, D. M., Bell, C., White, P., Manson, F. B. C., Reid, G. A., and Chapman, S. K., (1996b), *Biochemistry*, **35**, 6351-6357.
- Daum, G., Bohni, P. C., and Schatz, G. (1982) *J. Biol. Chem.* **257**, 13028-13033.
- Fewson, C. A. (1988) *FEMS. Microbiol. Rev.* **54**, 85-110
- Fürst, J. P., Pansegrau, W., Frank, R., Blöcker, H., Scholz, P., Bagdasarian, M. and Lanka, E. (1986) *Gene* **48**, 119-131.
- Gaume, B, Sharp, R. E., Manson, F. D. C., Chapman, S. K., Reid, G. A. and Lederer, F., *Biochimie*, **77**, 621-630, 1995.
- Ghisla, S. and Massey, V., *Eur. J. Biochem.*, **181**, 1-17, (1989)
- Ghisla, S., and Massey, V. (1991) in *Chemistry and Biochemistry of Flavoenzymes* (Muller, F., Ed) Vol. **2**, 243-289.
- Giegel, D.A., Williams, C. H., and Massey, V. (1990) *J. Biol. Chem.*, **265**, 12, 6626-6632.
- Gondry, M., Lê, K. H. D., Manson, F. D. C., Chapman, S. K., Mathews, F. S., Reid, G. A., and Lederer, F., (1995), *Protein Science*, **4**, 925-935.
- Guiard, B., (1985), *EMBO, J.*, **4**, 3265-3272.
- Harris, C. M., Ghisla, S., Pilone, M.S., and Pellegioni, L., University of Insubria, Varese, Italy, Unpublished results.
- Hayaishi, O., Sutton, W. B., (1957) *J. Am. Chem. Soc.* **79**, 4809.
- Jacq, C. and Lederer, F., (1974) *Eur. J. Biochem.* **41**, 311-320.
- Johnson, C. M., Copper, A. and Stockley, P. G., (1992), *Biochemistry*, **31**, 9717-9724.
- Koppenol, W. H. and Margoliash, E., (1982) *J. Biol. Chem.*, **257**, 4426-4437.
- Lê, K. H. D., Lederer, F. (1991) *J. Biol. Chem.* **266**, 31, 20877-20881.

- Lederer, F. (1991) in Chemistry and Biochemistry of Flavoenzymes, ed. Müller, F. VolII, 153-242.
- Lederer, F., Cortial, S., Becam, A. M., Haumont, P. Y., and Perez, L. (1985) *Eur. J. Biochem.* **139**, 59-65.
- Lindqvist, Y. (1989) *J. Mol. Biol.* **209**, 151-166.
- Lindqvist, Y., Branden, C. I., Mathews, F.S., Lederer, F. (1991) *J. Biol. Chem.* **266**, 5, 3198-3207.
- Lockridge, O., Massey, V., and Sullivan, P. A., (1972) *J. Biol. Chem.* 8097-8106.
- MacFie, R., 1998, Honours Project, Modelling the interaction between the flavocytochrome b_2 flavin domain and cytochrome c . University of Edinburgh.
- Macheroux, P., Kieweg, V, Massey, V., Söderland, E., Stenberg, K., and Lindqvist, (1993) *Eur. J. Biochem.*, **213**, 1047-1054.
- Maeda-Yorita, K., Aki, K., Sagai, H., Misaki, H and Massey, V. (1995) *Biochimie* **77**, 631-642.
- Massey, V., (1994) *J. Biol. Chem.*, **269**, 22459-22462.
- Mattevi, A., Vanoni, M. A., Todone, F., Rizzi, M., Teplyakov, A., Coda, A., Bolognesi, M. and Curti, B., *Proc. Natl. Acad. Sci.*, (1996) **93**, 7496-7501.
- Miles, C. S., Rouviere-Fourmy, N., Lederer, F., Mathews, F. S., Reid, G. A., Black, M. T., and Chapman, S. K., (1992) *Biochem. J.*, **285**, 187-192.
- Mitra, B., Gerlt, J. A., Babbitt, P. C., Kenyon, G. L., Joseph, D., Petsko, G. A. (1993) *Biochemistry*, **32**, 12959-12967.
- Moser, C. C., Page, C. C., Farid, R. and Dutton, P. L., (2000) *J. Bioenerg. And Biomemb.*, **27**, 263-274.
- Müh, U., Massey, V. and Williams, C. H., (1994) *J. Biol. Chem.* **269**, 11, 7982-7988.

- Østergard, L. H., PhD thesis, Engineering Oxidase Activity in Flavocytochrome *b*₂, University of Edinburgh 1997.
- Pace, C. and Stankovich, M., *Biochemistry*, **25**, 9, 2516-2522, 1986.
- Reid, G. A., White, S., Black, M. T., Lederer, F., Mathews, F. S., and Chapman, S. K., (1988) *Eur. J. Biochem.*, **178**, 329-333.
- Sanders, S. A., Williams, C. H., and Massey, V. (1999) *J. Biol. Chem.* **274**, 32, 22289-22295.
- Scrutton, N. S., (1994), *BioEssays*, **16**, 115-122.
- Sharp, R. E., White, P., Chapman, S., and Reid, G. A. (1994), *Biochemistry*, **33**, 5115-5120.
- Sharp, E. R., Chapman, S. K. and Reid, G.A., *Biochemistry*, **35**, 891-899, (1996a).
- Sharp, E. R., Chapman, S. K. and Reid, G.A., *Biochem. J.*, **316**, 507-513, (1996b).
- Short, D. M., Walkinshaw, M. D., Taylor, P., Reid, G. A. and Chapman, (1997), *Flavins and Flavoproteins*, University of Calgary Press, Calgary, Alberta, 575-578.
- Short, D. M., Walkinshaw, M. D., Taylor, P., Reid, G. A. and Chapman, S. K., (1998), *J. Biol. Inorg. Chem.*, **3**, 246-252.
- Sinclair, R., PhD thesis, The Kinetic Characterisation of *Rhodotorula graminis* L-Mandelate dehydrogenase, University of Edinburgh, 1998.
- Sinclair, R., Reid, G. A. and Chapman, S. K., (1998), *Biochem. J.*, **333**, 117-120.
- Steinberg, K., Clauen, T., Lindqvist, Y. and Macheroux, P., (1995) *Eur. J. Biochem.* **228**, 408-416.
- Sun, W., Williams, C. H., Massey, V. (1996) *J. Biol. Chem.*, **271**, 29, 17226-17233.
- Tegoni, M., Silvestrini, M. C., Guigliarelli, B., Asso, M., Brunori, M. and Bertrand, P., (1998), *Biochemistry*, **37**, 112761-112771.

- Tegoni, M., White, S. A., Roussel, A., Mathews, F. S. and Cambillau, C., (1993), *Proteins: Structure, Function, and Genetics*, **16**, 408-422.
- Tsou, A. Y., Rabson, S. C., Gerlt, J. A., Buechter, D. D., Babbit, P. C., Kenyon, G. L. (1990) *Biochemistry*, **29**, 9856-9862.
- Umhau, S., Pollegioni, L., Molla, G., Diederichs, K., Welte, W., Pilone, M. S. and Ghisla, S., *Proc. Natl. Acad. Sci.*, (2000) **23**, 12463-12468.
- Volkita, M., and Somerville, C. R. (1987) *J. Biol. Chem.* **262**, 15825-15828.
- Walsh, C. T., Schonbrunn, A., and Abeles, R., (1971), *J. Biol. Chem.*, **246**, 6855-6866.
- Welsh, F., PhD thesis, Flavocytochrome b_2 : Molecular Recognition, University of Edinburgh, 1998.
- White, P., Manson, F. D. C., Brunt, C. E., Chapman, S. K., and Reid, G. A. (1993) *Biochem. J.* **291**, 89-94).
- Xia, Z. X., and Mathews, F. S. (1990) *J. Mol. Biol.* **212**, 837-863.

Chapter 4

Introduction to Flavocytochrome c_3

4.0 Introduction

Shewanella frigidimarina is a facultative anaerobe that can respire anaerobically using an extremely broad range of terminal electron acceptors. These include metal oxides of Fe^{3+} and Mn^{4+} , thiosulphates, sulphates, sulphites and elemental sulphur, nitrates and nitrites, DMSO, TMAO and fumarate. Anaerobic growth of *S. frigidimarina* on fumarate results in the synthesis of several cytochromes, the most abundant of which is flavocytochrome c_3 (Morris *et al.*, 1994, Gordon *et al.*, 1998, Pealing *et al.*, 1992). This soluble periplasmic enzyme catalyses the reduction of fumarate to succinate (Figure 4.1). An isozyme of flavocytochrome c_3 , ifc_3 is expressed when *S. frigidimarina* is grown anaerobically in the presence of iron (50 mM iron citrate) but not in the presence of fumarate (Dobbin *et al.*, 1999). Similarly *Shewanella putrefaciens* MR1 expresses a fumarate reductase during anaerobic growth on fumarate (Myers and Myers, 1992, 1997b). This enzyme, also a flavocytochrome c_3 , is termed fcc_3 -MR1. In contrast to *Shewanella*, *E. coli* produces a membrane bound fumarate reductase. This enzyme expressed by the frdABCD operon (Zientz *et al.*, 1998, Cole *et al.*, 1985, Dickie and Weiner 1979, van Hellemond 1994) under anaerobic conditions is closely related in structure and function to succinate dehydrogenase which plays a prominent role as complex II of the aerobic respiratory chain (Rossi *et al.*, 1964, Cole 1982, Maklashina *et al.*, 1998). Succinate dehydrogenase (SDH) is expressed maximally during aerobic growth by the sdhABCD operon while the frdABCD operon is repressed. It couples the oxidation of succinate to fumarate with the reduction of quinone to quinol (Ackrell *et al.*, 1993, Cooley *et al.*, 2000).

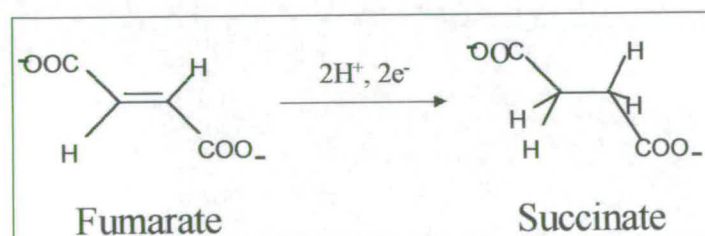


Figure 4.1 Fumarate reductases catalyse the reduction of fumarate to succinate.

4.1 Comparison of Fumarate Reductases

The recent determination of the crystal structures of the membrane bound fumarate reductases from *E. coli* (Iverson *et al.*, 1999) and *W. succinogenes* (Lancaster *et al.*, 1999), and the soluble flavoenzyme L-aspartate oxidase (LASPO) (Mattevi *et al.*, 1999) also from *E. coli* along with the flavocytochromes c_3 of *Shewanella frigidimarina* (Bamford *et al.*, 1999b, Taylor *et al.*, 1999) and *S. putrefaciens* (Leys *et al.*, 1999) allow aspects of the structure-function relationship to be examined. A summary of the different enzymes for which crystal structures are available is given in Table 4.1.

Organism	Enzyme	Location	Redox centres	FAD - binding
<i>E. coli</i>	FRD	Membrane bound	FAD [2Fe:2S], [4Fe:4S], [3Fe:4S], Q _P , Q _D	Covalent
<i>W. succinogenes</i>	FRD	Membrane bound	FAD, [2Fe:2S], [4Fe:4S], [3Fe:4S], 2 <i>b</i> -type haems	Covalent
<i>S. frigidimarina</i> NCIMB400	Fcc ₃	Periplasm Soluble	FAD 4 <i>c</i> -type haems	Non-covalent
<i>S. putrefaciens</i> MR1	Fcc ₃ -MR1	Periplasm Soluble	FAD 4 <i>c</i> -type haems	Non-covalent
<i>E. coli</i>	L-Aspartate oxidase (LASPO)	Soluble	FAD	Non-covalent
<i>S. frigidimarina</i> NCIMB400	Iron induced Ifc ₃	Periplasm Soluble	FAD 4 <i>c</i> -type haems	Non-covalent

Table 4.1 Comparison of the structure and redox cofactors contained within the fumarate reductases from *E. coli*, *W. succinogenes*, *S. frigidimarina*, and *S. putrefaciens*.

The flavocytochromes c_3 and LASPO are soluble fumarate reductases that contain non-covalently bound FAD. The reaction catalysed by these enzymes is essentially unidirectional. In contrast, the fumarate reductases from *E. coli* and *W. succinogenes* contain covalently bound FAD and the reaction is reversible. The interaction of the FAD with the protein environment and covalent linkage combine to raise the redox

potential of free FAD (-219 mV) to allow reduction of succinate (Blautt *et al.*, 1989). Thus the E_m of FAD/FADH₂ couple in fcc_3 (-152 mV) and LASPO (-216 mV) is appreciably lower than in, for example *W. succinogenes* (-20 mV) and *E. coli* (-55 mV) fumarate reductases.

4.1.1 Global structure

The crystal structure of flavocytochrome c_3 has been solved to 1.8 Å resolution (Taylor *et al.*, 1999). Flavocytochrome c_3 (fcc_3) is composed of a single polypeptide chain (M_r 63800) that forms three distinct domains (Figure 5.2). The N-terminal cytochrome domain (residues 1-107) contains four c -type haems. The flavin domain (residues 108-364, 503-568) contains a molecule of non-covalently bound FAD. The overall fold of the FAD binding region has structural and topological similarities with known FAD binding proteins, though sequence similarity is quite low. Buried within the flavin domain is an octahedrally coordinated sodium ion which is close to the active site. The haem domain contains four c -type haems which, together with the FAD, form a 40 Å 'molecular wire' providing efficient electron transfer to the active site. The clamp domain (residues 365-502) controls access to the active site. The isozyme of flavocytochrome c_3 , ifc_3 (Bamford *et al.*, 1999b) and the fumarate reductase from *S. putrefaciens* are essentially identical to fcc_3 . The crystal structure of the uncomplexed ifc_3 enzyme has been determined at 2.15 Å resolution (Figure 4.4). The fumarate reductase from *S. putrefaciens* MR1 (fcc_3 -MR1), also a flavocytochrome c_3 , shares 59% sequence identity with fcc_3 from *S. frigidimarina*. The same overall domain structure is observed but Leys *et al.*, (1999) distinguish a small section (domain IV residues 195-251) from the rest of the FAD binding domain (residues 125-168, 252-362). The clamp domain is, in the case of fcc_3 -MR1, termed the capping domain (residues 363-502) and these two terms shall be used interchangeably. The haem domain consists of residues 1-104. The crystal structure of this enzyme has been solved for the uncomplexed form (2.9 Å resolution), with fumarate bound (2.8 Å resolution, Figure 4.3) and with succinate bound (2.5 Å resolution) (Leys *et al.*, 1999).

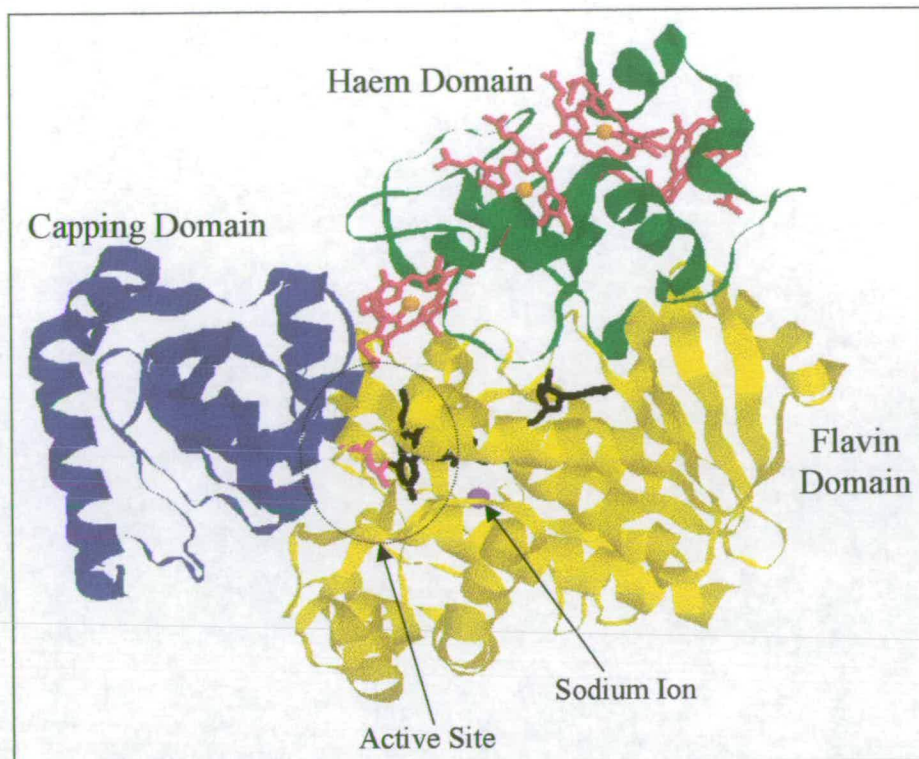


Figure 4.2 The crystal structure of flavocytochrome c_3 highlighting the flavin domain (yellow), the clamp domain (blue) and the haem domain (green). The active site located in the flavin domain is bordered on one side by FAD (black) and contains a malate-like molecule (pink). A structural sodium ion (purple) is buried in the flavin domain close to the active site. Four c -type haems (red) together with the FAD direct electrons to the active site for fumarate reduction.

L-aspartate oxidase is a flavoprotein that catalyses the oxidation of L-aspartate to iminoaspartate (Nasu *et al.*, 1982). It displays the ability to use fumarate as electron acceptor, so that the enzyme can function as an L-aspartate/fumarate oxidoreductase (Tedeschi *et al.*, 1999). This soluble enzyme has 30 % sequence identity with the flavoprotein subunit of the membrane bound fumarate reductase from *E. coli* and is related to the soluble fumarate reductases from *Shewanella* (Tedeschi *et al.*, 1996). The structure of the apof orm of L-aspartate oxidase from *E. coli* has been determined to 2.2 Å resolution (Bachela *et al.*, 1999, Mattevi *et al.*, 1999, Figure 4.3). The ability of LASPO to utilise fumarate but not succinate is in accordance with the non-covalent attachment of FAD. LASPO folds into three domains: the FAD binding domain (residues 2-241 and 353-410), the capping domain (242-352) and the helical domain (414-533). The interface between the FAD-binding domain and capping-domain

defines a cleft in which the active site is located. The capping domain establishes almost no interactions with the rest of the protein. FAD is bound relatively weakly ($K_m=0.67 \mu\text{M}$) in LASPO so dissociation of the cofactor in the crystal structure was not unexpected (Mortarino *et al.*, 1996).

The structures of the fumarate reductase from the facultative anaerobe *E. coli* (3.3 Å resolution) and the obligate anaerobe *Wolinella succinogenes* (2.2 Å resolution) both contain membrane spanning hydrophobic regions and an extramembrane hydrophilic region (Figure 4.3, Ohnishi *et al.*, 2000). The *E. coli* enzyme consists of four non-identical subunits (Robinson and Weiner 1982, Dickie and Weiner 1979, Cole *et al.*, 1985); a membrane extrinsic catalytic domain comprising FrdA (73 kDa) and FrdB, and a membrane intrinsic hydrophobic domain comprising FrdC and FrdD. FrdA contains one molecule of covalently bound FAD and is closely related to the flavin domain of the soluble fumarate reductases. The fumarate reductase from *W. succinogenes* encoded by the frdABC operon consists of three subunits (Simon *et al.*, 1998, Lorenzen *et al.*, 1993, Lancaster *et al.*, 1999); a flavoprotein subunit (subunit A, 73 kDa), a subunit containing three iron sulphur clusters and a membrane spanning subunit. Subunit A contains the site of fumarate reduction and a molecule of covalently bound FAD, subunit B contains three iron sulphur centres, the menaquinone oxidising subunit C consists of five membrane spanning helices and binds two *b*-type haems (Geisler *et al.*, 1993). These fumarate reductases most closely resemble the succinate dehydrogenase enzyme of the TCA cycle. Succinate dehydrogenase consists of a flavoprotein subunit (SdhA) which contains covalently bound FAD and the dicarboxylic acid binding site and an iron-sulphur protein subunit (SdhB) containing three distinct iron-sulphur clusters (Cammack *et al.*, 1992). This domain is bound to two small integral membrane subunits (SdhC and SdhD) which are necessary to form the quinone binding sites found in both FRD and SDH (Cecchini *et al.*, 1986a).

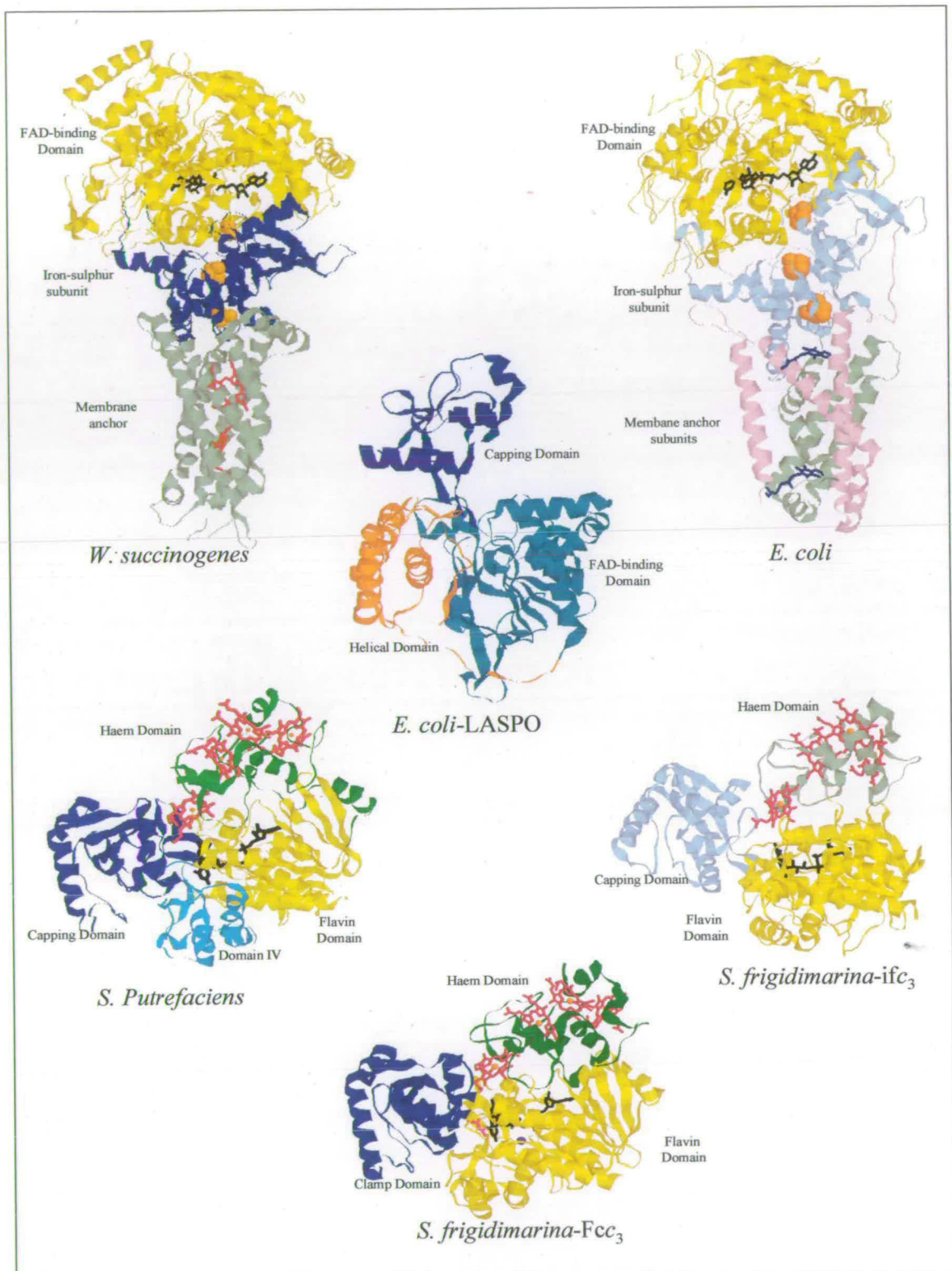


Figure 5.3 Structural comparison of the membrane bound fumarate reductases from *W. succinogenes* and *E. coli* with the soluble flavocytochromes c_3 from *S. frigidimarina* and *S. putrefaciens*, the isozyme of flavocytochrome c_3 from *S. frigidimarina* and L-aspartate oxidase from *E. coli*.

4.1.2 Flavoprotein Subunit

The flavin domain of fcc_3 contains a sodium ion octahedrally co-ordinated to four backbone carbonyls and two water molecules (Figure 4.4). Ligands are provided by Thr506, Met507, Gly508 and Glu534, the latter also hydrogen bonds to the FAD. A water molecule hydrogen bonds to His505 which lies adjacent to His504, a residue which is involved in the binding of fumarate. A sodium ion has also been found in the crystal structure of the tryptophan synthase $\alpha_2\beta_2$ complex (Rhee *et al.*, 1996). It has been suggested that this sodium ion plays a structural as well as a regulatory role. Therefore, in fcc_3 , the sodium ion could affect the potential of the FAD, substrate binding and the pK_a of His504.

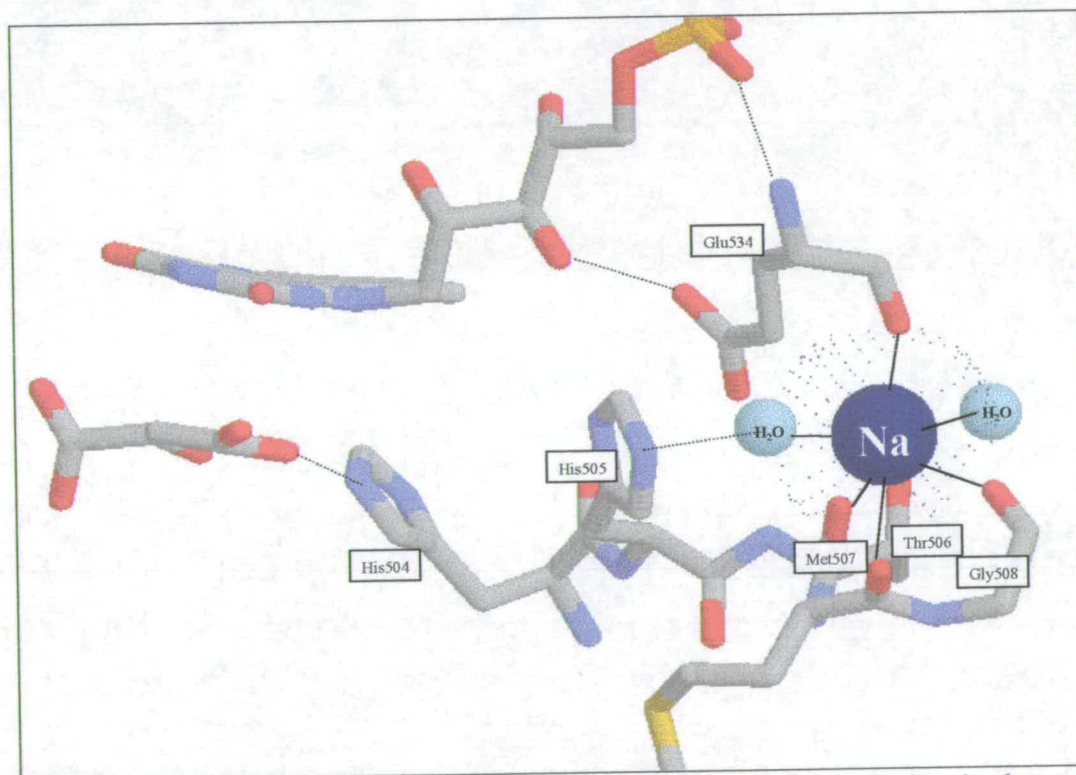


Figure 4.4 An octahedrally coordinated sodium ion is found buried in the flavin domain close to the active site. Ligands are provided by four backbone carbonyls from Met507, Thr506, Gly508 and Glu534. Two water molecules complete the coordination sphere.

The flavin binding subunit of the *E. coli* and *W. succinogenes* fumarate reductases bear striking resemblance to the soluble fumarate reductases from *Shewanella*. In *E. coli* the flavoprotein subunit (subunit A) is comprised of four domains (Cole 1982, Iverson *et al.*, 1999). The large FAD binding domain (residues 1-50, 130-231 and 354-414) and three other domains comprised of residues 51-129, 232-353 and 415-575. The flavoprotein subunit of *W. succinogenes* also contains a similar arrangement of four domains; the FAD domain (1-260 and 366-436), a capping domain (residues 260-366), a helical domain (residues 436-554) and C-terminal domain (residues 554-655). Strict conservation of active site residues indicates that the same mechanism operates within this family of fumarate reductases and succinate dehydrogenases (Schröder *et al.*, 1991, Figure 4.5).

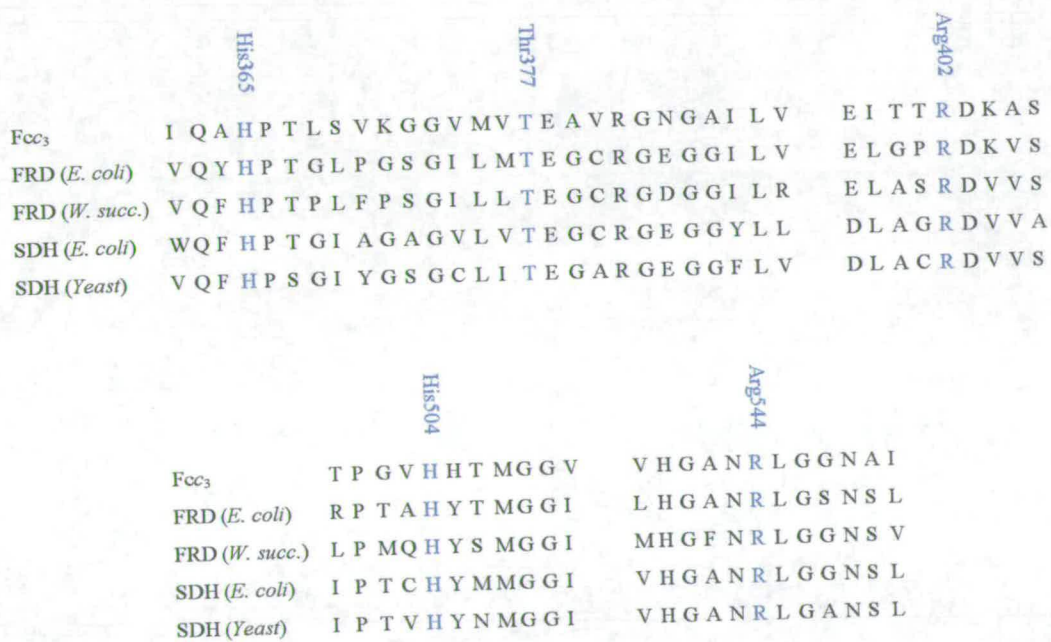


Figure 4.5 Conservation of active site residues in the fumarate reductases and succinate dehydrogenases. The sequence of fcc₃ is aligned with the corresponding region of the flavoprotein subunits of the fumarate reductases from *W. succinogenes*, *E. coli*, and the succinate dehydrogenases from *E. coli*, and *S. cerevisiae* (Arikawa *et al.*, 1998). The conserved residues are highlighted; His365 and Thr377, Arg402, His504 and Arg544.

4.1.2.1 Mechanism

The high resolution of the crystal structure of fcc_3 and the presence of a malate-like molecule in the active site has enabled a mechanism (Figure 4.7) to be proposed (Taylor *et al.*, 1999, Reid *et al.*, 2000). Catalysis is initiated by fumarate binding in the active site. The C4 carboxyl group is bound in a very polar environment forming two hydrogen bonds to Arg544 and one each to His504 and Arg402. The second carboxylate twists out of the plane of the molecule and forms hydrogen bonds to His365 and Thr377. Steric constraints imposed by the side chains of Met236 and Met375 are then removed resulting in closure of the clamp domain. The combination of these effects results in polarisation of the C2-C3 double bond and creates a δ^+ charge at C2. Catalysis is initiated by transfer of a hydride from the FAD (N5) to C2, a distance of 3.35 Å. The transient carbanion intermediate is stabilised by His504. Proton donation from Arg402 to C3 then occurs resulting in the formation of succinate. The malate-like molecule found in the active site is tightly bound and inaccessible to solvent. The crystallisation medium contained 10 mM fumarate, well above the K_m of 25 μ M. Therefore fumarate might be expected to occupy the active site. However under oxidising conditions hydride transfer is not possible and instead nucleophilic attack at C2 by a water molecule has occurred. A hydride would be transferred to the *si*-side of fumarate but with this approach blocked by the FAD the water molecule has attacked from the *re*-side of fumarate leading to the intermediate with R stereochemistry.

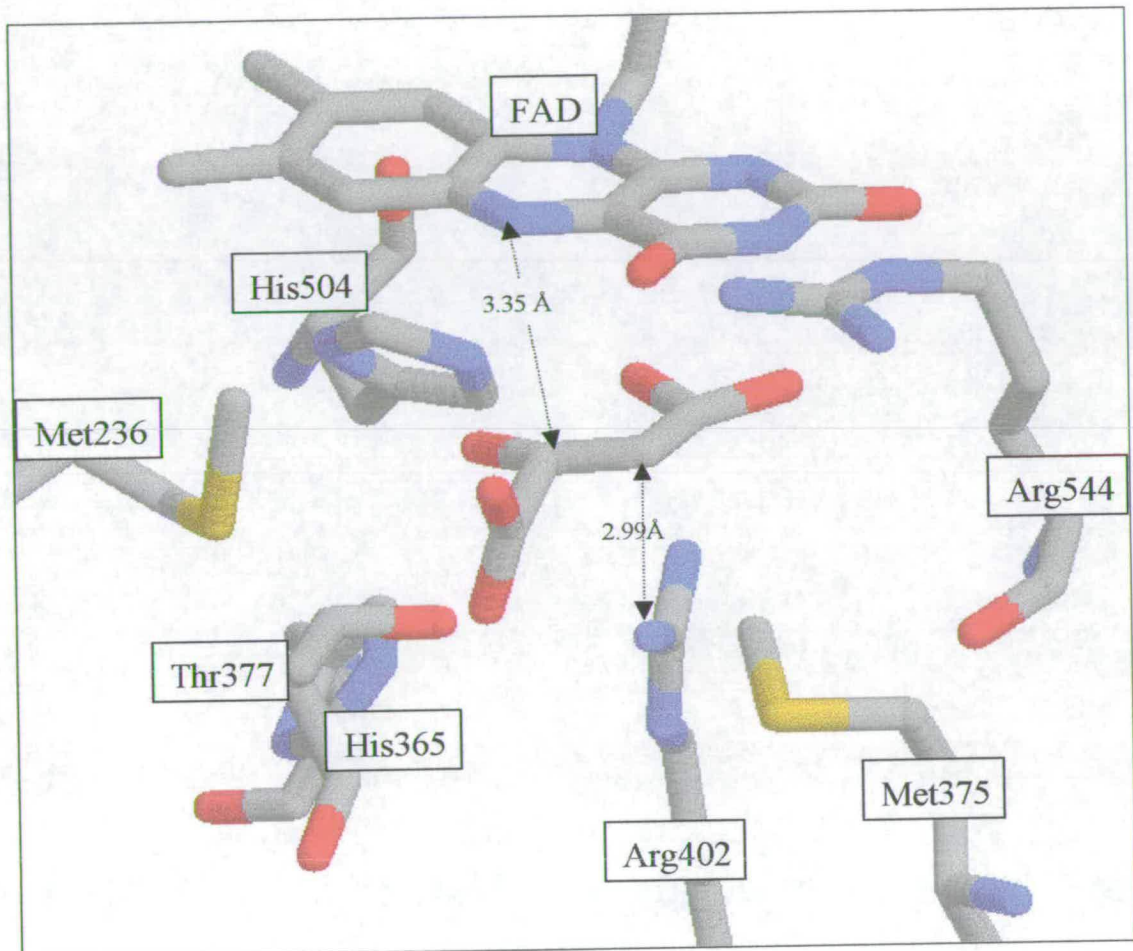


Figure 4.6 The active site of flavocytochrome c_3 containing a malate-like molecule. Distances for hydride transfer (Arg402 \rightarrow C3) and proton transfer (FAD(N5) \rightarrow C2) are shown.

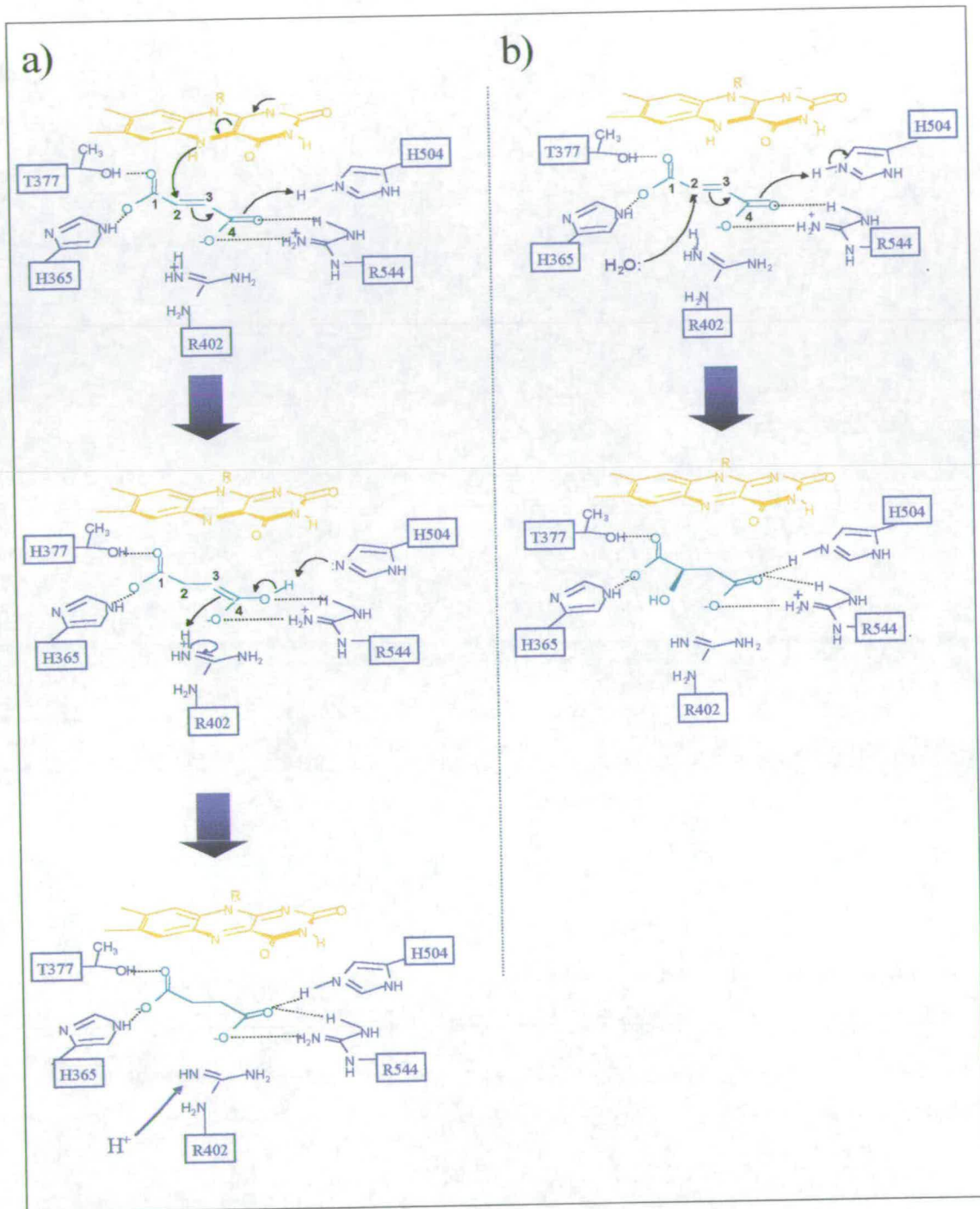


Figure 4.7 a) Schematic representation of the mechanism of fumarate reduction by Fcc₃, b) Formation of the hydrated intermediate found at the active site in the crystal structure of fcc₃.

4.1.2.2 Proton Delivery

Since the active site is inaccessible to solvent, proton delivery to Arg402 occurs via a pathway of residues (Figure 4.8). Glu378, the central residue in this pathway, forms hydrogen bonds from the same carboxylate oxygen to Arg381 and Arg402. These three residues are completely conserved, consistent with this essential function. Mutation of Arg381 to lysine was found to lower the k_{cat} 100-fold and mutation of Glu378 to alanine resulted in complete loss of activity (M. Doherty PhD thesis 1999).

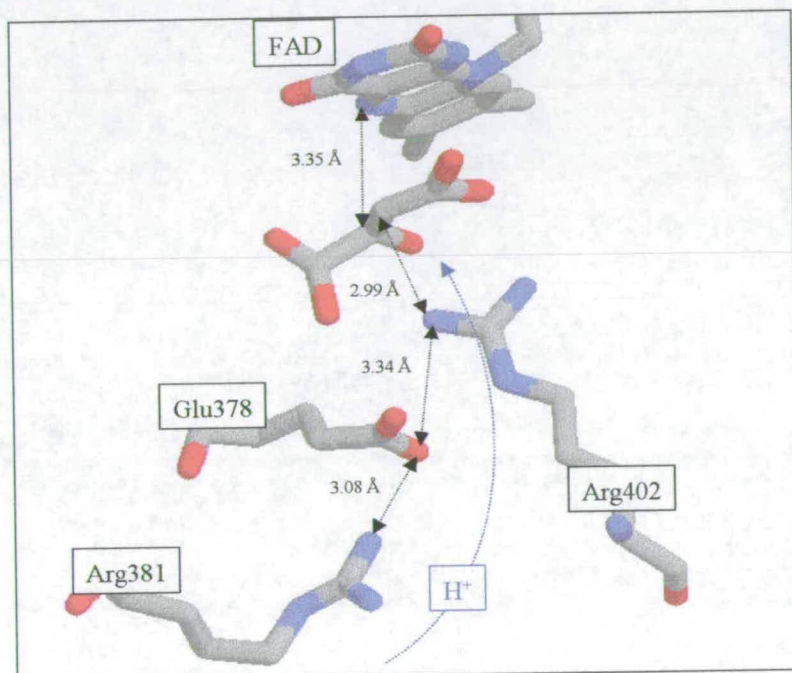


Figure 4.8 Arg381, Glu378 and Arg402 form a triad of residues which deliver protons to the active site.

The dicarboxylic acids found at the active site of the fumarate reductases from *W. succinogenes*, *E. coli* and *Shewanella* all adopt a conformation in which the second carboxyl group is twisted out of plane of the molecule (Figure 4.9). The fumarate reductase from *W. succinogenes* also shows some divergence in the positions of conserved residues. Although in this case fumarate is bound at the active site the enzyme is trapped in a slightly open conformation in the crystal structure. The location of active-site residues resembles more closely the open conformation of ifc_3 than the catalytically active closed form of the enzyme in the substrate bound fumarate reductases.

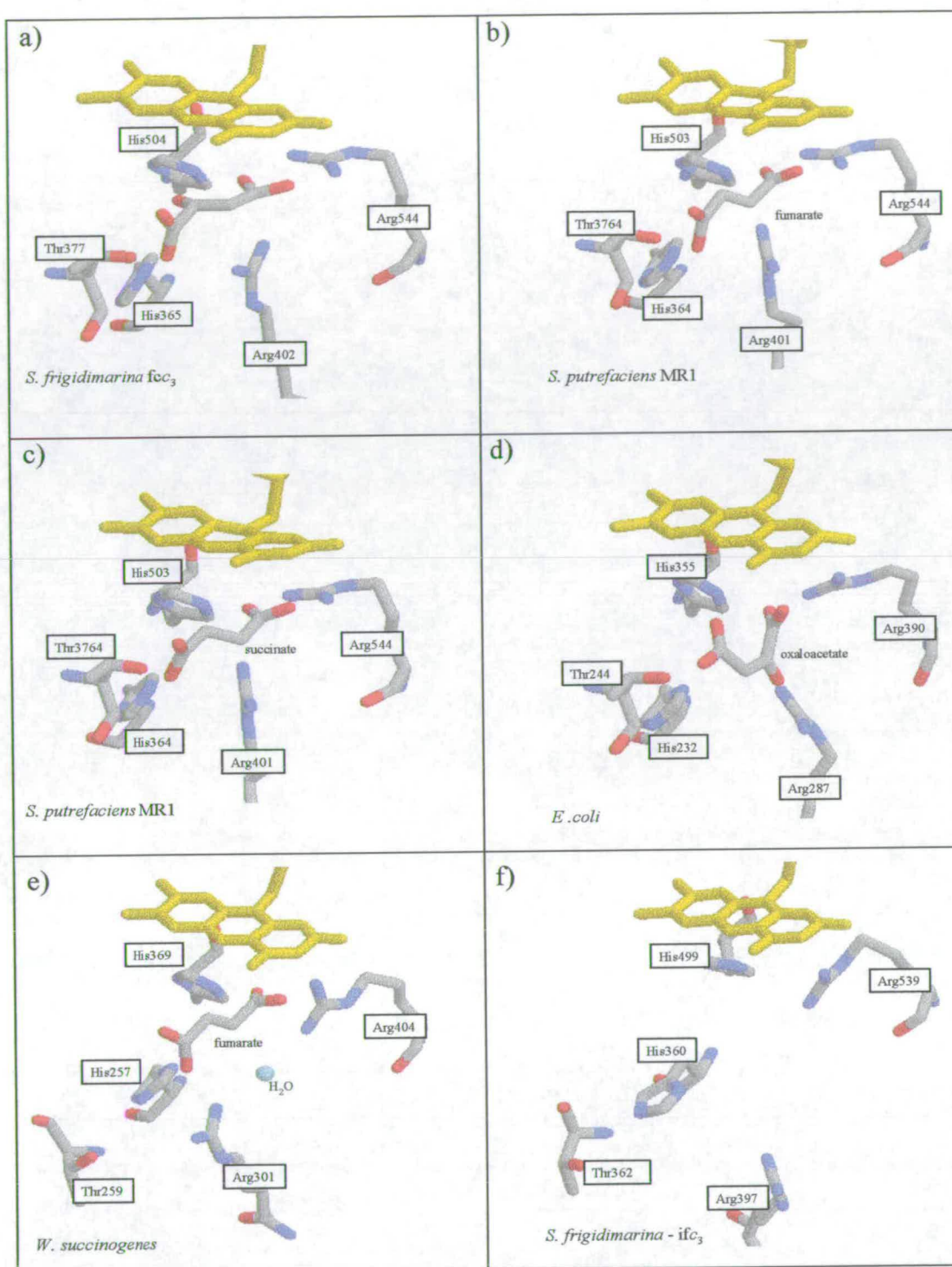


Figure 4.9 Comparison of the active site structures of fcc_3 (a) in which a malate-like molecule is bound with the fumarate reductases from *S. putrefaciens* complexed with fumarate (b) and succinate (c), *E. coli* complexed with oxaloacetate (d) *W. succinogenes* complexed with fumarate (e) and the open conformation of ifc_3 (f).

4.1.3 The Clamp Domain

Fcc_3 has been crystallised in the closed conformation with the active site inaccessible to solvent. Evidence from the structures of LASPO (Mattevi *et al.*, 1999) and Fcc_3 -MR1 (Leys *et al.*, 1999) indicates that movement of the clamp domain facilitates access to the active site. In LASPO the orientation of the capping domain may well reflect the open conformation of this protein (Figure 4.22). However it is feasible that it could adopt different conformations leading to the opening and closing of the active site cleft. Arg236 is positioned on α -helix 1 of the capping domain and points with its side chain to the active site cleft. His244 is located in proximity to the flavin binding site. On the basis of the LASPO apoenzyme structure, it is impossible to assign a specific role to the residues in the active site. Nevertheless, the presence of three conserved arginine residues (Arg236, Arg290, Arg386) and two conserved histidine residues (His244 and His351) in proximity to the active site is consistent with the mechanism of fumarate reduction proposed. The different structures available for fcc_3 -MR1 also indicate movement of the capping domain. In the uncomplexed enzyme the capping domain is rotated by approximately 12° relative to the capping domain of the fumarate bound enzyme and by 3° relative to the succinate complexed enzyme (Leys *et al.*, 1999, Figure 4.10). As the rotation axis is close to the active site movement near the substrate is small. This observation suggests that in solution, the capping domain can rotate about a hinge resulting in a transiently enlarged cleft allowing access to the active site.

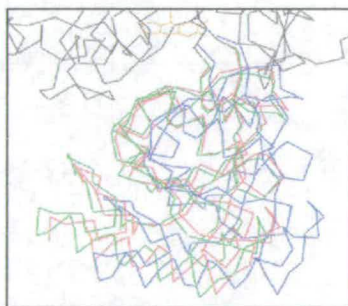


Figure 4.10 The position of the clamp domain in the structures of flavocytochrome c_3 from *S. putrefaciens* for the open form (blue), complexed with fumarate (red) and closed but no substrate present (green).

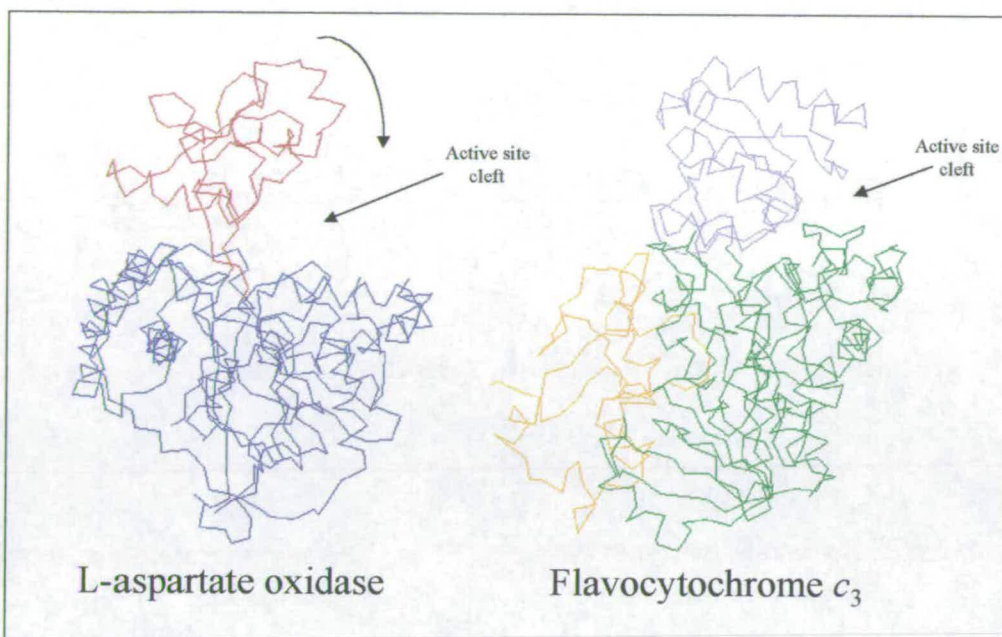


Figure 4.11 Comparison of the clamp domain positions of L-aspartate oxidase (open conformation) and flavocytochrome c_3 (closed conformation)

4.1.4 The Haem Domain

The haem domain of fcc_3 contains four c -type haems (Figure 4.12) each covalently linked to two cysteines in a CxxCH motif. Two histidines provide the fifth and sixth ligands (Pealing *et al.*, 1995). The potentials of the cofactors have been determined by redox potentiometry and protein film voltametry studies (Turner *et al.*, 1999). At pH 7.2 the FAD was found to have a reduction potential of -152 mV. The potential of the FAD was shown to vary with pH whereas the haems potentials (-238 mV, -196 mV, -146 mV, -102 mV) were found to be essentially independent of pH. The assignment of reduction potentials to individual haems is not possible using these techniques. However a similar structural arrangement of haems is found in cytochrome c_3 , a small electron transfer protein (11.8 kDa) also from *S. frigidimarina* (Tsapin *et al.*, 1996, Pike 1998). This protein is closely related to the haem domain of fcc_3 (Reid *et al.*, 1998). The three dimensional solution structure of the reduced enzyme has been determined using 2D $^1\text{H-NMR}$. The haems form a similar arrangement to those of fcc_3 (Figure 4.13). By monitoring the signals for each haem

as the protein was oxidised it was possible to correlate particular reduction potentials to the signals arising from individual haems. The reduction potentials were assigned in order of most readily oxidised as, haemIV (-58 mV), haemII (-113 mV), haemI (-184 mV) and haemIII (-223 mV). The close proximity of the redox centers assures sub-millisecond tunnelling rates through the sequence of cofactors despite the low reduction potential of haem3. Analogous chains with a mix of substantial endergonic and exergonic steps can be found in the iron sulphur cluster chain of NiFe hydrogenase and the haem chain of the photosynthetic reaction centre of *B. viridis* (Chen, I. P. *et al.*, 2000).

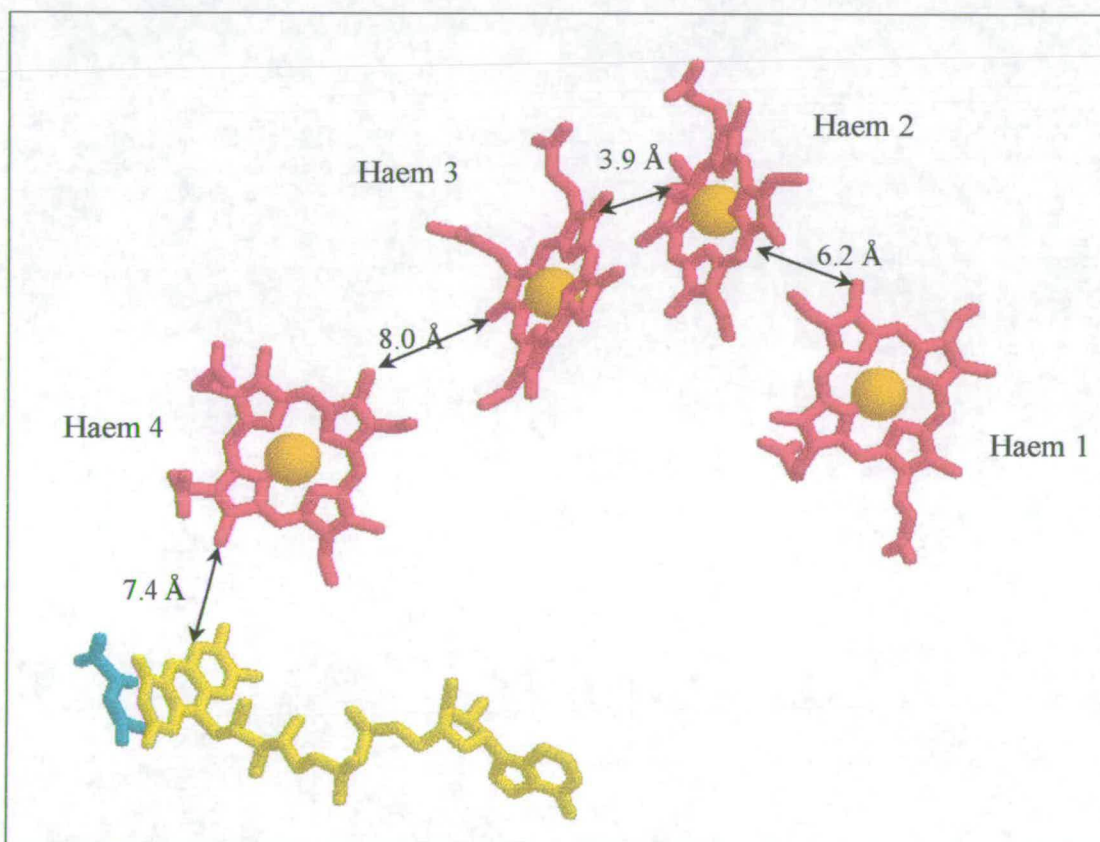


Figure 4.12 The arrangement of *c*-type haems and FAD which together form a 40 Å 'molecular wire' for efficient transfer of electrons to the active site. Edge-to-edge distances between redox cofactors are all 8Å or less.

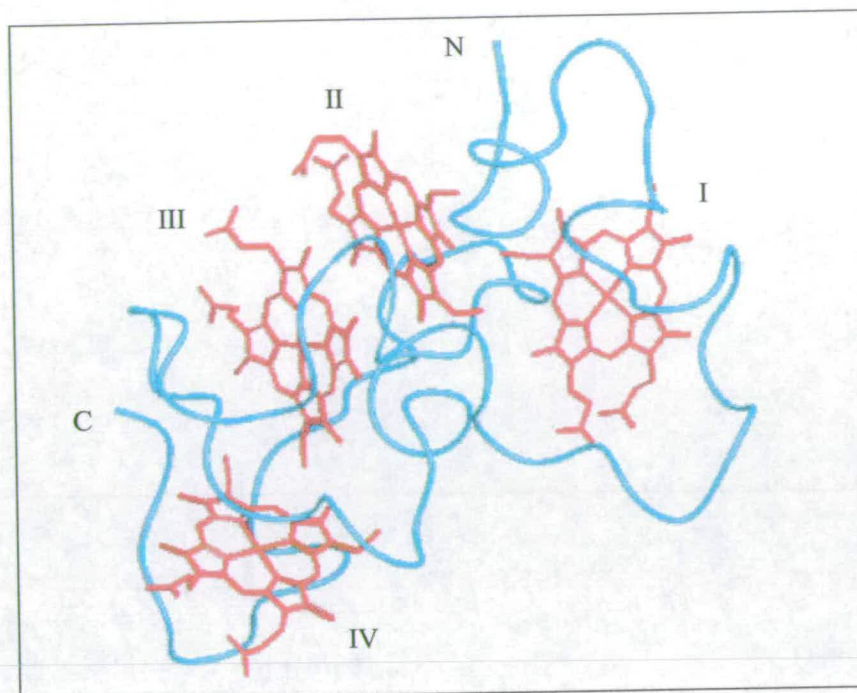


Figure 4.13 The NMR structure of cytochrome c_3 from *S. frigidimarina* which has a similar arrangement of haems to flavocytochrome c_3 .

4.1.5 The Membrane Anchor Subunits

The membrane anchor domain (subunit C) of the *E. coli* fumarate reductase contains two menaquinones which are located on opposite sides of the membrane-spanning region (Figure 4.14). Subunit B containing three iron sulphur clusters is solvent exposed. The six redox cofactors are organised into a chain with the sequence FAD-[2Fe:2S]-[4Fe:4S]-[3Fe:4S]-Qp-QD (Cecchini *et al.*, 1995, Weiner *et al.*, 1986, Werth *et al.*, 1990, Rothery and Weiner 1998, Simpkin *et al.*, 1985, Spencer *et al.*, 1973, Cammack *et al.*, 1986, Kowal *et al.*, 1995, Heering *et al.*, 1997, Tsapin 1995). With the exception of the 27 Å spacing between the two menaquinones, the redox cofactors are all separated by ~11-14 Å center to center distances. The membrane bound domain of the fumarate reductase from *W. succinogenes* also possesses three iron sulphur clusters but in addition two *b*-type haems (Lancaster *et al.*, 1999, 2000, Figure 4.15). The iron sulphur clusters: [2Fe-2S], [4Fe-4S] and [3Fe:4S] are coordinated by cysteine residues. The [3Fe:4S] centre is within segments that contact subunit C, which is comprised of five membrane spanning helices. The *b*-haems are

bound approximately perpendicular to the membrane surface. The axial histidine ligands to the haems are provided from the adjacent protein helices (Vibat *et al.*, 1998). Hydrogen bonds and salt bridges form between the haems and all four transmembrane helices. Distances of 9-12 Å are appropriate for the efficient transfer between FAD and quinone.

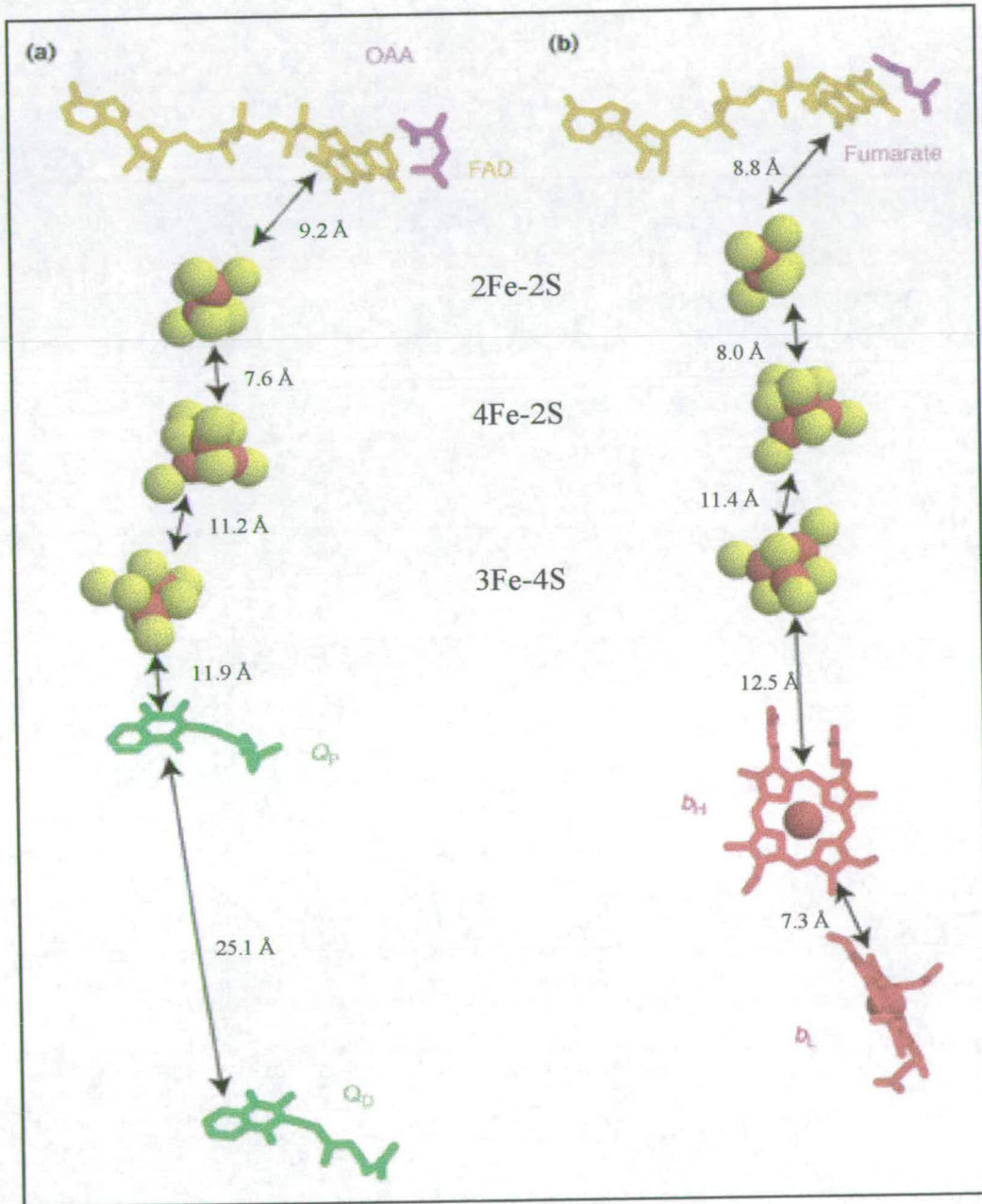


Figure 5.14 Redox cofactors found in the membrane bound fumarate reductases from *E. coli* (a) *W. succinogenes* (b). Q_p = proximal menaquinone, Q_d = distal menaquinone. OAA= oxaloacetate.

4.1.6 Electron Donors

E. coli is able to synthesise a variety of different quinones (Figure 4.16) which form an electron donor/acceptor pool (van Hellemond *et al.*, 1995). The cytoplasmic pH of *E. coli* is maintained between 7.6 and 7.8 and the composition of the quinone pool is controlled by oxygen. Aerobic growth induces ubiquinone production and represses menaquinone biosynthesis. In order to reduce terminal substrates which are lower in potential than oxygen under anaerobic conditions, menaquinones (-74 mV) and dimethylmenaquinone (+36 mV) predominate in the cell membrane. Fumarate reductases accept electrons from menaquinone ($E=-74$ mV) and dimethylmenaquinone ($E=+34$ mV) whereas succinate dehydrogenase transfers electrons to ubiquinone (Ohnishi *et al.*, 2000) which has a higher standard reduction potential ($E=+100$ mV). Menaquinone is reoxidised by fumarate reductase only in the presence of the membrane anchor subunits C and D (Zhao *et al.*, 1999, Cecchini *et al.*, 1986a, 1986b, Sucheta *et al.*, 1993). Analogous membrane-bound functions were discovered in SDH which reduces ubiquinone to ubiquinol.

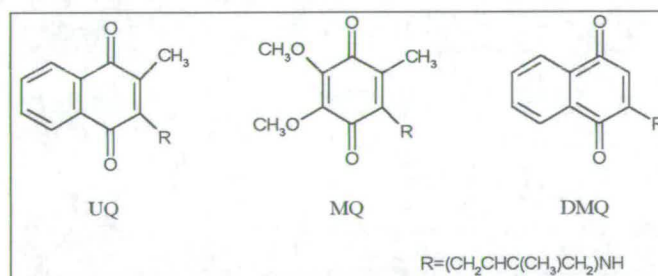


Figure 4.16 Ubiquinone (UQ), menaquinone (MQ) and dimethylmenaquinone (DMQ) are present in *E. coli*. R indicates a poly-isoprenyl chain.

The fumarate reductases of *S. frigidimarina* and *S. putrefaciens* are found in the periplasm and the physiological electron donor has not been determined. Electron transfer proteins in the periplasm could be one means of establishing a link between the quinol pool and the electron transport chain that supplies electrons to fcc_3 . CymA is a small cytochrome that is expressed by *Shewanella* during anaerobic growth

(Myers and Myers 1997a). The exact function of *cymA* is not established but studies with *S. putrefaciens* MR1 have shown it to be a requirement for anaerobic growth on fumarate (Myers and Myers 2000). It could therefore be an electron donor to the respiratory chain or direct to fcc_3 . The prominent position of the haems in fcc_3 , in which at least three are highly accessible to solvent, indicates that they would be easily reduced by a redox partner of suitable potential.

4.2 Project Aims

The aim of this project is to investigate the catalytic mechanism of fumarate reduction in flavocytochrome c_3 . The following areas are studied: i) The roles of active site residues in Michaelis complex formation; ii) Substrate specificity; iii) Differences in the active site structure of the open and closed conformation of the enzyme using inhibition experiments iv) To determine the identity of the active-site acid; v) The possibility of substituting other residues for the active site acid; vi) To elucidate whether the mechanism is a concerted or stepwise process.

Chapter 5
Materials and Methods

5.0 Materials and Methods

5.1 Media and Solutions

5.1.1 Growth Media (High Salt Luria Broth)

Bacto Tryptone	10 g
Yeast Extract	5 g
Sodium Chloride	10 g

All media was sterilised at 121 °C for twenty minutes in a Kestral autoclave prior to use. Antibiotics were added immediately prior to use from stock solutions giving final concentrations of 50 mg l⁻¹ streptomycin sulfate and 50 mg l⁻¹ kanamycin.

5.1.2 Buffers

50 mM Tris.HCl pH 7-9, I=0.5 M (Tris[hydroxymethyl]aminoethane)

dH ₂ O	500 ml
Trisma base	6.05 g
NaCl	5.265 g

Adjusted to required pH using 1M HCl and volume to 1 l with dH₂O

50 mM CHES pH 8.6-10, I= 0.5 M (2-[N-Cyclohexylamino]ethane sulfonic acid)

dH ₂ O	500 ml
CHES	10.36 g
NaCl	5.265 g

Adjusted to required pH using 1M NaOH and volume to 1 l with dH₂O

50 mM MES pH 5.5-6.7, I= 0.5 M (2-[N-Morpholino]ethanesulfonic acid)

dH ₂ O	500 ml
MES	10.66 g
NaCl	5.265 g

Adjusted to required pH using 1M NaOH and volume to 1 l with dH₂O

50 mM MOPS pH 6.5-7.9, I= 0.5 M (3-[N-Morpholino]propanesulfonic acid)dH₂O 500 ml

MOPS 10.46 g

NaCl 5.265 g

Adjusted to required pH using 1M NaOH and volume to 1 l with dH₂O.**Lysis Buffer**

10 mM Tris.HCl pH 7.0.

10 mM L-lactate

10 mM EDTA

1 mM PMSF

0.2 mg/ml egg white lysozyme

3 × SDS gel-loading buffer

50 mM Tris.HCl pH 6.8

100 mM dithiothreitol

2 % SDS (electrophoresis grade)

0.1 % bromophenol blue

10 % glycerol

SDS resolving Buffer (1.5 M Tris.HCl pH 8.8)

Tris 181.6 g

SDS 4.0 g

dH₂O 400 mladjust to pH 8.8 with 1M HCl and adjust volume to 1 l with dH₂O**Stacking Buffer (0.5 M Tris.HCl pH 6.8)**

Tris 30.28 g

SDS 2.0 g

dH₂O 450 mladjust to pH 6.8 with 1M HCl and adjust volume to 0.5 l with dH₂O

5×Tris glycine running buffer

Tris	15.1 g
glycine	94 g
SDS(10%)	50 ml

5.2 Protein Preparation

Recombinant enzyme was prepared using the pEGX₁/EG301 expression vector system (pEGX₁ plasmid - pMMB503EH fcc with signal sequence, EG301 - NCIMB 400 Rif^R, Δfcc:ahp Km^R). Bacterial Strains were stored long term as DMSO stocks (-80 °C) and up to two weeks on agar plates (+4 °C).

5.2.1 Growth of Recombinant and Mutant Forms of Fcc₃

Starter flasks (50 ml Luria Broth high salt media) containing kanamycin (50 mg l⁻¹) and streptomycin (25 mg l⁻¹) were grown overnight. Flasks (1 litre) containing 500 ml media, kanamycin (50 mg l⁻¹) and streptomycin (25 mg l⁻¹) were inoculated by the addition of 1 ml portions of starter culture and grown at 23 °C for 12 hours, 150 rpm. Cultures were then induced with IPTG (250 mg l⁻¹) and grown for 8 hours, 200 rpm. Cells were harvested by centrifugation at 8,000 rpm using a SLA1500 rotor and Sorval RC-5B centrifuge for 20 minutes and either frozen or used directly.

5.2.2 Protein Abstraction

Cells obtained from a 5 litre growth were resuspended in the minimum of lysis buffer and stirred for 1 hour at 4 °C. The cell solution was sonicated on ice at intensity 8-10 for 3 × 20 seconds using a MSE Soniprep150. The solution was centrifuged at 15,000 g for 20 minutes to remove cell debris. The supernatant was decanted off and precipitated with 40 % ammonium sulphate stirring at 4 °C for 2 hrs followed by

centrifugation for 15 minutes at 15,000 rpm (SS34 rotor, Sorval RC-5B centrifuge). The supernatant was retained and the ammonium sulphate concentration raised to 100%. After stirring at 4 °C for 2 hrs fcc_3 was collected by centrifuging for 15 minutes at 15,000 rpm (SS34 rotor, Sorval RC-5B centrifuge). The pellet was resuspended in the minimum volume of 10 mM Tris.HCl pH 8.4 and dialysed against several changes of buffer (~5-10 mM Tris.HCl pH 8.4).

5.2.3 Anion Exchange Chromatography (DE52)

Column material (DE52 Whatman) was resuspended in 0.1 M Tris.HCl pH 8.4 then equilibrated in 10 mM Tris.HCl pH 8.4. Protein solution was loaded onto a column 15 cm \times 4 cm diameter. Flavocytochrome c_3 bound over the top 2 cm indicated by a dark red band. The column was washed until the UV absorption at 270 nm was minimal (approx. 2 column volumes 10 mM Tris.HCl pH 8.4). A step gradient of 0.1 M NaCl increments was used for eluting protein.

5.2.4 Hydroxyapatite

Column material was prepared by equilibrating in 10 mM Tris.HCl pH 8.4. A column of length 4 cm \times 3 cm diameter was used. Protein solution was fully dialysed in 10 mM Tris.HCl pH 8.4 and concentrated to approximately 10 ml prior to loading. The column was washed with buffer until the absorption at 270 nm was minimal (approx. 2 column volumes) before eluting protein with 0.1 M K_2HPO_4 .

5.2.5 Gel Filtration Chromatography

Protein solution was concentrated to 5-10 mls before desalting by gel filtration chromatography (Sephadex G25). A column 15-20 cm \times 2 cm diameter was prepared with 10 mM Tris.HCl buffer pH 8.4 buffer. Buffer exchange into 10 mM MOPS pH 7.8 could also be carried out if the protein was to be further purified by FPLC.

5.2.6 FPLC

Protein for crystallisation was purified using an additional step. A resource Q column 25 mg, 1 ml capacity, was used. The column was equilibrated in 10 mM MOPS pH 7.8 using a flow rate of 4 ml/min with a pressure limit of 3 MPa. Protein was then loaded onto the column and washed with 5 ml of buffer. A linear gradient from 0 to 0.5 M NaCl over 20 ml was used to elute the protein. Fractions showing fumarate reductase activity and considered pure were combined. The column was regenerated by washing with 5 ml of 1M NaCl followed by 5 ml of 1 M NaOH, before washing with 5ml ethanol at a reduced flow rate of 1 ml/min prior to storing.

5.3 Purity Determination

Purity of flavocytochrome c_3 samples collected was assessed using a combination of spectrophotometric and electrophoretic techniques (Figure 5.1).

5.3.1 UV-Visible Spectroscopy

Spectra were obtained for oxidised and reduced flavocytochrome c_3 from 270 nm to 650 nm. A sample of known volume (typically 50-100 μ l) was diluted to 1 ml with 50 mM Tris.HCl buffer. The relative intensities of peaks were used to determine the level of purity of the sample. The intensity ratio of the haem peak (409 nm) to total protein present (270 nm) indicates the purity of the sample. A value of A_{409}/A_{280} greater than 4 is observed for pure protein. Reduced spectra were obtained on the addition of sodium dithionite. The Soret peak (418 nm) of the reduced sample was used to calculate the concentration of the protein sample ($\epsilon = 752800 \text{ cm}^{-1}$).

5.3.2 SDS Page Gel electrophoresis

	4 % Stacking Gel	10 % Separation Gel
dH ₂ O	3.05 μ l	4.02 ml
0.5 M Tris.HCl, pH 6.8	1.25 ml	-
1.5 M Tris.HCl, pH 8.8	-	2.5 ml
10% (w/v)SDS	50 μ l	100 μ l
Acrylamide (30 % stock)	0.65 ml	3.32 ml
Ammonium persulfate (10 %)	25 μ l	50 μ l
TEMED	8 μ l	5 μ l

The polyacrylamide gel was prepared in two phases, a stacking gel for the concentration of protein samples and a resolving gel for the separation of the protein samples. Gels were prepared by combining all solutions except initiators. Polymerisation was initiated by addition of TEMED and ammonium persulfate. The resolving gel was poured between two glass plates and overlaid with water saturated butanol. Once polymerised (30 minutes) the water saturated butanol was rinsed off with distilled water and the stacking gel was prepared. The stacking gel was mixed and then poured on top of the resolving gel. A comb was then inserted into the top of the stacking gel and the gel was allowed to polymerise for 30 minutes. Once polymerised the gel was clamped into a vertical electrophoresis tank with 1 \times running buffer. The comb was then carefully removed and the protein samples were loaded into the wells with one lane reserved for prestained protein markers (BioLabs, broadrange). Empty lanes were filled with loading buffer to ensure smooth running of samples. Gels were run at 180 volts for 45 minutes. The gels were stained with 1% Coomassie blue in 40 % MeOH/10 % HOAc for 30 minutes followed by destaining in 40 % MeOH/10 % HOAc until bands became visible (1-3 hours).

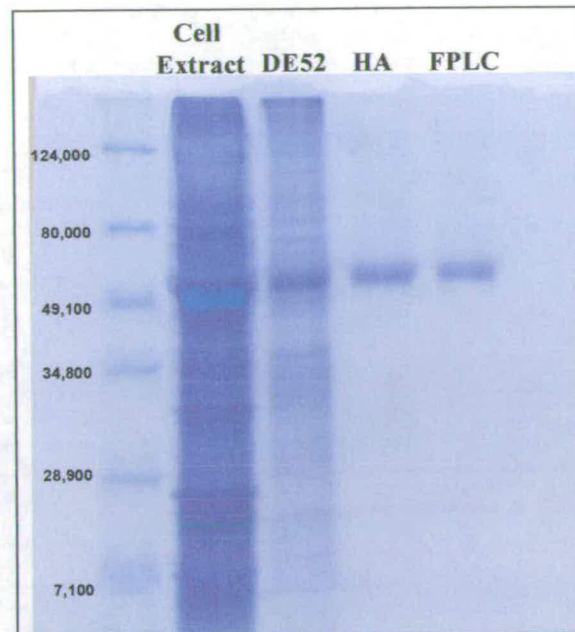


Figure 5. 1 Steps in the purification procedure. Crude cell extract, after anion exchange chromatography (DE52), after hydroxyapatite column (HA) and after FPLC.

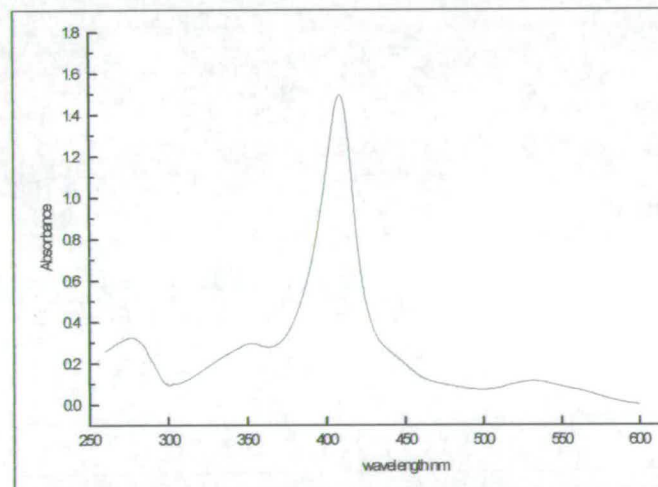


Figure 5.2 UV/vis spectrum of purified flavocytochrome c_3

5.3.4 FAD Content Determination

FAD content was determined by the method adapted from Macheroux *et al.*, (1999). To a solution of 250-300 μg of protein in 1 ml of 10mM Tris.HCl pH 8.4 buffer, 150 μl of trichloroacetic acid (50 %) was added and the solution mixed by inversion. The denatured protein was pelleted in a microcentrifuge at 13,000 rpm (microfuge, pico)

and the supernatant removed to a clean Eppendorf. Solid sodium carbonate was used to adjust the pH to 7.0. The UV/vis spectrum was recorded and the concentration of FAD calculated ($\epsilon=11100$) as a % of the protein concentration. Typical values of FAD content were between 65 and 80 %. All kinetics were readjusted to 100 % FAD.

5.3.5 Molecular Weight Determination by Mass Spectrometry

The molecular weight of wild-type and mutant proteins of flavocytochrome c_3 were determined by electrospray mass spectrometry.

5.4 Kinetic Analysis

5.4.1 Steady-State Kinetic Analysis

5.4.1.1 Fumarate Reductase Assay

Assays were carried out at 25 °C in 50 mM Tris.HCl pH 7.2 I=500 mM under a nitrogen atmosphere (<5 ppm) in a Belle Technology glovebox using a Shimadzu UV-PC 1201 spectrophotometer. Enzyme activity was measured by a method adapted from Thorneley (1974). Disposable cuvettes (3 ml volume) with a 1 cm pathlength were used. To a cuvette containing 3 ml buffer and 0.2 mM methyl viologen ($\epsilon=13,000 \text{ M}^{-1}\text{cm}^{-1}$), sodium dithionite was added until the absorption was in the range 1-1.5. Protein was then added to a concentration of 1-20 μM depending on how active the enzyme was. A control assay was carried out over 100 seconds to ensure there was no background O_2 activity. The reaction was initiated by the addition of fumarate and monitored at 600 nm over 50-500 seconds.

The following buffers systems were used for pH profiles:

pH 6.0-6.6, 50 mM MES, I=0.5 M

pH 6.6-7.8, 50 mM MOPS, I=0.5 M

pH 7.2-7.5, 50 mM Tris, I= I=0.5 M

pH 8.6- 9.5, 50 mM CHES, I=0.5 M

5.4.1.2 Succinate Oxidation Assay

Succinate oxidation by flavocytochrome c_3 was determined spectrophotometrically. Assays were carried out in a 1 ml cuvette with 1 cm pathlength. Dichloroindophenil (Sigma) was used as electron acceptor. This was prepared as a 4 mM stock with phenazine methosulfate added to a concentration of 0.27 mM. To 1 ml of buffer and protein, dichloroindophenil was added to a concentration of 40 μ M and the reaction initiated by addition of succinate. The absorption at 600 nm was monitored over 100-500 seconds. The rate of succinate oxidation was also monitored using potassium ferricyanide as electron acceptor.

5.4.1.3 Inhibition Studies

Inhibition studies were carried out using a range of molecules to test for their ability to inhibit fumarate reduction and/or succinate oxidation. Fumarate reductase inhibition assays were carried out with a fumarate concentration of 66 μ M ($K_m=25$ μ M). The activity was then determined in the absence and in the presence of each potential inhibitor (~200 mM). For those molecules which showed inhibitory behaviour individual inhibition assays were then carried out for a range of increasing inhibitor concentrations until fumarate reductase activity approached zero. To ascertain the type of inhibition Michaelis plots of fumarate reduction were determined at three or four different inhibitor concentrations and Lineweaver-Burk plots constructed. Succinate oxidation inhibition studies were carried out with a succinate concentration of 2 mM ($K_m=1$ mM). Assays were carried out in the absence and presence of 500 mM inhibitor.

5.4.2 Pre-Steady-State Kinetic

Stopped-flow measurements of fumarate reduction were carried out anaerobically using an Applied Photophysics SF.17MV stopped flow spectrophotometer contained in a Belle Technology glovebox under nitrogen atmosphere (<5 ppm). Stock solutions of enzyme (4-8 μM) and substrate (500 mM) were prepared in 50 mM Tris.HCl buffer, pH 7.2, I=0.5 M and fully degassed. Sodium dithionite was titrated into the enzyme solution until full reduction of the haems was observed spectrophotometrically. Excess sodium dithionite was removed by passing the protein solution through a gel filtration (G50) chromatography column (10 cm length \times 2 cm diameter) maintained under nitrogen. Substrate and enzyme solutions were allowed to equilibrate to 25 $^{\circ}\text{C}$ prior to analysis. Haem re-oxidation was monitored at 418 nm over a 500 ms time course.

5.5 Solvent Isotope Studies

Buffer and substrate solutions for solvent kinetic isotope studies were prepared by dissolving the appropriate reagents in D_2O . The pH of the solutions was adjusted by addition of concentrated DCl or NaOD using the equation $\text{pH} = \text{pD} + 0.4$ to correct for the reactivity of D_2O solutions towards the pH electrode. Concentrated enzyme stock solutions in H_2O were used so that a large dilution factor leaves the isotopic composition of the larger volume unaffected. Typically <5 μl was added to 3 ml giving the final proportion of D_2O >95 % including correction for the protium content of the buffer components. For proton inventory studies buffer solutions that had been previously adjusted to the appropriate pH were combined together to give the desired proportion of H_2O and D_2O . The reaction was monitored at 1 min and 30 minutes after preparing assays in D_2O buffer and similar rates were observed. The absence of any effect shows that all important hydrogenic sites are already exchanged or else are very slowly exchanging relative to the period of kinetic experiment.

Chapter 6

Structure and Function of Flavocytochrome c_3

6.0 Structure and Function of Flavocytochrome c_3

6.1 Probing The Active Site Structure

The crystal structure of fcc_3 features a malate-like molecule at the active site. This is an artefact of the crystallisation process in which fumarate has undergone nucleophilic attack by water at the C2 position (Taylor *et al.*, 1999) (Figure 6.1). The active site structure is therefore seen to be able to accommodate a hydroxyl group at this position. This raises the question - could small molecules other than fumarate be accommodated in the active site either as substrates or inhibitors? (Teipel *et al.*, 1968, Ackrell *et al.*, 1989)

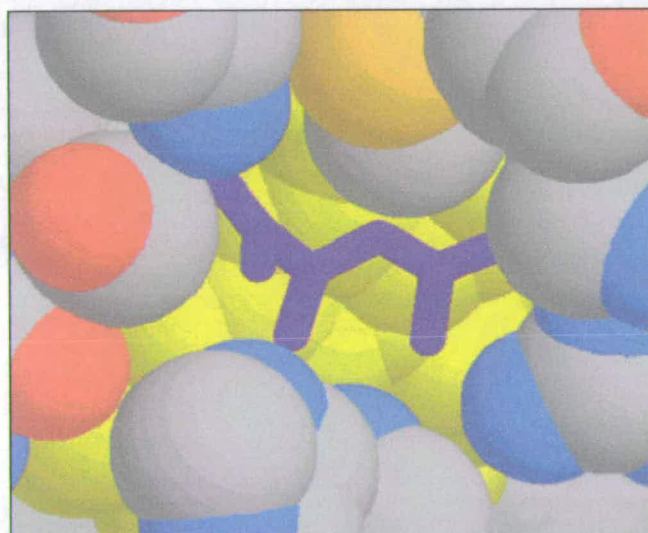


Figure 6.1 The active site cavity of fcc_3 containing a malate-like molecule. FAD (yellow) is visible below the substrate (purple). To obtain this view residues above the substrate have been removed.

From the crystal structures of fcc_3 from *Shewanella* MR1 with and without substrate/product it can be seen that there is movement of the clamp domain by 12° about a hinge at the flavin domain/clamp domain interface. This movement allows access to the active site by the substrate and diffusion out through a channel to release the product. In order to improve our understanding of the open-closed transition a

number of molecules were screened for their ability to act as inhibitors for both the reduced form of the enzyme and the oxidised form of the enzyme. Molecules found to be inhibitors could then be used in crystallisation trials.

The closely related methacrylate reductase from *Geobacter sulfurreducens* AM-1 catalyses the reduction of methacrylate to isobutyrate (Mikoulinskaia *et al.*, 1999). Its N-terminal amino acid sequence shows similarity to fcc_3 . In addition to reducing methacrylate, the enzyme catalyses the reduction of several α,β -unsaturated carboxylic acids such as acrylate, crotonate and pentenoate. A similar reaction is catalysed by the enoate reductase from *Clostridium kluyveri* which catalyses the reduction of a broad range of α,β -unsaturated carboxylic acids (enoates) (Simon *et al.*, 1992). From these observations fcc_3 might be expected to be able to utilise alternative substrates to fumarate. The structure at the active site and the mechanism of reduction were considered in the selection of potential substrates. Residues at the active site important for fumarate binding have been studied using site-directed mutagenesis (Doherty PhD thesis 1999) (Table 6.1).

	$k_{cat} s^{-1}$ (pH 7.2)	$K_m \mu M$ (pH 7.2)
F cc_3 WT	510 ± 15	25 ± 2
H365A	51 ± 2	259 ± 24
H504A	65 ± 3	256 ± 23
T377A	38 ± 1	650 ± 50
R544M	0.15 ± 0.01	715 ± 114

Table 6.1 Effect of active site mutations on k_{cat} and K_m (Doherty PhD thesis 1999, Pankhurst, personal communication).

The C1 carboxyl group forms hydrogen bonds to His504 and Thr377, whereas the C2 carboxyl forms hydrogen bonds to His365, Arg544 and Arg402 (Figure 6.2). The individual mutations; H504A, R544M, T377A and H365A were found to increase the K_m values from 25 μM to between 250 μM and 715 μM . There was a 10-fold decrease

in the k_{cat} values of each of the mutants H365A, H504A and T377A but a 100-fold lowering for R544M. The greater effect on k_{cat} of mutating Arg544, over the other active site residues, indicates that Arg544 is important not only in forming the Michaelis complex but also for activating the substrate by withdrawing electron density and polarising the double bond. Removal of hydrogen bonds to the C1 carboxyl group affects k_{cat} to a lesser extent.

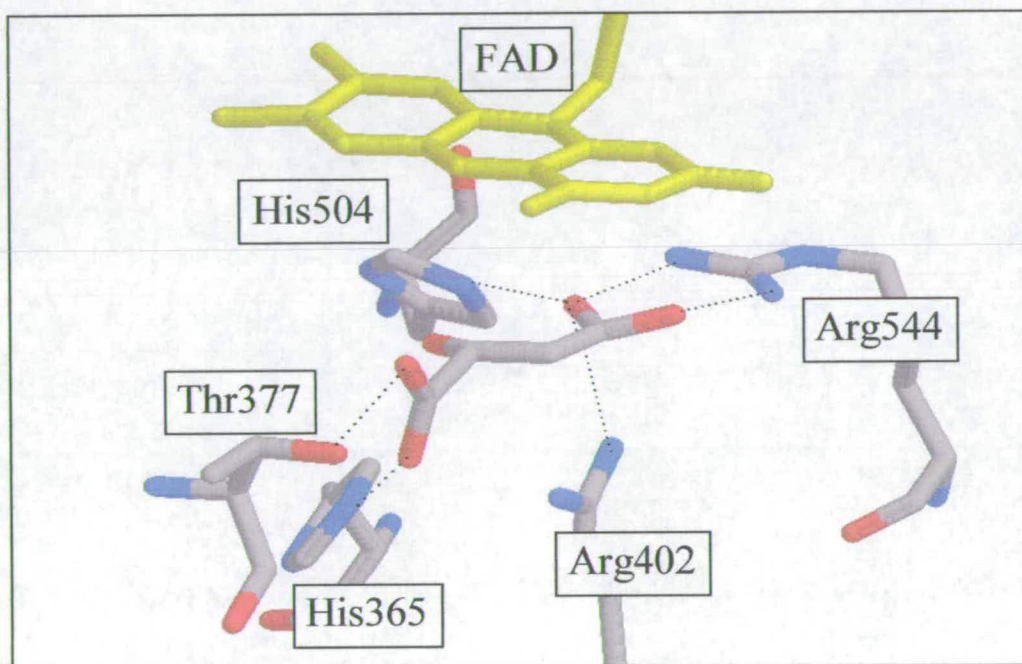


Figure 6.2 The active site of flavocytochrome c_3 highlighting the hydrogen bonding network. A malate-like molecule is bound at the active site.

6.1.1 Substrate Specificity

Potential substrates studied incorporate one carboxyl group and a double bond in the C2-C3 position (Figure 6.3). Functional groups were substituted at positions R_1 , R_2 and R_3 (Table 6.4). Acrylamide which features an amide group instead of a carboxylic acid group and propiolic acid containing a C-C triple bond were also tested.

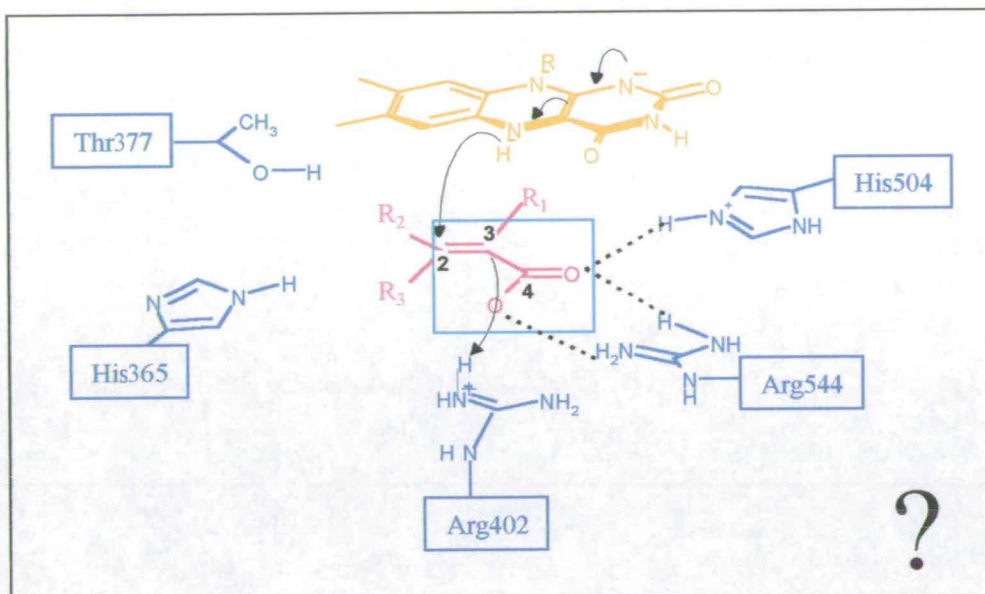


Figure 6.3 Schematic representation of the active site. Acrylate and derivatives of acrylate were studied as potential substrates.

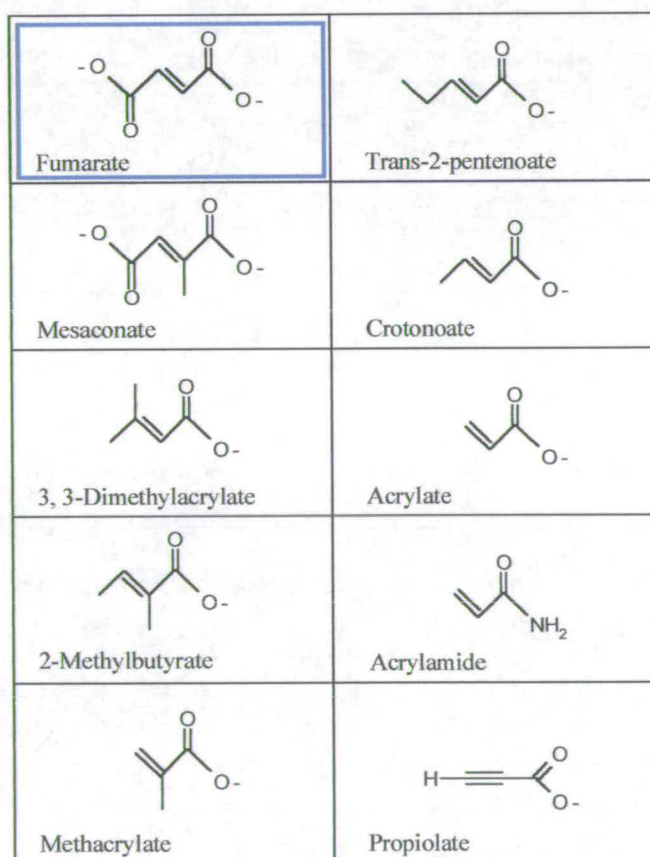


Figure 6.4 Structures of potential substrates in comparison to fumarate (top left)

Steady-state and pre-steady-state analyses of potential substrates were carried out as described in Section 5.4. To ensure low levels of activity would be detected steady-state assays were carried out using enzyme concentrations of 20 μM and were monitored over 5-10 minutes. Background traces were monitored to ensure no oxygen was present before the addition of 500 mM substrate. Acrylamide and propiolic acid were unable to be tested under steady-state conditions due to their own reactivity towards methylviologen.

All traces obtained were continuous straight lines and showed no change in absorbance indicating that none of the molecules tested were able to act as substrates. This was surprising for acrylate, crotonate and trans-2-pentenoate. These molecules only differ from fumarate by the absence of the second carboxyl group. If methacrylate reductase is able to reduce these substrates then why not fcc_3 ? There are several possible reasons why fcc_3 is unable to catalyse the reduction of these molecules. Whereas it is energetically favourable for the highly polar fumarate molecule to bind in the active site this may no longer be true for acrylate and derivatives. Even if acrylate does bind (in the active site) it may not align itself as fumarate does and the position of the double bond may have moved too far from the flavin N5 for hydride transfer to occur. It is highly unlikely that acrylate would bind to the pair of residues T377 and H365 through its sole carboxyl group instead of the H504/R544 combination, forming only two hydrogen bonds instead of a possible four. It may be that acrylate binds but it is no longer energetically favourable for the clamp domain to close. Consequently active site residues are not aligned as in the catalytically active form of the enzyme. With fumarate the resultant energy gained as the 2nd carboxyl group twists out of plane and forms two hydrogen bonds is the driving force for the closure of the clamp domain. As it is unable to form these two hydrogen bonds acrylate can not provide the system with this driving force. Fumarate binding is therefore a prerequisite for domain closure and the differences in structure of fumarate and acrylate may be enough to stop this taking place. Inferences drawn from acrylate also apply to other acrylate derivatives. Mesaconate, a known inhibitor

of fcc_3 , proved not to be a substrate either. With a K_i of 1 μM mesaconate binds extremely tightly in the active site in an orientation that prevents catalysis taking place.

6.1.2 Inhibition Studies

Potential inhibitors were screened for their ability to inhibit fumarate reduction and succinate oxidation. Fumarate assays using 66 μM fumarate were initiated before the addition of 200 mM inhibitor. Rates before and after addition of the inhibitor were compared and those compounds which decreased the rate of fumarate reduction were investigated further. The same procedure was used to screen potential inhibitors of succinate oxidation using 2 mM succinate ($K_m = 1.1$ mM) and 200 mM inhibitor (Figure 6.5). Molecules that did not show any inhibition at a concentration of 200 mM would not bind strongly enough to be of use in crystallisation studies. Inhibitors and other small molecules that were tested are shown in Figure 6.6.

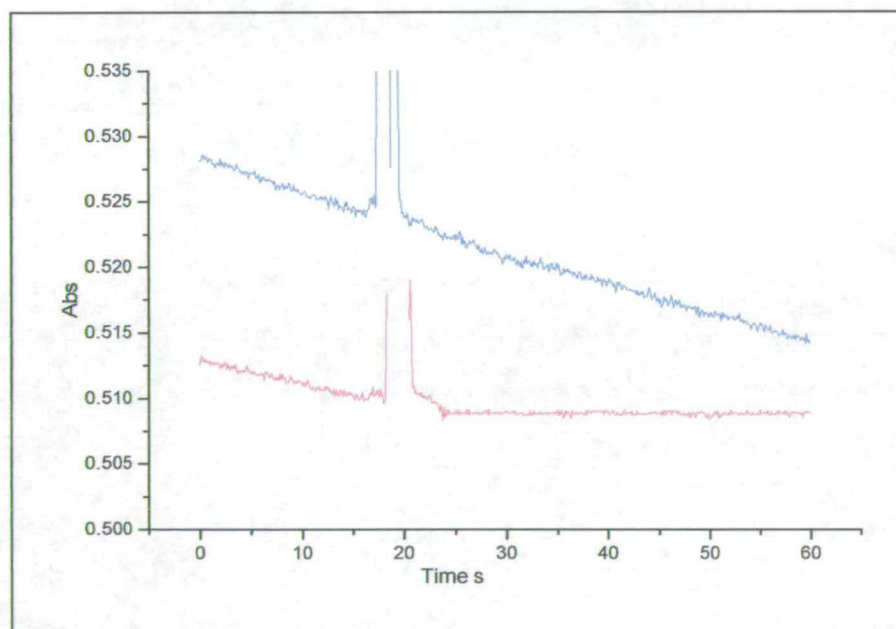


Figure 6.5 Steady-state traces obtained for succinate oxidation. The reaction was initiated by the addition of enzyme and monitored for 20 seconds before addition of crotonate (blue) and oxaloacetate (pink).

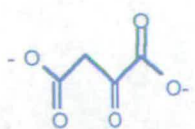
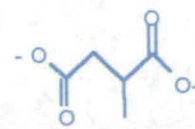
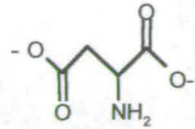
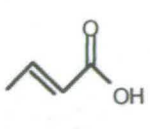
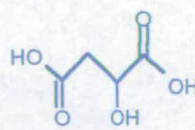
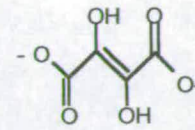
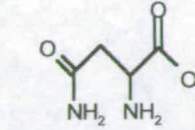
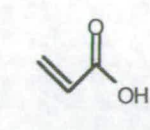
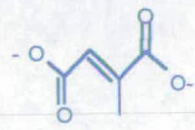
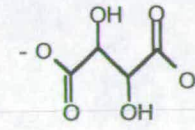
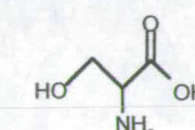
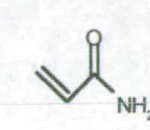
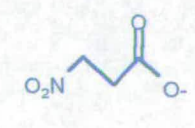
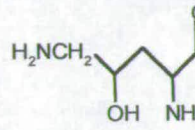
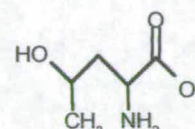
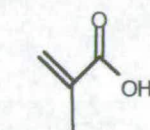
			
Oxaloacetate	Methyl Succinate	(D) and (L)-Aspartate	Crotonoate
			
(D) and (L)-Malate	Dihydroxyfumarate	(D) and (L)-Asparagine	Acrylate
			
Mesaconate	L-Tartarate(2R,3R)	(D) and (L)-Serine	Acrylamide
			
3-Nitropropionate	(D) and (L)-4-amino 3-hydroxybutyrate	(D) and (L)-Threonine	Methacrylate

Figure 6.6 The structure of inhibitors (blue) and other molecules tested (black).

Inhibition curves were then obtained for each inhibitor by measuring the rate of succinate oxidation with 2 mM succinate present over a range of inhibitor concentrations (Figure 6.7). Data were fitted to the Equation 6.1 and K_i , the inhibition constant calculated.

$$k_{\text{obs}} = k_0 - \left(\frac{[I] \times k_{\text{obs}}}{[I] + K_i \left(1 + \frac{[S]}{K_m} \right)} \right)$$

Equation 6.1 The equation used to calculate K_i , the inhibition constant.

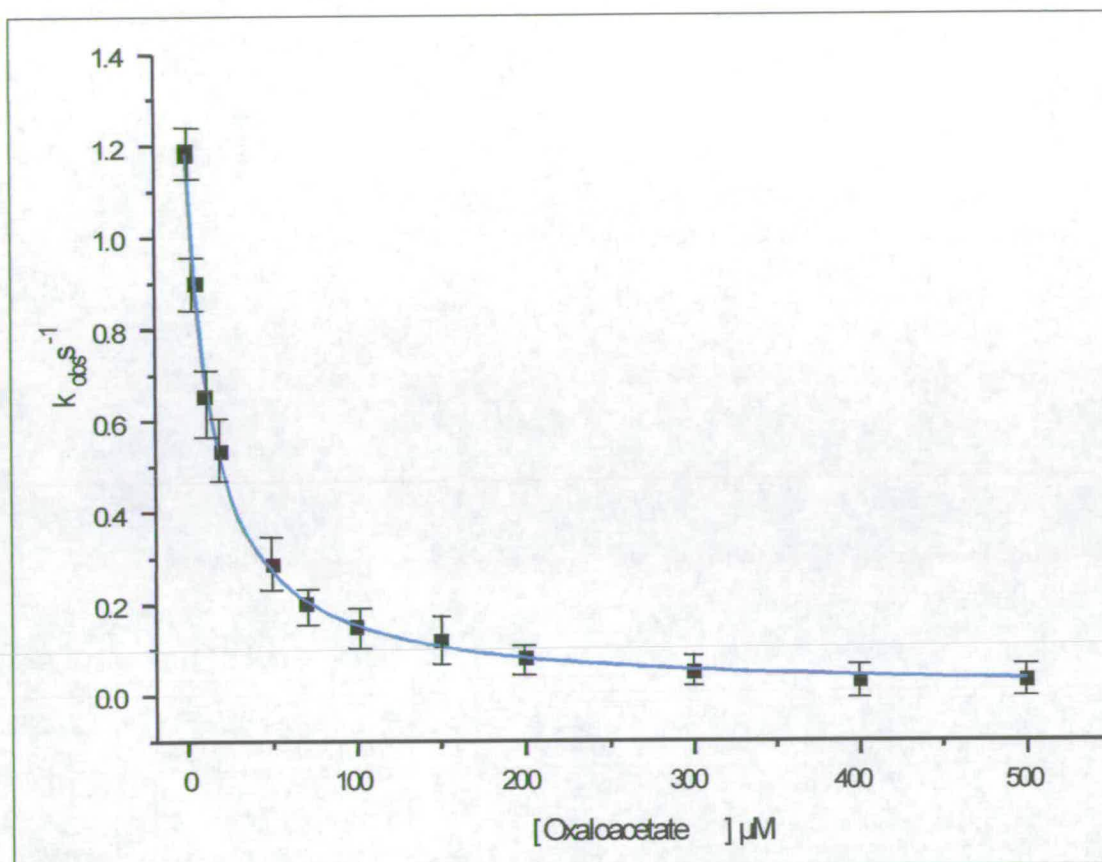


Figure 6.7 Inhibition plot of succinate oxidation by oxaloacetate. Assays were carried out in the presence of 2 mM succinate at pH 8.5. Data were fitted to Equation 6.1 using non-linear least squares regression analysis using the program Microcal Origin.

Michaelis plots for succinate oxidation were obtained in the presence of at least three different inhibitor concentrations (Figure 6.8). At low substrate concentrations the inhibitor competes for the binding site and the rate of the reaction is decreased. At higher substrate concentrations the inhibitor is much less successful at competing with the substrate for the available binding sites and the degree of inhibition is negligible. For a true competitive inhibitor the apparent K_m is increased as a result of the inhibition but k_{cat} remains unchanged (Table 6.2).

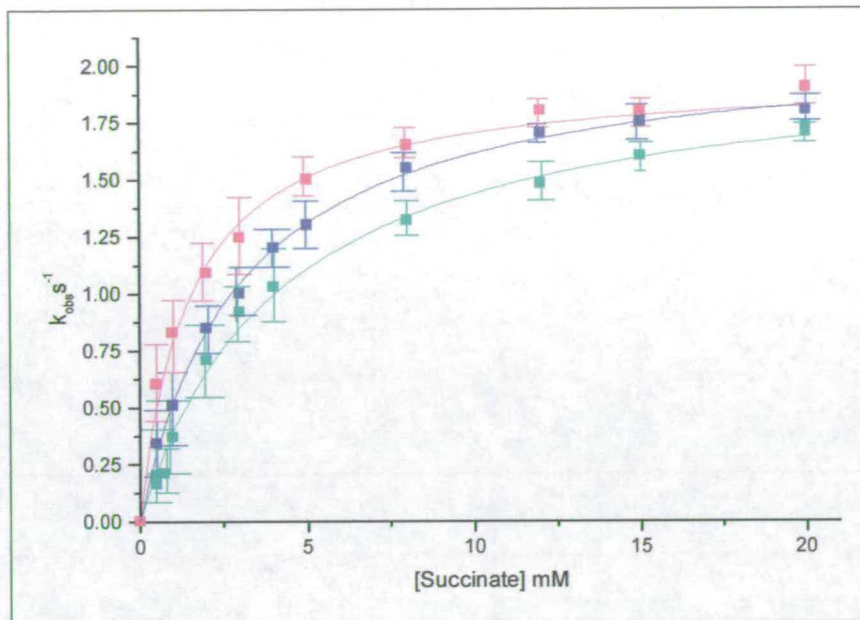


Figure 6.8. Michaelis-Menten plots for succinate oxidation at different oxaloacetate concentrations 20 μM (red), 40 μM (purple), 50 μM (blue). Individual points were calculated from steady-state assays. The data were fitted by least-squares regression analysis to the Michaelis-Menten equation.

[Oxaloacetic acid] μM	$k_{\text{cat}} \text{ s}^{-1}$ (pH 8.5)	Apparent K_m (mM)
0	2.1 ± 0.1	1.1 ± 0.2
20	2.0 ± 0.1	1.5 ± 0.2
40	2.2 ± 0.1	3.5 ± 0.3
50	2.0 ± 0.1	4.2 ± 0.3

Table 6.2 Data for succinate oxidation over a range of inhibitor concentrations

In the presence of a competitive inhibitor a plot of $1/V$ vs $1/[\text{succinate}]$ gives a straight line for each inhibitor concentration (Equation 6.2). These lines intercept in the first quadrant indicating the inhibition is competitive (Figure 6.9).

$$\frac{1}{v} = \frac{K_m}{V_{\text{max}}} \left(1 + \frac{[I]}{K_i} \right) \frac{1}{[S]} + \frac{1}{V_{\text{max}}}$$

Equation 6.2 The Lineweaver-Burk equation in the presence of a competitive inhibitor

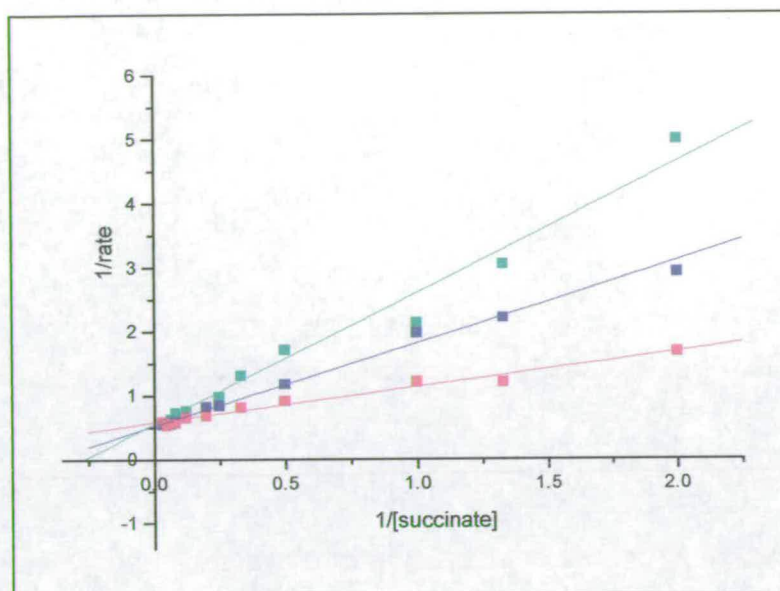


Figure 6.9 A plot of $1/v$ versus $1/[S]$ plot in the presence of different fixed inhibitor concentrations of $20 \mu\text{M}$ (red), $40 \mu\text{M}$ (purple), $50 \mu\text{M}$ (blue).

All inhibitors were found to be competitive. Values of K_i are shown in Table 6.3.

Inhibitor	Inhibition of fumarate reduction. (K_i)	Inhibition of succinate oxidation. (K_i)
Mesaconate	$1.0 \mu\text{M}$	$32.3 \mu\text{M}$
D-Malate	no inhibition	4.8 mM
L-Malate	no inhibition	6.2 mM
Methylsuccinate	no inhibition	1.7 mM
Oxaloacetate	no inhibition	$5.3 \mu\text{M}$
3-nitropropionate	no inhibition	0.5 mM

Table 6.3 Inhibition constants (K_i) for the inhibition of succinate oxidation and fumarate reduction. (Values for (D) and (L) malate are taken from M. Doherty PhD thesis 1999)

As mentioned previously mesaconate is a potent inhibitor of fumarate reduction (K_i of $1 \mu\text{M}$) but it also inhibits succinate oxidation, though less well with a K_i of $32.3 \mu\text{M}$. It was the only inhibitor found to bind to both the reduced and the oxidised forms of the enzyme. Methylsuccinate is structurally very similar to mesaconate in that it possesses

a methyl group at the C2 position but does not have a double bond. Methyl succinate was found to inhibit succinate oxidation with a K_i of 1.7 mM but not fumarate reduction. This suggests the double bond is an important feature facilitating fumarate and mesaconate binding in the reduced form of the enzyme. If the methyl group of methylsuccinate is replaced with a ketone group as in oxaloacetate, the polarity of the molecule is increased and it binds more tightly than methylsuccinate with a K_i of 5.3 μ M. The ability of oxaloacetate to bind to oxidised but not reduced fcc_3 has been observed during protein film voltammetry experiments. Cyclic voltammograms show that oxaloacetate will bind in the active site of the oxidised enzyme but is expelled on reduction (Jones, personal communication). Malate, in which a hydroxyl group is found at C2, inhibits succinate oxidation with a K_i of 4.8 mM for D-malate and 6.2 mM for L-malate. Groups favoured at this position are small and polar such as a methyl, hydroxy or ketone. Molecules with an amine group at this position e.g. (D) and (L) aspartate, asparagine, serine and threonine do not inhibit. An explanation for this might be that with a pK_a of 11.9 the secondary amine group will be protonated under the assay conditions (pH 8.4) thus preventing binding. Molecules that only possess one carboxyl group such as acrylic acid, crotonoate, methacrylate or an amide as in acrylamide do not inhibit fumarate reduction or succinate oxidation. 3-nitropropionic acid where the second carboxyl group is replaced with a polar nitro group is able to inhibit succinate oxidation with a K_i of 0.52 mM. The ability of inhibitors to bind to the oxidised enzyme but less well (mesaconate) or not at all to the reduced form might be due to redox linked structural changes at the active site. Alternatively the redox state of the FAD, in which FAD_{red} carries a charge of -2 and FAD_{ox} is neutral, could influence the binding of the inhibitors.

6.2 The Active Site Catalyst

6.2.1 The Roles of The Active Site Histidines

Although there is considerable kinetic and crystallographic evidence to suggest that Arg402 is the active site acid there has remained some controversy over whether His504 or His365 could fulfil this role. Alternatively, based on the crystal structure of the membrane bound fumarate reductase from *W. succinogenes*, it has been proposed that a water molecule carries out this function (Lancaster *et al.*, 1999). In this enzyme a water molecule is found close to fumarate in the active site at the position occupied by the guanidinium group of Arg402 in fcc_3 . Although fumarate is found in the active site the position of residues more closely resemble those of the uncomplexed ifc_3 (open conformation) than the closed conformation of fcc_3 (Figure 4.9). Therefore, although fumarate is found at the active site, the enzyme is trapped in a non-catalytically active form. The slightly open conformation gives misleading evidence as to the position of active-site residues involved in catalysis. Strict conservation of active site residues throughout this family implies that a common mechanism operates. With the same reaction being catalysed the mechanism will be conserved throughout this family of fumarate reductases. The fcc_3 mutants H365A and H504A have been characterised (Doherty PhD thesis 1999) (Figure 6.10). These enzymes retain approximately 25% of wild-type activity consistent with both these residues being important for Michaelis complex formation but not with being essential for catalysis. Additional evidence that His365 is not the active site acid comes from studies on the *E. coli* fumarate reductase. The equivalent residue in this enzyme, His232 was mutated to a serine and similarly retained approximately 25 % of original activity (Schröder *et al.*, 1991).

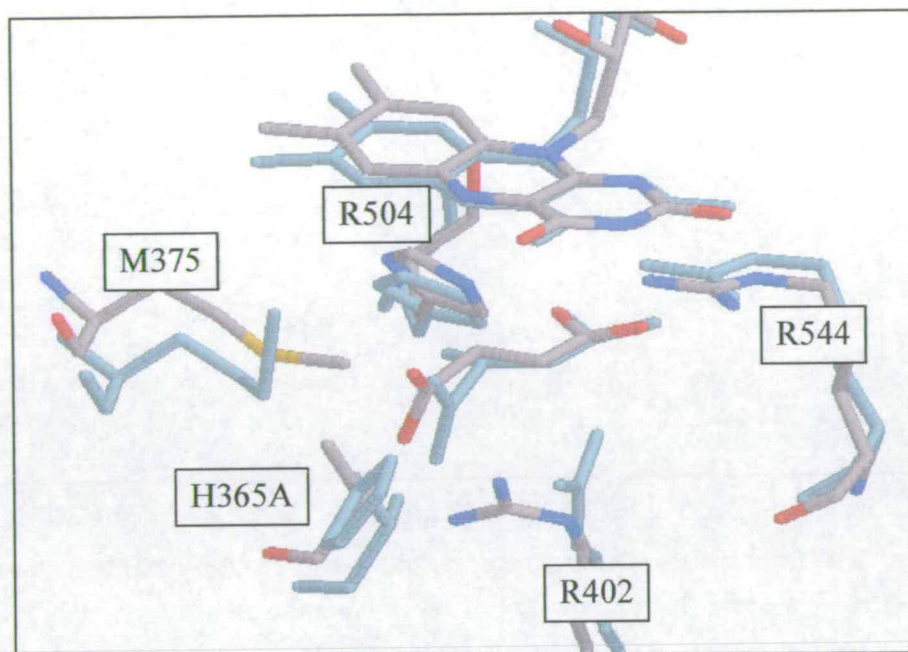


Figure 6.11 Comparison of the active site of H365A (atom coloured) which contains fumarate with wild-type (blue) in which a malate-like molecule is bound. The mutation has led to changes in the position of Arg402.

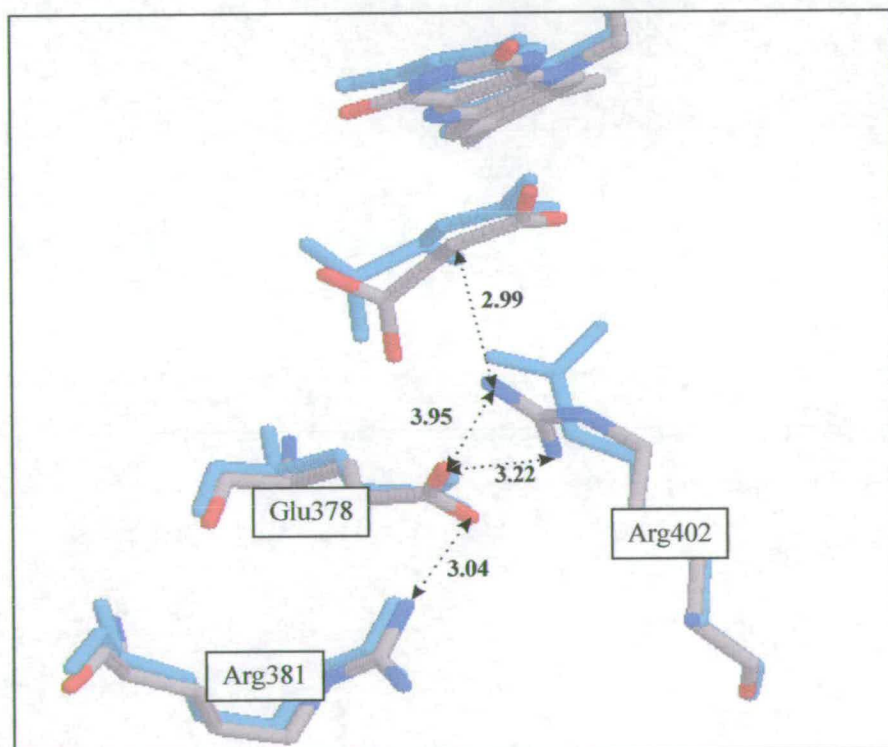


Figure 6.12 The proton transfer pathway of H365A (atom coloured) in comparison to wild-type (blue). Distances between residues for H365A are shown.

6.2.2 H365A:H504A- fcc_3

In D-amino acid transaminase Lys145, the catalytic residue, abstracts the α -proton of the amino-acid substrate (Yoshimura *et al.*, 1992). The mutant enzyme K145N still retains residual activity. Results suggest that in the mutant enzyme an amino-acid side chain other than Lys145 performs this function. Using the radiolabelled substrate D-serine, results show that Lys267 may substitute for the NH_2 group of Lys145 of the wild type enzyme to provide an alternative base that catalyses transamination although with reduced efficiency. To rule out the possibility that either H504 or H365 could compensate in the others absence as proton donor the double mutant H365A:H504A has been studied. The effect of the double mutation on kinetic parameters has been investigated. All rates have been corrected for FAD content. The molecular mass of H365A:H504A was compared to that of wild-type (63 033 Da) and the difference found to be 134 ± 6 Da (expected difference 132 Da). The mutations were also confirmed by DNA sequencing.

6.2.2.1 The effect of H365A:H504A on k_{cat} and K_m

The ability of the H365A:H504A- fcc_3 enzyme to catalyse fumarate reduction has been determined at a range of fumarate concentrations and pH values (Figure 6.13, Table 6.4). The fact that this enzyme is still active is compelling evidence that neither of these residues can be the active-site acid. Changes in the positions of active-site residues similar to those seen in the H365A- fcc_3 crystal structure might be expected in the H365A:H504A- fcc_3 mutant enzyme. This would explain the extremely low levels of activity observed.

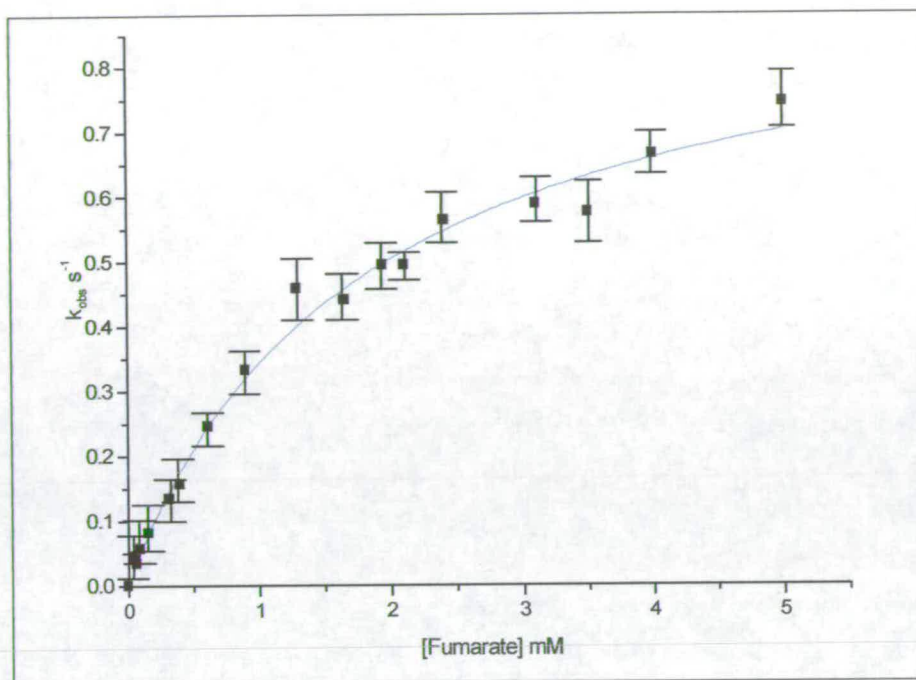


Figure 6.13 A Michaelis-Menten plot of fumarate reduction by H365A:H504A- fcc_3 at pH 7.2. Points were calculated from individual steady-state assays. The data was fitted by least-squares regression analysis to the Michaelis-Menten equation using the program Microcal Origin.

pH	Wild-Type k_{cat} (s^{-1})	H365A:H504A- fcc_3 k_{cat} (s^{-1})
6.0	658 ± 34	0.3 ± 0.1
7.2	509 ± 15	0.8 ± 0.1
7.5	370 ± 10	0.9 ± 0.1
9.0	210 ± 13	0.9 ± 0.1

Table 6.4 Comparison of k_{cat} values obtained for wild type and H365A:H504A- fcc_3 , $I=0.5$ M

The double substitution H365A:H504A- fcc_3 has a dramatic effect on the enzyme's ability to bind fumarate with a value for K_m in the low millimolar range (Table 6.5). This increase in K_m is not surprising considering that each of these histidine residues forms hydrogen bonds to the carboxylate oxygens of fumarate.

pH	Wild-Type K_m (μM)	H365A:H504A K_m (mM)
6.0	43 ± 10	~ 0.28
7.2	25 ± 2	~ 1.1
7.5	28 ± 3	~ 1.8
9.0	7 ± 1.5	~ 1.3

Table 3.6 Comparison of K_m values obtained for wild-type and H365A:H504A- fcc_3

6.2.2.2 The pH dependence of H365A:H504A- fcc_3

The pH profile of wild type fcc_3 gives a pK_a of 7.43 which is thought to correspond to the pK_a of His504. This residue, if protonated, would have a stabilising effect on the transient anion species formed following hydride transfer. The pH profile of H504A gives a very different trend to wild-type reaching a maximum rate at pH 8.5 (M. Doherty, PhD thesis 1999). Two pK_a values were obtained; 6.8 and 8.5. The rate of fumarate reduction for H365A- fcc_3 was essentially independent of pH. Electrochemical studies on H365A- fcc_3 confirmed that the rate-determining step in the reaction had been changed to hydride transfer from flavin to substrate (Turner, personal communication).

For H365A:H504A- fcc_3 the pH dependence has been modified in comparison to wild-type (Figure 6.14). The rate of fumarate reduction appears to increase as the pH becomes more basic, reaching a maximum at pH 7.8 after which the rate rapidly falls off. Two pK_a values were obtained; 6.9 ± 0.5 and 8.3 ± 0.5 . Interestingly these values are the same within error as those obtained for H504A- fcc_3 . This indicates that the same two protonation sites could be contributing to the observed pH profiles for H504A- fcc_3 and H365A:H504A- fcc_3 .

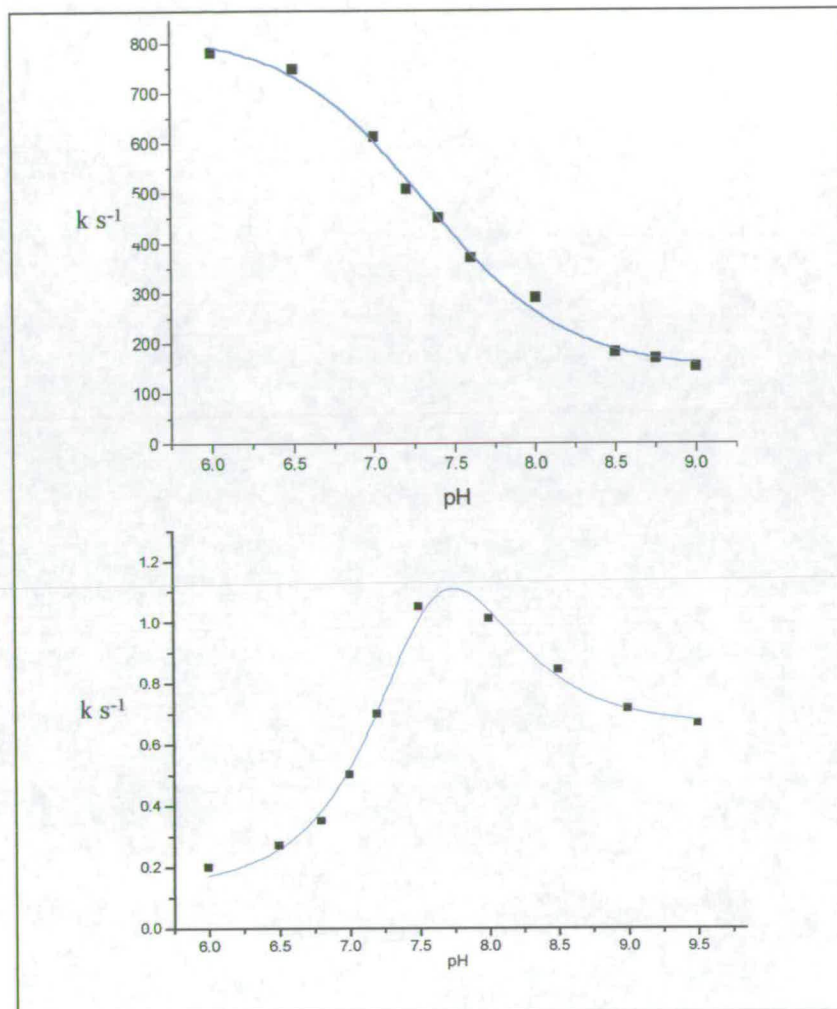


Figure 6.14 pH profiles of wild-type fcc_3 (top) and H365A:H504A- fcc_3 (bottom).

6.2.3 Substitution of the Active-Site Acid

The mechanism of fumarate reduction is thought to occur in a concerted reaction in which a hydride is transferred from N5 of FAD to the substrate C2 and a proton is donated from Arg402, the active-site acid to C3. The pK_a of the transient carbanion intermediate would be approximately 25, with a pK_a of arginine of ~ 12 . Therefore transfer of a proton from the guanidine group to C3 would be favoured. Residues which fulfil the role of active site acid/base catalyst in other enzymes are lysine

($pK_a=10.8$) or more commonly, histidine ($pK_a=6$). Histidine is conserved as the catalytic active site residue in the family of α -hydroxy acid dehydrogenases/oxidase enzymes (Ghisla *et al.*, 1989). Lysine is used as active site catalyst in aspartate aminotransferase (Toney *et al.*, 1993) (AspAT), *o*-acetylserine sulfhydrylase (Rege *et al.*, 1996) (OASS), D-amino acid transaminase (Yoshimura *et al.*, 1992), tryptophan synthase (Lu *et al.*, 1993) and 5-aminolevulinate synthase (Hunter *et al.*, 1999) (ALAS).

Studies on AspAT and ALAS have shown that it is possible to substitute one of these active site catalytic residues for another. AspAT reversibly interconverts the dicarboxylic substrates aspartate and α -ketoglutarate with glutamate and oxaloacetate. The active site residue Lys258 of chicken AspAT was replaced with a histidine residue by means of site-directed mutagenesis (Ziak *et al.*, 1990). The reaction comprises of transamination followed by tautomerisation and hydrolysis. The transamination requires a 1,3-prototropic shift to interconvert aldimine and ketimine intermediates. The rate of the transamination half-reaction was five orders of magnitude slower than the wild type enzyme and the reverse half reaction was three orders of magnitude slower. This suggests the histidine residue can to some extent substitute for Lys258 which is assumed to be the proton donor/acceptor. 5-Aminolevulinate synthase (ALAS) catalyses the condensation of glycine and succinyl-CoA to form CoA, carbon dioxide and 5-aminolevulinate. A conserved lysine residue is the active-site base. Following substrate binding the conserved lysine removes the C- α proton of the amino acid substrate to form a transiently observed quinonoid intermediate. The active site base, Lys313, was replaced by glycine, histidine and arginine (Hunter *et al.*, 1999). In the case of glycine no quinonoid was formed indicating removal of the C- α proton from the substrate was not possible. The more conservative K313H and K313R mutants retain partial capacity to form a quinonoid intermediate indicating that they can substitute for lysine as the active site base.

6.2.3.1 Substitutions of Arg402

A series of residues were substituted for Arg402. The mutant R402A was designed to illustrate the crucial role of arginine. The mutations; R402K, R402H and R402Y were designed to substitute arginine with residues which might be able to function as proton donors. The volume occupied and the length of the side chain will determine whether their size can be accommodated in place of arginine without major structural alterations (Figure 6.15).

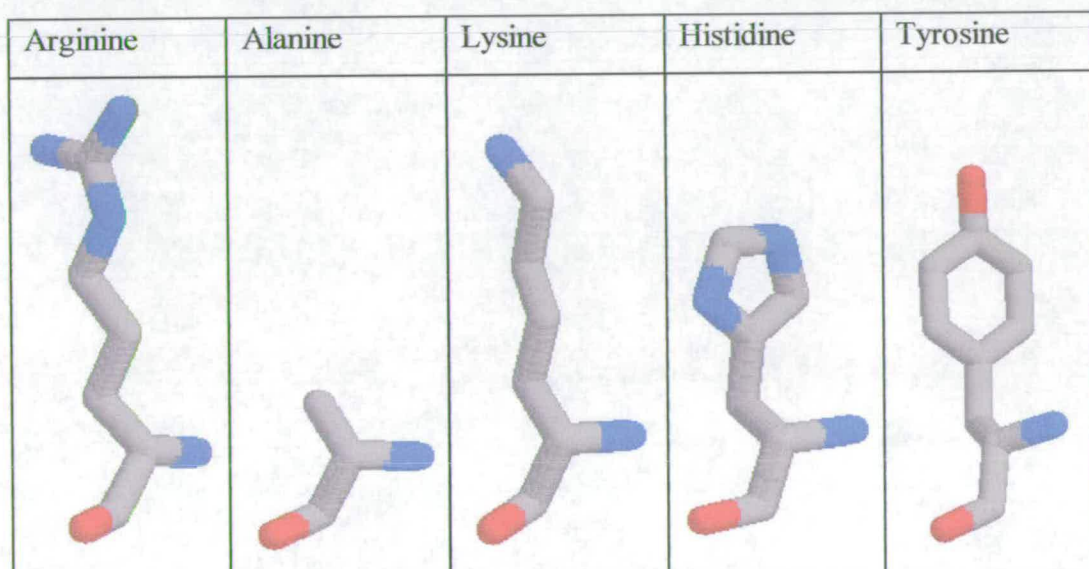


Figure 6.15 Structure of amino acid residues substitute for Arg402.

The pK_a values of the functional groups will affect their ability to donate protons to C3 of fumarate. The pK_a values of the ionizable groups of arginine, lysine, histidine and tyrosine for the free amino acids are shown in Figure 6.16. The pK_a values depend to a considerable extent upon the environment within the protein.

Group	Ionization Reaction	pK_a
Gaunidium (of arginine)		12.5
α -Amino (of lysine)		10.8
Imidazolium (of histidine)		6.0
Phenolic OH (of tyrosine)		10.1

Figure 6.16 The approximate pK_a values of the protonatable side chains of arginine, lysine, histidine and tyrosine. These values can vary by several pH units according to their environment within the protein.

6.2.4 The Crystal Structure of R402A

The R402A mutant as expected is completely inactive (Doherty PhD thesis). To confirm that the mutation had not adversely affected the position of other residues in the active site the enzyme was crystallised and its structure determined to 2.3 Å resolution (Figure 6.17). Bound at the active site is a molecule of fumarate. The positions of active-site residues in the R402A structure overlay almost exactly with the equivalent residues in wild-type. The C4 carboxyl group of fumarate is bound in the same position as that of the malate-like molecule in the wild-type structure. The C1 carboxyl of fumarate lies at a distance of 3.67 Å from Met375 and 3.52 Å from Met236. These distances are slightly shorter than the equivalent distances in wild-type of 3.93 Å and 4.03 Å respectively. The space made vacant by removal of the arginine is now occupied by a water molecule which lies at a distance of 3.51 Å from C3 of fumarate. C2 of Fumarate lies at a distance of 3.67 Å from N5 of FAD compared to 3.93 Å for the equivalent distance in wild-type. The presence of a water molecule

close to fumarate confirms that a mechanism involving water as the active site acid as proposed by Lancaster et al (1999) can not be operational. Loss of activity is not due to detrimental changes in the structure of R402A but in loss of the active site catalytic residue.

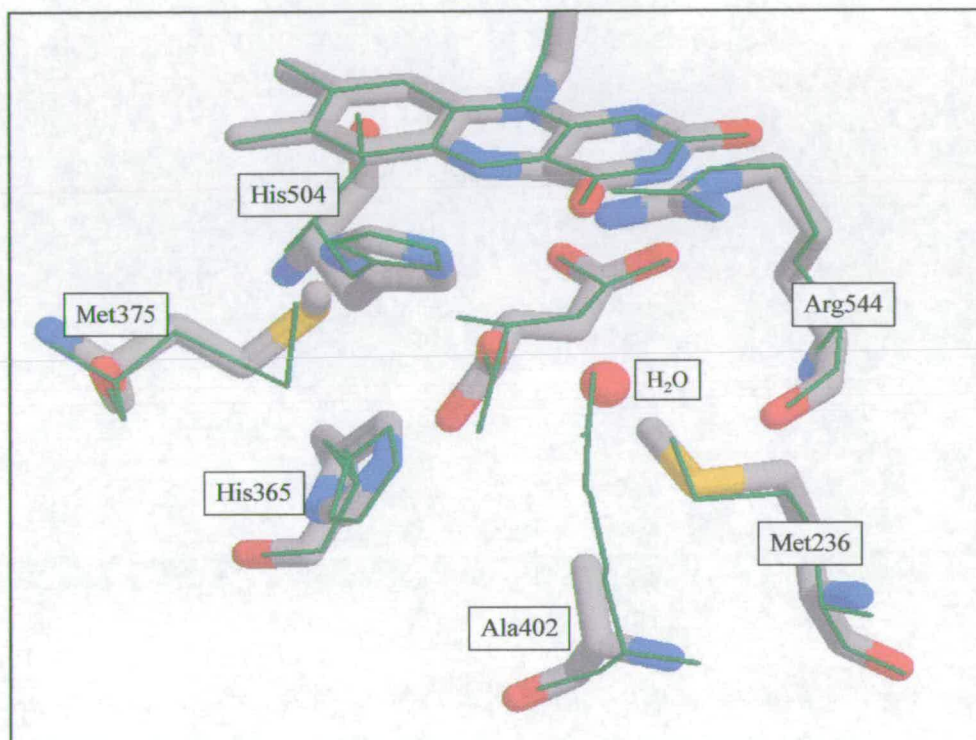


Figure 6.17 Comparison of the active site of R402A (atom coloured) and wild-type (green). A water molecule is located close to fumarate in the R402A structure.

6.2.5 R402K- fcc_3

The conservative mutation R402K has been studied by steady-state analysis and the crystal structure determined to 2.0 Å resolution. The ability of R402K to catalyse fumarate reduction has been investigated at various pH values. All rates have been corrected for FAD content. The difference in molecular mass of R402K in comparison to wild-type was found to be -36 ± 10 Da (expected difference -28 Da). The mutation was also confirmed by DNA sequencing. Due to the extremely low activity of R402K, assays were carried out using enzyme concentrations of 10 μ M and were monitored

over 5-10 minutes (Section 5.8.1) (Figure 6.18). The kinetic parameters, k_{cat} and K_m are shown in Table 6.7.

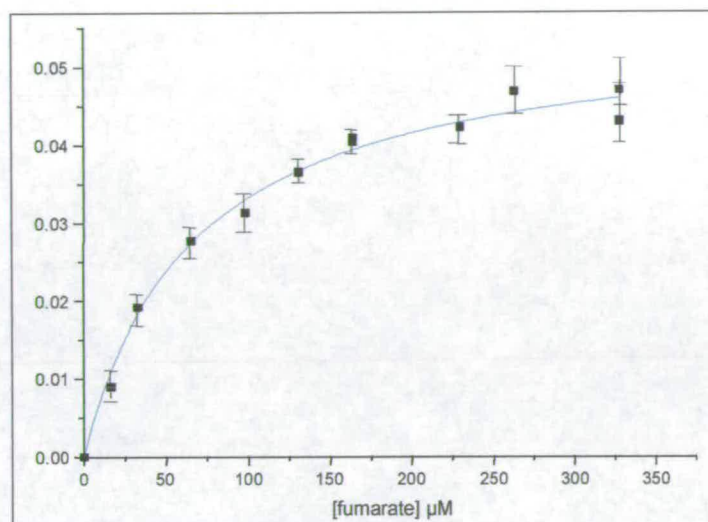


Figure 6.18 A Michaelis-Menten plot of fumarate reduction at pH 7.2 for the mutant R402K. Individual points were calculated from steady-state assays. The data were fitted by least squares regression analysis to the Michaelis-Menten equation using the program Microcal Origin.

At pH 7.2 the enzyme is 10^4 -fold less active than wild-type and above pH 7.5 the enzyme is inactive. The narrow pH range in which the enzyme is active peaks at pH 6.8 (Figure 6.21). The ability of R402K to bind fumarate has also been affected. The K_m value for fumarate is approximately twice that of wild-type at pH 7.2. Arg402 is able to form a hydrogen bond from the guanidinium group to the carboxylate group of fumarate (a distance of 2.83 Å). Lysine is unable to hydrogen bond to fumarate and consequently K_m is increased.

	k_{cat} (s^{-1})		K_m (μM)	
	Wild-type	R402K- fcc_3	Wild-type	R402K- fcc_3
pH 6.0	658 ± 34	0.02 ± 0.01	43 ± 10	18 ± 4
pH 7.2	509 ± 15	0.06 ± 0.01	25 ± 2	66 ± 14
pH 7.5	370 ± 10	Inactive	28 ± 3	Inactive
pH 9.0	210 ± 13	Inactive	17 ± 2	Inactive

Table 6.7 Kinetic data for fumarate reduction at various pH values by R402K- fcc_3 in comparison to wild-type.

6.2.5.1 Crystal Structure of R402K

The R402K structure shows that lysine occupies the same space that was previously filled by arginine (Figure 6.19). The lysine side-chain extends to within 3.14 Å of fumarate. The equivalent distance to C3 of the malate like molecule in wild-type is 2.99 Å. Evidently this has an effect on the rate of proton donation. Fumarate adopts a slightly bent conformation in the active site which enables the C2 carbon to be positioned just 3.25 Å from the N5 of the flavin, closer than for wild-type at 3.35 Å. Once hydride transfer occurs it is possible that fumarate moves closer to Lys402 to receive a proton. The proton transfer pathway has also been affected (Figure 6.20). The greatest change is in the distance between Glu378 and Arg/Lys402. This is 3.34 Å in the case of arginine and 3.50 Å in the case of lysine. In wild-type Arg402 and Arg381 hydrogen bond to the same oxygen of the glutamate (378) side chain. For R402K, lysine hydrogen bonds to the opposite oxygen to that of Arg381. Arginine possessing a guanidinium group and a guanidino group is able to accept and donate protons in a concerted reaction. Lysine on the other hand only possessing an amine group can only receive or donate protons one at a time. It is predicted that this together with the increase in distance from proton donor to C3 of fumarate contributes to the slow rate of fumarate reduction.

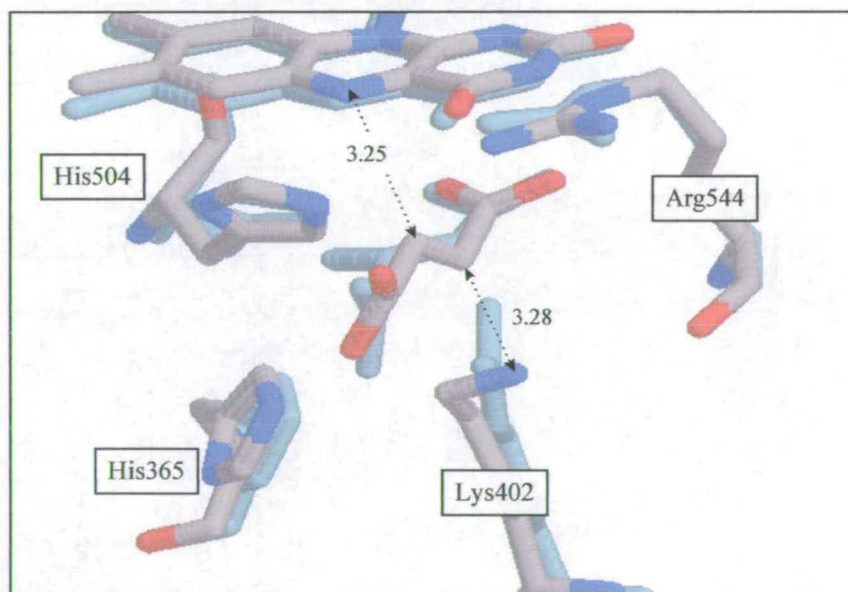


Figure 6.19 Overlay of the active site of R402K- fcc_3 (atom coloured) which contains fumarate with wild-type (blue) which is complexed with a malate-like molecule.

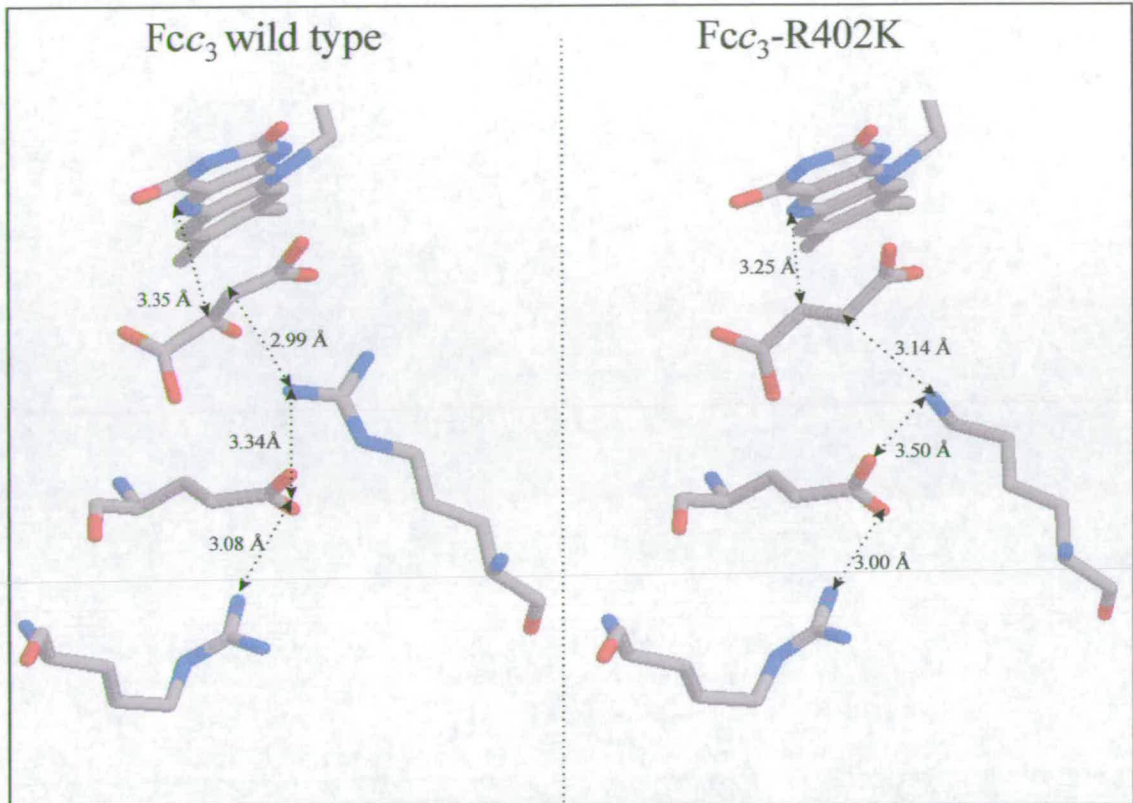


Figure 6.20 Effects seen in the changes to the proton pathway in R402K compared to wild-type.

6.2.6 R402H- fcc_3

The molecular mass of R402H was determined to be (63017 ± 5) Da. A difference of 22 Da in comparison to wild-type (expected difference -19 Da). The mutation was also confirmed by DNA sequencing. The ability of R402H to catalyse fumarate reduction was measured over a range of pH's (Table 6.8). At pH 7.2 this enzyme was approximately 3-fold more active than R402K. This is thought to be due to the ability of the histidine, like arginine to receive and donate protons to fumarate in a concerted process. One nitrogen of the imidazole ring could receive protons from glutamate 378 while the other could donate protons to fumarate.

The ability of this enzyme to bind fumarate at pH 7.2 and above has decreased compared to wild-type. The active site is clearly able to accommodate the bulk of

histidine in place of arginine but it is likely the positions of active-site residues involved in substrate binding have been adversely affected by this mutation.

	k_{cat} (s^{-1})		K_M (μM)	
	Wild-type	R402H-fcc ₃	Wild-type	R402H-fcc ₃
pH 6.0	658 ± 34	0.03 ± 0.01	43 ± 10	20 ± 5
pH 7.2	509 ± 15	0.09 ± 0.01	25 ± 2	98 ± 5
pH 7.5	370 ± 10	0.81 ± 0.01	28 ± 3	133 ± 17
pH 9.0	210 ± 13	0.12 ± 0.01	17 ± 2	892 ± 100

Table 6.8 Kinetic data for R402H-fcc₃ at various pH values in comparison to wild-type.

6.3.7 R402Y-fcc₃

The fumarate reductase activity of R402Y was determined over a range of fumarate concentrations and pH values (Table 6.9). All rates have been corrected for FAD content. The molecular mass of R402Y was determined to be (63038 ± 7) Da. A difference of 5 Da in comparison to wild-type (expected difference 7 Da). The mutation was also confirmed by DNA sequencing. This enzyme is active over the pH range 7.5-9.0. Remarkably at its optimum pH this enzyme is more active than R402K.

	k_{cat} (s^{-1})		K_m (μM)	
	Wild-type	R402Y-fcc ₃	Wild-type	R402Y-fcc ₃
pH 6.0	658 ± 34	0.02 ± 0.01	43 ± 10	207 ± 25
pH 7.2	509 ± 15	0.05 ± 0.01	25 ± 2	267 ± 44
pH 7.5	370 ± 10	0.14 ± 0.01	28 ± 3	213 ± 24
pH 9.0	210 ± 13	Inactive	17 ± 2	Inactive

Table 6.9 Kinetic data for R402Y-fcc₃ at various pH values in comparison with wild-type.

6.3.7.1 Comparison of the pH Profiles of R402K- fcc_3 , R402H- fcc_3 and R402Y- fcc_3

Fumarate reductase activities of R402K, R402H and R402Y mutant enzymes were measured over the pH range 6.0-9.0 (Figure 6.21). Each mutant exhibits a distinctly different trend in activity with pH. The optimum pH values for WT- fcc_3 , R402K, R402H, and R402Y are 6.0, 6.8, 7.5 and 8.0 respectively with corresponding maximum rates of 660 s^{-1} , 0.15 s^{-1} , 0.075 s^{-1} and 0.14 s^{-1} respectively. R402K is inactive above pH 7.5 and R402Y is unable to catalyse fumarate reduction above pH 8.0. It is not clear why R402K and R402Y should only be able to function over such narrow pH ranges.

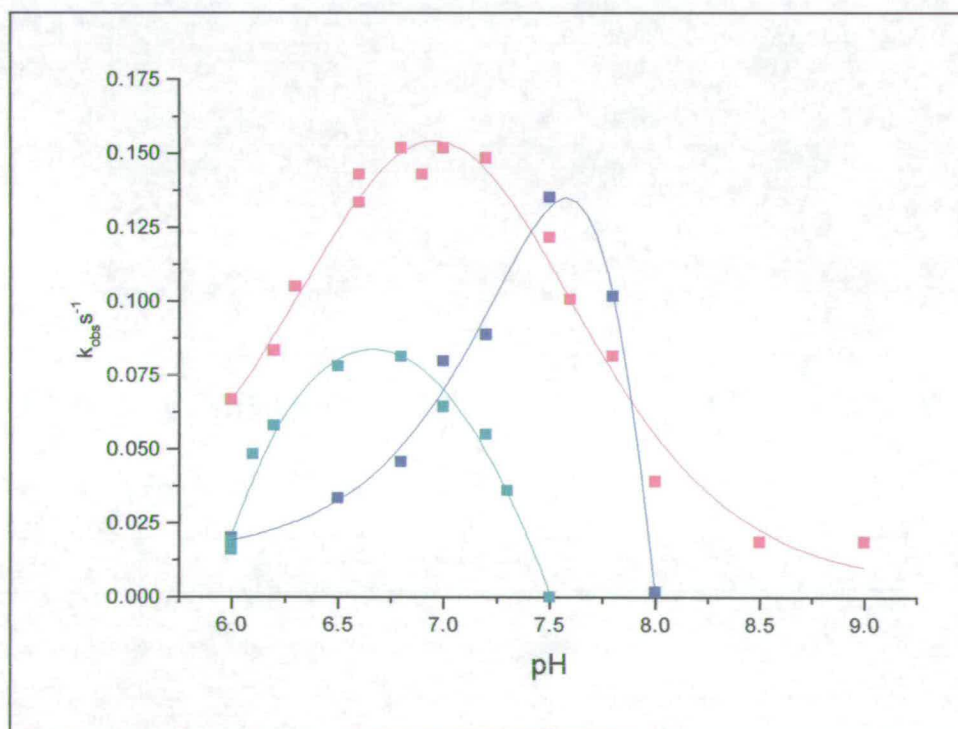


Figure 6.21 Comparison of pH profiles for R402H (RED), R402K (green) and R402Y (blue) Data has been fitted to equation 1 described in appendix 7.4 enabling the resolution of two pKa values.

6.4 Solvent Isotope Effect

6.4.1 Introduction

Many enzymatic properties differ when the enzyme is dissolved in deuterium oxide rather than H_2O . (Katz 1970). The solvent isotope effect arises from the isotopic free-energy differences for the reactant state (Michaelis complex) and transition state (Figure 6.22) (Schöwen 1981). Kinetic studies of solvent isotope effects in a series of mixtures of H_2O and D_2O can in some cases allow the dissection of the isotope effect into its component contributions from different sites in the reactant and transition states (Schöwen *et al.*, 1982). Each exchangeable hydrogenic site dissolved in H_2O/D_2O mixtures will, at equilibrium, contain a mixture of protium and deuterium. The ratio of protium to deuterium in a particular site will be equal to the ratio present in the bulk solvent only if the binding in the site equals the binding of an average water molecule. If the solute site binds its hydrogen more weakly, protium will accumulate while if the binding is tighter deuterium will be preferred. In order to identify isotopic effects for individual hydrogenic positions, rather than the aggregate effects, isotopic fractionation factors (ϕ) can be used (Schöwen 1978).

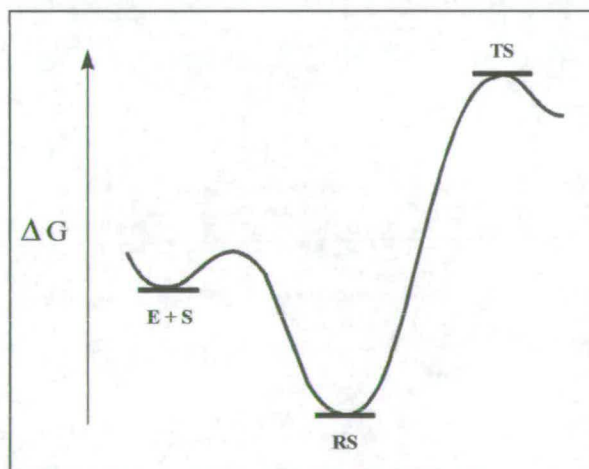


Figure 6.22 Free energy diagram for enzyme catalyzed reactions. E = enzyme, S = substrate. The reactant state (RS) and transition state (TS) free energy will be effected as a result of deuterium exchanging for protium.

It has been shown that Arg402 is the active site acid (Doherty *et al.*, 2000). However there is no direct evidence to suggest that fumarate reduction occurs in a concerted mechanism or in a stepwise process. However in the R402K and R402H mutant enzymes a stepwise mechanism might operate. For a stepwise process, in which proton transfer was the rate-limiting step, contributions to the solvent isotope effect would arise from transfer of a single protium species. In a concerted mechanism two protium species should be accounted for. The solvent isotope effect can be separated into its separate components using the Equation 6.3.

$$\frac{k_D}{k_H} = \frac{\prod_i^y \phi_i^T}{\prod_j^y \phi_i^R}$$

Equation 6.3 Solvent isotope effect arising from contributions from the fractionation factors in the reactant (ϕ_i^R) and transition (ϕ_i^T) state.

6.4.2 Solvent isotope studies on Fcc₃

Proton inventories were carried out for fumarate reduction by fcc₃-WT under steady-state conditions at pH 7.2 (Figure 6.23) (section 5.5). The data were fitted to a multiple z site model. (Appendix 7.2). It was not possible to assign contributions to a particular site in either reactant or transition state. However the data are not consistent with a mechanism in which only one proton is involved in either the reactant or transition state (appendix 7.3). This is in agreement with the proposed mechanism whereby hydride transfer from the flavin N5 to C2 of fumarate and proton transfer from Arg402 to C3 of fumarate occurs in a concerted process and involves two hydrogens.

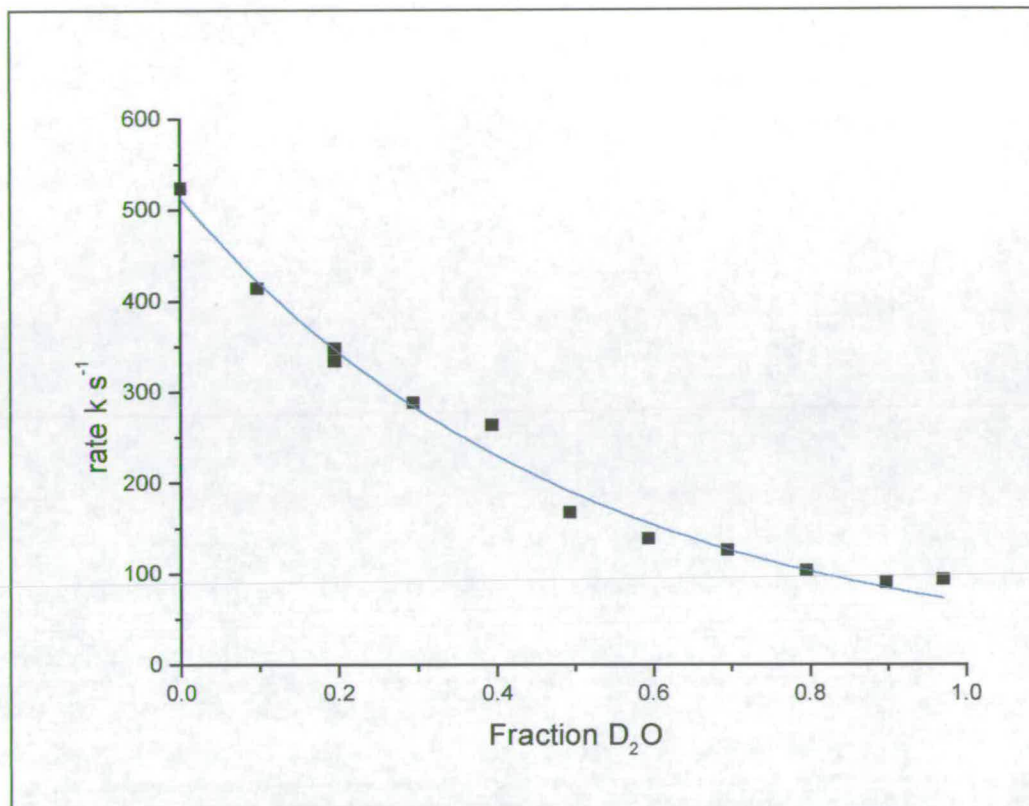


Figure 6.23 Solvent isotope effect observed for wild-type at pH 7.2 fitted to a model for multiple z sites. Individual points were calculated from steady-state assays.

To simplify the interpretation of experimental data the studies were repeated at pH 9.5 (Figure 6.24). Whereas pH 7.2 is close to the pK_a value of 7.32 for wild-type, at pH 9.5 many residues which may have contributed to the observed isotope effect of 7 will be unprotonated and therefore the influences from these proton sites will be removed. There is a reduction in the solvent isotope effect from 7 at pH 7.2 to 3.7 at pH 9.5 (Figure 6.24). However it was still not possible to attribute the effects observed to particular sites.

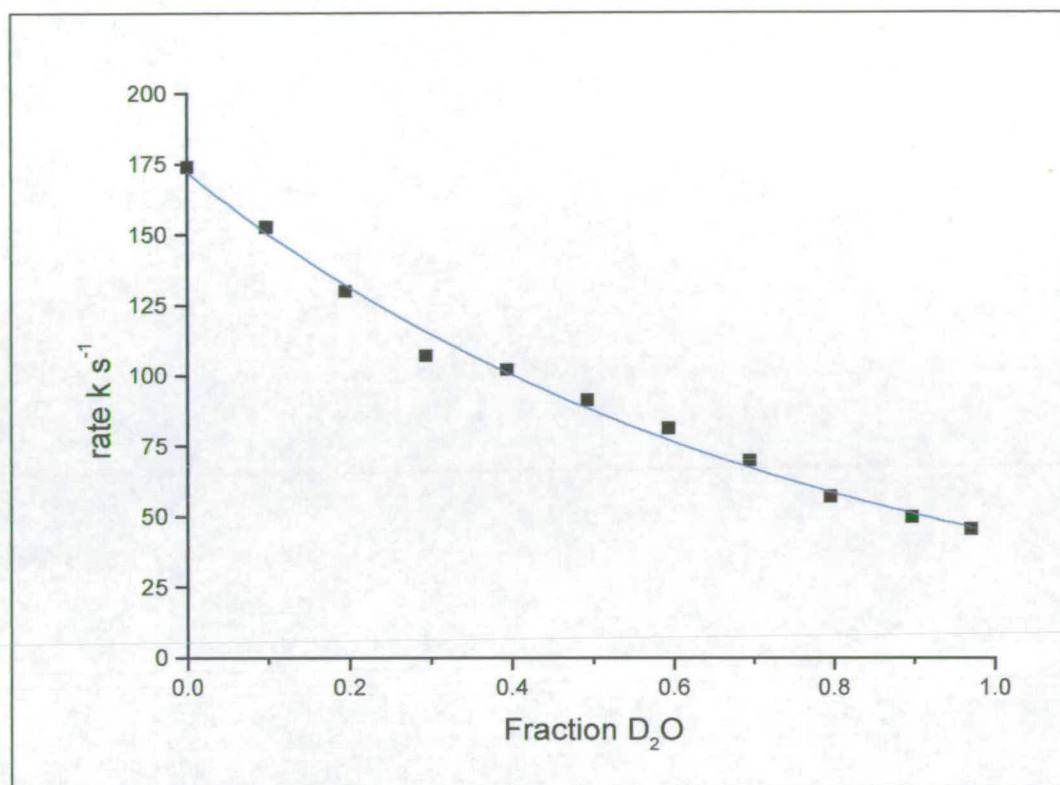


Figure 6.24 Solvent isotope effect observed for wild-type at pH 9.5. Data are fitted to a model for multiple z sites. Individual points were calculated from steady-state assays.

6.4.3 Solvent Isotope Studies on R402K- fcc_3 and R402H- fcc_3

Under steady-state conditions contributions to the solvent isotope effect observed in wild-type might arise from many different steps in the catalytic cycle. For the mutant enzymes R402K- fcc_3 and R402H- fcc_3 proton transfer from Lys402 or His402 to C3 of fumarate might be expected to be significantly slower than other steps in the catalytic cycle. This would enable the rate-limiting step in isolation to be examined. Proton inventories were carried out at pH 7.2 where these mutant enzymes showed a reasonable level of activity. Solvent isotope effects for R402K and R402H were found to be 2.2 (Figure 6.25) and 6.4 (Figure 6.26) respectively. However results could only be interpreted to give aggregate fractionation values and data was fitted to a multiple z site model.

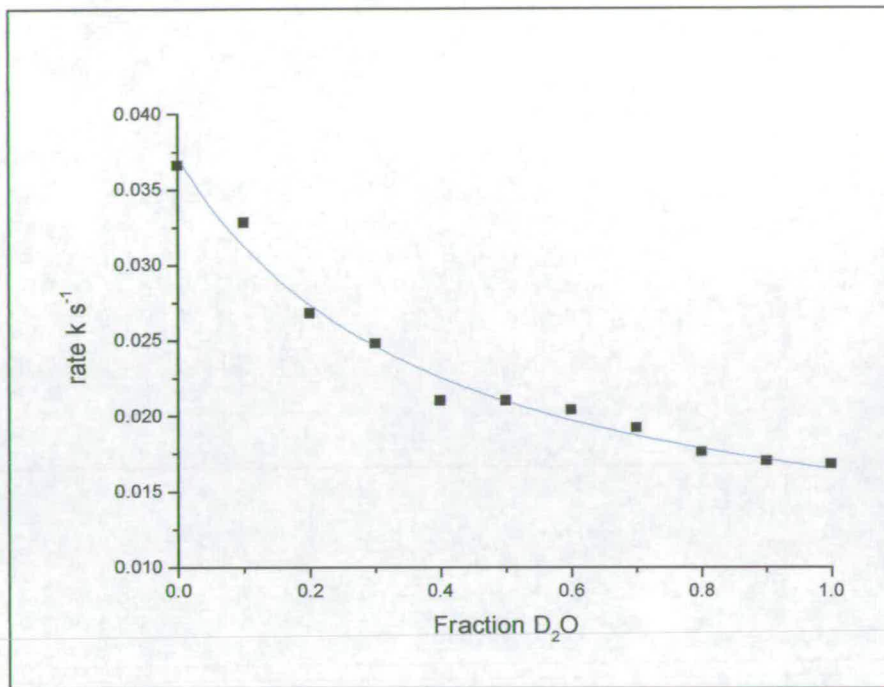


Figure 6.25 Solvent isotope effect for R402K-fcc₃. Steady-state assays were carried out at saturating fumarate concentrations and pH 7.2. Data is fitted to a multiple z site model.

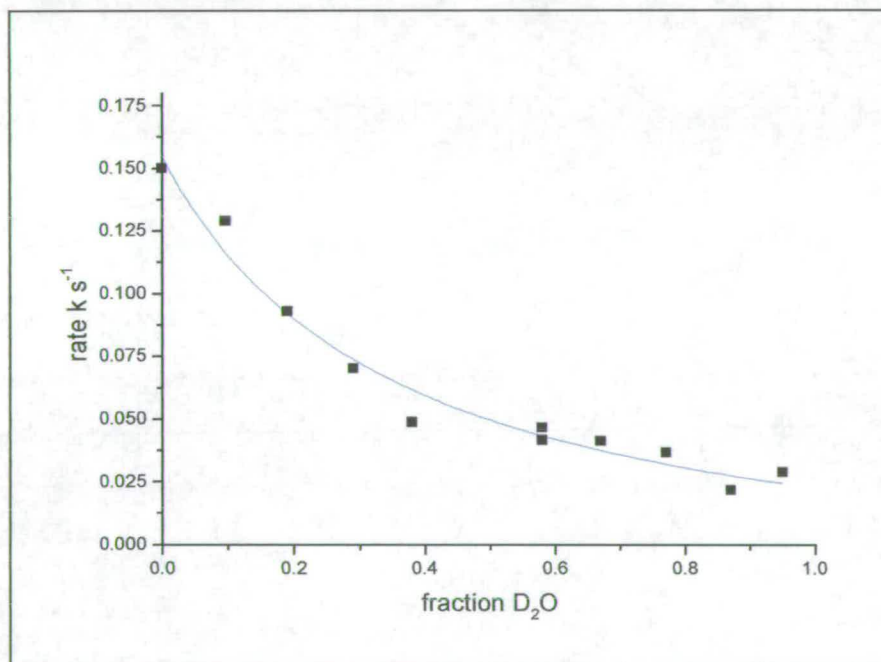


Figure 6.26 Solvent isotope effect for R402H-fcc₃ at pH 7.2. Steady-state assays were carried out at saturating fumarate concentrations and pH 7.2. Data is fitted to a multiple z site model.

Many different protons contribute to the observed solvent isotope effect. Data for wild-type, R402K and R402H fitted well to a model for multiple z sites in which many small isotope effects add up to a much more significant aggregate effect. It was not possible to assign effects to individual protons. Proton hydrogenic sites are generally considered exchangeable if hydrogen is bound to O, N or S. Many active-site residues will therefore have an influence on the solvent isotope effect. At pH 9.5 the solvent isotope effect is less than at pH 7.2 (7.0 and 3.7 respectively) suggesting that deprotonation of certain residues removes their contributions. Additionally, contributions may arise from the proton-transfer pathway (Figure 6.27). For fumarate reduction to occur protons are delivered to the active site via the triad of residues Arg381, Glu378 and Arg402. Individual steps or the cumulative effect from the complete pathway may add to the solvent isotope effect observed.

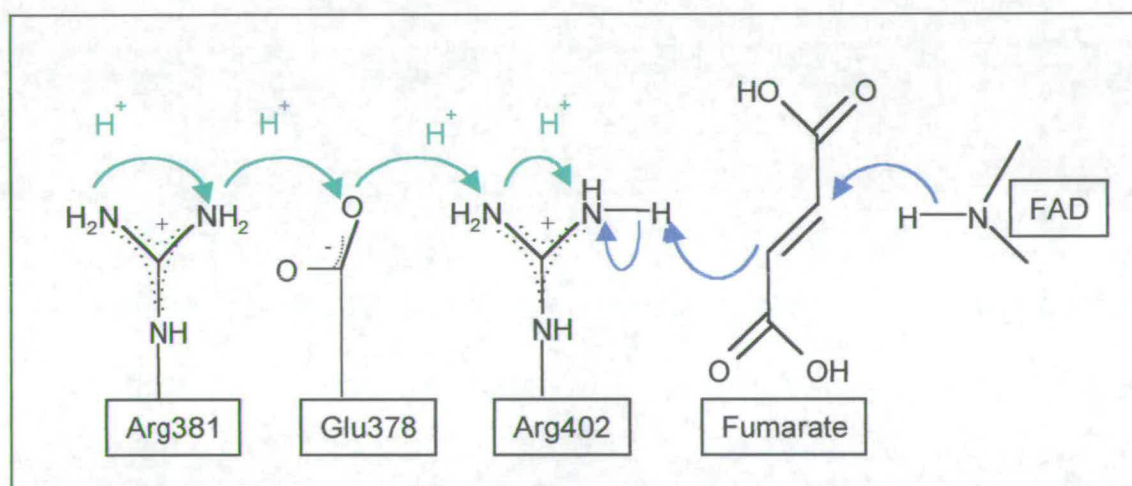


Figure 6.27 The proton-transfer pathway. Blue arrows represent electron flow and green arrows show proton transfer.

6.4 Conclusions

The aim of this work was to investigate the role of active site residues in flavocytochrome c_3 , in particular the identity of the active site acid. Site directed mutagenesis has been used to confirm that Arg402 is the active site acid. Mutation of the active site histidines (His504 and His365) individually and in the double mutant (H365A:H504A- fcc_3) resulted in enzymes which retained low levels of fumarate reductase activity confirming that neither of these residues are essential for catalysis. However, mutation of Arg402 to alanine results in complete loss of activity. The crystal structure of the R402A enzyme has been solved to 2.3 Å resolution. The presence of a water molecule close to fumarate at the active site suggests that a mechanism involving water as the active site acid as proposed by Lancaster *et al* (1999) can not be operational. The conservative mutation R402K has been constructed and characterised by kinetic analysis and the crystal structure solved to 2.0 Å resolution. The enzyme retains fumarate reductase activity showing that lysine is able to substitute for arginine as the active site acid. The crystal structure shows that lysine occupies the same space that was previously filled by arginine. In addition the position of residues involved in Michaelis complex formation are almost identical with that seen in the wild-type structure. The lysine side-chain extends to within 3.14 Å of the C3 position of fumarate. The equivalent distance to C3 of the malate like molecule in wild-type is 2.99 Å. However lysine is no longer positioned optimally to receive protons from Glu378. It is predicted that this together with the increased distance from proton donor to C3 of fumarate contributes to the slow rate of fumarate reduction. Construction of the mutant enzymes R402H- fcc_3 and R402Y- fcc_3 has demonstrated that histidine and tyrosine are also able to substitute for Arg402. At pH 7.2 the R402H enzyme is approximately 3-fold more active than R402K. This is thought to be due to the ability of the histidine, like arginine, to receive and donate protons to fumarate in a concerted process.

The proposed mechanism for fumarate reduction involves hydride transfer from the flavin N5 to C2 of fumarate and proton transfer from Arg402 to C3 of fumarate.

However there is no direct evidence to suggest that fumarate reduction occurs in a concerted mechanism rather than as a stepwise process. This has been investigated using solvent isotope studies. Although the data does not prove that a concerted mechanism operates it is not consistent with a mechanism in which only one proton is transferred at a time.

Substrate specificity studies and inhibition studies have been carried out to probe the active site structure. Flavocytochrome c_3 was unable to catalyse the reduction of alternative enoates to fumarate. However, oxaloacetate, methyl succinate and 3-nitropropionate were found to be inhibitors of succinate oxidation with K_i values of 5.3 μM , 1.7 mM and 0.5 mM respectively.

Future Work

The roles of key active residues have been investigated using site-directed mutagenesis but there is much scope for future work. The series of mutants constructed to investigate residues able to substitute for Arg402 has been extended to include glutamine. Preliminary studies show that this enzyme is also able to catalyse fumarate reduction. The crystal structure of the R402H mutant is currently being refined and work is underway to crystallise R402Y and R402Q. The importance of the Met 236 and Met375 which induce the twist in fumarate, in order to activate the substrate, are being investigated.

The reduction potentials of the four haem cofactors have been determined by redox potentiometry and protein film voltametry but it is not possible to assign potentials to individual haems using these techniques. To overcome this a series of mutants have been designed in which the axial ligands of individual haems have been mutated to alanine residues. These enzymes are being studied by protein film voltametry enabling the effected haem to be detected as a result of its change in reduction potential.

Part 2

References

- Ackrell, B. A. C., Armstrong, F. A., Cochran, B., Sucheta, A., and Yu, T., (1993) *FEBS Letters*, **326**, 92-94.
- Ackrell, B. A. C., Cochran, B., and Cecchini, G., (1989) *Archives of Biochemistry and Biophysics*, **268**, 1, 26-34.
- Arikawa, Y., Enomoto, K., Muratsubaki, and H., Okazaki, M., (1998) *FEMS*, **165**, 111-116.
- Bachela, L., Lina, C., Todone, F., Negri, A., Tedeschi, G., Ronchi, S., and Mattevi, A., *Acta Crystallographica*, **D55**, 549-551 (1999)
- Bamford, V., Dobbin, P.S., Lee, S. Reilly, A., Powell, A. K., Richardson, D. J., and Hemming, A. M., (1999a), *Acta Crystallographica*, **D55**, 1222-1225.
- Bamford, V., Dobbin, P.S., Richardson, D. J., and Hemmings, A. M., (1999b) *Nature Structural Biology*, **6**, 12, p1104-1107.
- Blautt, M., Whittaker, K., Valdovinos, A., Ackrell, B. A. C., Gunsalus, R. P., and Cecchini, G., (1989) *J. Biological Chemistry*, **264**, 23, 13599-13604.
- Cammack, R., Patil, D. S., and Weiner, J. H., (1986) *Biochimica et Biophysica Acta*, **870**, 545-551.
- Cammack, R., (1992), *Nature*, **356**, 288-289.
- Cecchini, G., Thompson, C. R., Ackrell, B.A.C., Westenberg, N. D., and Gunsalus, R. P., (1986a) *P. Natl. Acad. Sci.*, **83**, 8898-8902.
- Cecchini, G., Ackrell, B. A. C., Deshler, J. O., and Gunsalus, R. P., (1986b) *J. Biol. Chem.*, **261**, 4, 1808-1814.
- Cecchini, G., Sices, H., Shroder, I., and Gunsalus, R. P., (1995) *J. Bacteriol.* **177**, 16, 4587-4592.
- Chen, I-P., Maths, P., Koepke, J., and Michel, H., (2000), *Biochemistry*, **39**, 3592-3602.
- Cole, S., (1982) *Eur. J. Biochem.*, **122**, 479-484.
- Cole, S., Candon, C., Lemire, B. D., and Weiner, J. H., (1985) *Biochimica et Biophysica Acta*, **811**, 381-403.
- Cooley, J. W., Howitt, C. A., and Vermaas, W. F. J., (2000), *J. Bacteriology*, **182**, 3, 714-722.
- Dickie, P., and Weiner, J. H., (1979), *Can. J. Biochem.*, **57**, 813-821.

- Dobbin, P. S., Butt, J. N., Powell, A.K., Reid, G.A., and Richardson, D. J., (1999) *Biochem. J.*, **342**, 439-448.
- Doherty, M. K., Pealing, S. L., Miles, C. S., Moysey, R., Taylor, P., Walkinshaw, M. D., Reid, G. A., and Chapman, S. K., (2000) *Biochemistry*, **39**, 10695-10701.
- Doherty, M., PhD thesis, Mechanistic Characterisation of Flavocytochrome c_3 , the Fumarate Reductase from *Shewanella frigidimarina* NCIMB400, University of Edinburgh, (1999)
- Geisler, V., Ullmann, R., and Kroger, A., (1994) *Biochimica et Biophysica Acta*, **1184**, 219-226.
- Ghisla, S. and Massey, V., (1989), *Eur. J. Biochem.*, **181**, 1-17.
- Gordon, E. H. J., Pealing, S. L., Chapman, S. K., Ward, B., and Reid, G. A., (1998), *Microbiology*, **144**, 937-945.
- Heering, H. A., Weiner, J. H., and Armstrong, F. A., (1997), *J. Am. Chem. Soc.*, **119**, 48, 11628-11638.
- Hunter, G. A., and Ferreira, G. C., (1999), *Biochemistry*, **38**, 3711-3718.
- Iverson, T. M., Luna-Chavez, C., Cecchini, G., and Rees, D. C., (1999) *Science*, **284** 1960-1966.
- Katz, J. J., and Crespi, H. L., in 'Isotope Effects In Chemical Reactions', P. 286, Van Nostrand-Rheinhold, Princetown, New Jersey (1970)
- Kowal, A. T., Werth, M.T., Manodori, A., Cecchini, G., Schröder, I., Gunsalus, R. P. and Johnson, M. K., (1995), *Biochemistry*, **34**, 12284-12293,
- Lancaster, C. R. D., Kroger, A., Auer, M., and Michel, H., (1999), *Nature*, **402**, 37-385.
- Lancaster, C. R. D., and Kroger, A., (2000), *Biochimica et Biophysica Acta*, **1459**, 422-431.
- Leys, D. Tsapin, A. S., Nealsen, K. H., Meyer, T. E., Cusanovich, M. A., and Van Beeumen, J. J., (1999), *Nature Structural Biology*, **6**, 12.
- Lorenzen, J. P., Kroger, A., and Udden, G., (1993), *Arch. Microbiol.* **159**, 477-483.
- Lu, Z., Nagata, S., McPhie, P., and Wilson Miles, E., (1993), *J. Biol. Chem.*, **268**, 12, 8727-8734.
- Macheroux, P., (1999) Methods in Molecular Biology, 131 in 'Flavoprotein Protocols' (Ed. Chapman, S. K., and Reid, G. A.) 1-7.

- Maklashina, E., Berthold, D. A., and Cechini, G., (1998), *J. Bacteriology*, **180**, 22, 5989-5996.
- Mattevi, A., Tedeschi, G., Bacchella, L., Coda, A., Negri, A., and Ronchi, S., (1999), *Structure*, **7**, 7, 745-757.
- Mikouliniskaia, O., Akimenko, V., Galouchko, A., Thauer, R., and Hedderich, R., (1999), *Eur. J. Biochem.*, **263**, 346-352.
- Morris, C. J., Black, A. C., Pealing, S. L., Manson, F. D., Chapman, S. K., Reid, A. G., Gibson, D. M., and Ward, F. B., (1994). *J. Biochem*, **302**, 587-593,
- Mortarino, M., Negri, A., Tedeschi, G., Simonic, T., Duga, S., Gassen, H. G., and Ronchi, S., (1996), *Eur. J. Biochem.*, **239**, 418-426,
- Myers, C. R., and Myers, J. M., (1992), *FEMS Microbiol. Lett.*, **98**, 13-20.
- Myers, C. R., and Myers, J. M., (1997a), *J. Bacteriology*, **179**, 4, 1143-1152.
- Myers, C. R., and Myers, J. M., (1997b), *Lett. In Appl. Microbiol.*, **25**, 162.
- Myer, J. M., and Myer, C. R., (2000), *J. Biol. Chem.*, **182**, 1, 67-75
- Nasu, S., Wicks, F. D. and Gholson, R. K., (1982), *J. Biol. Chem.*, **257**, 626-632.
- Ohnishi, T., Moser, C.C., Page, C. C., Dutton, P.L. and Yano, T., (2000), *Structure* **8**, 2, 23-32.
- Pealing, S. L., Black, A. C., Manson, F. D. C., Ward, B., Chapman, S. K., and Reid, G. A., (1992), *Biochemistry.*, **31**, 12132-12140.
- Pealing, S. L., Cheesman, M. R., Reid, G. A., Thompson, A. J., Ward, B., and Chapman, S. K., (1995), *Biochemistry*, **34**, 6153-6158.
- Pealing, S. PhD Thesis, Flavocytochrome *c*₃ from *Shewanella Putrefaciens*: A soluble Fumarate Reductase, University of Edinburgh, (1994)
- Pike, A. PhD thesis, A study of the Cytochrome *c*₃ from *Shewanella* NCIMB400 and The Flavocytochrome *b*₂ from *Saccharomyces Cerivisiae*, University of Edinburgh, (1998)
- Rege, V. D., Kredich, N. M., Tai, C., Karsten, W. E., Schnackerz, K. D., and Cook, P., (1996), *Biochemistry*, **35**, 13485-13494.
- Reid, G. A., Gorden, E. H., Hill, A. E., Doherty, M., Turner, K., Holt, R., and Chapman, S. K., (1998), *Biochem. Soc. Trans.*, **26**, 418-421.
- Reid, G. A., Miles, C. S., Moysey, R. K., Pankhurst, K. L., and Chapman, S. K., (2000), *Biochimica et Biophysica Acta*, **1459**, 310-315.

- Rhee, S., Parris, K. D., Ahmed, A., Wilson Miles, E., Davies, D. R., (1996), *Biochemistry*, **35**, 4211-4221.
- Robinson, J. J., and Weiner, J. H., (1982), *Can. J. Biochem*, **60**, 811-816.
- Rossi, C., Hauber, J., and Singer, T. P., (1964), *Nature*, **204**, 167-170.
- Rothery, R. A., and Weiner, J. H., (1998), *Eur. J. Biochem.*, **254**, 588-595,
- Schöwen, R. L., in 'Transition States of Biochemical Processes' P. 225, Plenum, New York (1978).
- Schöwen, K. B., and Showen, R. L., (1982), *Methods in Enzymology*, vol **87**, p27
- Schöwen, R. L., in 'Isotope Effects on Enzyme-catalyses Reactions' P. 64 University Park Press, Baltimore, Maryland.
- Schröder, I., Gunsalus, R. P., Ackrell, B. A. C., Cochran, B., and Cecchini, G., (1991), *J. Biol. Chem.*, **266**, 21, 13572-13579.
- Simon, J., Gross, R., Ringel, M., Schimdt, E., and Kroger, A., (1998), *Eur. J. Biochem.*, **251**, 418-426.
- Simpkin, D., and Ingeldew, W. J., (1985), *Biochem. Soc. Trans.*, **13**, 602-607.
- Spencer, M. E., and Geuest, J. R., (1973), *J. Bacteriology*, **114**, 563-570.
- Sucheta, A., Ackrell, B. A. C., Cochran, B. and Armstrong, F. A., (1992) *Nature*, **356**, 361-362.
- Sucheta, A., Cammack, R., Weiner, J., and Armstrong, F. A., (1993), *Biochemistry*, **32**, 5455-5465.
- Taylor, P., Pealing, S. L., Reid, G. A., Chapman, S. K., and Walkinshaw, M. D., (1999), *Nature Structural Biology*, **6**, 12, 1108-1112.
- Tedeschi, G., Negri, A., Motarino, M., Ceciliani, F., Simonic, T., Faotto, L., and Ronchi, S., (1996), *Eur. J. Biochem.*, **239**, 427-433.
- Tedeschi, G., Zetta, L., Negri, A., Motarino, M., Ceciliani, F., Ronchi, S., (1997), *Biochemistry*, **36**, 16221-16230.
- Tedeschi, G., Negri, A., Ceciliani, F., Mattevi, A., and Ronchi, S., (1999), *Eur. J. Biochem.*, **260**, 896-903.
- Teipel, J. W., Hass, G. M., and Hill, R. L., (1968), *J. Biol. Chem.*, **243**, 21, 5684-5694.
- Thorneley, R. N. F., *Biochemica et Biophysica Acta*, **333**, 487-496.

- Toney, M. D., and Firsch, J. F., (1993), *Biochemistry*, **32**, 1471-1479.
- Tsapin, A. T., Bubaev, D. S., Nealson, K. H., and Keppen, O.I., (1995), *Appl. Magn. Reson.*, **9**, 509-516.
- Tsapin, I. A., Nealson, K. H., Meyers, T., Cusanovich, M. A., Van Beuumen, J., Crosby, L. D., Feinberg, B. A., and Zang, C., (1996), *J. Bacteriology*, **178**, 21, 6386-6388.
- Turner, K. L., Doherty, M. K., Heering, H. A., Armstrong, F. A., Reid, G. A., and Chapman, S. K., *Biochemistry*, **38**, 11, 3302-3309, (1999)
- Unden, G., Hackenberg, and H., Kroger, A., (1980), *Biochimica et Biophysica Acta*, **591**, 275-288.
- van Hellemond, J. J., and Tielens, G. M., (1994), *Biochemical Journal.*, **304**, 321-331.
- van Hellemond, J. J., Klockiewicz, M., Gaasenbeek, C. P. H., Roos, M. H., and Tielens, A. G. M., (1995), *J. Biol. Chem.*, **270**, 52, 31065-31070.
- Vibat, C. T., Cecchini, G., Nakamura, K., Kita, K., Gennis, R. B., (1998), *Biochemistry*, **37**, 4148-4159.
- Weiner, J. H., Cammack, R., Cole, S., Candon, C., Honore, N., Lemire, B. D., and Shaw, G., (1986), *P. Natl. Acad. Sci.*, **83**, 2056-2060.
- Werth, M. T., Cecchini, G., Manodori, A., Ackrell, B. A. C., Schroder, I., Gunsalus, R. P., and Johnson, M. K., (1990), *P. Natl. Acad. Sci.*, **87**, 8965-8969.
- Yoshimura, T., Bhatia, M. B., and Manning, M., (1992) *Biochem. J.*, **31**, 11748-11754.
- Zhao, Z., Rothery, R. A., and Weiner, J. H., (1999), *Eur. J Biochem.* **260**, 50-56.
- Ziak, M., Jaussi, R., Gehring, H., Christen, P., (1990), *Eur. J. Biochem.*, **187**, 329-333.
- Zientz, E. Bongaerts, J., and Unden, G., (1998), *J. Bacteriology*, **180**, 20, 5421-5425.

Appendix

7.0 Appendix

7.1 Abbreviations

7.1.1 Amino Acids

Alanine	Ala	A
Arginine	Arg	R
Asparagine	Asn	N
Aspartic acid	Asp	D
Cysteine	Cys	C
Glutamic acid	Glu	E
Glutamine	Gln	Q
Glycine	Gly	G
Histidine	His	H
Isoleucine	Ile	I
Leucine	Leu	L
Lysine	Lys	K
Methionine	Met	M
Phenylalanine	Phe	F
Proline	Pro	P
Serine	Ser	S
Threonine	Thr	T
Tryptophan	Trp	W
Tyrosine	Tyr	Y
Valine	Val	V

7.1.2 Kinetic parameters

k_{cat}	Rate constant under saturating conditions
k_{obs}	Observed rate
k_{lim}	Rate constant under pre-steady-state conditions
K_{m}	Michaelis constant
K_{d}	Binding constant
K_{I}	Inhibitor binding constant

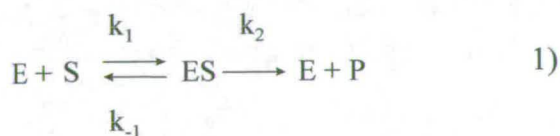
7.1.3 Standard units

m	metre	°C	degrees Celsius
g	gram	M	molar
s	second	Da	dalton units
l	litre	Å	angstrom

7.1.4 Abbreviations

Abs	Absorbance
APS	Ammonium persulfate
ATP	Adenosine triphosphate
D ₂ O	deuterated water
DCIP	Dichloroindophenol
DMSO	Dimethyl Sulphoxide
DTT	Dithiothreitol
<i>E. coli</i>	<i>Escherichia coli</i>
EDTA	Ethylene diamine tetraacetic acid
FAD	Flavin Adenine Dinucleotide
FMN	Flavin Mononucleotide
FPLC	Fast protein liquid chromatography
FRD	Fumarate reductase
I	Ionic strength
IPTG	Isopropyl-β-thiogalactoside
LB	Luria broth
NMR	Nuclear magnetic resonance
ox	Oxidised
PAGE	Polyacrylamide gel electrophoresis
PFV	Protein film voltammetry
red	Reduced
R _i	Ionic radius
SDH	Succinate Dehydrogenase
SDS	Sodium dodecyl sulfate
TCA	Tricarboxylic acid cycle
TEMED	N,N,N',N'-tetramethylene diamine
Tris	Tris(hydroxymethyl) aminomethane
UV	Ultra-violet

7.2 Derivation of the Michaelis-Menten Equation.



E = enzyme, S = substrate, P = product, ES = enzyme-substrate complex.

$$V = \text{catalytic rate} = k_2 [ES] \quad 2)$$

$$\text{rate of formation of ES} = k_1 [E][S] \quad 3)$$

$$\text{rate of dissociation of ES} = (k_{-1} + k_2) [ES] \quad 4)$$

k_2 = turnover number *i.e.* the number of substrate molecules converted into product by an enzyme molecule in a unit time when under saturating conditions = k_{cat}

Assumption 1

Under steady-state the concentrations of intermediates stay the same while the concentrations of starting materials and products are changing. This occurs when the rates of formation and breakdown of ES are equal.

$$k_1 [E][S] = (k_{-1} + k_2) [ES] \quad 5)$$

$$[ES] = \frac{k_1 [E][S]}{(k_{-1} + k_2)} \quad 6)$$

$$K_m = \frac{(k_{-1} + k_2)}{k_1} \quad [ES] = \frac{[E][S]}{K_m} \quad 7)$$

The concentration of substrate-free enzyme, [E], is equal to the total enzyme concentration, $[E_0]$, minus the concentration of the ES complex.

$$[E_0] = [E] + [ES] \quad [E] = [E_0] - [ES] \quad 8)$$

Assumption 2

If the substrate concentration far exceeds that of the substrate-free enzyme the rate of the reaction is unaffected by the depletion of substrate throughout the course of the reaction *i.e.* $[S] = [S_0]$. Substituting expression 8 for [E] into equation 7,

$$[ES] = \frac{([E_0] - [ES])[S]}{K_m} \quad 9)$$

$$[ES] = \frac{[E_0][S]}{[S] + K_m} \quad (10)$$

By substituting this expression for [ES] into equation 4 gives the Michaelis-Menten equation (11),

$V = k_{cat} [ES]$
and

$$V = \frac{k_2 [E_0] [S]}{[S] + K_m} \quad (11)$$

Case 1

The maximal rate, V_{max} is attained when the enzyme sites are saturated with substrate, when $[S] \gg K_m$.

$$V_{max} = k_2 [E_0] = k_{cat} [E_0]$$

Case 2

When the substrate concentration is much less than K_m , then the rate is directly proportional to [S]

$$\frac{[S]}{[S] + K_m} \approx \frac{[S]}{K_m} \quad \text{and} \quad V = \frac{k_{cat} [E_0] [S]}{K_m}$$

Case 3

The substrate concentration equals the value of K_m ,

$$\frac{[S]}{[S] + K_m} \approx \frac{[S]}{2[S]} \approx \frac{1}{2} \quad \text{and} \quad V = \frac{k_{cat} [S_0]}{2} = \frac{V_{max}}{2}$$

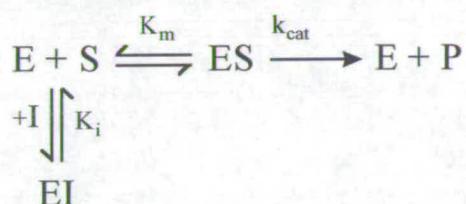
Case 4

The dissociation of the ES complex is more rapid than its conversion of substrate to product, $k_{-1} \gg k_{cat}$, K_m is equal to the dissociation constant, K_d , and is a measure of the strength of the ES complex.

$$K_d = \frac{[E][S]}{[ES]} = \frac{k_{-1}}{k_1} \quad \text{and} \quad K_m = \frac{k_{-1} + k_{cat}}{k_1} \approx \frac{k_{-1}}{k_1}$$

7.2.1 Competitive Inhibition

Competitive inhibition occurs when substrate and inhibitor compete for the active site.



The dissociation constant, K_i is defined as,

$$K_i = \frac{[E][I]}{[EI]}$$

$$K_m = \frac{[E][S]}{[ES]}$$

$$[EI] = \frac{[E][I]}{[K_i]}$$

The total enzyme concentration, $[E]_t$ is given by,

$$[E]_t = [E] + [ES] + [EI]$$

Substitution of $[EI]$ gives,

$$V = \frac{k_{\text{cat}} [E]_0 [S]}{[S] + K_m (1 + [I] / K_i)}$$

7.3 Debye-Hückel theory

The picture underlying the Debye-Hückel theory is of a tendency for oppositely charged ions to attract each other. As a result, cations and anions are not uniformly distributed in solution: anions are more likely to be found near cations, and vice versa. The energy, and therefore chemical potential, of any given central ion is lowered by electrostatic interactions with its ionic atmosphere. At low concentrations, the activity coefficient can be calculated from the Debye-Hückel limiting law,

$$(1) \quad \log \gamma_{\pm} = -Az_i^2 \sqrt{I}$$

γ = activity coefficient of ion.

z_i = charge on the ion.

I = ionic strength of solution.

$A = 0.509 \text{ mole}^{-1/2} \text{ l}^{1/2}$ for an aqueous solution at 25°C (in general, A depends on temperature and solvent)

The limiting law assumes that ions are point charges and ignores some solvent effect which are important when studying macromolecules at high ionic strength. In order to take into account these effects the equation is incorporated into the Brønsted's kinetic relation.

$$(2) \quad \log k_2 = \log k_0 + 2Az_+z_- \sqrt{I}$$

k_2 = second order rate constant.

k_0 = second order rate constant at I_0

Plotting $\log k_2$ vs \sqrt{I} generates a straight line allowing calculation of the charges involved in the reaction between two species. It should also be noted that the equation

does not fit satisfactorily to data obtained at high ionic strength. However, the extended Debye-Brønsted equation (3) introduces a term which is linearly dependent on ionic strength.

$$(3) \quad \log k_2 = \log k_0 + 2Az_+z_- \sqrt{I} - BI$$

In this case a plot of $\log k_2$ vs \sqrt{I} generates a parabola which fits more accurately to high ionic strength data. The coefficient, B, has no simple definition but is designed to compensate for deviations due to short-range solvent interactions and the increasing dominance of the ionic radius at high ionic strength.

(Robinson & Stokes, 1973; Perlmutter-Hayman, 1959)

7.4 pH Dependence

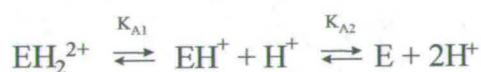
The ionisation constants for acids and bases can be described using the following equations.

$$K_a = \frac{[A^-][H^+]}{[AH]}$$

The pK_a of such systems is defined by;

$$pK_a = -\log K_a$$

Rearrangement of the above equations allows derivation of the Henderson-Hasselbach equation;



$$K_{A1} = \frac{[H^+][EH^+]}{[EH_2^{2+}]} \quad K_{A2} = \frac{[E][H^+]}{[EH^+]}$$

Therefore the pK_a can be described as the pH at which the concentration of protonated and deprotonated species are equal, i.e. the species is half neutralised.

$$pH = pK_{A1} - \text{Log} \left(\frac{[EH^+]}{[EH_2^{2+}]} \right)$$

$$pH = pK_{A2} - \text{Log} \left(\frac{[E]}{[EH^+]} \right)$$

Equations for the three individual species can be obtained,

$$[E] = \frac{10^{(pK_{A1} - pH)}}{1 + 10^{(pK_{A1} - pH)} + 10^{(pH - pK_{A2})}} \quad [EH^+] = \frac{1}{1 + 10^{(pK_{A1} - pH)} + 10^{(pH - pK_{A2})}}$$

$$[EH_2^{2+}] = \frac{10^{(pH - pK_{A2})}}{1 + 10^{(pK_{A1} - pH)} + 10^{(pH - pK_{A2})}}$$

The total activity measured at any pH value will be a sum of the contributions from the three species,

$$\text{Activity} = k_0[E] + k_1[EH^+] + k_2[EH_2^{2+}]$$

Fitting of the experimental data to the final equation, allows the resolution of two pK_a values.

$$\text{Activity} = \frac{k_0 10^{(pK_{A1} - pH)} + k_1 + k_2 10^{(pH - pK_{A2})}}{1 + 10^{(pK_{A1} - pH)} + 10^{(pH - pK_{A2})}}$$

7.5 Solvent Isotope Effects

If the fraction of deuterium in a mixed isotopic solvent is called n , then the isotopic fractionation factor, ϕ_i is simply the ratio of D:H at the i^{th} hydrogenic site relative to water (Figure 7.1).

$$\phi_i = \frac{D_i}{H_i} \bigg/ \frac{n}{(1-n)}$$

Figure 7.1 Fractionation factor, ϕ denotes the ratio of deuterium to hydrogen at a particular hydrogenic site.

A simple case, in which a reactant RH, with one exchangeable hydrogen forms a transition state TH also with one exchangeable hydrogen, is represented in Figure 7.2.

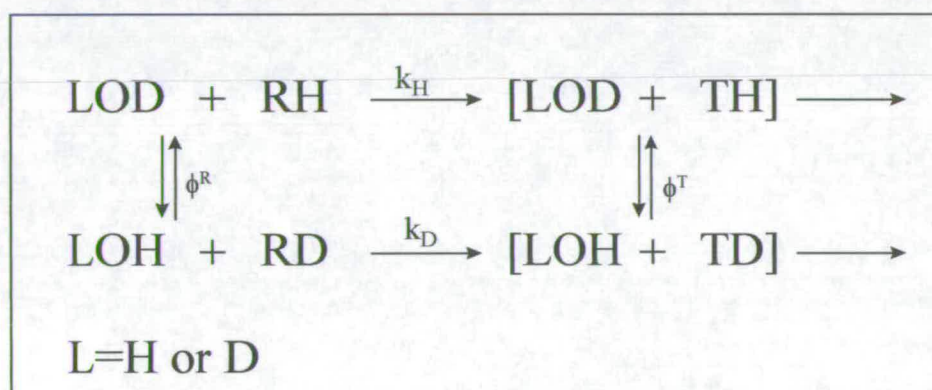


Figure 7.2 Fractionation factors for a simple case involving one exchangeable hydrogen in the reactant state and one in the transition state.

The solvent isotope effect observed can be expressed in terms of the fractionation factors for the single reactant and transition sites.

$$\frac{k_D}{k_H} = \frac{\phi^T}{\phi^R}$$

Figure 7.3 The solvent isotope effect expressed in terms of fractionation factors.

The kinetic isotope effect is then determined by the reactant state and transition state fractionation factors which change on activation. A considerable number of isotopic fractionation factors have been determined experimentally and they can be generalised to form the functional-group rule. This simplification means that values of ϕ_i depend on the functional group in which the i^{th} site is located and not on more remote features of the molecular environment. Thus, all alcohols can be expected to show the same fractionation factor, all amines the same one, etc.

In order to identify isotopic effects for individual hydrogenic positions rather than the aggregate effects described by free energies of transfer isotopic fractionation factors can be used (Schöwen 1978). Protein hydrogenic sites are generally considered exchangeable if hydrogen is bound to O, N or S and non exchangeable if bound to carbon. Hydrogenic sites can be classified into:

- 1) Internal sites - exchangeable hydrogenic sites in the protein giving substantial effect on the free energy of transfer.
- 2) External sites - sites in water molecules that are strongly interacting with the protein.
- 3) Z sites-hydrogenic sites in weakly interacting water molecules or in exchangeable sites in proteins where the binding potential is close to bulk water so that only small isotope effects are produced. Such sites will be important if their aggregate isotope effect becomes significant.

7.4.1 Proton Inventories

Kinetic studies of solvent isotope effects in a series of mixtures of H_2O and D_2O can in some cases allow the dissection of the isotope effect into its component contributions from different sites in the reactant and transition states (Schöwen *et al.*, 1982). A solvent isotope effect of $k_{\text{H}}k_{\text{D}} < 1$ indicates an inverse isotope effect and net binding at contributing hydrogenic sites is tighter in effective transition states than in effective reactant state. If $k_{\text{H}}k_{\text{D}} > 1$, a normal isotope effect indicates net binding is

looser in effective transition state than in effective reactant state. Proton inventories corresponding to an overall isotope effect $k_0 > k_n$ will give a general 'tilt' of the curve downwards. A number of model curves can be generated to which data can be fitted (Figure 7.4). For a single site in the transition state, k_n is linear (a), for a single site in the reactant state, k_n is a steep bowl shape and k_n^{-1} is linear (d). For two sites in the transition state there is the opportunity even at small n , for both sites to be deuterated, thus the rate drops off initially more rapidly than for the one proton effect resulting in the downward bowing of the curve and data can be fitted to a quadratic (b). The larger the number of sites in the transition state the greater the curvature, but this effect is opposed when sites in the reactant state also contribute. If both reactant and transition state contribute to a solvent isotope effect possibly with multiple z sites in each then influences begin to oppose each other and it becomes impossible to ascribe the sites to a particular state and the models converge on a curve for multiple z sites (c).

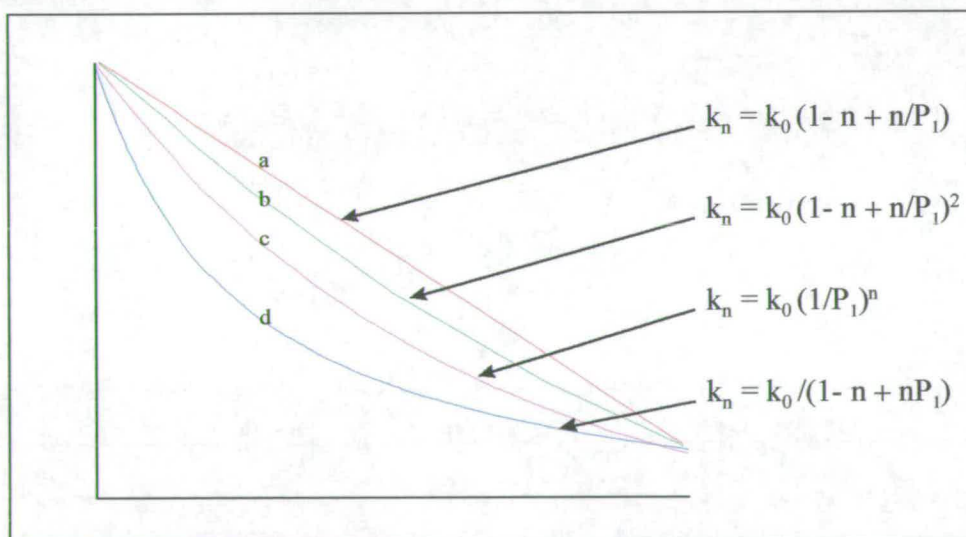


Figure 7.4 Model curves generated from solvent isotope effect. A linear curve is obtained for a single site in the transition state (a) or a steep curve for a single site in the reactant state (d). Curve b corresponds to two sites in the transition state and curve c to a multiple z site model.

7.7 Conferences and Courses Attended

Department of Chemistry Colloquia

ISTAS Summer School, Structure and Function of Metalloenzymes, Oeiras, Portugal, Sept. 7th-19th 1998

Biochemical Society Meeting (redox enzymes section), University of Leicester, Sept. 1998

13th International Congress on Flavins and Flavoproteins, University of Konstanz, Germany, 29th Aug - 4th Sept. 1999 (Abstract and Poster presented)

3rd Furbush Redox Enzymes Meeting, University of Edinburgh, 1998

4th Furbush Redox Enzymes Meeting, University of Edinburgh, 2000 (speaker)

Inorganic Chemistry Group Meeting, Furbush Field centre, Scotland 2000 (speaker)

7.7 Publications

Chapman, S. K., Welsh, F., Moysey, R., Mowat, C., Doherty, M. K., Turner, K. L., Munro, A. W., Reid, G. A. (1999): Flavocytochromes: transceivers and relays in biological electron transfer. *Biochemical Society Transactions*, **27**, 185-189.

Moysey, R., Welsh, F., and Chapman, S. K., (1999) Flavins and Flavoproteins, *Molecular Recognition in the Flavin Domain of Flavocytochrome *b*₂*.

Doherty, M. K., Pealing, S. L., Miles, C. S., Moysey, R., Taylor, P., Walkinshaw, M. D., Reid, G. A., and Chapman, S. K., (2000): Identification of the active site acid/base catalyst in a bacterial fumarate reductase: A kinetic and Crystallographic Study, *39*, 35, 10695-10701.

Reid, G. A., Miles, C. S., Moysey, R., Pankhurst, K. L., and Chapman, S. K., (2000) Catalysis in fumarate reductase. *Biochimica et Biophysica Acta*, **1459**, 310-315.

Flavocytochromes: transceivers and relays in biological electron transfer

S. K. Chapman¹, F. Welsh*, R. Moysey*, C. Mowat*, M. K. Doherty*, K. L. Turner*, A. W. Munro*
and G. A. Reid†

*Department of Chemistry, University of Edinburgh, West Mains Road, Edinburgh EH9 3JJ, Scotland, U.K., and

†Institute of Cell and Molecular Biology, University of Edinburgh, Mayfield Road, Edinburgh EH9 3JR, Scotland, U.K.

Introduction

Flavocytochromes are multi-centre redox proteins containing both flavin and haem [1,2]. They catalyse a wide range of biologically important redox processes, including the oxidation and reduction of organic molecules, simple electron-transfer reactions and the activation of molecular oxygen. This diversity of function is made possible by the combination of flavin and haem cofactors, which allows the direct coupling of two-electron to one-electron oxido-reductions. Thus flavins can act as molecular transceivers receiving the redox equivalents, as a hydride for example, and transmitting them as electrons or vice versa. Haem groups can function both as efficient one-electron relays or as catalytic centres for the activation of small molecules such as dioxygen [1]. The combination of these cofactors produces flavocytochromes with great catalytic versatility, e.g. flavocytochrome *P*-450 BM3 (a fatty acid mono-oxygenase), flavocytochromes *b*₂ (lactate and mandelate dehydrogenases) and flavocytochrome *c*₃ (a fumarate reductase). These three flavocytochromes, although very different in reactivity, have certain structural features in common. They all have subunit arrangements in which there are two distinct domains connected by a short linker region of peptide (Figure 1). Each of these domains contains either flavin or haem prosthetic groups. Here we compare the ways in which redox equivalents are transmitted through the individual centres of these flavocytochromes.

Flavocytochrome *P*-450 BM3

Flavocytochrome *P*-450 BM3 from *Bacillus megaterium* catalyses the subterminal mono-oxygenation of a range of fatty acids with chain lengths of 12–20 carbon atoms. The enzyme is composed of a diflavin *P*-450 reductase fused to a cytochrome *P*-450 fatty acid mono-oxygenase in a single polypeptide chain (Figure 1A). Recent potentiometric and kinetic studies have resulted in a clearer understanding of the electron flow through this flavocytochrome [3,4]. Thus the

FAD is initially reduced by hydride transfer from NADPH. The driving force for electron transfer from FAD to FMN is high [3], so there is rapid electron transfer between the two flavins. The next step requires electron transfer from FMN to the *P*-450 haem. However, the reduction potential of the haem is very dependent on substrate binding and, in the absence of substrate, electron transfer from flavin to haem is thermodynamically disfavoured. On binding of fatty acid, the haem reduction potential is elevated by more than 130 mV [3] and electron transfer from FMN to haem occurs. In essence, this substrate-induced switch regulates electron transfer in flavocytochrome *P*-450 BM3 and effectively prevents the enzyme from cycling in a futile manner, which would waste reducing equivalents in the production of H₂O₂. Reduction of the *P*-450 haem is followed by dioxygen binding and this initiates a classic *P*-450 catalytic cycle in which the transient formation of an oxyferryl intermediate leads ultimately to the mono-oxygenation of the fatty acid substrate [1,2]. In this case, therefore, we have a flavocytochrome that couples the reducing equivalents of NADPH to the activation of molecular oxygen, resulting in the hydroxylation of a fatty acid substrate.

Flavocytochromes *b*₂

Unlike flavocytochrome *P*-450 BM3, the flavocytochromes *b*₂ show little or no reactivity towards dioxygen. These enzymes are in fact 2-hydroxyacid dehydrogenases; they are found in the intermembrane space of yeast mitochondria. Examples are the enzymes from *Saccharomyces cerevisiae* and *Hansenula anomala*, both of which are L-lactate dehydrogenases [2], and the enzyme from *Rhodotorula graminis*, which is an L-mandelate dehydrogenase [5]. All of these flavocytochromes *b*₂ are homotetramers with subunit molecular masses of close to 60 kDa; each subunit contains one flavin (FMN) and one haem. A three-dimensional structure is available for the enzyme from *S. cerevisiae* both in native [6] and recombinant (from *Escherichia coli*) forms [7]. The subunit composition is as shown

¹To whom correspondence should be addressed.

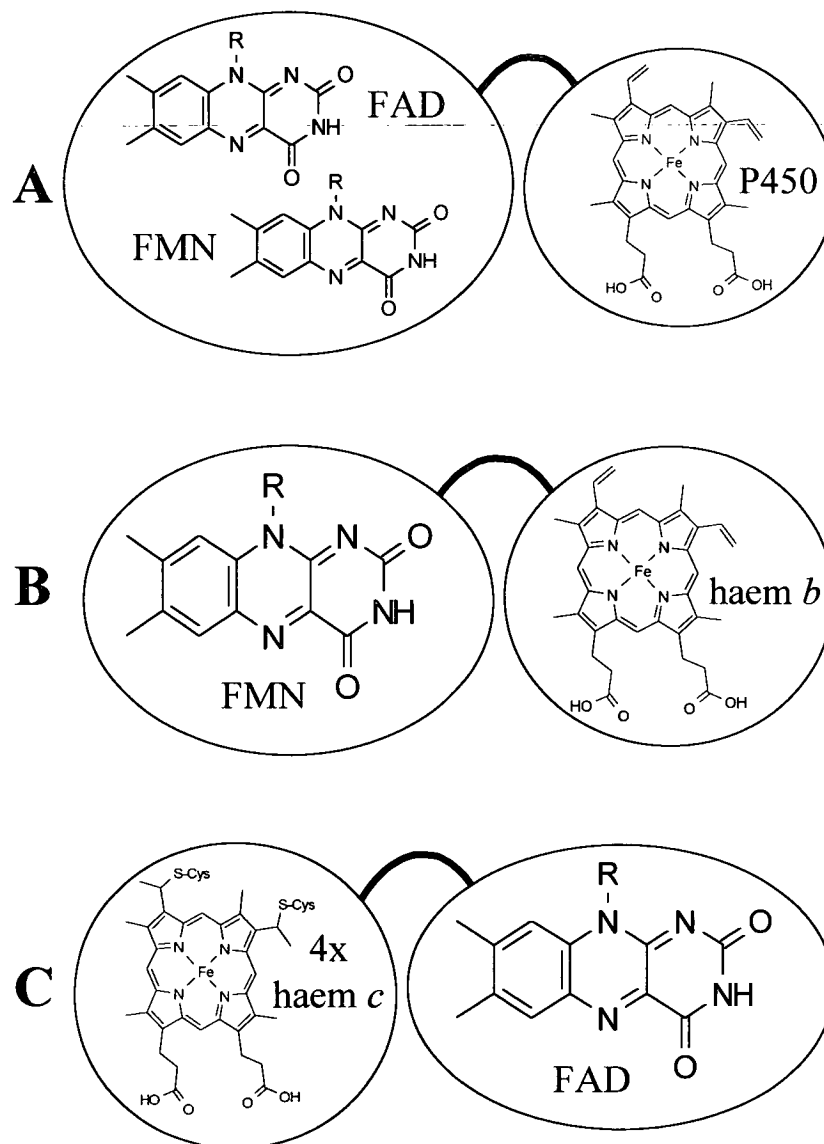
schematically in Figure 1(B) with an N-terminal (100 residues) cytochrome domain connected via a short hinge region to a C-terminal (400 residues) flavodehydrogenase domain. Electron flow through flavocytochrome b_2 is now fairly well understood [8–10] (Scheme 1). First the FMN is reduced by L-lactate (Step 1, Scheme 1). A carbanion mechanism has been proposed for this redox step [11], although a hydride transfer from lactate to flavin N-5 is equally plausible, as has already been suggested for D-amino acid oxidase

[12]. Two-electron reduction of FMN is followed by intramolecular electron transfer from flavin to haem, generating flavin semiquinone and reduced haem [8] (Step 2, Scheme 1). There follows the first of two intermolecular electron transfers from b_2 haem to cytochrome c [13] (Step 3, Scheme 1). This results in an oxidized b_2 haem, which is then re-reduced by the flavin semiquinone. The electron transfer from semiquinone to haem (Step 4, Scheme 1) is the slowest step in the catalytic cycle and is approx.

Figure 1

Schematic representation of the subunit structure of three flavocytochromes

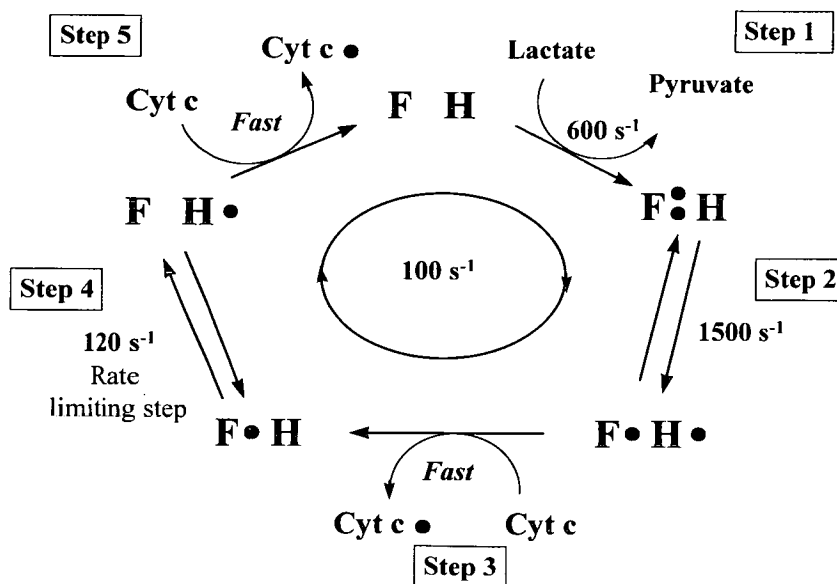
All three flavocytochromes have subunits in which a flavin-containing domain is fused to a cytochrome domain via a 'hinge' or 'linker' region of peptide. The domains are shown as ovals or spheres with the appropriate cofactors indicated. The linker is shown as a curved black line. (A) Flavocytochrome P-450 BM3; (B) flavocytochrome b_2 ; (C) flavocytochrome c_3 .



Scheme 1

Catalytic cycle for flavocytochrome b_2

All rate constants shown are at 25°C, pH 7.5 and $I = 0.10$. Abbreviations: F, flavin; H, haem; Cyt c , cytochrome c . Electrons are represented by filled circles. Descriptions of the individual steps can be found in the text.



one-tenth as fast as the electron transfer from hydroquinone to haem [8]. Finally, the second electron is transferred from the b_2 haem to cytochrome c (Step 5, Scheme 1). Thus in this case the flavocytochrome couples the two-electron oxidation of L-lactate to the reduction of two molecules of cytochrome c .

One area of recent controversy has concerned the nature of the complex formed between flavocytochrome b_2 and cytochrome c , which must be formed to permit efficient inter-protein electron transfer. Tegoni et al. [14] reported a computer-generated model of what the flavocytochrome b_2 -cytochrome c complex might look like. Unfortunately, mutagenesis studies that examined the predictions made by this model led to the conclusion that it was not likely to represent a kinetically competent complex [10,13]. More recently a new modelling study, consistent with mutagenesis results, has suggested a cytochrome c docking site on flavocytochrome b_2 involving the acidic residues Glu-63, Asp-72 and Glu-237 [10]. The study concluded that cytochrome c could 'sample' a number of different, yet similar, binding modes on this docking surface and that in each of these binding modes the edge-to-edge distance for electron transfer remains essentially the same [10].

An interesting question about electron flow through flavocytochrome b_2 is as follows: Why is the b_2 cytochrome domain required for electron transfer to cytochrome c ? This is actually quite a fundamental question because the b_2 flavin group is quite capable of transferring electrons singly; the driving force for electron transfer to cytochrome c , directly from the flavin, is more than 300 mV. There is therefore no thermodynamic problem for electron transfer from b_2 flavin to cytochrome c and yet the individually expressed flavodehydrogenase domain (i.e. that lacking the N-terminal cytochrome domain) has virtually no cytochrome c reductase activity. An explanation for this is that there is very poor molecular recognition between the flavodehydrogenase domain and cytochrome c .

For efficient electron transfer to occur between these two proteins their redox centres should come as close together as possible. However, an examination of the surface around the exposed haem-edge of cytochrome c and the surface of the flavodehydrogenase domain closest to the flavin indicates that these two faces are almost totally incompatible. Both surfaces are predominantly positively charged and this must present a substantial coulombic barrier to complexation between the proteins. In addition to this electrostatic effect there is also a possible

steric problem to consider. In the crystal structure of flavocytochrome b_2 there is a length of peptide (residues 299–318) that shows no electron density. This portion of sequence forms a proteolytically sensitive loop on the surface of the protein. In the absence of crystal structure information we have used computational methods to model the folding and location of this loop (Figure 2). Results from these modelling studies indicate that the loop might fold directly over the docking site closest to the flavin. Thus there are both electrostatic and steric explanations for the slow reactivity of the flavodehydrogenase domain with cytochrome c .

To try to overcome these problems we have embarked on extensive protein engineering of the flavodehydrogenase domain to remove the steric block and build in a favourable recognition site for cytochrome c . This will involve the replacement of residues 298–320 with a sequence of seven glycine residues coupled with a triple mutation on the surface, of Lys-210→Glu, Lys-324→Ala and Phe-325→Glu. We believe that this redesign of the flavodehydrogenase domain surface will make an excellent docking site for cytochrome c , which should permit efficient interprotein electron transfer to occur.

Flavocytochrome c_3

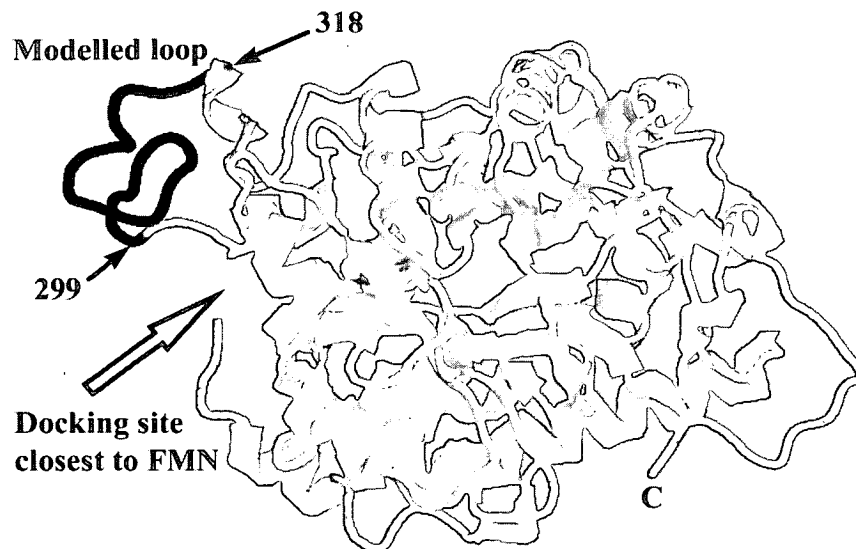
Flavocytochrome c_3 is a fumarate reductase isolated from the periplasm of the marine bacterium *Shewanella frigidimarina* NCIMB400 (previously described as *S. putrefaciens*) [15]. Production of flavocytochrome c_3 is induced, under anaerobic growth conditions, by the addition of fumarate [16]. Flavocytochrome c_3 differs from the previously characterized fumarate reductases, which are multi-subunit and anchored to the inner face of the cytoplasmic membrane [17]. In contrast, flavocytochrome c_3 is a soluble, single-subunit enzyme found in the periplasm [18]. The flavocytochrome c_3 subunit is composed of two domains, shown schematically in Figure 1(C), a tetrahaem cytochrome domain (117 residues) and a flavin domain (454 residues) that contains non-covalently bound FAD [18]. The cytochrome domain, located at the N-terminus of the protein, encapsulates four, bis-His ligated, c -type haems [19]. It has been proposed that this domain is structurally similar to the family of cytochromes c_3 [18].

The mechanism of electron flow through flavocytochrome c_3 is far less well understood than for flavocytochrome b_2 and flavocytochrome P -450 BM3. The physiological donor to the

Figure 2

Structure of the flavocytochrome b_2 flavodehydrogenase domain, showing the modelled structure of the disordered loop

The structure contains arrows indicating β -sheet and ribbons indicating μ -helix. The modelled proteolytically sensitive loop is shown in black with the start and end points indicated by residue numbers. The site for cytochrome c to dock closest to the flavin is arrowed.



enzyme has not yet been defined. One possibility might be a membrane-bound tetrahaem cytochrome *c* related to the Nap C family, because such a protein has been identified in the closely related organism *S. putrefaciens* MR-1 [20]. Potentiometric and voltammetric studies on flavocytochrome *c*₃ indicate that the electrons would first flow through the haem groups (reduction potentials ranging from -240 to -100 mV) then to the FAD (two-electron reduction potential -152 mV at 25°C, pH 7.0). The fully reduced FAD would then reduce fumarate by donation of a hydride ion, as outlined elsewhere [18].

Conclusion

The examples described here should have made it clear that flavocytochromes represent a very versatile group of enzymes. This versatility of function is being exemplified with the isolation of new flavocytochromes with even more variations in reactivity.

We thank Rhiannon Macfie, Scott Mathews, Florence Lederer, Malcolm Walkinshaw and Fraser Armstrong for their helpful discussions. We are grateful to the BBSRC, EPSRC, the Leverhulme Trust and Zeneca for their support of this work.

- 1 Chapman, S. K., Daff, S. and Munro, A. W. (1979) *Struct. Bond.* **88**, 39-70
- 2 Chapman, S. K., Reid, G. A. and Munro, A. W. (1998) in *Biological Electron Transfer Chains: Genetics, Composition and Mode of Operation* (Canters, G. W. and Vijgenboom, E., eds.), pp. 165-184, Kluwer, Dordrecht
- 3 Daff, S. N., Chapman, S. K., Turner, K. L., Holt, R. A., Govindaraj, S., Poulos, T. L. and Munro, A. W. (1997) *Biochemistry* **36**, 13816-13823
- 4 Munro, A. W., Daff, S., Coggins, J. R., Lindsay, J. G. and Chapman, S. K. (1996) *Eur. J. Biochem.* **239**, 403-409
- 5 Ilias, R. M., Sinclair, R., Robertson, D., Neu, A., Chapman, S. K. and Reid, G. A. (1998) *Biochem. J.* **333**, 107-115
- 6 Xia, Z.-X. and Mathews, F. S. (1990) *J. Mol. Biol.* **212**, 837-863
- 7 Tegoni, M. and Cambillau, C. (1994) *Protein Sci.* **3**, 303-313
- 8 Daff, S., Ingeldew, W. J., Reid, G. A. and Chapman, S. K. (1996) *Biochemistry* **35**, 6345-6350
- 9 Chapman, S. K., Reid, G. A., Daff, S., Sharp, R. E., White, P., Manson, F. D. C. and Lederer, F. (1994) *Biochem. Soc. Trans.* **22**, 713-718
- 10 Short, D. M., Walkinshaw, M. D., Taylor, P., Reid, G. A. and Chapman, S. K. (1998) *J. Biol. Inorg. Chem.* **3**, 246-252
- 11 Lederer, F. (1991) in *Chemistry and Biochemistry of Flavoenzymes*, vol. 2 (Müller, F., ed.), pp. 153-242, CRC Press, Boca Raton
- 12 Mattevi, A., Vanoni, M. A. and Curti, B. (1997) *Curr. Opin. Struct. Biol.* **7**, 804-810
- 13 Daff, S., Sharp, R. E., Short, D. M., White, P., Manson, F. D. C., Reid, G. A. and Chapman, S. K. (1996) *Biochemistry* **35**, 6351-6357
- 14 Tegoni, M., White, S. A., Roussel, A., Mathews, F. S. and Cambillau, C. (1993) *Prot. Struct. Funct. Genet.* **16**, 408-422
- 15 Reid, G. A. and Gordon, E. H. J. (1998) *Int. J. Syst. Bacteriol.*, in the press
- 16 Pealing, S. L., Black, A. C., Manson, F. D. C., Ward, F. B., Chapman, S. K. and Reid, G. A. (1992) *Biochemistry* **31**, 12132-12140
- 17 Ackrell, B. A. C., Johnson, M. K., Gunsalus, R. P. and Cecchini, G. (1992) in *Chemistry and Biochemistry of Flavoenzymes*, vol. 3 (Müller, F., ed.), pp. 229-297, CRC Press, Boca Raton
- 18 Reid, G. A., Gordon, E. H. J., Hill, A. E., Doherty, M., Turner, K., Holt, R. and Chapman, S. K. (1998) *Biochem. Soc. Trans.* **26**, 418-421
- 19 Pealing, S. L., Cheesman, M. R., Reid, G. A., Thomson, A. J., Ward, F. B. and Chapman, S. K. (1995) *Biochemistry* **34**, 6153-6158
- 20 Myers, C. R. and Myers, J. M. (1997) *J. Bacteriol.* **179**, 1143-1152

Received 19 August 1998

Flavocytochrome *P*-450 BM3: a paradigm for the analysis of electron transfer and its control in the *P*-450s

A. W. Munro^{*1}, M. A. Noble^{*}, C. S. Miles^{*}, S. N. Daff^{*}, A. J. Green^{*}, L. Quaroni[†], S. Rivers[‡], T. W. B. Ost^{*}, G. A. Reid[‡] and S. K. Chapman^{*}

^{*}Department of Chemistry, University of Edinburgh, West Mains Road, Edinburgh RH9 3JJ, Scotland, U.K.,

[†]Department of Chemistry, Iowa State University, Ames, IA 50011, U.S.A., and [‡]Institute of Cell and Molecular Biology, University of Edinburgh, Mayfield Road, Edinburgh EH9 3JR, Scotland, U.K.

Introduction

The cytochromes *P*-450 (*P*-450s) are a 'super-family' of haem *b*-containing oxidase proteins [1,2], which catalyse an array of oxidative reactions with a plethora of organic substrates. *P*-450 enzymes are found throughout Nature, from organisms as simple as bacteria (and archaeons [3]) to higher eukaryotes. The *P*-450s have enormous biotechnological potential because they catalyse the controlled activation of O₂, with the potential for stereospecific and regiospecific insertion of oxygen atoms into organic molecules. This potential has already been realized with the use of the *P*-450s in the commercial manufacture of steroids [4], and the process is continually being developed and improved [5].

Mammals have numerous forms of membrane-bound *P*-450 that catalyse various forms of reaction (e.g. hydroxylation, epoxidation, N-oxidation and reductive dehalogenation) [6] and are vital to a number of physiological processes, including steroid syntheses and interconversions, the manufacture of eicosanoid derivatives for cellular signalling, and xenobiotic detoxification. The importance of mammalian hepatic *P*-450s in the metabolism of drugs is a subject of great importance to the pharmaceutical industry. The *P*-450s, the so-called 'phase I' enzymes, represent a 'first line of defence' when the body is exposed to xenobiotics, and the multiple hepatic forms of *P*-450 catalyse oxidative reactions on thousands of drugs and other foreign chemicals to which the body is exposed. Examples are the oxidations of ethanol, aspirin, chloroform and polycyclic aromatic hydrocarbons. These oxidations are often designed to increase the water-solubility of xenobiotics to facilitate their excretion directly, or to provide functional groups for recognition by 'phase II' drug-metabolizing enzymes, such as glutathione S-transferases or UDP-glucuronyl transferases. However, factors

such as industrial pollution and the massive development of the pharmaceutical industry in the past century has meant that we have been exposed to a vast number of new chemicals that can act as substrates for the *P*-450s (many forms of mammalian *P*-450 are rather non-specific). It is now well recognized that the *P*-450s are capable of converting a number of compounds into more dangerous, even genotoxic, derivatives. Examples are the epoxidations of benzo[*a*]pyrene (*P*-450 1A1) and aflatoxin B1 (*P*-450 3A4) [7]. It is ironic that an enzyme system that evolved to defend the body against harmful organic compounds can also be tricked into acting against it, due to the rate of human evolution of new chemicals outstripping the genetic evolution of the *P*-450s.

Although there is intense medical and pharmaceutical interest in the mammalian *P*-450s, the expression and study of the structural properties of these enzymes is hampered by the fact that they are integral membrane proteins (as are their redox partners). However, the bacterial *P*-450s are soluble; this has simplified the overexpression and purification of these forms [8]. In many respects, the entire *P*-450 field has been led forward by the advances made through kinetic, spectroscopic and structural analysis of a small number of bacterial forms. There are currently six atomic structures available for bacterial *P*-450s [9–14]. For the two most important of these enzymes (*P*-450cam and *P*-450 BM3), the structures of both substrate-bound and free forms have been determined [9,10,15,16]. The camphor hydroxylase *P*-450cam from *Pseudomonas putida* has been one of the most intensely studied of all enzymes over the last quarter of a century [17]; the analysis of this enzyme has provided us with most of our knowledge on the structure and mechanism of *P*-450. However, in the past 5–10 years there has been enormous interest in the characterization of the fatty acid hydroxylase *P*-450 BM3 from *Bacillus megaterium* [18]. This shift in emphasis results from the realization that *P*-450 BM3 uses a simi-

Abbreviations used: hq, hydroquinone; ox, oxidized; sq, semiquinone.

¹To whom correspondence should be addressed.

**Identification of the Active Site Acid/Base
Catalyst in a Bacterial Fumarate
Reductase: A Kinetic and
Crystallographic Study**

**Mary K. Doherty, Sara L. Pealing, Caroline S. Miles,
Ruth Moysey, Paul Taylor, Malcolm D. Walkinshaw,
Graeme A. Reid, and Stephen K. Chapman**

Department of Chemistry, University of Edinburgh, West Mains
Road, Edinburgh EH9 3JJ, U.K., and Institute of Cell and Molecular
Biology, University of Edinburgh, Mayfield Road,
Edinburgh EH9 3JR, U.K.

Biochemistry[®]

Reprinted from
Volume 39, Number 35, Pages 10695–10701

Identification of the Active Site Acid/Base Catalyst in a Bacterial Fumarate Reductase: A Kinetic and Crystallographic Study[†]

Mary K. Doherty,[‡] Sara L. Pealing,^{‡,§} Caroline S. Miles,[§] Ruth Moysey,[‡] Paul Taylor,[§] Malcolm D. Walkinshaw,[§] Graeme A. Reid,[§] and Stephen K. Chapman^{*‡}

Department of Chemistry, University of Edinburgh, West Mains Road, Edinburgh EH9 3JJ, U.K., and Institute of Cell and Molecular Biology, University of Edinburgh, Mayfield Road, Edinburgh EH9 3JR, U.K.

Received April 17, 2000; Revised Manuscript Received May 31, 2000

ABSTRACT: The active sites of respiratory fumarate reductases are highly conserved, indicating a common mechanism of action involving hydride and proton transfer. Evidence from the X-ray structures of substrate-bound fumarate reductases, including that for the enzyme from *Shewanella frigidimarina* [Taylor, P., Pealing, S. L., Reid, G. A., Chapman, S. K., and Walkinshaw, M. D. (1999) *Nat. Struct. Biol.* 6, 1108–1112], indicates that the substrate is well positioned to accept a hydride from N5 of the FAD. However, the identity of the proton donor has been the subject of recent debate and has been variously proposed to be (using numbering for the *S. frigidimarina* enzyme) His365, His504, and Arg402. We have used site-directed mutagenesis to examine the roles of these residues in the *S. frigidimarina* enzyme. The H365A and H504A mutant enzymes exhibited lower k_{cat} values than the wild-type enzyme but only by factors of 3–15, depending on pH. This, coupled with the increase in K_m observed for these enzymes, indicates that His365 and His504 are involved in Michaelis complex formation and are not essential catalytic residues. In fact, examination of the crystal structure of *S. frigidimarina* fumarate reductase has led to the proposal that Arg402 is the only plausible active site acid. Consistent with this proposal, we report that the R402A mutant enzyme has no detectable fumarate reductase activity. The crystal structure of the H365A mutant enzyme shows that, in addition to the replacement at position 365, there have been some adjustments in the positions of active site residues. In particular, the observed change in the orientation of the Arg402 side chain could account for the decrease in k_{cat} seen with the H365A enzyme. These results demonstrate that an active site arginine and not a histidine residue is the proton donor for fumarate reduction.

Fumarate reductases enable bacteria to respire anaerobically with fumarate as a terminal electron acceptor. In most cases these enzymes are membrane-bound complexes, closely related to succinate dehydrogenase, but in *Shewanella* the fumarate reductase is a soluble, periplasmic, tetraheme flavocytochrome c_3 (Fcc₃,¹ M_r 63 800). The gene encoding Fcc₃ has been cloned and sequenced (Swissprot entry FRDA_SHEPU), and the protein product has been shown to be a novel respiratory fumarate reductase (1, 2).

Fumarate reductases from several other bacteria have been identified as complexes of three or, more commonly, four subunits that are anchored to the inner face of the cytoplasmic membrane (3, 4). The largest of these, FrdA, is a flavoprotein containing the site of substrate reduction, and this is tightly associated with the FrdB subunit which contains three iron–sulfur centers that feed electrons to the flavin. These two

subunits are very closely related to succinate dehydrogenase subunits that catalyze the reverse reaction. The A and B subunits are peripheral membrane proteins that are associated with smaller, integral membrane proteins that transfer electrons from the lipophilic hydrogen carrier, menaquinone, to the iron–sulfur centers. Fumarate reductase from *Escherichia coli* contains two membrane anchor subunits, FrdC and FrdD, that are devoid of prosthetic groups (3) whereas the equivalent enzyme from *Wolinella succinogenes* contains a single membrane subunit that is a diheme cytochrome *b* (4).

In contrast to these cytoplasmic membrane enzymes, Fcc₃ is a soluble, single-chain enzyme found in the periplasm (5). Despite the differences in architecture and location, its function has been shown to be analogous to that of the membrane-bound enzymes since disruption of the gene encoding Fcc₃ resulted in the specific loss of the ability to respire with fumarate as the electron acceptor (6). The recently determined crystal structure of Fcc₃ (7–10) shows it to be composed of three domains. These have been termed the cytochrome domain, the flavin domain, and the clamp domain (7). The flavin binding domain is clearly related by sequence to the flavoprotein subunits of the membrane-bound fumarate reductases and succinate dehydrogenases (2), and all of the amino acid residues that have been implicated in substrate binding and catalysis, on the basis of chemical modification and mutagenesis experiments, are conserved.

[†] This work was funded by the U.K. Biotechnology and Biological Sciences Research Council, BBSRC. M.K.D. and R.M. acknowledge studentships from the BBSRC and EPSRC. We thank SRS Daresbury for use of synchrotron data collection facilities.

^{*} Corresponding author: e.mail, S.K.Chapman@ed.ac.uk; fax/phone, (44) 131 650 4760.

[‡] Department of Chemistry, University of Edinburgh.

[§] Institute of Cell and Molecular Biology, University of Edinburgh.

¹ Abbreviations: Fcc₃, flavocytochrome c_3 ; H365A, histidine 365 → alanine mutation; H504A, histidine 504 → alanine mutation; R402A, arginine 402 → alanine mutation; FAD, flavin adenine dinucleotide.

One particular histidine residue (His365 in Fcc₃, equivalent to His232 in *E. coli* fumarate reductase) has been proposed as a possible active site acid/base catalyst for fumarate reduction/succinate oxidation (11, 12). In *E. coli* fumarate reductase, the substitution of His232 by serine resulted in an enzyme which retained 25% of its fumarate reductase activity but only 2% of its succinate dehydrogenase activity (12). Such data are consistent with this residue having a significant but nonessential role in enzyme activity. Retention of 25% of the wild-type fumarate reductase activity clearly indicates that an alternative proton donor must be operational. The recently determined high-resolution crystal structure of Fcc₃ supports the idea that His365 is unlikely to be the active site acid (7). First, the structure shows that N5 of His365 is hydrogen bonded to a backbone amide group, indicating that the imidazole ring must be neutral. Second, N3 of His365 is hydrogen bonded to one of the carboxylate groups of the substrate with the imidazole ring too far (4.88 Å) from the C3 carbon to which the proton must be donated (7).

The possibility of an alternative histidine (residue 504 in the Fcc₃ sequence) acting as the active site acid has been suggested on the basis of the recent structure of an isozyme of Fcc₃ known as iron-induced flavocytochrome *c*₃ (10). There is no supporting evidence for this suggestion since the active site in this structure is unoccupied. Indeed, the suggestion is incompatible with evidence from the structures of the *E. coli* fumarate reductase (3) and the other *Shewanella* enzymes (7, 8), all of which have substrate- or inhibitor-like molecules bound at the active site. In these cases the structures indicate a role in the binding of substrate but not in the donation of a proton to substrate C3. The highest resolution Fcc₃ structure (7) clearly indicates that Arg402 is the most likely active site acid. This is supported by the structure of the related Fcc₃ from *Shewanella putrefaciens* MR-1 (9).

To further investigate the nature of the active site acid catalyst, we have examined the roles of residues His365, Arg402, and His504 by substituting each by alanine and in addition have made the H365A:H504A double substitution. In the present paper we describe the kinetic characterization of these mutant enzymes. In addition, we report the 1.8 Å resolution crystal structure of H365A Fcc₃.

MATERIALS AND METHODS

DNA Manipulation, Strains, Media, and Growth. The mutant enzymes H365A Fcc₃, R402A Fcc₃, and H504A Fcc₃ were generated by site-directed mutagenesis using the method described by Kunkel and Roberts (13). The *fccA* coding sequence was cloned into the phagemid vector pTZ18R (14) on an ~1.8 kbp *EcoRI/HindIII* fragment (6) to provide the template.

Mutagenic oligonucleotides GTATATCCAAGCTGCTC-CAACACTATCTG (which substitutes histidine 365 with alanine), CGAAATTACTACTGCTGATAAAGCATC (which substitutes arginine 402 with alanine), and GTTACACCTG-GTGTGCTCACAATGATGGGTG (which substitutes histidine 504 with alanine) were obtained from PE-Applied Biosystems U.K. Mismatched bases are underlined. Single-stranded DNA was screened for the required mutations by dideoxy chain termination sequencing (15) using the Sequenase version 2.0 kit (United States Biochemicals). To verify that no secondary mutations had been introduced, the mutated

fccA coding sequences were fully sequenced from single-stranded DNA: H365A *fccA* as above and R402A and H504A *fccA* using a Perkin-Elmer ABI Prism 377 DNA sequencer.

To enable expression of H365A, R402A, and H504A Fcc₃, the modified coding sequences were cloned individually into the IPTG-inducible, broad-host range expression vector pMMB503EH (16) on an ~1.8 kbp *EcoRI/HindIII* fragment to give pCM15, pCM68, and pCM67, respectively. Following transformation of *E. coli* SM10 (17), the above plasmids were transferred to the $\Delta fccA$ *Shewanella frigidimarina* strain EG301 (6) by conjugation. Recombinant wild-type Fcc₃ was expressed in the same manner (6). To generate H365A:H504A Fcc₃, an ~1.1 kbp *NheI/MfeI* fragment was excised from pCM67 (H504A *fccA*/pMMB503EH) and replaced with the corresponding fragment from pCM14 (H365A *fccA*/pTZ18R). Expression was as described above.

Protein Purification and Kinetic Analysis. Wild-type and mutant forms of Fcc₃ were purified as previously reported (1). Protein samples for crystallization were subjected to an additional purification step using FPLC with a Mono Q column as described by Pealing et al. (18). Protein concentrations were determined using the Soret band absorption coefficient for the reduced enzyme (752.8 mM⁻¹ cm⁻¹ at 419 nm) (1).

The FAD content of recombinant Fcc₃ was determined using the method of Macheroux (19), and all steady-state rate constants were corrected for the percentage of FAD present.

The steady-state kinetics of fumarate reduction were followed at 25.0 ± 0.1 °C as described by Turner et al. (20). The fumarate-dependent reoxidation of reduced methyl viologen was monitored at 600 nm using a Shimadzu UV-PC 1201 spectrophotometer. To ensure anaerobicity the spectrophotometer was housed in a Belle Technology glove-box under a nitrogen atmosphere with the O₂ level maintained below 5 ppm. Assay buffers contained 0.45 M NaCl and 0.2 mM methyl viologen and were adjusted to the appropriate pH values using 0.05 M HCl or NaOH as follows: Tris·HCl (pH 7.0–9.0), MES/NaOH (pH 5.4–6.8), CHES/NaOH (pH 8.6–10), and CAPS/NaOH (pH 9.7–11.1). The viologen was reduced by addition of sodium dithionite until an absorbance reading of around 1 was obtained (corresponding to around 80 μM reduced methyl viologen). The concentration of reduced methyl viologen could be varied between 100 and 20 μM with no effect on the rate of reaction. Fumarate was added to give a range of concentrations (0–350 μM), and the reaction was initiated by addition of a known concentration of enzyme.

Kinetic parameters *K*_m and *k*_{cat} were determined from the steady-state results using nonlinear regression analysis (Microcal Origin software).

Crystallization and Refinement. Crystallization was carried out by hanging drop vapor diffusion at 4 °C in Linbro plates. Crystals were obtained with a well solution comprising 100 mM Tris·HCl, pH 7.4 (measured at 25 °C), 80 mM NaCl, 17–20% PEG 8000, and 10 mM fumarate. Hanging drops of 4 μL were prepared by adding 2 μL of 6 mg/mL protein (in 10 mM Tris·HCl, pH 8.4) to 2 μL of well solution. Needles of up to 1 × 0.2 × 0.2 mm were formed after about 2 weeks.

Crystals were immersed in well solution containing 23% glycerol as cryoprotectant, before being mounted in loops

Table 1: Refinement Statistics

refinement	24.0–1.8 Å
total no. of reflections	265 858
unique reflections	54 333
completeness (%)	90.7
$\langle I \rangle / \langle \sigma(I) \rangle$	13.8
$R_{\text{merge}} (\%)^a$	4.9
R_{merge} in outer shell (1.83–1.80) (%)	11.7
$R_{\text{cryst}} (\%)^b$	18.14
$R_{\text{free}} (\%)^b$	24.70
rmsd from restraint values	
bond length (Å)	0.007
bond angle distance (Å)	0.022
Ramachandran analysis	
most favored (%)	89.1
additionally allowed (%)	10.9

^a $R_{\text{merge}} = \sum |I| - I / \sum I$ over all reflections. ^b $R_{\text{cryst}} = \sum |F_o - F_c| / F_o$; R_{free} calculated with 10.7% data withheld from refinement.

and frozen in liquid nitrogen. A data set was collected to 1.8 Å ($\lambda = 0.87$ Å) on station 9.6 at Daresbury synchrotron source using an ADSC Quantum 4 detector. The crystals are isomorphous with wild-type Fcc₃ with space group $P2_1$ and cell dimensions $a = 45.571$ Å, $b = 92.172$ Å, $c = 78.489$ Å, and $\beta = 91.09^\circ$. This compares with the wild-type crystal cell dimensions of $a = 45.393$ Å, $b = 91.946$ Å, $c = 78.288$ Å, and $\beta = 91.09^\circ$.

Data processing was carried out using the HKL package (21) (Table 1). The wild-type Fcc₃ structure (1qjd), stripped of water, was used as the initial model. Electron density fitting was carried out using the graphics program WITNOTP (22). Restraints for the heme group were calculated from the CNS parameter file and for the FAD from two small molecule crystal structures (Cambridge Crystallographic Database codes HAMADPH and VEFHUI10). Structure refinement was carried out using SHELXL-97 (23).

The atomic coordinates have been deposited in the Protein Data Bank (accession code 1E39).

RESULTS AND DISCUSSION

Characterization of Recombinant Enzymes. The molecular mass of the recombinant wild-type enzyme was confirmed by electrospray mass spectroscopy to be 63 033 Da. The masses of the mutant enzymes were lower than this by 68 Da for H365A (expected difference 66), 84 Da for R402A (expected difference 85), 59 Da for H504A (expected difference 66), and 134 Da for H365A:H504A (expected difference 132). All the mutations were further verified by DNA sequencing. The average FAD content of the recombinant enzymes was found to be the following: 73%, wild-type; 69%, H365A; 78%, R402A; 70%, H504A; and 68%, H365A:H504A. This compares with typical values for the native (nonrecombinant) enzyme from *Shewanella* of around

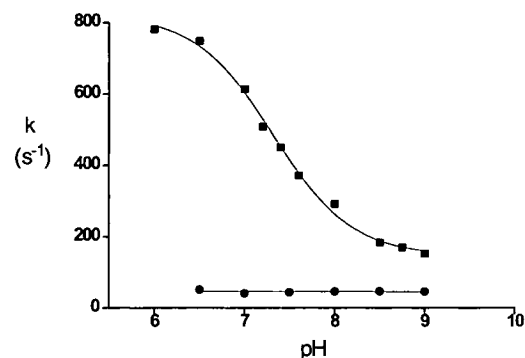


FIGURE 1: pH dependence of fumarate reduction activity (under saturating conditions) at 25 °C: wild-type flavocytochrome c_3 (solid squares); H365A flavocytochrome c_3 (solid circles).

98%. The lower flavin content of the recombinant forms is most likely due to the higher levels of expression in these cases. All catalytic rates were corrected for the variation in FAD content.

The ability of wild-type and mutant forms of Fcc₃ to catalyze fumarate reduction was determined over a range of pH values. The resulting k_{cat} and K_m parameters for wild-type and mutant forms of Fcc₃ are listed in Table 2. The pH dependence of the rate of fumarate reduction under saturating substrate conditions seen with wild-type and H365A Fcc₃ is shown in Figure 1. The pK_a value seen for the wild-type enzyme is 7.4 ± 0.2 , as previously reported (20). However, it is clear from the results shown in Figure 1 and Table 2 that the catalytic rate of fumarate reduction seen for the H365A mutant enzyme is essentially independent of pH over the range 6.0–9.0. At pH 6.0 the value of k_{cat} for the H365A enzyme has fallen to approximately 7% of that seen with wild-type Fcc₃. This effect is less dramatic at pH 9.0 where the k_{cat} for the H365A enzyme is 25% of the value seen with the wild-type enzyme. The magnitude of the effect of this mutation on activity is similar to that seen for the His232→Ser mutation made in the *E. coli* enzyme (9).

The fact that up to 25% of the value of k_{cat} is retained in the H365A mutant enzyme is not consistent with this residue being an essential active site acid/base catalyst. Rather, we propose that the major role of this residue is in stabilizing the Michaelis complex. This is supported by the values of K_m reported in Table 2. At pH 9.0 the K_m value for the H365A mutant is some 30-fold larger than that seen for the wild-type enzyme. Previous results on the wild-type enzyme from pre-steady-state experiments (1) and inhibition studies (5) suggest that the K_m for fumarate is similar to the K_d value. We have therefore used the variation in the value of K_m as a means of determining approximate changes in the free energies of fumarate binding between wild-type and mutant enzymes. For example, at pH 9.0 the change in K_m between

Table 2: Comparison of k_{cat} and K_m Values for Wild-Type, H365A, H504A, and the Double Mutant H365A:H504A Fcc₃ (25 °C, $I = 0.45$ M)^a

pH	wild-type Fcc ₃		H365A Fcc ₃		H504A Fcc ₃		H365A:H504A Fcc ₃	
	k_{cat} (s ⁻¹)	K_m (μM)	k_{cat} (s ⁻¹)	K_m (μM)	k_{cat} (s ⁻¹)	K_m (μM)	k_{cat} (s ⁻¹)	K_m (mM) ^b
6.0	658 ± 34	43 ± 10	47 ± 2	113 ± 20	26 ± 1	38 ± 3	0.28 ± 0.02	~0.08
7.2	509 ± 15	25 ± 10	51 ± 2	259 ± 24	65 ± 3	256 ± 23	0.84 ± 0.10	~1.1
7.5	370 ± 10	28 ± 3	54 ± 2	143 ± 21	68 ± 2	200 ± 15	0.95 ± 0.10	~1.8
9.0	210 ± 13	7.0 ± 1.5	52 ± 2	224 ± 25	76 ± 3	635 ± 37	0.95 ± 0.10	~1.3

^a The R402A enzyme was inactive under all conditions. ^b Values of K_m (millimolar) for fumarate with the H365A:H505A enzyme were difficult to determine accurately due to the very low activity of the enzyme.

wild-type and H365A enzymes equates to a difference in free energy for the binding of substrate of approximately 8.6 kJ mol^{-1} . In addition, the value of k_{cat}/K_m , a measure of enzyme efficiency, varies between 2×10^5 and $4 \times 10^5 \text{ M}^{-1} \text{ s}^{-1}$ over the pH range 6–9. A catalytic efficiency of 10^5 is typical for many native enzymes and is certainly not consistent with an enzyme in which the key active site acid/base catalyst has been removed.

The possibility of an alternative histidine (His504) acting as the acid/base catalyst has been recently suggested (10). However, substitution of this histidine by alanine leads to effects similar to those seen for the H365A mutant enzyme. For H504A Fcc₃ the value of k_{cat} varies from 4% of the wild-type value (at pH 6.0) to 36% of the wild-type value (at pH 9.0). As for H365A, the H504A mutation has large effects on the value of K_m particularly at high pH. For example, at pH 9.0 the K_m value for fumarate seen with the H504A enzyme is some 90-fold larger than that seen for the wild-type enzyme (Table 2), equating to a change in free energy for the binding of substrate of around 11.2 kJ mol^{-1} . Again, it is clear that His504 is not essential for catalysis but is important for Michaelis complex formation.

Even for the case in which both histidines are replaced by alanine (H365A:H504A Fcc₃), there is still some residual activity. Not surprisingly, the double mutation has a large effect on the K_m value for fumarate, with the value now in the millimolar range (Table 2). In fact, the effect of the mutations is additive since, at pH 7.2, the loss in binding energy with respect to wild-type enzyme, seen for the double mutant ($\sim 10 \text{ kJ mol}^{-1}$), is almost exactly the sum of the loss in binding energies for the two single mutants ($\sim 5 \text{ kJ mol}^{-1}$). The effect on k_{cat} is also dramatic (Table 1); however, the fact that there is any activity at all indicates that an alternative acid/base catalyst must still be operating.

These results clearly indicate that a group other than His365 or His504 operates as the crucial proton donor/acceptor. The most likely candidate for this role has previously been suggested to be Arg402 (7, 9). The effect of substituting Arg402 by Ala is far more dramatic than that seen for either of the histidine mutations. In this case the R402A mutant enzyme was found to be completely inactive under all conditions. This abolition of activity is clearly not due to the loss of redox cofactors since the FAD complement was found to be equivalent to that of the recombinant wild-type enzyme. A possible explanation for this abolition of all activity is that Arg402 is indeed the essential active site acid catalyst required for fumarate reduction. This idea is further supported by an inspection of the high-resolution X-ray structure of the wild-type enzyme which shows that the NH₂ of Arg402 is ideally positioned for proton donation at only 2.99 \AA from the C3 carbon of the substrate (7). The mechanism proposed for the reduction of fumarate based on the wild-type enzyme structure (7) is shown in Figure 2. This mechanism is shown proceeding in a stepwise rather than in a concerted fashion. The only evidence for the reaction being stepwise comes from the crystallographic identification of a trapped malate-like molecule (an artifact of the crystallization procedure) in the Fcc₃ structure which may represent an unprotonated intermediate (7). Clearly, further solution studies will be required to confirm the stepwise nature of the mechanism. Nevertheless, the mechanism shown in Figure 2 is entirely consistent with the roles of His365 and

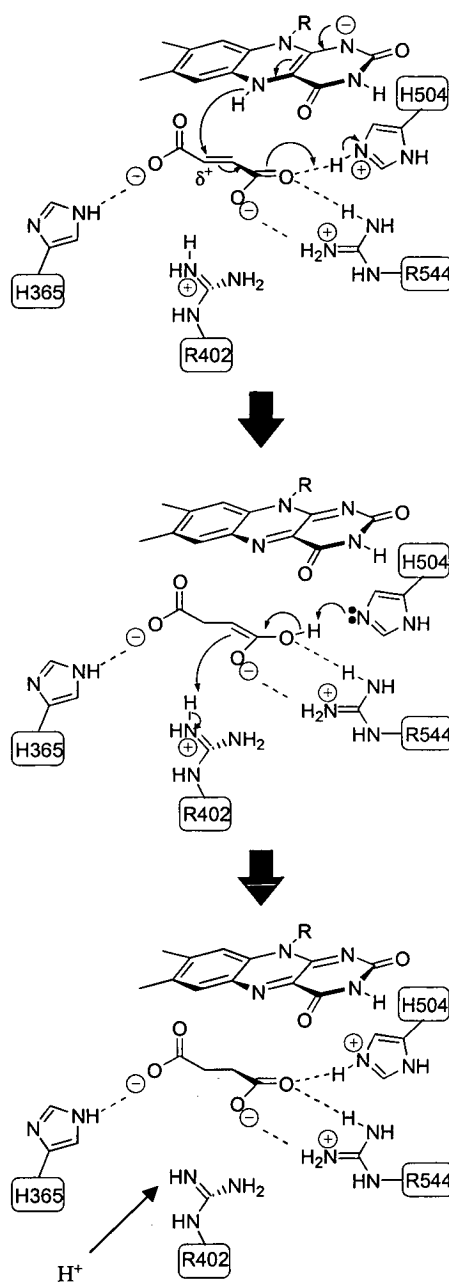


FIGURE 2: Reaction mechanism for fumarate reduction as proposed by Taylor et al. (7). Catalysis is initiated by the twisting out of plane of the C1' carboxylate group (on the left) of fumarate. The substrate is polarized by interactions with charged residues facilitating hydride transfer from N5 of reduced FAD to the substrate C2. Arg402 (2.99 \AA from C3) is ideally positioned to donate a proton to the substrate C3, resulting in the formation of succinate. Arg402 is immediately reprotonated via a proton pathway involving Arg381 and Glu378 (Figure 3).

Arg402 that we propose on the basis of our mutagenesis results. The mechanism also shows His504 protonating the C4 carboxylate to facilitate the transient formation of a carbanion at C3. While such a role for His504 would clearly facilitate the reaction, it is obviously not essential since removal of the imidazole ring causes only around a 10-fold decrease in the k_{cat} value. It is possible that His504 is the residue with the pK_a of 7.4 observed in the wild-type enzyme. If so, this again shows that a protonated imidazole can enhance the rate of reaction but is not essential for it, since the rate constant at high pH, where the imidazole would be

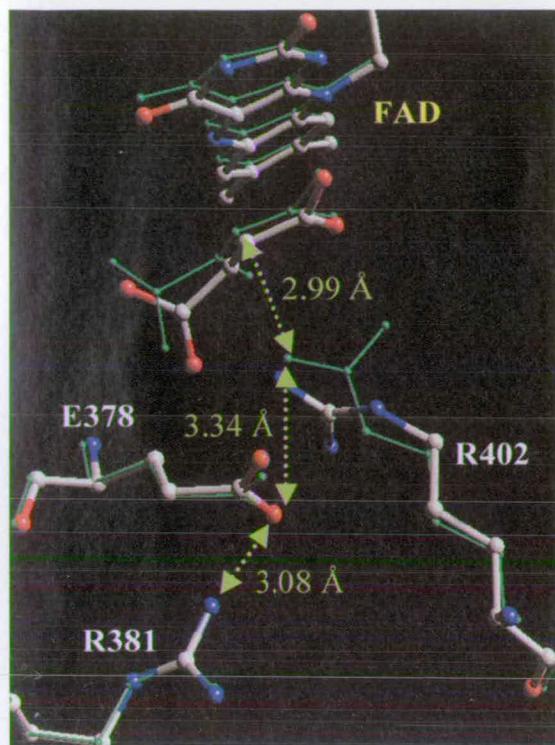


FIGURE 3: Overlay of the structures of wild-type Fcc_3 (green) and H365A Fcc_3 (atom-type colors) showing the proposed proton delivery pathway to the substrate C3 atom involving Arg381, Glu378, and Arg402. The distances indicated are for the wild-type enzyme. The altered conformation of Arg402 in the mutant enzyme is clearly visible.

fully deprotonated, would be around 150 s^{-1} (5–6-fold lower than the value for the fully protonated state).

The use of Arg402 as an active site acid to protonate the substrate clearly requires the guanidine moiety to be reprotonated. Since the active site is completely closed to solvent, we propose that a proton transfer pathway operates involving Arg381, Glu378, and Arg402. This pathway (Figure 3) may facilitate the rapid delivery/removal of protons for catalysis.

The Crystal Structure of H365A Fcc_3 . Data to 1.8 \AA were used to refine the H365A mutant enzyme structure to a final R -factor of 18.1% (Table 1). The final model consists of residues 1–568, 4 hemes, the FAD, 1 substrate molecule, 1

sodium ion, and 584 water molecules. As in wild-type Fcc_3 , one *cis*-peptide between Ala175 and Trp176 was clearly identified. The three C-terminal residues (569–571) were not located in the electron density maps. The rmsd fit of all backbone atoms for the wild-type and H365A mutant enzyme is 0.15 \AA , showing no significant structural differences between the two structures.

Both wild-type and H365A enzymes were crystallized in the presence of 10 mM fumarate. In the crystal structure of the mutant enzyme, a molecule of fumarate was found at the active site in a twisted conformation (Figure 4). This is in marked contrast to the wild-type structure in which (although found in the same twisted conformation) the molecule at the active site is hydroxylated at the C2 position (7).

The active sites of the two structures are compared in Figure 5. A major difference is, of course, the replacement of the histidine by alanine at position 365, removing the original hydrogen bond between His365 N3 and a carboxylate oxygen of the substrate. The removal of this hydrogen bond is entirely consistent with the increased K_m value seen for the mutant enzyme. The void produced by the H365A mutation is compensated by significant changes in side-chain conformations of Met375 and Arg402. Significantly, there is now room for a water molecule which forms a hydrogen bond to the backbone NH of Thr367 ($\text{N} \cdots \text{O} = 3.2 \text{ \AA}$). This water is also hydrogen bonded to the side chains of Thr367 ($\text{O} \cdots \text{O} = 2.95 \text{ \AA}$) and Arg402 ($\text{O} \cdots \text{N} = 3.14 \text{ \AA}$). This latter interaction may contribute toward stabilizing the rather different conformation of the Arg402 side chain, decreasing its effectiveness as a proton donor in fumarate reduction. In other words, the lower activity seen for the mutant enzyme arises from a less favorable orientation for proton donation from Arg402, rather than the loss of the imidazole ring. However, although the side chain of Arg402 has been altered, the closest distance between Arg NH2 and substrate C3 remains at 2.99 \AA .

The new conformation of Met375 in the H365A structure also triggers a flip in the orientation of the carbonyl group of Ala169, which swings down, allowing the incorporation of an additional bridging water molecule between A169 (O) and Val253 (N). It is probable that the repositioning of

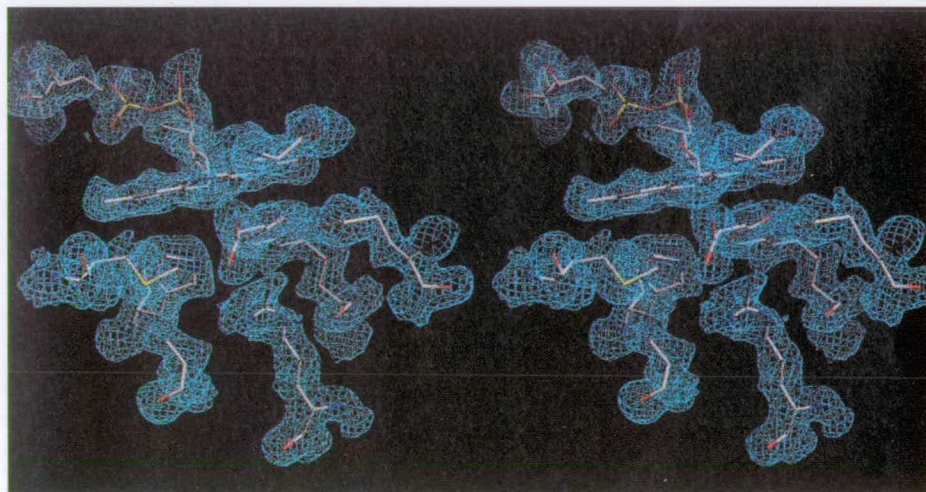


FIGURE 4: Stereoview of the electron density around the active site of the H365A mutant enzyme. The $2F_o - F_c$ map is contoured at the 1.25σ level. The FMN group is clearly visible at the top of the figure with the alanine residue at position 365 at the bottom left and Arg402 at the bottom center.

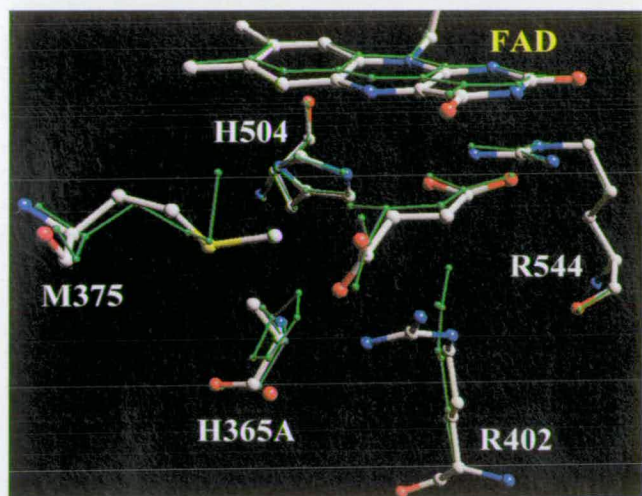


FIGURE 5: Overlay of the structures of wild-type Fcc₃ (green) and H365A Fcc₃ (atom-type colors). The substrate molecule is shown in the center surrounded by key active site residues. The substituted residue is labeled as H365A. Significant shifts in the positions of Met375 and Arg402 can be clearly seen.

Met375 prevents the hydroxylation of fumarate as seen in the wild-type structure, since in the H365A structure, much of the space that would have been taken up by this hydroxyl-group is now occupied by the side chain of Met375.

Comparison with Other Fumarate Reductases. The active sites of each of the known fumarate reductase structures (3, 7–9, 24) are largely well conserved structurally. In all cases, the bound substrate is well positioned to accept a hydride from N5 of the FAD cofactor, and this is clearly a key step in the chemical mechanism of fumarate reduction. The source of the proton needed to complete formation of the product succinate is somewhat less clear from direct observation of the structures and, as already discussed, has been variously proposed to be (using Fcc₃ numbering) His365 (12), His504 (10), and Arg402 (7–9). It would be very surprising if these closely related enzymes were to use different proton donors, especially when the residues listed above are conserved in all known fumarate reductases. Prior to the crystallographic results, it was generally expected that a histidine would act as the acid/base catalyst in fumarate reductases and succinate dehydrogenases. This expectation was based on the widespread use of histidines in this role in many types of enzyme and the fact that chemical modification studies with succinate dehydrogenase indicated that a histidine residue played an important catalytic role (25). However, results from mutagenesis studies reported in this paper rule out His365 and His504 as the active site acid. In addition, crystallographic analysis shows that His365 and His504 are each hydrogen bonded to substrate carboxylate oxygens and are not well positioned for proton transfer, being too distant from the substrate C3. Thus, the results described here for Fcc₃ confirm the importance of these histidine residues in substrate binding but rule out a key role in substrate protonation.

The structures of two of the *Shewanella* enzymes (7, 9) and *E. coli* fumarate reductase (3) clearly show NH₂ of Arg402 close to the substrate C3, the eventual proton acceptor. In the structure of the *Wolinella* enzyme, the position of the equivalent arginine (Arg301) has moved by about 3 Å compared to the *Shewanella* and *E. coli* enzyme structures. An overlay of the flavin binding domains of all

structures shows that the conserved catalytic residues of the flavin binding domain are very similar. The residues on the clamp domain differ by between 1 and 3 Å, which corresponds to an opening of the clamp in the *Wolinella* structures (24). Interestingly, both *Wolinella* structures (with and without fumarate) are similar, though the clamp has closed a little (less than 0.5 Å) when the substrate is present. In addition, the temperature factors of the fumarate and the fumarate binding residues are raised (24), suggesting that the protein has been trapped in a partially open conformation. This can be compared to the substrate-free open conformation seen in the structure of the iron-induced flavocytochrome *c*₃ (10). The fact that the arginine side chain is somewhat altered in the *Wolinella* fumarate reductase (24) (too distant for efficient proton transfer) has led Lancaster and colleagues to propose that the proton comes instead from a water molecule (24). This proposal suffers several weaknesses. The water positioned in the active site of the *Wolinella* enzyme is absent from all other substrate-bound fumarate reductase structures, indicating that if it is used for substrate protonation, then this enzyme is fundamentally different from its close homologues in this key mechanistic aspect. We believe that the equivalent of Arg402 is the true acid catalyst, and we further suggest that if the *Wolinella* enzyme had crystallized in the closed (catalytically active) form, then the position of the arginine side chain would have been comparable to all the other structures.

In conclusion, the combined kinetic and structural evidence strongly suggests that Arg402 is the active site acid catalyst in the fumarate reductase from *Shewanella*. We believe that this conserved arginine residue fulfills this role in all members of the fumarate reductase family.

REFERENCES

1. Pealing, S. L., Cheesman, M. R., Reid, G. A., Thomson, A. J., Ward, F. B., and Chapman, S. K. (1995) *Biochemistry* 34, 6153–6158.
2. Pealing, S. L., Black, A. C., Manson, F. D. C., Ward, F. B., Chapman, S. K., and Reid, G. A. (1992) *Biochemistry* 31, 12132–12140.
3. Iverson, T. M., Luna-Chavez, C., Cecchini, G., and Rees, D. C. (1999) *Science* 284, 1961–1966.
4. Körtner, C., Lauterbach, F., Tripiet, D., Unden, G., and Kroger, A. (1990) *Mol. Microbiol.* 4, 855–860.
5. Morris, C. J., Black, A. C., Pealing, S. L., Manson, F. D. C., Chapman, S. K., Reid, G. A., and Ward, F. B. (1994) *Biochem. J.* 302, 587–593.
6. Gordon, E. H. J., Pealing, S. L., Chapman, S. K., Ward, F. B., and Reid, G. A. (1998) *Microbiology* 4, 937–945.
7. Taylor, P., Pealing, S. L., Reid, G. A., Chapman, S. K., and Walkinshaw, M. D. (1999) *Nat. Struct. Biol.* 6, 1108–1112.
8. Chapman, S. K., Morrison, C. A., Reid, G. A., Pealing, S. L., Taylor, P., and Walkinshaw, M. D. (1999) *Flavins Flavoproteins 1999*, 105–113.
9. Leys, D., Tsapin, A. S., Nealson, K. H., Meyer, T. E., Cusanovich, M. A., and Van Beeumen, J. J. (1999) *Nat. Struct. Biol.* 6, 1113–1117.
10. Bamford, V., Dobbin, P. S., Richardson, D. J., and Hemmings, M. (1999) *Nat. Struct. Biol.* 6, 1104–1107.
11. Reid, G. A., Gordon, E. H. J., Hill, A. E., Doherty, M., Turner, K., Holt, R., and Chapman, S. K. (1998) *Biochem. Soc. Trans.* 26, 418–421.
12. Schröder, I., Gunsalus, R. P., Ackrell, B. A. C., Cochran, B., and Cecchini, G. (1991) *J. Biol. Chem.* 266, 13572–13579.
13. Kunkel, T. A., and Roberts, J. D. (1987) *Methods Enzymol.* 154, 367–382.

14. Rokeach, L. A., Haselby, J. A., and Hoch, S. O. (1988) *Proc. Natl. Acad. Sci. U.S.A.* 85, 4832–4836.
15. Sanger, F., Nicklen, S., and Coulson, A. R. (1977) *Proc. Natl. Acad. Sci. U.S.A.* 74, 5463–5467.
16. Michel, L. O., Sandkvist, M., and Bagdasarian, M. (1995) *Gene* 152, 41–45.
17. Simon, R., Priefer, U., and Puhler, A. (1983) *Bio/Technology* 1, 784–791.
18. Pealing, S. L., Lysek, D. A., Taylor, P., Alexeev, D., Reid, G. A., Chapman, S. K., and Walkinshaw, M. D. (1999) *J. Struct. Biol.* 127, 76–78.
19. Macheroux, P. (1999) in *Flavoprotein Protocols: Methods in Molecular Biology* (Chapman, S. K., and Reid, G. A., Eds.) Vol. 131, pp 1–7, Humana Press, Totowa, NJ.
20. Turner, K. L., Doherty, M. K., Heering, H. A., Armstrong, F. A., Reid, G. A., and Chapman, S. K. (1999) *Biochemistry* 38, 3302–3309.
21. Otwinowski, Z., and Minor, W. (1997) *Methods Enzymol.* 276, 307–326.
22. Widmer, A. (1997) Novartis AG, Basel.
23. Sheldrick, G. M. (1997) SHELX-97, University of Goettingen, Germany.
24. Lancaster, C. D., Kröger, A., Auer, M., and Michel, H. (1999) *Nature* 402, 377–385.
25. Vinogradov, A. D. (1986) *Biokhimiya* 51, 1944–1973.

BI000871L

Catalysis in fumarate reductase

Graeme A. Reid ^{a,*}, Caroline S. Miles ^a, Ruth K. Moysey ^b, Katherine L. Pankhurst ^b,
Stephen K. Chapman ^b

^a

^b

Received 15 May 2000; accepted 12 June 2000

Abstract

In the absence of oxygen many bacteria are able to utilise fumarate as a terminal oxidant for respiration. In most known organisms the fumarate reductases are membrane-bound iron-sulfur flavoproteins but *Shewanella* species produce a soluble, periplasmic flavocytochrome c_3 that catalyses this reaction. The active sites of all fumarate reductases are clearly conserved at the structural level, indicating a common mechanism. The structures of fumarate reductases from two *Shewanella* species have been determined. Fumarate, succinate and a partially hydrated fumarate ligand are found in equivalent locations in different crystals, tightly bound in the active site and close to N5 of the FAD cofactor, allowing identification of amino acid residues that are involved in substrate binding and catalysis. Conversion of fumarate to succinate requires hydride transfer from FAD and protonation by an active site acid. The identity of the proton donor has been open to question but we have used structural considerations to suggest that this function is provided by an arginine side chain. We have confirmed this experimentally by analysing the effects of site-directed mutations on enzyme activity. Substitutions of Arg402 lead to a dramatic loss of activity whereas neither of the two active site histidine residues is required for catalysis. © 2000 Elsevier Science B.V. All rights reserved.

Bacterial respiration; Fumarate reductase; *Shewanella*; Flavoprotein

1. Introduction

Shewanella species are widespread Gram-negative proteobacteria and are particularly abundant in marine and freshwater sediments. They are remarkable in their diversity of respiratory pathways [1,2] and can utilise many inorganic and organic electron acceptors, including fumarate, nitrate, trimethylamine *N*-oxide, thiosulphate and, more unusually, insoluble oxides of Fe(III) and Mn(IV). The diversity of

known respiratory pathways is matched by a large number of redox proteins. Several have been identified biochemically but it is clear from examination of the genome sequence of *Shewanella* MR-1 (available at www.tigr.org) that a very large number of uncharacterised cytochromes and other electron transfer proteins are produced. When

NCIMB400 (formerly *Shewanella*) is grown anaerobically, it produces large quantities of several *c*-type cytochromes [3]. The most abundant of these is a 64 kDa flavocytochrome that catalyses methyl viologen-dependent fumarate reduction *in vitro* [4,5]. The role of this flavocytochrome c_3 (Fcc₃) in fumarate respiration has been shown using a null

* Corresponding author. Fax: +44 (131) 6508650;
E-mail: graeme.reid@ed.ac.uk

mutant constructed by gene disruption [6]. The mutant is incapable of fumarate respiration but pathways to other electron acceptors are unaffected. This specific defect shows not only that flavocytochrome $_3$ is required for fumarate respiration but its function cannot be performed by other proteins produced under these conditions. This implies that no membrane-bound fumarate reductase is produced. It appears, surprisingly, that the genome of

MR-1 includes an operon that is very similar to the operon that encodes the membrane-bound fumarate reductase, even though this strain also produces a soluble flavocytochrome $_3$ fumarate reductase [7]. Whether a similar operon is present in NCIMB400 is not yet known. If so then its role in fumarate respiration is unclear since the Fcc $_3$ knockout strain failed to grow with fumarate as terminal electron acceptor. It has been shown that NCIMB400 produces a second flavocytochrome $_3$ (Ifc $_3$) which also efficiently reduces fumarate in vitro [8]. However, this protein is specifically induced by Fe(III) and its physiological function is poorly understood.

species are the only bacteria known to produce soluble respiratory fumarate reductases. In other organisms fumarate is reduced by a membrane-

bound complex of either three or four subunits [9]. These enzymes are closely related in structure and activity to succinate dehydrogenases which catalyse the reverse reaction. All fumarate reductases and succinate dehydrogenases contain FAD at the active site but electron transfer to the flavin is mediated by three iron-sulfur centres in the membrane-bound enzymes whereas the four haem centres of flavocytochrome $_3$ perform the equivalent function. The FAD-binding catalytic domain or subunit is highly conserved within and between these groups of enzymes indicating that the catalytic mechanism is likely to be very similar in all cases.

2. Fumarate reductase structure

The determination of the high-resolution crystal structure of fumarate reductase ([10,11]; PDB references 1QJD, 1D4C) has provided major insights into substrate binding and catalysis. The protein consists of a single polypeptide organised into three distinct domains (Fig. 1). The small, N-terminal, cytochrome domain containing four haem groups is tethered to the flavin domain by a charged bent helix linker (residues 100–110). The flavin do-

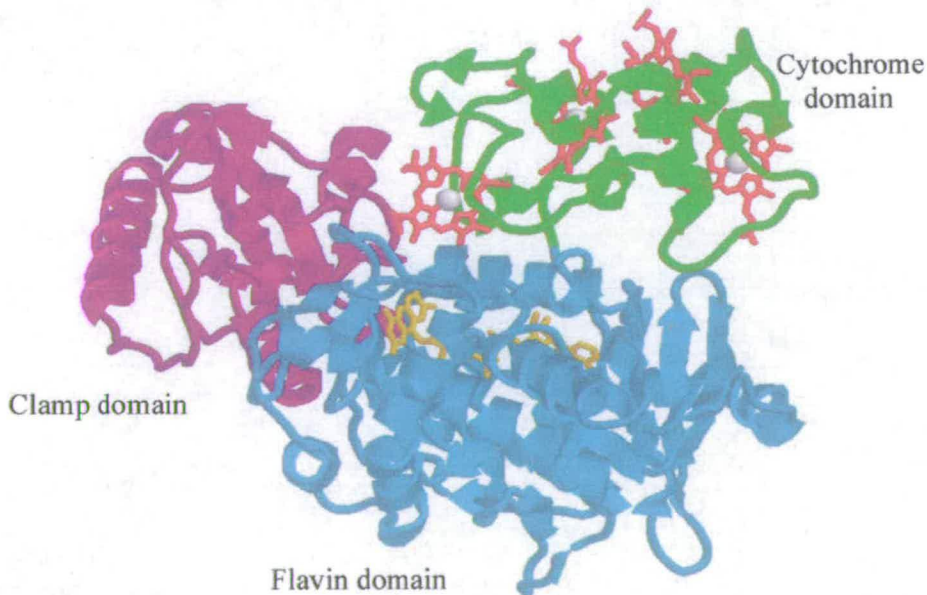


Fig. 1. Domain structure of fumarate reductase. The polypeptide chain is shown as a ribbon diagram with the cytochrome, flavin-binding and clamp domains coloured green, cyan and magenta, respectively. The haem groups are shown in red (with the iron in grey) and the flavin is in yellow.

main (residues 111–364 and 503–571, coloured cyan in Fig. 1) holds the non-covalently bound FAD group. The overall fold of the FAD binding domain has a structural and topological similarity with known FAD binding proteins, though sequence similarity is poor [12]. Buried within the flavin domain is an octahedrally coordinated sodium ion which is close to the active site and may well play a structural or regulatory role. The clamp domain of Fcc₃ (residues 365–502) is likely to be involved in controlling access of substrate to the active site. It consists of seven short helical stretches wrapped round a four-stranded antiparallel sheet.

The crystallisation medium contained a 10 mM solution of fumarate, well above the K_m of 25 μ M, suggesting that the active site of Fcc₃ should be fully occupied. However, the electron density map clearly shows the presence of a hydrated, malate-like molecule in the active site of Fcc₃ (Fig. 2). It is unlikely that this molecule is oxaloacetate because the protein is crystallised from fully active enzyme in the complete absence of this compound. The malate-like molecule is held tightly by several hydrogen bonds and sits in a close-fitting binding site that is completely inaccessible to solvent [10].

The absence of a solvent-accessible channel to the active site implies that there must be significant domain movement to enable substrate binding and product release. The active site is at the interface between the flavin-binding and clamp domains, both of which contribute important active site residues. We presume that the closed conformation that we observe when crystals are grown in the presence of fumarate represents a close approximation to the catalytically competent state. The enzyme is found in this form with either substrate or product bound in the active site [10] and it also appears that, in the absence of available reducing equivalents, the enzyme is still capable of modifying the substrate by nucleophilic attack [11]. The relative positions of the two domains are somewhat variable in the different fumarate reductase structures and more especially in *L*-aspartate oxidase [13], a closely related enzyme that can also reduce fumarate. This protein was crystallised in an open conformation with no substrate bound – indeed the FAD cofactor had also dissociated. We conclude that domain movement is an important feature of these enzymes with

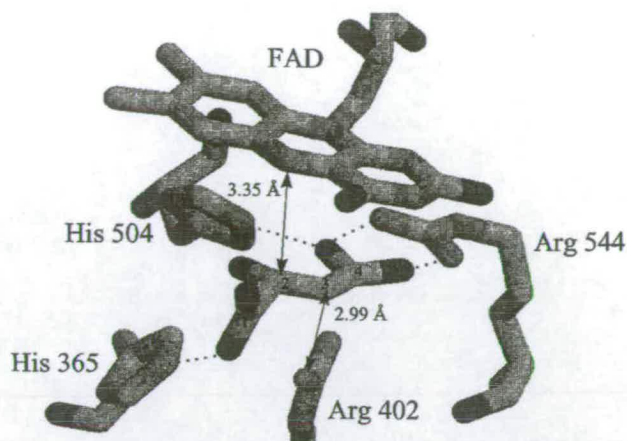


Fig. 2. The environment of the modified substrate in the active site. The malate-like molecule is shown with hydrogen bonds to Arg544, His504 and His 365 as dotted lines. The distances relevant for hydride and proton transfer are indicated.

opening being necessary for access to the active site and closure being essential for catalysis as described below.

3. Electron transfer

The pathway from membrane-bound quinols to the fumarate reductase in *E. coli* is not well understood, but a membrane-bound tetrahaem cytochrome *c*₂ has been implicated in electron transfer to fumarate reductase and other terminal reductases. This protein, CymA [14], is related to the NirT/NapC family. It is not known whether this protein directly reduces flavocytochrome *c*₂ but the organisation of the Fcc₃ cytochrome domain, with at least three of its four haems highly accessible to solvent, indicates that electron transfer should be facile. The edge-to-edge distances between pairs of haems in Fcc₃ range from a mere 3.9 Å to 8.0 Å and the shortest haem-FAD distance is just 7.4 Å. All of these distances are commensurate with very rapid internal electron transfer. The thermodynamic properties of the redox centres have been determined by potentiometric measurements and by protein film voltammetry [15]. The reduction potentials of the haems are low, ranging from –238 to –102 mV at pH 7.0 and 25°C with the FAD potential at –154 mV, giving a substantial driving force for fumarate reduction.

4. Substrate binding and catalysis

The malate-like molecule found in the active site is tightly bound and inaccessible to solvent. Its binding is indistinguishable from fumarate bound in the active site of fumarate reductase from MR-1 [11]. The C4 carboxylate is bound in a highly polar environment by electrostatic interaction and hydrogen bonds to Arg544 and Arg402 and by a hydrogen bond to His504 (Fig. 2). The environment of the C1 carboxylate is much less polar but hydrogen bond interactions with Thr377 and His365 are observed.

Two significant features of substrate binding appear critical for the reaction mechanism (Fig. 3). Normally fumarate is a symmetrical, planar, substrate. Reduction to succinate involves the transfer of a hydride from N5 of the FAD to C2 and a proton to C3 resulting in a non-planar product. This reaction is facilitated by an induced polarisation of the substrate, resulting from the charge asymmetry in the binding pocket and by an induced loss of planarity upon binding to the enzyme. This results from the close interaction of the C1 carboxylate with the side chains of Met236 and Met375, too close to allow substrate to bind as a planar molecule. Met236 is in the flavin-binding domain whereas Met375 is a clamp domain residue so it seems that the substrate distortion is a feature of domain closure around the active site. The orientation of the C1 carboxylate by hydrogen bonds to His365 and Thr377 may facilitate domain closure and provide the drive to twist the substrate out of the planar conformation with the additional effect of weakening the conjugated double bonds. The exceptionally polar hydrogen bonding environment of the C4 carboxyl group with contributions from two arginines and a histidine, acts to polarise the fumarate. The combined steric and electronic effects then reinforce each other to generate considerable positive charge at C2 making it amenable to nucleophilic attack.

The flavin N5 is positioned less than 3.2 Å from fumarate C2, poised to attack the si-face of the C2 centre. Hydride transfer to C2 is followed by protonation of C3, resulting in formation of succinate; the only residue sufficiently close to C3 for protonation is Arg402 at a distance of 2.99 Å. The role of this residue is discussed in detail below. Under the oxi-

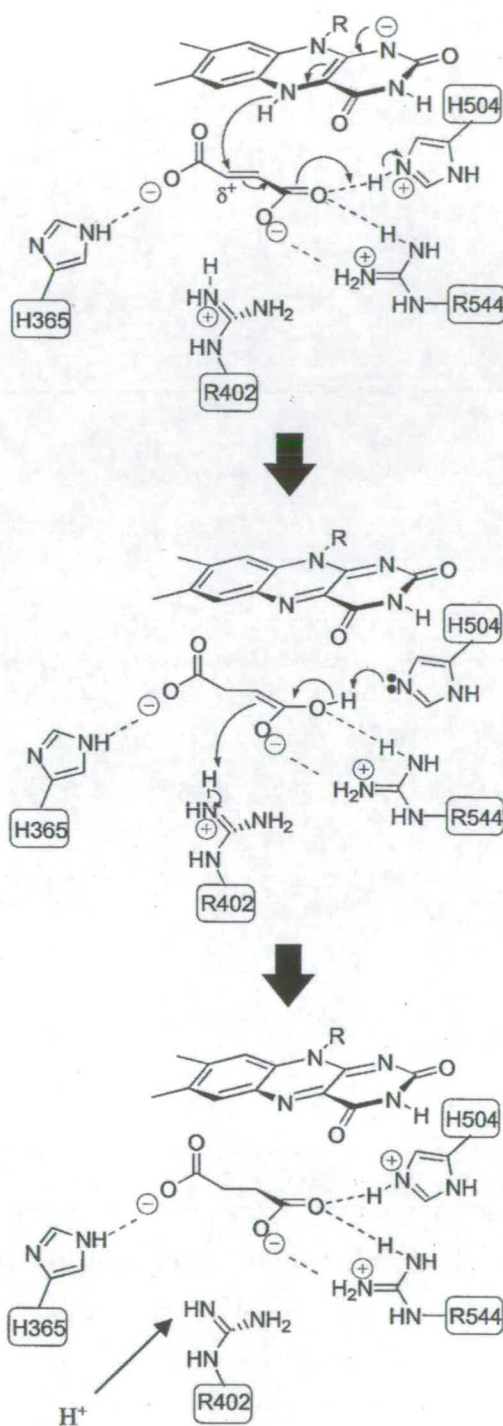


Fig. 3. The mechanism of fumarate reduction. The key residues are shown schematically with hydrogen bonds as dashed lines. The proposed mechanism is described in the text.

dising conditions that were used for crystal growth, hydride attack is not possible and instead there is attack by H_2O on the re-face to provide the observed product which has α -stereochemistry at C2 [10].

5. Proton transfer

The structures of five fumarate reductases from [10,11,16], [17] and [18] indicate a common mechanism for substrate binding and activation, suitably positioned for hydride transfer. Completion of product formation also requires protonation at C3 and the source of the proton has been the subject of some debate.

Prior to the crystallographic results, it was generally expected that a histidine would act as the acid/base catalyst in fumarate reductases and succinate dehydrogenases. This expectation was based on the widespread use of histidines in proton transfer in many types of enzyme and the fact that chemical modification studies with succinate dehydrogenase indicated that a histidine residue played an important catalytic role [19]. Analysis of the structure shows that the two active site histidines, His365 and His504, are each hydrogen-bonded to substrate carboxylate oxygens and not well positioned for proton transfer, being too distant from the substrate C3. To probe the roles of these residues and their possible involvement in substrate protonation as suggested elsewhere (e.g. [16]) we have used site-directed mutagenesis to convert each to alanine [20]. The H365A and H504A mutant enzymes exhibited lower k_{cat} values than the wild-type enzyme (Table 1) but only by factors of 3–15, depending on pH. This, coupled with the increase in K_m observed for these enzymes, indicates that His365 and His504 are primarily involved

Table 1
Comparison of k_{cat} and K_m values for wild-type, H365A, H504A and R402K Fcc₃ (pH 7.2, 25°C, $[F] = 0.45$ M)

Form of Fcc ₃	k_{cat} (s ⁻¹)	K_m (μM)
Wild-type	509 ± 15	25 ± 10
H365A	51 ± 2	259 ± 24
H504A	65 ± 3	256 ± 23
R402K	0.055 ± 0.004	66 ± 14

No activity was detected with the R402A enzyme.

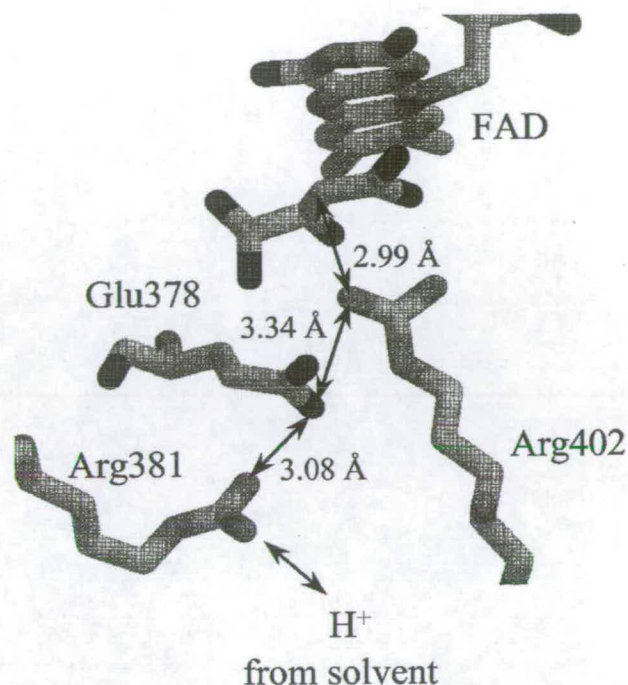


Fig. 4. The putative proton delivery pathway. Arg381 is exposed to solvent and close interactions indicate a pathway for rapid proton transfer to the substrate via Glu378 and Arg402.

in Michaelis complex formation and are not essential catalytic residues.

The structures of two of the enzymes [10,11] and fumarate reductase [17] clearly show NH₂ of Arg402 close to the substrate C3, the eventual proton acceptor. When we altered Arg402 to Ala we could not detect fumarate reductase assay in the recombinant enzyme, indicating a key role for this arginine. Interestingly we have recently substituted Arg402 with a lysine residue and the enzyme now exhibits activity, albeit at an extremely low level (Table 1).

Since the active site is inaccessible to solvent, delivery of a proton to Arg402 may appear problematic. However, a putative pathway for proton transfer is readily observed in that Glu378 forms a bridge between Arg402 and a conserved surface residue, Arg381 (Fig. 4). These residues are completely conserved, consistent with such an important function.

In the structure of the fumarate reductase [18], the position of the residue equivalent to Arg402 in the enzyme (Arg301) has moved by about 3 Å compared to the

and enzyme structures. An overlay of the flavin binding domains of all structures shows that the conserved catalytic residues of the flavin-binding domain are very similar. The residues on the clamp domain differ in position by between 1 and 3 Å, corresponding to an opening of the clamp in the enzyme structure [18]. It should be noted that this structure was determined with crystals that had had substrate diffused in – they may have been trapped in a slightly open conformation. The fact that the position of the arginine side chain is somewhat altered in the fumarate reductase has led Lancaster and colleagues to propose that the proton comes instead from a water molecule [18]. However, if the clamp domain in the enzyme is moved to the orientation (i.e. the closed form) seen in the other fumarate reductases then the position of the arginine side chain is comparable to that seen in all the other structures. Thus we are convinced that our mechanism (Fig. 3), involving hydride transfer from flavin N5 and proton transfer from this conserved arginine residue, applies for all members of the fumarate reductase family.

Acknowledgements

We thank Malcolm Walkinshaw, Paul Taylor and David Leys for useful discussions and the Biotechnology and Biological Sciences Research Council for their financial support.

References

- [1] C.R. Myers, K.H. Nealson, *Science* 240 (1988) 1319–1321.
- [2] K.H. Nealson, D.A. Saffarini, *Annu. Rev. Microbiol.* 48 (1994) 311–343.
- [3] C.J. Morris, D.M. Gibson, F.B. Ward, *FEMS Microbiol. Lett.* 69 (1990) 259–262.
- [4] S.L. Pealing, A.C. Black, F.D.C. Manson, F.B. Ward, S.K. Chapman, G.A. Reid, *Biochemistry* 31 (1992) 12132–12140.
- [5] S.L. Pealing, M.R. Cheesman, G.A. Reid, A.J. Thomson, F.B. Ward, S.K. Chapman, *Biochemistry* 34 (1995) 6153–6158.
- [6] E.H.J. Gordon, S.L. Pealing, S.K. Chapman, F.B. Ward, G.A. Reid, *Microbiology* 4 (1998) 937–945.
- [7] C.R. Myers, J.M. Myers, *FEMS Microbiol. Lett.* 98 (1992) 13–19.
- [8] P.S. Dobbin, J.N. Butt, A.K. Powell, G.A. Reid, D.J. Richardson, *Biochem. J.* 342 (1999) 439–448.
- [9] T. Ohnishi, C.C. Moser, C.C. Page, P.L. Dutton, T. Yano, *Structure* 8 (2000) R23–R32.
- [10] P. Taylor, S.L. Pealing, G.A. Reid, S.K. Chapman, M.D. Walkinshaw, *Nat. Struct. Biol.* 6 (1999) 1108–1112.
- [11] D. Leys, A.S. Tsapin, K.H. Nealson, T.E. Meyer, M.A. Cusanovich, J.J. van Beeumen, *Nat. Struct. Biol.* 6 (1999) 1113–1117.
- [12] M.W. Fraaije, A. Mattevi, *Trends Biochem. Sci.* 25 (2000) 126–132.
- [13] A. Mattevi, G. Tedeschi, L. Bacchella, A. Coda, A. Negri, S. Ronchi, *Structure* 7 (1999) 745–756.
- [14] C.R. Myers, J.M. Myers, *J. Bacteriol.* 179 (1997) 1143–1152.
- [15] K.L. Turner, M.K. Doherty, H.A. Heering, F.A. Armstrong, G.A. Reid, S.K. Chapman, *Biochemistry* 38 (1999) 3302–3309.
- [16] V. Bamford, P.S. Dobbin, D.J. Richardson, A.M. Hemmings, *Nat. Struct. Biol.* 6 (1999) 1104–1107.
- [17] T.M. Iverson, C. Luna-Chavez, G. Cecchini, D.C. Rees, *Science* 284 (1999) 1961–1966.
- [18] C.D. Lancaster, A. Kröger, M. Auer, H. Michel, *Nature* 402 (1999) 377–385.
- [19] A.D. Vinogradov, *Biokhimiya* 51 (1986) 1944–1973.
- [20] M.K. Doherty, S.L. Pealing, C.S. Miles, R. Moysey, P. Taylor, M.D. Walkinshaw, G.A. Reid, S.K. Chapman, *Biochemistry* (2000) in press.